# AN ABSTRACT OF THE DISSERTATION OF

Matthew D. Wolhowe for the degree of Doctor of Philosophy in Oceanography presented on September 5, 2014.

Title: Hydrogen Isotopic Composition of $C_{37}$ Alkenones and the Ecology and Physiology of Coccolithophores.

Abstract approved: _____

Fredrick G. Prahl

A three-part study was conducted into the impact of physiological and ecological variables on the net isotopic fractionation of hydrogen, $\alpha_{K37}$, expressed in $C_{37}$ alkenones. First, alkenone-producer production, abundance, and export were characterized in the summertime Gulf of California and Eastern Tropical North Pacific using compound-specific, labeled *in situ* incubations. It was found that these organisms routinely exhibited maximum production rates at depths associated with subsurface chlorophyll features and the nitracline, as opposed to the N-depleted surface, and that the relative contribution of coccolithophore productivity to overall productivity was decoupled from nutrient conditions. Our observations suggest that, in sufficiently well-stratified settings, a coccolithophore-favorable 'mid-to-low nutrient' niche may be absent. Second, results from a culture study were compared to samples from the initial field campaign in order to more firmly establish the physiological controls on the δD of alkenones. Nutrient-limitation experiments in culture, combined with previously published data, show that net fractionation between the growth medium and alkenones ($\alpha_{K37}$) increases rapidly with increasing cellular alkenone content and production rate, and, by extension, growth phase. To explain these results, a mechanism is proposed in which changing NADPH sources result in isotopically-depleted lipids at both high growth rates and in stationary phase growth. Comparison of these results to the field samples suggests that, in the water column, this dynamic (a relationship $\alpha_{K37}$ and growth rate) drives correlations between

$\alpha_{K37}$ and both cell abundance and the carbon-fractionation term $\varepsilon_p$. Lastly, the chemical and isotopic composition of alkenones was measured in sediment samples along a transect of the North-American Pacific margin from ~42°N to the tip of Baja California. It was found that both core-top and LGM intervals expressed a strong relationship between the temperature proxy $U_{37}^{K'}$ and estimated $\alpha_{K37}$. If covariation between $U_{37}^{K'}$ and estimated $\alpha_{K37}$ is robust in settings such as these, then paired analysis of $U_{37}^{K'}$ and alkenone δD may enable paleoceanographic estimates water δD. In light of the results of the second study, it is proposed that this relationship derives from a control of temperature on cellular division rate on sedimentary time scales. Deviations from this relationship were tentatively interpreted as indicative of export from locations where alkenone producers are/are not subjected to nutrient deprivation before sedimentation. Overall, the results of this three-part study suggest A) that coccolithophore-derived inorganic carbon export may serve as a weaker positive feedback on atmospheric $CO_2$, in the future, than previously suggested; B) that $\alpha_{K37}$ may lend valuable context to studies of alkenone-producer ecology, and C) that alkenone δD may prove a better than expected hydrologic proxy in marine settings and/or a coccolithophore-specific growth rate proxy.

# Hydrogen Isotopic Composition of $C_{37}$ Alkenones and the Ecology and Physiology of Coccolithophores.

by
Matthew D. Wolhowe

A DISSERTATION

submitted to

Oregon State University

in partial fulfillment of
the requirements for the
degree of

Doctor of Philosophy

Presented September 5, 2014
Commencement June 2015

Doctor of Philosophy dissertation of Matthew D. Wolhowe presented on September 5, 2014.

APPROVED:

Major Professor, representing Oceanography

Dean of the College of Earth, Ocean, and Atmospheric Sciences

Dean of the Graduate School

I understand that my dissertation will become part of the permanent collection of Oregon State University libraries. My signature below authorizes release of my dissertation to any reader upon request.

Matthew D. Wolhowe, Author

# ACKNOWLEDGEMENTS

Support for this work was project was provided by NSF OCE-0726422 and 1103434, while the work detailed in Chapter 2 was also supported in part by NSF OCE-0726543. Special thanks go to Dr. Russell Desiderio, who provided programming acumen, chemistry and physics expertise, mathematic instruction, humor, friendship, and extensive assistance authoring a section of Chapter 3 only to see it removed entirely; to Margaret Sparrow who taught me all my bench-top techniques, put up with my constant complaints, and kept the lab sufficiently irreverent while providing elemental and pigment data to my cause; to Dr. Jennifer McKay, a constant advocate of my ability who let me use her over-booked instruments whenever I needed to and trusted me to both take things apart and to put them back together; to June Padman, who always provided warm conversation and a ready smile, and was smart enough to realize that picking forams for me was faster than watching me do it myself; to Andy Ross for always having a helping hand to lend when it came to making things happen in the lab and an ear to lend when it came to anything else; and to Lori Hartline for consistently being the only person who could figure out how I was supposed to navigate through graduate school and how to fill the holes I invariably dug for myself. Personal thanks go to my friends Maxine Davies and Michelle Stowell, who helped keep me sane these last few years, Dr. Maureen Davies, who helped keep me sane for even longer, and to my dearest friend Joshua Chester who has kept me sane for most of my life.

Particular thanks go to committee member and former advisor Dr. Alan Mix, who recruited me, let me change projects and primary advisors with a smile and a handshake in lieu of complaint, and provided me with two years of funding for, in the end, no real benefit to himself; and to committee members Dr. Angelicque White (for making CEOAS a better place to work) and Dr. Allen Milligan (for putting up with my continued inability to keep him informed). Lastly, thanks go to my advisor Dr. Fredrick Prahl. He has made me a better scientist and writer, has bent over backwards to keep me gainfully employed, has stood next to me in the trenches, and has generally made graduate school a bearable (and even enjoyable, on occasion) experience despite my eternal delay of his retirement. None of this would have been possible without his patience.

# CONTRIBUTION OF AUTHORS

In the course of preparing Chapter 2 "A Biomarker Perspective on Coccolithophorid Growth and Export in a Stratified Sea", Dr. Angelicque E. White, Dr. Brian N. Popp, and Anaid Rosas-Navarro assisted as co-authors. Dr. White provided editorial assistance and provided data from ancillary analyses. These included primary productivity, chlorophyll, and particulate organic carbon analyses, the data from which was a component of previous manuscripts of which she was the primary author. Dr. Popp provided editorial assistance, and was responsible for the operation of the *in situ* incubation arrays, the quantitative and isotopic analysis of the dissolved $CO_2$ system, and isotopic analysis of the majority of the incubated alkenone samples. Mrs. Anaid Rosas-Navarro provided coccolithophorid taxonomic and abundance data for the 2008 field campaign.

In the course of preparing Chapter 3 "Alkenone δD As an Ecological Indicator: A Culture and Field Study of Physiologically-Controlled Chemical and Hydrogen-Isotopic Variation in $C_{37}$ Alkenones", Dr. Gerald Langer, Angela Maria Oviedo, and Dr. Patrizia Ziveri assisted as co-authors. Dr. Langer, Mrs. Oviedo, and Dr. Ziveri were responsible for the culture experiments and provided the associated alkenone and media samples, in addition to cell count data.

In the course of preparing Chapter 4 "Core-Top and LGM Covariation of $U_{37}^{K'}$ and Alkenone D/H Fractionation in Sediments: Implications for Paleohydrology and the Study of Coccolithophore Ecology", Dr. Alan C. Mix assisted as a co-author. He provided editorial assistance, access to prepared planktonic foraminiferal samples, and $\delta^{18}O$ stratigraphic data for many of the sampled cores.

# TABLE OF CONTENTS

TABLE OF CONTENTS (Continued)

Page

TABLE OF CONTENTS (Continued)

Page

# LIST OF FIGURES

# LIST OF FIGURES (Continued)

# LIST OF TABLES

# LIST OF APPENDICES

# LIST OF APPENDIX FIGURES

# LIST OF APPENDIX TABLES

# Dedication

This work is dedicated to my father, James C. Wolhowe, who would hate that this wrote ‘James’ instead of ‘Jim’. He was a good man and a good father, to whom I owe both my interest in, and whatever skill I possess at, both science and art. He was a smart, thoughtful, kind man who dealt with a war he’d never talk about and a life that took him different directions than he’d intended when he was my age. He always loved me, was always so, so proud of me, and felt every one of my struggles, whether he talked about it or not. I held his hand as his body failed him before he could see me crest this mountain, or do many other things. I won’t let him down again.

# 1. General Introduction

Coccolithophores, calcifying prymnesiophytes (unicellular phytoplankton) of the division Haptophyta, are an important producer of particulate inorganic carbon (PIC) in the past and modern oceans (Baumann et al. 2004; Hay 2004). They are also, coincidently, producers of alkenones, an important class of lipid biomarker. These compounds are largely produced in modern marine settings by the coccolithophores *Emiliania huxleyi* and species of the genus Gephyrocapsa (Volkman et al. 1980, 1995; Marlowe et al. 1984). These species are found throughout the world ocean (Winter et al. 1994; Bollmann 1997) and primarily produce di- and tri-unsaturated 37-carbon methyl ketones, referred to as K37:2 and K37:3. The ratio in which these compounds are produced varies, for still-unknown reasons, as a function of growth temperature (e.g. Prahl et al. 1988; Volkman et al. 1995), providing these compounds utility as the $U_{37}^{K'}$ paleo-temperature proxy (e.g. Herbert 2003). The source specificity of 'K37' alkenones has also led to the (partially successful) development of their carbon isotopic composition as a $pCO_2$ proxy (e.g. Pagani 2014). Due to the role of coccolithophores A) as PIC producers in a changing marine carbon cycle, B) their role in generating a large portion of the paleoceanographic community's paleotemperature records, and C) their potential to enable $pCO_2$ reconstructions, significant research has gone into better understanding coccolithophorid physiology (e.g. Müller et al. 2008), ecology (e.g. De Bernardi et al. 2005), and biogeochemical cycling (e.g. Balch and Utgoff 2009) for the last two decades. This work has already provided important insights into mechanisms of the inorganic carbon pump and the subtleties of making alkenone paleotemperature estimates. Potential changes in the ecology and chemistry of the ocean in the face of rising atmospheric $CO_2$ (e.g. Zondervan et al. 2001) and the development of alkenones as hydrogen-isotopic archive, however, continue to fuel efforts to understand when, where, and how coccolithophores grow.

The hydrogen isotopic composition of plant and algal lipids has received considerable attention from the oceanographic and paleoclimate communities since the 1970s. Lipids produced by photoautotrophs encode the D/H composition of environmental water in their non-exchangeable hydrogen (Estep and Hoering 1980),

spurring attempts to develop hydrologic proxies from these compounds (e.g. Estep and Hoering 1981; Sauer et al 2001; Huang et al. 2004). There are large and variable species-specific vital effects relating water and lipid isotopic compositions, however, and these make general lipid classes or biomarkers with multiple potential sources problematic as climate archives (e.g. Zhang and Sachs 2007). The need for source specificity has, as it did in the case of carbon isotopes as an indicator of $pCO_2$, lead to research on $C_{37}$ alkenones. With limited source organisms, a net fractionation factor, $\alpha_{K37}$, can be determined and used to relate measured alkenone composition ($\delta D_{K37}$) with the composition of the water ($\delta D_{H2O}$) from which the compounds were synthesized. The potential to determine water-compound fractionation factors, and the previous development of these compounds as a temperature proxy, makes alkenones an attractive target for development as a sedimentary hydrologic proxy. Attempts to relate $\delta D_{K37}$ to $\delta D_{H2O}$ via laboratory- or field-determined values of $\alpha_{K37}$ have yielded promising results (Englebrecht and Sachs 2005). However, it has become clear that, even with limited source organisms, $\alpha_{K37}$ (a net, apparent factor integrating an unknown number of fractionating biochemical processes) is highly variable, and may respond to a number of physiological influences. In addition to differences between species, such as open-ocean alkenone producers *E. huxleyi* and *G. oceanica* (Schouten et al. 2006) and coastal species *I. galbana* (M'boule et al. 2014) and *C. lamellose* (Chivall et al. 2014b), factors suggested to control $\alpha_{K37}$ include growth rate and salinity (Schouten et al. 2006; M'boule et al. 2014), growth phase (Wolhowe et al. 2009; Chivall et al. 2014b), and temperature (Wolhowe et al. 2009; Zhang et al. 2009). There is an additional 'temperature effect' in that an isotopic offset exists between K37:2 and K37:3 ($\alpha_{K37:3\text{-}K37:2}$) and appears to vary in magnitude with temperature (D'Andrea et al. 2007; Schwab and Sachs 2009, 2011; van der Meer et al. 2013).

In high-salinity contrast, high-$\delta D_{H2O}$ contrast environments, most of these proposed physiological influences, save the 'amplifying' salinity effect (Schouten et al. 2006) are theoretically minimized (relative to the impact of changing $\delta D_{H2O}$ on $\delta D_{K37}$), and alkenones have been employed to reconstruct changing hydrology. These include inland seas (van der Meer et al. 2008; Vasiliev et al. 2014), estuarine systems (Schwab and

Sachs 2011), and areas of high freshwater discharge (Pahnke et al. 2007). Even in highly-variable hypersaline environments, however, $\delta D_{K37}$ has been suggested to be impacted more by physiology more than salinity (Romero-Viana et al. 2013). In locations with lower-amplitude $\delta D_{H2O}$ variations, physiological controls on $\alpha_{K37}$ almost certainly make $\delta D_{K37}$ a poor hydrologic proxy (Wolhowe et al. 2009). In these locations, can $\delta D_{K37}$, responding primarily to changes in $\alpha_{K37}$, instead be used as an indicator of the physiological condition of coccolithophores?

This question drives the following work, an investigation of coccolithophore ecology and isotope systematics in three parts. The first component of this work, Chapter 2, assesses coccolithophore production in a novel study environment, the summertime Gulf of California (GoCal) and Eastern Tropical North Pacific (ETNP). This provides the necessary context for the second component (Chapter 3), a detailed study of hydrogen isotopic fractionation in alkenones that compares culture experiments and modeling results to field samples from the Chapter 2 study area. Lastly, Chapter 4 examines the chemical and isotopic composition of alkenones in sediments (both Holocene and glacial) from the eastern margin of the North Pacific and interprets these data in light of the systematics illustrated in Chapter 3. The general goals of these chapters are, respectively, A) to gain insight into the possible response of coccolithophores, as occupants of a low-nutrient ecological niche, to future warming and oligotrophic shifts in the ocean, B) to determine how the physiological factors that empirically control $\alpha_{K37}$ mechanistically impact $\delta D_{K37}$ in order to identify cellular properties that more directly explain observed isotopic variability, and C) to test whether $\delta D_{K37}$ varies in the marine sedimentary record in a manner, consistent with these controlling properties, that is useful to the paleoclimatological or paleoecological communities. As such, they address the following specific research questions and hypotheses:

<u>Chapter 2</u>

Q1: Is coccolithophorid production enhanced under stratified, nutrient-depleted conditions in the GoCal/ETNP study area? If so, why is the relative coccolithophorid abundance so low?

Q2: Does any perceived dependence of production on nutrient conditions alter the contribution of these plankton to carbon export?

Chapter 3

Q1: Can a consistent mechanistic explanation be given for the previously-observed, simultaneous dependence of $\delta D_{K37}$ and alkenone abundance on growth rate, temperature, and the exponential/stationary phase transition? Are common trends evident in the apparently-conflicting, available experimental data?

H1: $\delta D_{K37}$ in a natural water column can be interpreted based on the physiological dynamics observed in culture. Samples from the nutrient-depleted and nutrient-replete levels of a stratified water column will possess $\delta D_{K37}$ values consistent with nutrient-stressed and actively-dividing physiological states, respectively.

Chapter 4

H1: $\alpha_{K37}$ signals indicative of nutrient-replete, high-growth rate conditions will be observed in core-top sediments under the upwelling-dominated Oregon/California portion of the modern North American margin. Conversely, $\alpha_{K37}$ signals indicative of low growth rates will be observed further south, where summer stratification holds sway.

H2: This north-south pattern will shift northward at the LGM, as the California Current retreated away from the Southern California Bight and upwelling weakened along the coast.

In addressing these questions and hypotheses, my co-authors and I present a unique set of *in situ* coccolithophore productivity measurements, the first measurements of $\delta D_{K37}$ from a natural water column, and a first-of-its-kind survey of $U_{37}^{K'}$ and $\delta D_{K37}$ in spatially-distributed marine sediments. The following manuscripts detail these findings.

# 2. A Biomarker Perspective on Coccolithophorid Growth and Export in a Stratified Sea

Matthew D. Wolhowe, Fredrick G. Prahl, Angelicque E. White, Brian N. Popp, and Anaid Rosas-Navarro

Progress in Oceanography
Elsevier Inc.
225 Wyman Street
Waltham, MA 02144
www.elsevier.com/progress-in-oceanography

**Abstract:** Summer cruises to the Gulf of California and adjacent Eastern Tropical North Pacific between 2004 and 2008 provided data on non-bloom coccolithophorid abundance and production in nitrate-depleted surface waters. Using lipid biomarkers specific to the dominant coccolithophorids in this region, it was found that these organisms routinely exhibited maximum production rates at depths associated with subsurface chlorophyll features and the nitracline, as opposed to the N-depleted surface. Estimates of integrated coccolithophorid production, relative to bulk primary production, showed no systematic relationship to availability of the limiting macronutrient (nitrate) in the euphotic zone. Our observations suggest that, in sufficiently well-stratified settings, the nutrient-depleted and nutrient-replete portions of the euphotic zone may become so sharply partitioned and temporally stable that a coccolithophorid-favorable 'mid-to-low nutrient' niche is absent. Consequently, the relative abundance and production rate of coccolithophorids are low, and the relative contribution of alkenones to carbon export is driven by variability in the significantly larger bulk carbon component. Study of this region provides important insights into the ecology of these calcifying organisms in a warm, quiescent ocean. Our findings suggest that, if water columns akin to those surveyed become more common, coccolithophorid-derived inorganic carbon export may serve as a weaker positive feedback on atmospheric $CO_2$ than previously suggested.

## 2.1. Introduction:

As a dominant producer of particulate inorganic carbon (PIC) in the global ocean (Baumann et al. 2004; Hay 2004), coccolithophorids have received significant research focus for the last two decades. An increased understanding of coccolithophorid physiology (e.g. Müller et al. 2008), ecology (e.g. De Bernardi et al. 2005), and biogeochemical cycling (e.g. Balch and Utgoff 2009) has provided important insights into fluctuations in the inorganic carbon pump, the evolution of past climates, and changes in the ecology and chemistry of the ocean in the face of rising atmospheric $CO_2$ (e.g. Zondervan et al. 2001). This last subject is of particular importance. The predictability of future climate change is dependant, in part, on the understanding of

positive or negative feedbacks between algal calcite production and sea surface temperature (SST), upper ocean stratification, atmospheric $CO_2$ and ocean pH (Holligan and Robertson 1996; Tyrrell 2008; Beaufort et al. 2011). This situation has stimulated an effort to understand how modern coccolithophorid production relates to prognostic ocean parameters (e.g. Iglesias-Rodríguez et al. 2002; Cermeño et al. 2008). It remains unclear, however, which perspective is most relevant for the future ocean: bloom-dominated or steady-state/subsurface 'background' production. In oligotrophic surface waters, the low nutrient half-saturation constants and high light tolerance of coccolithophorids give them a competitive advantage over larger plankton such as diatoms (Tozzi et al. 2004; Litchman et al. 2007). These physiological attributes may also be a key component in coccolithophorids' successional niche in the North Sea (Head et al. 1998) and the North Atlantic (Lochte et al. 1996) blooms. However, coccolithophorids have also been observed or inferred to exhibit production maxima associated with the nitracline (Fernández et al. 1993; Prahl et al. 1993; Popp et al. 2006b), and it has been estimated that the bulk of global coccolithophorid production takes place under non-bloom conditions (Brown and Yoder 1994). Currently, it is unclear to what extent nutrient gradients with depth, in stratified settings, provide the same coccolithophorid-favorable niche provided by temporal nutrient gradients in more regularly-mixed regions (e.g. Iglesias-Rodríguez et al. 2002).

Cruises to the Gulf of California (GC) were conducted in the summers of 2004, 2005 and 2008, with the latter cruise also extending to the Gulf's entrance zone (EZ) and the adjacent Eastern Tropical North Pacific (ETNP) (White et al. 2007, 2013; Malinverno et al. 2008). These cruises (Table 2.1, Figure 2.1) provided an excellent opportunity to study the dynamics of coccolithophorid production in stratified water columns, across a broad temperature range, in a location where subsurface maxima in coccolithophorid abundance have been reported (Hernández-Becerril 1987). Furthermore, estimates of coccolithophorid and diatom abundance in the GC from the summer of 2005 correspond to coccolithophorid:diatom ratios on the order of ~0.01-0.08 (chlorophyll a basis; Malinverno et al. 2008). This ratio is lower than expected for what should be a coccolithophorid-favorable high light, low nutrient setting. For comparison,

ratios >1 (carbon basis) were observed along the majority of the longitudinal Atlantic Ocean transect surveyed by Cermeño et al. (2008). This difference suggests unusual coccolithophorid ecology in the GC, warranting further investigation.

**Table 2.1.** Summary of descriptive hydrographic parameters measured at stations in this study. Surface temperature is given as the mean temperature observed in the surface-most density bin over the course of station occupation (see Section 2.2.2). Mixed layer depth (density offset of 0.125 kg $m^{-3}$ from the surface value), top-of-nitracline depth ($[NO_3^-]$ = 1 μmol $L^{-1}$) and 1% light level (vs. simultaneous surface PAR) are interpolated from the mean profiles described in Section 2.2.2 (Appendix A). Uncertainty values are given as half the depth range between the two density bins bracketing the interpolated values. ChlA maximum depths are given as the average depth of the density bin with the highest average ChlA fluorescence (Appendix A), and uncertainty is given as the standard deviation of depth of this isopycnal.

**Table 2.1.** Station Summary

| Station | Occupation Date | Lat (ºN) | Lon (ºW) | SST (ºC) | Mean Mixed Layer Depth (m) | ± | Nitracline Depth (m) | ± | Depth of 1% Light (m) | ± | DCML Depth (m) | ± | Averaged Casts |
|---|---|---|---|---|---|---|---|---|---|---|---|---|---|
| | *Gulf of California (GC)* | | | | | | | | | | | | |
| 1-1 | July 13-15 2004 | 27.50 | 111.33 | 28.5 | 6 | 2 | 23 | 1 | 19 | 1 | 26 | 2 | 15 |
| 3-1 | Aug. 5-7 2005 | 27.02 | 111.42 | 30.9 | 4 | <1 | 47 | 7 | 43 | 1 | 32 | 4 | 12 |
| 3-2 | July 27-30 2005 | 27.50 | 111.33 | 29.4 | 8 | 1 | 33 | 4 | 29 | 1 | 34 | 2 | 7 |
| 3-3 | July 31-Aug. 3 2005 | 30.10 | 113.87 | 30.1 | 5 | 1 | 33 | 2 | 34 | 1 | 32 | 3 | 9 |
| 3-4 | Aug. 3-5 2005 | 26.07 | 110.12 | 29.8 | 14 | 3 | 46 | 3 | 42 | 1 | 44 | 3 | 9 |
| 4-1 | July 11-13 2008 | 26.50 | 110.50 | 28.8 | 9 | 2 | 35 | 5 | 42 | 1 | 35 | 6 | 16 |
| 4-2a | July 14-16 2008 | 24.50 | 109.00 | 29.4 | 10 | <1 | 36 | 3 | 55 | <1 | 39 | 6 | 19 |
| 4-2b | July 22-24 2008 | 24.50 | 109.00 | 29.7 | 8 | 2 | 40 | 9 | 45 | 2 | 46 | 1 | 14 |
| | *Entrance Zone (EZ)* | | | | | | | | | | | | |
| 4-8 | July 18-21 2008 | 20.50 | 106.50 | 29.5 | 8 | 1 | 69 | 1 | 67 | 1 | 60 | 8 | 19 |
| 4-9 | July 25-27 2008 | 21.50 | 109.50 | 28.8 | 8 | 1 | 34 | 3 | 44 | 1 | 43 | 4 | 16 |
| | *Eastern Tropical North Pacific (ETNP)* | | | | | | | | | | | | |
| 4-10 | July 28-31 2008 | 24.70 | 113.30 | 24.2 | 9 | 1 | 40 | 10 | 47 | 2 | 50 | 3 | 17 |
| 4-11 | Aug. 1-3 2008 | 27.50 | 117.50 | 21.0 | 12 | 3 | 51 | 3 | 42 | 1 | 50 | 6 | 15 |
| 4-12 | Aug. 5-7 2008 | 32.50 | 120.50 | 16.9 | 15 | 3 | 22 | 3 | 32 | 1 | 23 | 4 | 14 |

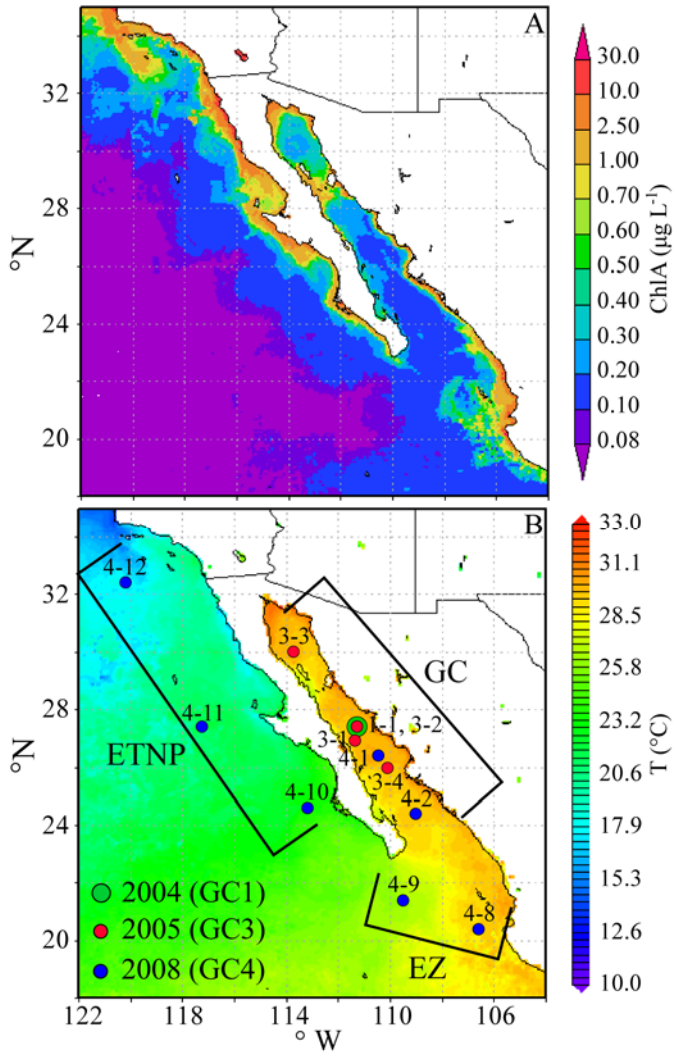


**Figure 2.1**. Seasonal composites of Aqua MODIS level-3 4km sea surface ChlA (µg $L^{-1}$) and 11µm nighttime SST (ºC) (**A** and **B**, respectively) in the Gulf of California for the summer (July-September) of 2005 (NASA Giovanni visualization). Sampling locations for 'GC' cruises 1 (2004), 3 (2005) and 4 (2008) are shown in **B**. Stations 4-8 and 4-9 are referred to herein as 'entrance zone' stations (EZ), and 4-10, 11, and 12 are referred to as 'ETNP'. The remaining stations are classified as 'GC'. See Table 2.1 for occupation coordinates and dates.

We have estimated coccolithophorid production and export relative to key water column features including mixed layer and nutricline depth, net primary production (NPP), and chlorophyll a (ChlA) concentration profiles during these cruises. This information allowed the following questions to be addressed:

1. Is coccolithophorid production enhanced under stratified, nutrient-depleted conditions in our study area? If so, why is the relative coccolithophorid abundance so low?
2. Does any perceived dependence of production on nutrient conditions alter the contribution of these plankton to carbon export?

Using the compound-specific $^{13}C$ incubation techniques developed by Popp et al. (2006a) and detailed further in Popp et al. (2006b), we employed $C_{37}$ alkenones as a sensitive tracer of coccolithophorid-specific production in this low-abundance, low PIC:particulate organic carbon (POC) setting. Alkenone biomarkers are unique to specific prymnesiophytes, and are largely produced by *Emiliania huxleyi* and members of the genus Gephyrocapsa (Volkman et al. 1980, 1995; Marlowe et al. 1984). These species are the predominant coccolithophorids in the Gulf of California (Thunell et al. 1996; Malinverno et al. 2008) and throughout the world ocean (Winter et al. 1994). The primary alkenones produced in marine settings, including the GC and adjacent ETNP, are the di- and tri-unsaturated 37-carbon methyl ketones K37:2 and K37:3. Using these two alkenones and previously reported cell abundances, we compare estimated coccolithophorid production and export to NPP and POC flux in the context of nutrient conditions and stratification.

## 2.2. Methods:

### 2.2.1 Study Area

The Gulf of California (GC) is an enclosed sea characterized by strong seasonal cycles in wind forcing and, consequently, strong variations in surface water temperature and mixed layer depth. Unlike the adjacent California Current System, northerly winds in winter drive upwelling along the eastern margin of the basin (Thunell et al. 1996), while weaker southeasterly winds in summer produce more sporadic upwelling that is

restricted to a narrow band along the western margin (Figure 2.1A). Coupled with high insolation, this wind forcing allows a warm, highly stratified water column to develop over most of the summertime GC (Hernández-Becerril 1987). For example, sea surface temperature (SST) determined by satellite during the summer of 2005 was >27ºC throughout the gulf (seasonal mean, Figure 2.1B; see also White et al. 2007). This resulted in a pronounced deep chlorophyll maximum layer (DCML) within the thermocline, at or near the depth of the nitracline (White et al. 2013). While satellite estimates of surface chlorophyll are highest during the upwelling-dominated winters, the highest alkenone (Goñi et al. 2001) and coccolith (Ziveri and Thunell 2000) fluxes have been observed during the stratified, low-surface nutrient summers. Despite sustained POC flux during the summer (Thunell 1998), satellite-detectable bloom events are restricted to the upwelling areas, the mixed region around the Midriff Islands, or sporadic $N_2$ fixation events (White et al. 2007).

Thorough descriptions of the regional variability of NPP, photosynthetically active radiation (PAR), POC export, temperature, nutrient, and ChlA fields observed at 'GC', 'EZ', and 'ETNP' sites (defined in Table 2.1 and Figure 2.1B) are provided by White et al. (2007, 2013). Malinverno et al. (2008) have published detailed analysis of the coccolithophorid species assemblages sampled on the 2004 and 2005 cruises; similar analysis will be forthcoming for the 2008 cruise from author Rosas-Navarro and Dr. Patrizia Ziveri.

### 2.2.2 Sampling

To account for the vertical movement of isopycnals over ~2 days of sampling at each station, discrete water samples and CTD profile measurements were binned according to density. For each site, the bin width was set by dividing the observed density range (the difference between the minimum and maximum density observed in the top 200m of the water column) into 50 equally spaced intervals. CTD measurements were then distributed into the bins based on the *in situ* density at the time of collection. The number of casts included in each data reduction varied with occupation (15 for 2004, 7-12 for 2005 and 14-19 for 2008; see Table 2.1). Each bin was then assigned the

average depth associated with its density range over the included set of casts, with uncertainty defined by the standard deviation. The resulting density vs. depth profiles have ~1m resolution in the steepest portion of the observed gradient, just below the base of the surface mixed layer (SML). These profiles and binned values for other properties measured continuously by CTD (T, S, ChlA fluorescence, and % PAR) are tabulated in Appendix A. Discrete measurements (e.g. alkenone abundance and production rate) are assigned the average depth of the density bin from which they were sampled. This processing allows for comparison of biogeochemical samples collected up to 48 hours apart at a given station, as well as comparison with the site's mean hydrographic profiles. The previously reported NPP, ChlA, nutrient, and cell abundance profiles (White et al. 2007, 2013; Malinverno et al. 2008; Anaid Rosas-Navarro, personal communication) have also been re-assessed on this basis. Depth-integrated production at each station (trapezoidal integration of values from each production rate profile, after making the density-depth adjustment described above) was calculated from the surface to the greatest depth at which an *in situ* incubation (Section 2.2.3) was conducted. This depth ranged from ~32 to 67m (Table 2.2), and, as such, discussion of integrated values is limited to comparison of relative properties (e.g. the ratio of integrated K37 production to integrated NPP).

### 2.2.3 *In Situ* Production Rate Arrays

K37:2 production rates (Popp et al. 2006a, b) were determined at each site using free-floating *in situ* incubation arrays (Prahl et al. 2005; White et al. 2007, 2013). Briefly, water (25 L) was collected before dawn, a solution of $^{13}$C-labeled bicarbonate (99%, Cambridge Isotope Laboratories) added to achieve an initial $\delta^{13}$C-DIC (dissolved inorganic carbon) composition of ~190‰ vs. PDB, and the water incubated for ~24 hours in clear polycarbonate carboys at 4-6 depths. The incubation depths ranged from just below the surface to ~60m and corresponded approximately to the initial collection depths. Each array included a Vertex style (Buesseler et al. 2007) sediment trap deployed at 100m depth. Collection tubes were filled with NaCl brine for sample preservation prior to deployment (Knauer et al. 1984).

2.2.4 Alkenone Quantification

Suspended particulate material (SPM) in ~40-70L of water from each of several depths in the euphotic zone, 25L of water from each *in situ* array incubation carboy, and the contents of the sediment trap collection tubes from each array deployment were collected on glass fiber filters (0.7 μm pore size, Whatman) using pressure (<10 psi) filtration and frozen until analysis. Total lipids were extracted from the filters using a Dionex ASE-200 automated solvent extraction system and partitioned into hexane via a standard procedure (Walinsky et al. 2009). Alkenone fractions were isolated by silica gel chromatography (Prahl and Pinto 1987), saponified in basic ethanol to remove alkenoates (Christie 2003), and characterized/quantified by capillary gas chromatography with flame ionization detection (Walinsky et al. 2009). Alkenone concentrations are reported as values corrected for recovery (typically 80-90%) of hexatriacontan-2-one (K36:0), a synthetic alkanone added to each sample prior to beginning the extraction procedure. Due to a lack of true sample replication, conservative uncertainties of 10% (as per Popp et al. 2006b) were assumed in the quantification of K37:2 and K37:3. These uncertainties were then propagated into calculation of suspended alkenone concentration ([K37]), alkenone flux measured in sediment traps ($F_{K37}$) and the unsaturation index $U_{37}^{K'}$ measured in both types of samples. The latter index is defined as:

$$U_{37}^{K'} = \frac{[K37:2]}{[K37:2]+[K37:3]} \qquad \textbf{2.2.1}$$

2.2.5 Production Rates

Compound-specific carbon isotopic analysis of alkenones and calculation of alkenone production rates followed the procedures outlined in Popp et al. (2006a, b). Both the natural-abundance and post-incubation isotopic composition of K37:2 (the dominant $C_{37}$ compound in all GC samples) was determined via gas chromatography-combustion isotope ratio mass spectrometry using methods discussed in Hayes et al. (1990). K37:2 production rates (ng $L^{-1}$ $d^{-1}$) are defined as:

$$PR_{K37:2} = [K37:2] * TR_{K37:2} \quad \textbf{2.2.2}$$

where $TR_{K37:2}$ is the turnover rate of K37:2. Turnover rate is traditionally defined as:

$$TR = \frac{A_{is} - A_{ns}}{T(A_{ic} - A_{ns})} \quad \textbf{2.2.3}$$

Equations 2.2.2 and 2.2.3 are modified from Equation 2 in Popp et al. (2006b). [K37:2] is the concentration K37:2 in the incubation bottle at the end of the experiment and $T$ is the ~24 hour incubation period. $A_{is}$ and $A_{ns}$ are the atom percent $^{13}C$ of K37:2 in post-incubation samples and in natural abundance samples collected from the same depth, respectively. $A_{ic}$ is the isotopic composition of $CO_{2(aq)}$ in the incubation bottle. This equation is based on analogous formulations in Hama et al. (1993, 1983). In turn, these formulations are based on a mass balance, from the treatment of early radio-tracer work in Sheppard (1962), where material newly added to the product pool possesses the same tracer concentration as the tracer-enriched reactant pool. In these prior formulations, $A_{ic} - A_{ns}$ (see Equation 2.2.3) represents the difference between the starting composition of the product pool and the value it approaches at 100% turnover. In reality, an isotopic offset exists between the DIC pool and new organic products due to fractionation during biosynthesis (Laws 1984). This effect is quantified here by α, the fractionation factor between alkenones and $CO_{2(aq)}$. For our incubation experiments, α can be determined by comparing the natural $^{13}C$ composition of $CO_{2(aq)}$ and K37:2 sampled at the incubation depth:

$$\alpha_{ns-nc} = \frac{\delta^{13}C_{ns} + 1000}{\delta^{13}C_{nc} + 1000} \quad \textbf{2.2.4}$$

The isotopic composition that the labeled product pool approaches with time, $\delta^{13}C_L$, is then defined by this fractionation factor and the composition of the $^{13}C$-enriched $CO_{2(aq)}$ pool:

$$\delta^{13}C_L = (\delta^{13}C_{ic} + 1000)(\alpha_{ns-nc}) - 1000 \quad \textbf{2.2.5}$$

Written in terms of atom-percent values, this equation becomes:

$$A_L = \frac{100\alpha_{ns-nc} * A_{ic}}{\alpha_{ns-nc} * A_{ic} + A_{ic} - 100} \quad \textbf{2.2.6}$$

Substituting $A_L$ for $A_{ic}$ in Equation 2.2.3 and including a factor of 1.025 (to account for the uptake rate difference between $^{13}CO_2$ and $^{12}CO_2$) yields the formula we use for turnover rate:

$$TR_{K37:2} = \frac{1.025(A_{is} - A_{ns})}{T(A_L - A_{ns})} \qquad \textbf{2.2.7}$$

For sufficiently high isotopic enrichments, $(A_{is} - A_{ns}):(A_{ic} - A_{ns}) \approx (A_{is} - A_{ns}):(A_L - A_{ns})$. For low-enrichment experiments or processes with large isotopic fractionations, however, the difference between the two formulations can be significant. In our work, $\delta^{13}C_L$ was ~18‰ to 27‰ more negative than $\delta^{13}C_{ic}$. This difference is a significant portion of the ~190‰ enrichment and would result in a ~10% to 14% under-estimation of derived production rates if $A_{ic}$ was used instead of $A_L$ in Equation 2.2.7.

Rate uncertainties were calculated given the alkenone abundance uncertainties discussed above, standard deviations of 2 or 3 replicate isotopic analyses of alkenones (typically ~0.1‰ v. PDB), analytical uncertainty of $\delta^{13}$C-DIC measurements (~0.1‰ v. PDB), and an assumed incubation time uncertainty of ±0.5 hr. Dissolved $CO_2$ isotopic compositions were calculated from $\delta^{13}$C-DIC knowing the concentration of DIC and carbonate alkalinity as per Laws et al. (1995) and Popp et al. (2006b). $\delta^{13}$C-DIC was determined as per Revesz et al. (2001).

Total $C_{37}$ alkenone production rates gauged by K37:2 alone will exhibit variation driven by temperature gradients with depth (small) and location (large) due to the temperature dependence of the ratio of K37:2 and K37:3 (Volkman et al. 1980). K37:3 was not abundant enough for isotopic analysis in most samples, and this compound has been found to acquire isotopic labeling at a lower rate than K37:2 (Popp et al. 2006a), making direct comparison of their measured production rates difficult. However, if $U_{37}^{K'}$ at a given depth is roughly constant over the course of the 24 hour experiment, then the relative production rates of K37:2 and K37:3 must be proportional to their relative abundance. Therefore, the 'production unsaturation index', $(PR_{K37:2})(PR_{K37:2}+PR_{K37:3})^{-1}$ (Hamanaka et al. 2000) must equal to Equation 2.2.1. Consequently,

$$PR_{K37:3} = PR_{K37:2}\left(\frac{1}{U_{37}^{K'}} - 1\right) \quad \textbf{2.2.8}$$

and therefore,

$$PR_{K37} = PR_{K37:2} + PR_{K37:3} = \frac{PR_{K37:2}}{U_{37}^{K'}} \quad \textbf{2.2.9}$$

Using this estimated production rate for total K37s ($PR_{K37}$), we can compare integrated biomarker production values between sites, while accounting for differences in temperature.

## 2.3. Results:

### 2.3.1 Hydrography

In general, the upper water column at all GC sites displayed similar hydrographic characteristics (SST, depths of the SML, nitracline, 1% light level, and DCML, see Table 2.1). A set of example profiles for Station 1-1 are illustrated in Figure 2.2. The depths of these hydrographic features, as well as several ecological features discussed below, are compared for all sites in Figure 2.3. Each GC station was highly stratified, with the base of the SML (defined by a density offset of 0.125 kg $m^{-3}$ from surface values, as per Kara et al. 2000) at an average depth of 8m (maximum: 14m) and surface water temperatures >28.5ºC. The concentration of nitrate (the stoichiometrically limiting macronutrient in this system) in the SML was at or below detection limits (≤0.01 μmol $L^{-1}$) (White et al. 2007, 2013; Appendix A). This depletion extended down to the top of the nitracline, defined as the depth (23-47m) at which the nitrate concentration reached 1 μmol $L^{-1}$ (depth determined from linear interpolation between samples with bracketing concentrations). The vertical nitrate gradient at the nitracline ranged from 0.2 to 0.9 μmol $L^{-1}$ $m^{-1}$. A thin SML (~8m), deep nitracline (34 and 62m), and sharp nitrate gradient (~0.5 μmol $L^{-1}$ $m^{-1}$) were also apparent at both EZ sites (4-8 and 4-9, respectively) occupied in 2008 (Table 2.1).

The ETNP sites sampled in 2008 (Figure 2.1B) were located along a surface temperature gradient from ~24ºC at 4-10 to ~17ºC at 4-12. However, SML depths (9-

15m) were not markedly different from those in the GC (Figure 2.3). As in the GC, the nitraclines at sites 4-10 and 4-11 were separated from the base of the SML by ~30 to 40m and displayed similar nitrate concentration gradients with depth (~0.4 μmol $L^{-1}$ $m^{-1}$). At the northernmost site (4-12), however, there was no separation between the base of the SML (15m) and the nitracline (22m) that was significant within the resolution of nutrient sampling.

**Table 2.2.** Abundance, integrated production and settling flux estimates from each sampling location. Included are the alkenone-related properties: 24-hour K37 100m sediment trap flux ($F_{K37}$; Section 2.2.3), integrated K37:2 and estimated total K37 production ($\int PR_{K37:2}$ and $\int PR_{K37}$; Section 2.2.5), and calculated K37 export efficiency. Also shown are estimated alkenone-producing cell production rates ($\int PR_{cocco}$; Section 2.4.1) and estimated cell flux ($F_{cocco}$; Section 2.4.3). For context, integrated net primary production ($\int NPP$), POC flux, and POC export efficiency (from White et al. 2013; Appendix A) are

**Table 2.2.** Integrated Properties

| Station | Integration Depth | $\int PR_{K37:2}$ | | $\int PR_{K37}$ | | $F_{K37}$ | | K37 Export Efficiency | | $\int NPP$ | | $F_{POC}$ | | POC Export Efficiency | | $\int PR_{cocco}$ | | $F_{cocco}$ | |
|---|---|---|---|---|---|---|---|---|---|---|---|---|---|---|---|---|---|---|---|
| | (m) | ($\mu g\ m^{-2}\ d^{-1}$) | ± | ($\mu g\ m^{-2}\ d^{-1}$) | ± | ($\mu g\ m^{-2}\ d^{-1}$) | ± | (%) | ± | ($mg\ m^{-2}\ d^{-1}$) | ± | ($mg\ m^{-2}\ d^{-1}$) | ± | (%) | ± | ($cs\ m^{-2}\ d^{-1} x10^{9}$) | ± | ($cs\ m^{-2}\ d^{-1} x10^{9}$) | ± |
| *Gulf of California* | | | | | | | | | | | | | | | | | | | |
| 1-1 | 35 | 64 | 7 | 67 | 7 | 15 | 2 | 23 | 3 | 1481 | 148 | 184 | 19 | 12 | 2 | 0.15 | 0.05 | 0.03 | 0.01 |
| 3-1 | 40 | 320 | 33 | 323 | 33 | 80 | 8 | 25 | 4 | 537 | 52 | 228 | 13 | 42 | 5 | 0.24 | 0.05 | 0.06 | 0.01 |
| 3-2 | 32 | 43 | 5 | 46 | 5 | 32 | 3 | 70 | 10 | 545 | 84 | 206 | 13 | 38 | 6 | 0.14 | 0.03 | 0.10 | 0.02 |
| 3-3 | 40 | 140 | 14 | 147 | 15 | 19 | 2 | 13 | 2 | 500 | 228 | 150 | 18 | 30 | 14 | 0.16 | 0.03 | 0.021 | 0.005 |
| 3-4 | 39 | 191 | 20 | 193 | 20 | 27 | 3 | 14 | 2 | 797 | 73 | 138 | 12 | 17 | 2 | 0.16 | 0.03 | 0.02 | 0.01 |
| 4-1 | 45 | 375 | 40 | 411 | 45 | 22 | 2 | 5 | 1 | 893 | 141 | 216 | 22 | 24 | 5 | 0.46 | 0.06 | 0.024 | 0.005 |
| 4-2a | 39 | 125 | 13 | 126 | 13 | 36 | 4 | 29 | 4 | 461 | 40 | 322 | 32 | 70 | 9 | 0.45 | 0.06 | 0.13 | 0.03 |
| 4-2b | 43 | - | | - | | 39 | 4 | - | | 365 | 37 | 264 | 27 | 72 | 10 | - | | - | |
| *Entrance Zone* | | | | | | | | | | | | | | | | | | | |
| 4-8 | 41 | 196 | 21 | 200 | 21 | 57 | 6 | 28 | 4 | 365 | 42 | 336 | 33 | 92 | 14 | 0.23 | 0.03 | 0.07 | 0.01 |
| 4-9 | 43 | - | | - | | 22 | 2 | - | | 304 | 55 | 138 | 14 | 45 | 9 | - | | - | |
| *Eastern Tropical North Pacific* | | | | | | | | | | | | | | | | | | | |
| 4-10 | 57 | - | | - | | 103 | 11 | - | | 533 | 53 | 209 | 21 | 39 | 6 | - | | - | |
| 4-11 | 67 | - | | - | | 23 | 2 | - | | 393 | 51 | 175 | 17 | 44 | 7 | - | | - | |
| 4-12 | 60 | 182 | 21 | 338 | 45 | 60 | 6 | 18 | 3 | 1269 | 89 | 253 | 25 | 20 | 2 | 0.56 | 0.08 | 0.10 | 0.02 |

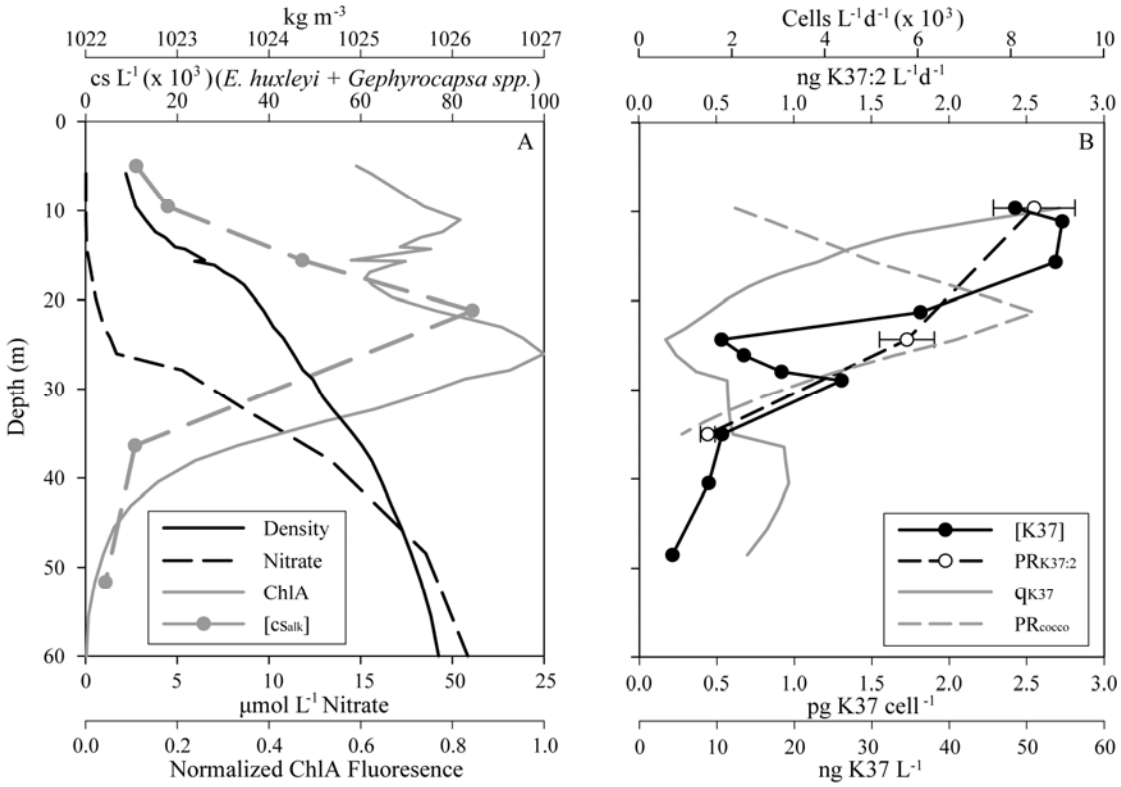


**Figure 2.2. A)** Alkenone-producing cell abundance ([$cs_{alk}$]) and relative ChlA fluorescence (fluorescence:maximum fluorescence) profiles for the 2004 GC station 1-1, compared to the nitracline and the density profile. **B)** K37 abundance ([K37]) and K37 production rates ($PR_{K37}$, Equation 2.2.9) measured at this station. These are compared to the estimated alkenone-producing cell production profile ($PR_{cocco}$, Equation 2.4.1) and estimated profile of K37 cell quotas $q_{K37}$ (see section 2.4.1). Error bars have been omitted from all but $PR_{K37}$ for clarity; see Appendix A for uncertainty estimates.

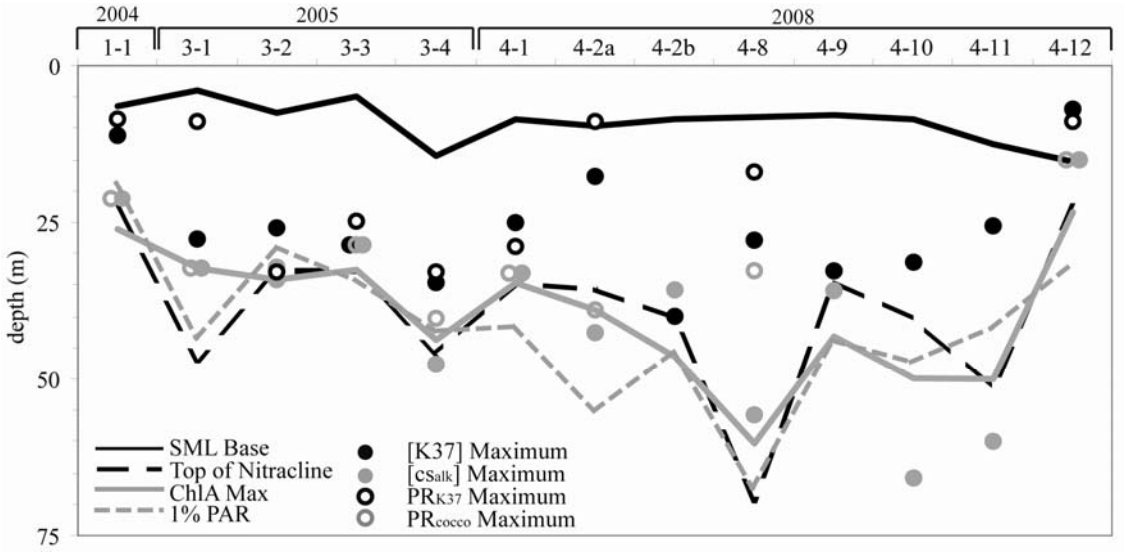


**Figure 2.3.** Depth of the [K37] and $PR_{K37}$ (Equation 2.2.8) maxima for each station, compared to the depths of the base of the mixed layer (Section 2.3.1), the top of the nitracline, the 1% light level, and DCML (from White et al. 2013), and the *E. huxleyi* + Gephyrocapsa cell density maximum (from Malinverno et al. 2008; Anaid Rosas-Navarro, personal communication). Scaling the cell density profiles by alkenone turnover rate (Equation 2.4.1) generates maxima of $PR_{cocco}$. Note that at station 3-2 the maximum values of $PR_{K37}$ and $PR_{cocco}$ occur at the deepest incubation depth (see Figure 2.4), and thus the indicated depth is a minimum estimate for the feature.

2.3.2 Alkenone Stocks, Production, and Export Rates

Alkenone concentration profiles generally exhibited low values in the SML and a shallow subsurface maximum (see Appendix A). The exception to this pattern was 4-12, the northernmost ETNP site, where [K37] decreased monotonically with depth from a maximum in the SML. For all other sites, [K37] ranged from ~0 to 60 ng $L^{-1}$ in the SML and from ~10 to 140 ng $L^{-1}$ at the subsurface maximum. To the extent that sampling density allowed resolution of the two features, [K37] profiles displayed maxima that were ~4 to 32m shallower (mean: 14m; Figure 2.3) than the [ChlA] maxima described by White et al. (2007, 2013; Appendix A).

Similar to depth profiles of [K37], $PR_{K37}$ profiles (Figure 2.4) showed distinct subsurface features in most years and locations, with values typically maximizing between the nitracline and the SML (Figure 2.3). In 2005, subsurface peaks in both standing stock and production rates were observed at all sites, though these maxima occurred at different depths (Figure 2.3). Site 3-2 was unique, displaying $PR_{K37}$ enhancement near the surface that was not reflected by [K37]. Although $PR_{K37}$ profiles are only available for a subset of the 2008 stations (4-1, 4-2a, 4-8 and 4-12), the same pattern is evident. Over all occupations, depth-integrated alkenone production rates ($\int PR_{K37}$) derived from these profiles ranged from 46 to 411 μg $m^{-2}$ $d^{-1}$ (Table 2.2). The highest rates were estimated at sites displaying both high and low depth-integrated NPP ($\int NPP$, White et al. 2013; Table 2.2), e.g. 4-12 in the ETNP (high) and 3-1 and 4-1 in the GC (low).

K37 export rates assessed by sediment trap ranged from ~15 to 80 μg $m^{-2}$ $d^{-1}$ for sites with corresponding production rate measurements, a magnitude of variation similar to that observed for $\int PR_{K37}$ (Table 2.2). This co-variation resulted in a narrow range of export efficiency estimates (5-29%, Figure 2.5A). Site 3-2 was an exception, displaying an export efficiency of 70%. However, the deepest incubation depth at this station exhibited the highest K37 production rate measurement, coincident with the DCML (34m, Figure 2.4). Thus, $\int PR_{K37}$ is likely underestimated here, artificially inflating the estimate of biomarker export efficiency.

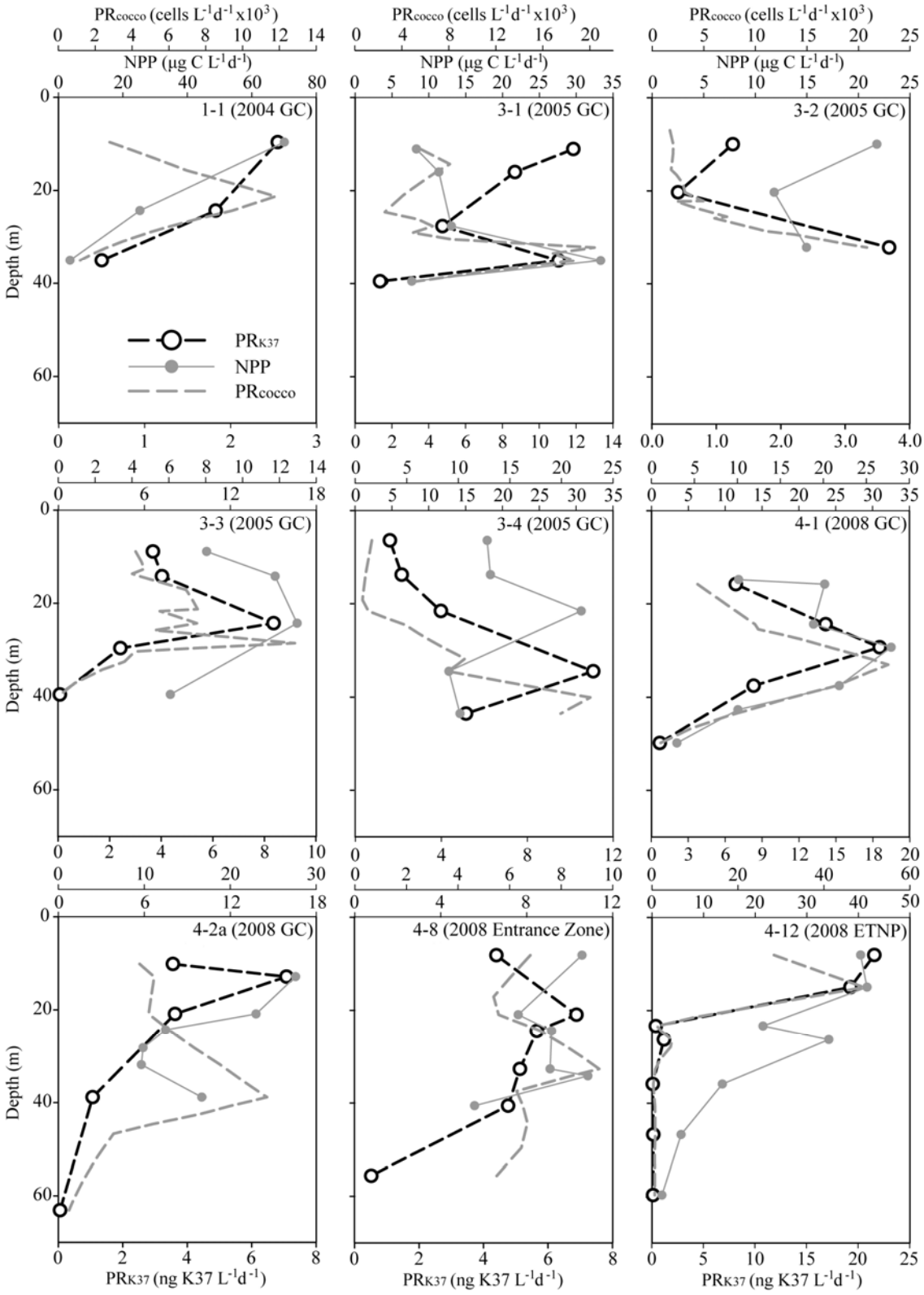
PRcocco (cells L-1d-1 x103)
NPP (µg C L-1d-1)
Depth (m)
1-1 (2004 GC)
3-1 (2005 GC)
3-2 (2005 GC)
3-3 (2005 GC)
3-4 (2005 GC)
4-1 (2008 GC)
4-2a (2008 GC)
4-8 (2008 Entrance Zone)
4-12 (2008 ETNP)
PRK37
NPP
PRcocco
PRK37 (ng K37 L-1d-1)

**Figure 2.4.** Profiles of $PR_{K37}$ (Equation 2.2.7) from *in situ* incubation arrays, compared to calculated profiles of $PR_{cocco}$ (Equation 2.4.1) and NPP (from White et al. 2013). Note that alkenone production rates are only available for a subset of the 2008 stations. Error bars have been omitted for clarity; see Appendix A for uncertainty estimates.

## 2.4. Discussion:

### 2.4.1 Alkenones as a Proxy for Coccolithophorids

Alkenones provide a tool for both measuring coccolithophorid-specific production and estimating coccolithophorid sinking flux in settings with low relative coccolithophorid abundance. These biomarkers are not, however, ubiquitous in coccolithophorids, nor do they constitute a constant proportion of biomass in the species which produce them (Conte et al. 1998; Prahl et al. 2003). Care must be taken, then, when relating [K37], $PR_{K37}$, and $F_{K37}$, which are representative of the activity of a limited number of alkenone-producing species, to overall coccolithophorid abundance, production rate, and export, respectively.

First, we must evaluate the degree to which alkenone producers are representative of the bulk coccolithophorid assemblage. Alkenone producers *E. huxleyi* and Gephyrocapsa *spp.* (includes *oceanica*, *muellerae*, *ericsonii*, and *ornata*) are the dominant coccolithophorids observed in these occupations, constituting 71 ± 12% of the integrated cell inventory (Malinverno et al. 2008; Anaid Rosas-Navarro, personal communication; Appendix A). These combined species ($cs_{alk}$) have previously been noted to be the dominant contributors to coccolith flux in the Guaymas Basin (Ziveri and Thunell 2000). Even at station 4-9, which possessed the lowest percentage of alkenone-producing coccolithophorids (53% on a depth-integrated basis; Anaid Rosas-Navarro, personal communication), the depth profile of $cs_{alk}$ abundance ([$cs_{alk}$]) was similar to the profile of total coccosphere abundance ($R^2$ value of 0.88 for the two profiles). Thus, we consider alkenone producing coccolithophorids in this setting to be reliable proxies for coccolithophorids as a whole.

Second, we must evaluate how well alkenones quantitatively represent these coccolithophorid species. While the sampling resolution of the two measures is low, the maximum of a given [K37] profile typically appears shallower than that of the corresponding [$cs_{alk}$] profile (Figure 2.3). Malinverno et al. (2008) provide evidence that per-cell K37 quotas ($q_{K37}$) were variable at the GC sites in 2004 and 2005, spanning a range from ~0.25 to 2 pg cell$^{-1}$. We have re-evaluated these data using our density binning scheme (Section 2.2.2) and extended the analysis to the 2008 stations. The

resulting estimated $q_{K37}$ profiles (e.g. Figure 2.2B) generally show higher values above the nitracline than below (see Appendix A for remaining profiles). The presence of higher $q_{K37}$ values near the surface is consistent with previously-documented increases in alkenone cell quota associated with nutrient deprivation (e.g. Prahl et al. 2003). The range of values we estimate (~0.1 to 3 pg cell$^{-1}$) is similar to that reported for these species in culture (Conte et al. 1998; Epstein et al. 2001; Prahl et al. 2003).

As estimated $q_{K37}$ values appear to vary in a manner consistent with nutrient conditions, the presence of non-calcifying alkenone producers (not detectable by the microscopic techniques of Malinverno et al. and Rosas-Navarro; de Vargas and Probert 2004) is not required to explain the biomarker abundance data. However, variability in $q_{K37}$ means that $PR_{K37}$ alone can not describe coccolithophorid production. One way to account for this variability is to assume $q_{K37}$ was constant at a given location and depth over the timescale of our incubations. An estimate of cellular production rate (cells L$^{-1}$ d$^{-1}$) can then be provided by dividing $PR_{K37}$ by $q_{K37}$ estimated at the same depth. Substituting the expression for $PR_{K37:2}$ (Equation 2.2.2) into equation 2.9 and dividing the result by $q_{K37}$ yields:

$$PR_{cocco} = \frac{PR_{K37}}{q_{K37}} = \frac{[cs_{alk}]}{[K37]} * \frac{[K37:2] * TR_{K37:2}}{U_{37}^{K'}} = [cs_{alk}] * TR_{K37:2} \qquad \textbf{2.4.1}$$

This estimated rate provides no information about the potentially variable per-cell production of organic or inorganic carbon biomass. Nonetheless, comparing these cellular production rates to NPP and other environmental parameters should reveal trends that are more ecologically meaningful than is possible using biomarker production data alone. The resulting $PR_{cocco}$ profiles are shown in Figure 2.4 (tabulated in Appendix A) and depth-integrated values, $\int PR_{cocco}$, are given in Table 2.2.

### 2.4.2 Patterns of Alkenone Production

Overall, depth profiles of alkenone production ($PR_{K37}$) and estimated coccolithophorid cell production ($PR_{cocco}$) appear to follow the NPP patterns reported by White et al. (2013). $PR_{K37}$ estimates show enhancements both near the surface and in subsurface maxima that are coincident with high NPP (Figure 2.4). Only at station 3-1 is

$PR_{K37}$ elevated at a depth where NPP is relatively low. Given the low nitrate half-saturation constants of coccolithophorids and the traditional view that they are 'low nutrient' specialists (e.g. Litchman et al. 2007), it is expected that coccolithophorids would thrive at shallower depths than the bulk phytoplankton community. Thus, the absence of $PR_{K37}$ maxima at depths shallower than the NPP maxima is surprising. $PR_{K37}$ profiles appear to deviate even further from the expectation of shallow enrichments when $PR_{cocco}$ is used to account for higher $q_{K37}$ values near the surface. Maxima in $PR_{cocco}$ occur deeper than the corresponding maxima in $PR_{K37}$ wherever definable (all sites but 3-2; Figure 2.4). Furthermore, at some sites (e.g. 1-1; Figure 2.2B), the subsurface maximum in $PR_{cocco}$ is significantly more pronounced than that of $PR_{K37}$. On average, maxima in estimated cell growth occur ~5m above the nitracline. The one exception is Site 4-8, where the nitracline was exceptionally deep (Figure 2.3). These observations suggest that coccolithophorid production is tightly coupled to the nitracline in our study area.

On a depth-integrated basis, alkenone production ($\int PR_{K37}$) appears decoupled ($R^2$ = 0.01) from bulk primary productivity ($\int NPP$). Given the presumed 'oligotrophic niche' of coccolithophorids, the ratio of $\int PR_{K37}$:$\int NPP$ may be expected to vary with nutrient availability in the euphotic zone, rather than these two production rates co-varying directly. Nitrate concentrations are meaningless as a basis for comparison in this case, as they are generally either analytically zero above the nitracline or well in excess of the half-saturation range for coccolithophorids (~0.45 μmol $L^{-1}$ for *E. huxleyi*; Riegman et al. 2000) below it (e.g. Figure 2.2; Appendix A). If, starting at the base of the SML, the nitracline is driven deeper with time after a mixing event, a meaningful measure of the 'degree' of nitrate drawdown at a site may be the amount of the nitrate-depleted euphotic zone below the SML. For stations 3-3 and 4-1, -2, -10, and -12, where the nitracline lies above the maximum euphotic depth (taken as the 1% light level; Table 2.1), this quantity is defined by the distance ($Z_d$) between the top of the nitracline and the base of the SML. For stations 3-1, -2, -4 and 4-8, -9, and -11 where the 1% light level lies above the nitracline (Table 2.1), $Z_d$ is approximated by the depth difference between the 1% light level and the base of the SML. This 'drawdown depth', $Z_d$, correlates

positively with the ratio of $\int PR_{K37}$:$\int NPP$ ($R^2$ = 0.68, Figure 2.6A). This relationship implies higher relative importance of alkenone production at sites with more complete nutrient removal from the euphotic zone, consistent with observations from open-ocean settings relating coccolithophorid:diatom abundance to nitracline depth (Cermeño et al. 2008).

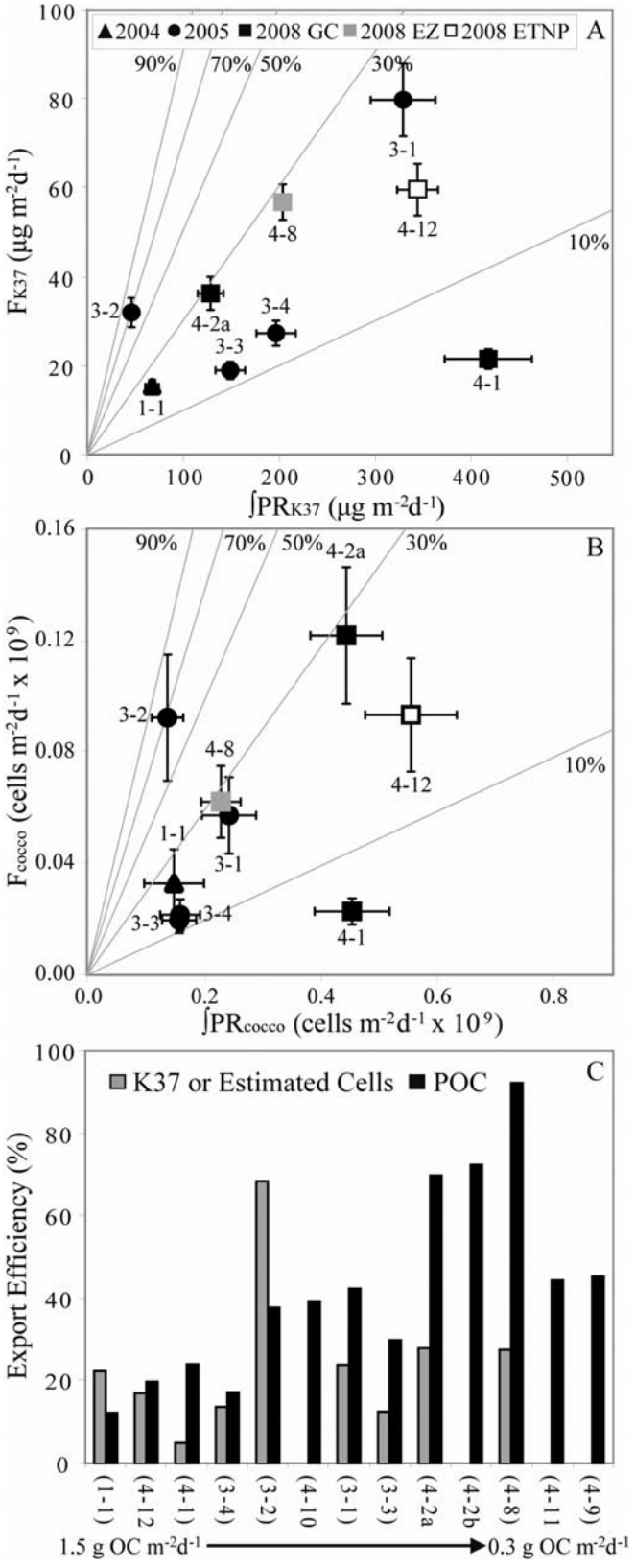
A
2004 2005 2008 GC 2008 EZ 2008 ETNP
90%
70%
50%
30%
10%
3-1
4-12
4-8
3-2
4-2a
3-4
3-3
4-1
1-1
$F_{K37}$ (µg m$^{-2}$d$^{-1}$)
$\int PR_{K37}$ (µg m$^{-2}$d$^{-1}$)
B
90%
70%
50%
4-2a
30%
10%
3-2
4-8
4-12
1-1
3-1
3-3
3-4
4-1
$F_{cocco}$ (cells m$^{-2}$d$^{-1}$ x 10$^9$)
$\int PR_{cocco}$ (cells m$^{-2}$d$^{-1}$ x 10$^9$)
C
K37 or Estimated Cells
POC
Export Efficiency (%)
(1-1)
(4-12
(4-1)
(3-4)
(3-2)
(4-10
(3-1)
(3-3)
(4-2a
(4-2b
(4-8)
(4-11
(4-9)
1.5 g OC m$^{-2}$d$^{-1}$
0.3 g OC m$^{-2}$d$^{-1}$

**Figure 2.5. A)** Sediment trap-derived flux measurements ($F_{K37}$) and depth-integrated production rate estimates ($\int PR_{K37}$, Equation 2.2.7 summed over all density bins) for K37 alkenones. Contours denote export efficiency, $F_{K37}$:$\int PR_{K37}$. Export rates for stations without corresponding $\int PR_{K37}$ measurements are reported in Table 2.2. **B)** The analogous plot of $F_{cocco}$ (Equation 2.4.2) and $\int PR_{cocco}$ (Equation 2.4.1 summed over all density bins). **C)** Comparison of export efficiencies for K37 and POC, where the sites have been ordered from highest to lowest integrated NPP.

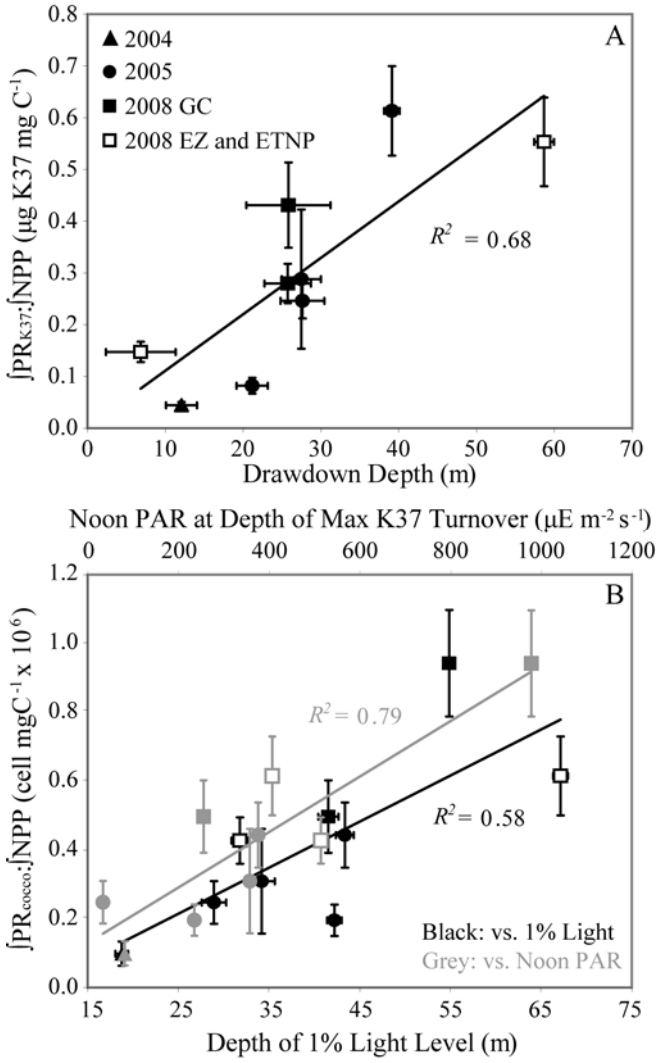


**Figure 2.6. A)** The positive relationship between the production ratio $\int PR_{K37}:\int NPP$ and nitrate 'drawdown depth' $Z_d$ (depth of nitrate-limited euphotic zone beneath the mixed layer, see section 2.4.2). **B)** The positive relationships between the estimated ratio $\int PR_{cocco}:\int NPP$ and the depth of the 1% light level (black) and the noon PAR at the most productive *in situ* incubation depth (grey).

However, if coccolithophorid cell growth is tied to the nitracline in this setting, then there is no *a priori* reason why coccolithophorid production:bulk production should increase with vertically-increasing nutrient depletion. Comparing $\int PR_{cocco}$ to $\int NPP$, and thus adjusting for $PR_{K37}$'s 'overrepresentation' of coccolithophorid production at shallow depths by taking variable $q_{K37}$ into account (Equation 2.4.1; Figure 2.4), reveals no trend relative to $Z_d$ ($\int PR_{cocco}$:$\int NPP$ vs. $Z_d$, $R^2 = 0.13$). Likewise, no significant relationship is observed between this 'adjusted' production ratio and any of the following parameters that could serve as indicators of nitrate availability to the euphotic zone: nitracline depth, SML depth, average nitrate concentration or nitrate inventory above the 1% light level, or the nitrate gradient at the base of the euphotic zone.

If $\int PR_{cocco}$:$\int NPP$ does not vary with nutrient conditions, it suggests that a fundamentally different coccolithophorid succession/niche dynamic may operate in our study area than in other oceanographic settings dominated by mixing-induced blooms. In the latter case, nutrients may be taken up by larger, faster growing taxa until they are reduced to a point where coccolithophorids are ecologically favored. For example, Iglesias-Rodríguez et al. (2002) relate coccolithophorid blooms specifically to areas of temporally decreasing surface nitrate. In settings like the summertime GC, concentrations of the limiting macronutrient (nitrate in this case) are consistently below analytical detection limits above a persistent nutricline. Thus, the presumably low frequency of disturbance may only allow for niche differentiation with depth, and not with time. At all stations besides 4-12, the phytoplankton groups that vary in abundance with nutrient conditions appear to be pico-plankton (predominantly cyanobacteria) above the nitracline and micro-plankton (predominately diatoms) below (White et al. 2013). At these sites, waters above and below the sharp nutricline may be too infertile and too nutrient-replete, respectively, for coccolithophorids (or nano-plankton in general) to have a competitive advantage anywhere in the euphotic zone. Assuming this paradigm is appropriate, removal of a 'mid-low nutrient niche' in extremely stratified conditions may explain the low relative coccolithophorid abundance (Malinverno et al. 2008) in the summertime GC relative to more open-ocean sites (e.g. Cermeño et al 2008; see Section 2.1).

In our study area, light penetration, rather than the dynamics of nutrient supply, appears to be the factor controlling relative coccolithophorid production. The only properties of water column structure that correlate clearly with $\int PR_{cocco}$:$\int NPP$ are the depth of the 1% light level ($R^2 = 0.58$) and PAR at the depth of the $PR_{K37}$ maximum ($R^2 = 0.79$; Figure 2.6B). As $PR_{cocco}$ is generally highest at light-limited, rather than nitrate-limited depths (i.e. associated with the DCML), it follows that the production ratio $\int PR_{cocco}$:$\int NPP$ would respond to how well this narrow zone of $cs_{alk}$ productivity is illuminated. The consequences of this relationship are discussed further in Section 2.4.4.

2.4.3 Relative Contribution to Export

In our study area, there appears to be a decoupling of the export efficiencies of bulk carbon production and of the coccolithophorid component. While alkenone export efficiency ranges from 5-29% (disregarding Station 3-2, see 2.3.2), the export efficiency of bulk POC is far more variable (12-92%), with the highest POC export efficiency typically occurring at the sites with the lowest integrated POC production rates (Figure 2.5C). White et al. (2013) suggest that pico-plankton support higher, aggregation-driven export efficiencies in the GC, and that these plankton dominate the community at the sites with the lowest $\int NPP$ (i.e. 4-2, -8, -9). This provides a mechanism by which the most effective bulk carbon export may occur at the least productive sites. Conversely, the lower and more constant efficiency of alkenone export suggests a distinct mode of export for coccolithophorids/nano-plankton, such as a separate grazer community or aggregation mechanism (e.g. Burd and Jackson, 2009). Regardless of mechanism, alkenones appear to less effectively exported, and therefore presumably more strongly recycled, than bulk POC at most of the sites for which measurements of both processes are available.

The decreased POC export efficiency at the more productive stations precludes the expected, proportional relationship between POC:alkenone production rates and POC:alkenone export rates. The ratio of $F_{K37}$ to $F_{POC}$ (POC values from White et al. 2013) at 100m, in fact, shows no apparent relationship with $\int PR_{K37}$:$\int NPP$ ($R^2 = 0.27$). To determine if this decoupling between alkenone:POC production ratios and export ratios

extends to the 'adjusted' production estimate $\int PR_{cocco}$, we must estimate 'cell flux', $F_{cocco}$. Assuming that coccolithophorid cells and alkenone biomarkers are exported proportionately to their integrated production rates, then:

$$F_{cocco} = F_{K37} \frac{\int PR_{cocco}}{\int PR_{K37}} \qquad \textbf{2.4.2}$$

By definition, the export efficiency calculated from $F_{cocco}$ and $\int PR_{cocco}$ is identical to the efficiency derived directly from alkenone measurements, as this formulation demands that the two components have identical flux attenuation. These cell fluxes (0.02 to 0.13 cells $m^{-2}$ $d^{-1}$ x $10^9$) and integrated production rates, however, vary site to site quite differently than alkenone fluxes and production rates (Figure 2.5B). While $F_{K37}$:$F_{POC}$ showed only weak correlation with $\int PR_{K37}$:$\int NPP$, no correlation at all is apparent between $F_{cocco}$:$F_{POC}$ and the corresponding production ratio $\int PR_{cocco}$:$\int NPP$ ($R^2$ = 0.0). Thus, while systematic trends are evident in the relative contribution of coccolithophorids to carbon production ($\int PR_{K37}$:$\int NPP$ vs. $Z_d$ or $\int PR_{cocco}$:$\int NPP$ vs. PAR, Section 2.4.2), these trends do not appear to extend to the relative contribution of coccolithophorids to bulk carbon flux.

Given estimates of export rates for coccolithophorid cells, our results can be compared to existing coccolith flux data. Assuming a PIC content of 1.25 pmols $cell^{-1}$ (based on ~15 pg OC $cell^{-1}$ and a ~1:1 $CaCO_3$:OC ratio; Fernández et al. 1996; Sciandra et al. 2003; Leonardos and Geider 2005), our export rate estimates yield a coccolith PIC flux at 100m depth ranging from ~0.3 to 1.8 mg $m^{-2}$ $day^{-1}$. These estimates are of a similar magnitude to measures of coccolith calcite flux at 500m depth (0.14-9.08 mg $m^{-2}$ $day^{-1}$) in the Carmen (1990) and Guaymas (1991-1992) Basins (Ziveri and Thunell 2000). In addition to inter-annual variability in production, the lower range of our estimates is likely due at least in part to our method accounting only for alkenone-producing species.

### 2.4.4 Summary and Implications for PIC/POC Export Ratios

In our study area, we have determined that:

1) the highest coccolithophorid biomarker or estimated cell production rates are associated with a nitracline dominated by micro-plankton rather than a nutrient-depleted, upper euphotic zone dominated by pico-plankton;
2) integrated estimated coccolithophorid cell production varies, relative to integrated NPP, in response to light availability at depth as opposed to nutrient depletion; and
3) the contribution of alkenones and estimated coccolithophorid biomass to export, relative to bulk POC, is driven by POC export efficiency and not by the relative production rates of the coccolithophorid and bulk components.

We can now describe, in simplified form, the system that we hypothesize to account for these observations and determine the implications of such a system for the PIC dynamics of our study area and similar locations. For the general case of a 'GC-like' euphotic zone, we assume a two layer system: (1) a nutrient-limited surface layer extending to the nutricline and (2) a light-limited region between the nutricline and the base of the euphotic zone (e.g. Coale and Bruland 1987; Small et al. 1987). We then assume that only pico-plankton can survive in the upper layer on a fixed diffusive, regenerative, or aeolian input of the limiting nutrient. Conversely, only micro-plankton and nano-plankton (i.e. coccolithophorids) are assumed to be competitively relevant in the lower layer (Figure 2.7A). As the water column warms, stability increases and the nutricline deepens. This increases the thickness of the upper layer, but reduces the volume-specific availability of its limited nutrient sources. Consequently, the volume-specific production rate and standing stock of phytoplankton is reduced, allowing more light to penetrate (per unit depth) through the layer. The result is constant integrated carbon fixation in the upper layer, and, assuming no change in the surface irradiance, co-variation of the nutricline and euphotic depth. As the lower layer is still nutrient-replete and receives the same downwelling irradiance through a thicker-but-clearer upper water column, micro- and nano-plankton production rates are also relatively unchanged. The ratio of nano-plankton production to bulk community photosynthetic rates is thus unaffected by nutricline depth.

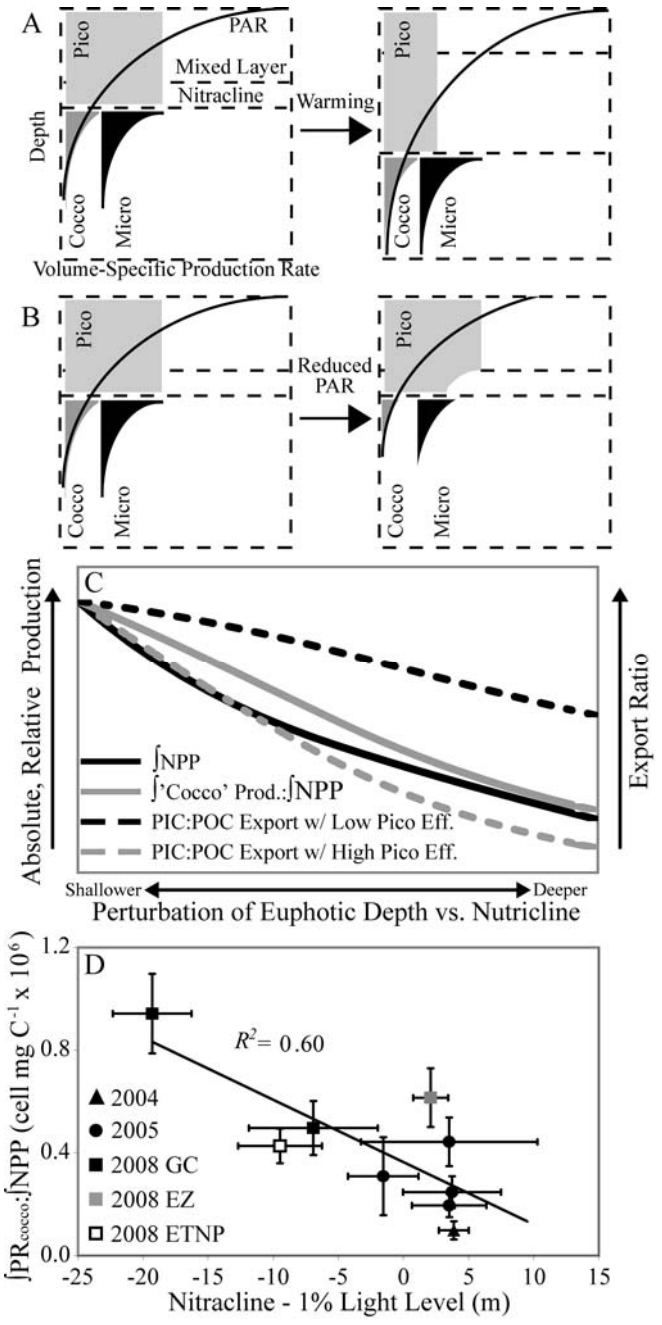
A
Pico
PAR
Mixed Layer
Nitracline
Depth
Cocco
Micro
Warming
Volume-Specific Production Rate
B
Reduced PAR
C
Absolute, Relative Production
Export Ratio
∫NPP
∫'Cocco' Prod.:∫NPP
PIC:POC Export w/ Low Pico Eff.
PIC:POC Export w/ High Pico Eff.
Shallower
Deeper
Perturbation of Euphotic Depth vs. Nutricline
D
$R^2$= 0.60
2004
2005
2008 GC
2008 EZ
2008 ETNP
∫PR$_{cocco}$:∫NPP (cell mg C$^{-1}$ x 10$^6$)
Nitracline - 1% Light Level (m)

**Figure 2.7.** Schematic of the structure and dynamics of an idealized euphotic zone in the summertime Gulf of California. The upper panels (**A**) illustrate how relative production rates of different phytoplankton size classes (distributed as per Section 2.4.4) are insensitive to changes in nutricline depth, as compensating changes occur to the light field. The shaded areas labeled 'pico' 'micro' and 'nano' denote depth profiles of these size classes' respective volume-specific production rates. A decrease in the light field that is independent of nutricline movement (**B**) reduces production in the lower layer (micro- and nano-plankton) more than it does that in the upper layer (pico-plankton), thereby changing production ratios. Panel **C** illustrates the shifts in NPP and relative nano-plankton production (where nano-plankton ≈ coccolithophorids for our purposes) that occur in response to positive and negative perturbations of the euphotic depth relative to the nitracline. The PIC:POC export ratios that result from these perturbations are also shown, where pico-plankton export efficiency is either 0.5x (black) or 2x (grey) that of nano-plankton. All curves are plotted as normalized values. The bottom panel (**D**) compares the estimated values of $\int PR_{cocco}$:$\int NPP$ at our study locations to nitracline depth minus the 1% light level, and shows a similar decreasing trend.

Now, let us decouple the euphotic depth from the nutricline (Figure 2.7B). Decoupling can occur for a variety of reasons, such as a reduction in surface irradiance (to which the nutricline cannot adjust due to stratification) or changes in light attenuation due to altered allochthonous particle input. A decoupled nutricline and euphotic depth allows for construction of a more specific case to explain our short-timescale Gulf of California data. For a given nutricline depth, decreasing the euphotic depth has little effect on the upper layer, as most of its extent will still be nutrient-limited. In the lower, light-limited layer, however, both micro- and nano-plankton will produce at lower rates, reducing the depth-integrated ratio of nano-plankton production to bulk production (Figure 2.7C). Over time, diffusion of the limiting nutrient into the newly-darkened portion of the water column will return the system to the general, coupled case described above. An increase in the euphotic depth also has no effect on the upper layer, as it remains nutrient-limited. Production in the lower layer will increase, however, elevating the ratio of integrated nano-plankton:bulk photosynthetic rates. In this instance, the system will eventually be returned to the coupled case by nutrient consumption in the newly-lit zone.

If upward and downward perturbations of the euphotic depth are uncorrelated with the depth of the nutricline, then relative integrated production rates will not correlate with nitracline depth. They will correlate, however, with measures of how well the lower layer is illuminated, as suggested by our data (Figure 2.6). In the proposed model, the factor controlling relative production rates in settings like the GC is the depth offset between the base of the euphotic zone and the top of the nitracline (Figure 2.7C). Our field data tentatively show the predicted negative relationship (Figure 2.7D).

Apart from changes that may be induced in the composition of the nano-plankton community itself, the overall effect of this proposed euphotic zone dynamic on PIC:POC export will be to decouple variation in this ratio from stratification. On long time scales, PIC:POC production will remain constant with respect to increased stratification and nutrient drawdown, weakening or removing any nutricline-driven feedback of coccolithophorid production (positive or negative) on atmospheric $pCO_2$. In this case, export ratios would depend on other factors that control relative production, such as

altered calcification rates (Zondervan et al. 2007; Langer et al. 2011), or that alter flux attenuation of the two components (Helmke et al. 2010). On shorter time scales, if decoupling of the light and nutrient fields alters the ratio of PIC to POC production, the effect on export will be modulated by the relative export efficiencies of nano-plankton/coccolithophorids and pico-plankton (Figure 2.7C). If a mechanism by which pico-plankton express proportionally more efficient export is present, as is now suggested for the Gulf of California (White et al. 2013) and several of other oceanographic settings (Richardson and Jackson 2007; Lomas and Moran 2011), PIC:POC export will vary more strongly with the light perturbation than otherwise.

## 2.5. Conclusions:

Our study posed two primary questions: Is coccolithophorid production enhanced under stratified, nutrient-depleted conditions in our study area? If so, does the enhancement alter the contribution to particle export? The results of our novel, biomarker-specific isotope incubation techniques have provided the following three responses, which illustrate a potential for coccolithophorids to lose their mid-to-low nutrient niche in areas of sharp, persistent nutrient gradients such as the highly stratified summertime Gulf of California:

1) Production of alkenone biomarkers is a more important component of overall carbon fixation under more nutrient-stratified conditions in this study area. However, this pattern appears indicative of cellular biomarker quotas that vary with nutrient availability rather than of greater coccolithophorid production, relative to other taxa, at lower-nutrient sites.
2) Depth integrated estimates of production rates for coccolithophorid cells, relative to bulk carbon fixation, do not vary with nutrient conditions. A simple model can be formulated in which relative coccolithophorid:bulk production in strongly stratified settings is altered when changes in illumination below the nutricline are decoupled from the depth of the nitracline itself. We propose that these shifts impact the relative production rates of a pico-plankton dominated upper layer and a coccolithophorid-containing lower layer.

3) Patterns in alkenone:carbon production or estimated coccolithophorid cell:carbon production do not parallel patterns in alkenone:POC export or estimated coccolithophorid cell:POC export. We suggest that this decoupling is due to large variations in the export efficiency of bulk organic carbon paired with low variation in the export efficiency of the much-less-significant alkenone-producing component.

These observations have ramifications for warming/$pCO_2$ feedback. In more common, open ocean settings where phytoplankton succession and/or biogeography is currently controlled by mixing, warming-driven decreases in surface-ocean nutrients (resulting in enhanced relative coccolithophorid production, and thus enhanced PIC:POC export ratios) may yield a positive feedback on atmospheric $pCO_2$ (e.g. Cermeño et al. 2008). However, our work in the GC suggests that a threshold of temporal stability exists beyond which the euphotic zone becomes much less favorable for coccolithophorid production. Initially, this response would represent a negative feedback on warming-driven stratification. Beyond this threshold, however, if nutricline depth no longer controls relative coccolithophorid production (point 2 above), but rather shifts production between larger or smaller plankton classes, no mixing-modulated feedback on PIC:POC ratios would result. The warm, enclosed GC is an atypical region relative to the modern open ocean. However, the appearance of similar alkenone production patterns with depth at sites in the entrance zone and the adjacent ETNP suggests that expansion of such environments in a warmer, future ocean may favor an increase in these coccolithophorid dynamics.

## 2.6. References:


Balch W.M. and Utgoff P.E. (2009) Potential interactions among ocean acidification, coccolithophores, and the optical properties of seawater. *Oceanogr.* **22**, 146-159.

Baumann K.-H., Backel B. and Frenz M. (2004) Coccolith contribution to South Atlantic carbonate sedimentation, p. 368-402. *In* H.R. Thierstein and J.R. Young [eds.], *Coccolithophores*. Springer.

Beaufort L., Probert I., de Garidel-Thoron T., Bendif E.M., Ruiz-Pino D., Metzl N., Goyet C., Buchet N., Coupel P., Grelaud M., Rost B., Rickaby R.E.M. and de Vargas C. (2011) Sensitivity of coccolithophores to carbonate chemistry and ocean acidification. *Nature* **476**, 80-83.

Brown C.W. and Yoder J.A. (1994) Coccolithophorid blooms in the global ocean. *J. Geophys. Res.* **99,** 7467-7482.

Buesseler K.O., Antia A.N., Chen M., Fowler S.W., Gardner W.D., Gustafsson O., Harada K., Michaels A.F., van der Loeff M.R., Sarin M., Steinberg D.K. and Trull T. (2007) An assessment of the use of sediment traps for estimating upper ocean particle fluxes. *J. Mar. Res.* **65,** 345-416.

Burd A.B. and Jackson G.A. (2009) Particle aggregation. *Annu. Rev. Mar. Sci.* **1**, 65-90.

Cermeño P., Dutkiewicz S., Harris R.P., Follows M., Schofield O. and Falkowski P.G. (2008) The role of nutricline depth in regulating the ocean carbon cycle. *P. Natl. Acad. Sci. USA* **105**, 20344-20349.

Christie W. W. (2003) *Lipid Analysis: Isolation, Separation, Identification and Structural Analysis of Lipids*. The Oily Press.

Coale K.H. and Bruland K.W. (1987) Oceanic stratified euphotic zone as elucidated by $^{234}$Th:$^{238}$U disequilibria. *Limnol. Oceanogr.* **32**, 189-200.

Conte M.H., Thompson A., Lesley D. and Harris R.P. (1998) Genetic and physiological influences on the alkenone/alkenoate versus growth temperature relationship in *Emiliania huxleyi* and *Gephyrocapsa oceanica*. *Geochim. Cosmochim. Ac.* **62**, 51-68.

De Bernardi B., Ziveri P., Erba E. and Thunell R.C. (2005) Coccolithophore export production during the 1997-1998 El Nino event in Santa Barbara Basin (California). *Mar. Micropaleo.* **55**, 107-125.

de Vargas C. and Probert I. (2004) New keys to the past: current and future DNA studies in Coccolithophores. *Micropaleontol.* **50**, 45-54.

Epstein B.L., D'Hondt S. and Hargraves P.E. (2001) The possible metabolic role of C37 alkenones in *Emiliania huxleyi*. *Org. Geochem.* **32**, 867-875.

Fernández E., Boyd P., Holligan P.M. and Harbour D.S. (1993) Production of organic and inorganic carbon within a large-scale coccolithophore bloom in the northeast Atlantic Ocean. *Mar. Ecol.-Prog. Ser.* **97**, 271-285.

Fernández E., Fritz J.J. and Balch W.M. (1996) Chemical composition of the coccolithophorid *Emiliania huxleyi* under light-limited steady state growth. *J. Exp. Mar. Biol. Ecol.* **207**, 149-160.

Goñi M.A., Hartz D.M., Thunell R.C. and Tappa E. (2001) Oceanographic considerations for the application of the alkenone-based paleotemperature $U_{37}^{K'}$ index in the Gulf of California. *Geochim. Cosmochim. Ac.* **65**, 545-557.

Hama T., Miyazaki T., Ogawa Y., Iwakuma T., Takahashi M., Otsuki A. and Ichimura S. (1983) Measurement of photosynthetic production of a marine phytoplankton population using a stable $^{13}C$ isotope. *Mar. Bio.* **73**, 31-36.

Hama T., Hama J. and Handa N. (1993) $^{13}C$ Tracer methodology in microbial ecology with special reference to primary production processes in aquatic environments, p. 39-83. *In* J. Gwynfryn [ed.], *Advances in Microbial Ecology*, Springer.

Hamanaka J., Sawada K. and Tanoue E. (2000) Production rates of $C_{37}$ alkenones determined by $^{13}C$-labeling technique in the euphotic zone of Sagami Bay, Japan. *Org. Geochem.* **31**, 1095-1102.

Hay W.W. (2004) Carbonate fluxes and calcareous phytoplankton, p. 509-528. *In* H.R. Thierstein and J.R. Young [eds.], *Coccolithophores*. Springer.

Hayes J.M., Freeman K.H., Popp B.N. and Hoham C.H. (1990) Compound-specific isotopic analyses: A novel tool for reconstruction of ancient biogeochemical processes. *Org. Geochem.* **16**, 1115-1128.

Head R.N., Crawford D.W., Egge J.K., Harris R.P., Kristiansen S., Lesley D.J., Marañón E., Pond D. and Purdie D.A. (1998) The hydrography and biology of a bloom of the coccolithophorid *Emiliania huxleyi* in the northern North Sea. *J. Sea Res.* **39**, 255-266.

Helmke P., Neuer S., Lomas M.W., Conte M. and Freudenthal T. (2010) Cross-Basin differences in particulate organic carbon export and flux attenuation in the subtropical North Atlantic gyre. *Deep-Sea Res. Pt. I* **57**, 213-227.

Hernández-Becerril D.U. (1987) Vertical distribution of phytoplankton in the central and northern part of the Gulf of California (June 1982). *Mar. Ecol.* **8**, 237-251.

Holligan P.M. and Robertson J.E. (1996) Significance of ocean carbonate budgets for the global carbon cycle. *Glob. Change Biol.* **2**, 85-95.

Iglesias-Rodríguez M.D., Brown C.W., Doney S.C., Kleypas J., Kolber D., Hayes P.K. and Falkowski P.G. (2002) Representing key phytoplankton functional groups in ocean carbon cycle models: Coccolithophorids. *Global Biogeochem. Cy.* **16**, doi:10.1029/2001GB001454.

Kara A.B., Rochford P.A. and Hurlburt H.E. (2000) An optimal definition for ocean mixed layer depth. *J. Geophys. Res.* **105**, 16803-16821.

Knauer G.A., Karl D.M., Martin J. and Hunter C. (1984) In situ effects of selected preservatives on total carbon, nitrogen and metals collected in sediment traps. *J. Mar. Res.* **42**, 445-462.

Langer G., Probert I., Nehrke G. and Ziveri P. (2011) The morphological response of *Emiliania huxleyi* to seawater carbonate chemistry changes: an inter-strain comparison. *J. Nanoplankton Res.* **32**, 29-34.

Laws E. A. (1984) Improved estimates of phytoplankton carbon based on $^{14}C$ incorporation into chlorophyll a. *J. Theor. Biol.* **110**, 425-434.

Laws E.A., Popp B.N., Bidigare R.R., Kennicutt M.C. and Macko S.A. (1995) Dependence of phytoplankton carbon isotopic composition on growth rate and

$[CO_2]_{aq}$: Theoretical considerations and experimental results. *Geochim. Cosmochim. Ac.* **59**, 1131-1138.

Leonardos N. and Geider R.J. (2005) Elevated atmospheric carbon dioxide increases organic carbon fixation by *Emiliania huxleyi* (Haptophyta), under nutrient-limited high-light conditions. *J. Phycol.* **41**, 1196-1203.

Litchman E., Klausmeier C.A., Schofield O.M. and Falkowski P.G. (2007) The role of functional traits and trade-offs in structuring phytoplankton communities: scaling from cellular to ecosystem level. *Ecol. Lett.* **10**, 1170-1181.

Lochte K., Ducklow H.W., Fasham M.J.R. and Stienen C. (1993) Plankton succession and carbon cycling at 47°N 20°W during the JGOFS North Atlantic Bloom Experiment. *Deep-Sea Res. Pt. II* **40**, 91-114.

Lomas M.W. and Moran S.B. (2011) Evidence for aggregation and export of cyanobacteria and nano-eukaryotes from the Sargasso Sea euphotic zone. *Biogeosci.* **8**, 203-216.

Malinverno E., Prahl F.G., Popp B.N. and Ziveri P. (2008) Alkenone abundance and its relationship to the coccolithophore assemblage in Gulf of California surface waters. *Deep-Sea Res. Pt. I* **55**, 1118-1130.

Marlowe I.T., Green J.C., Neal A.C., Brassell S.C., Eglinton G. and Course P.A. (1984) Long chain (n-$C_{37}$-$C_{39}$) alkenones in the Prymnesiophyceae. Distribution of alkenones and other lipids and their taxonomic significance. *Brit. Phycol. J.* **19**, 203-216.

Müller M.N., Antia A.N. and LaRoche J. (2008) Influence of cell cycle phase on calcification in the coccolithophore *Emiliania huxleyi*. *Limnol. Oceanogr.* **53**, 506-512.

Popp B.N., Bidigare R.R., Deschenes B., Laws E.A., Prahl F.G., Tanimoto J.K. and Wallsgrove R.J. (2006a). A new method for estimating growth rates of alkenone producing haptophytes. *Limnol. Oceanogr.-Meth.* **4**, 114-129.

Popp B.N., Prahl F.G., Wallsgrove R.J. and Tanimoto J. (2006b) Seasonal patterns of alkenone production in the subtropical oligotrophic North Pacific. *Paleoceanogr.* **21**, doi:10.1029/2005PA001165.

Prahl F.G. and Pinto L.A. (1987) A geochemical study of long-chain n-aldehydes in Washington coastal sediments. *Geochim. Cosmochim. Ac.* **51**, 1573-1582.

Prahl F.G., Collier R.B., Dymond J., Lyle M. and Sparrow M.A. (1993) A biomarker perspective on prymnesiophyte productivity in the northeast Pacific Ocean. *Deep-sea Res. Pt. I* **40**, 2061-2076.

Prahl F.G., Wolfe G.V. and Sparrow M.A. (2003) Physiological impacts on alkenone paleothermometry. *Paleoceanogr.* **18**, doi:10.1029/2002PA000803.

Prahl F.G., Popp B.N., Karl D.M. and Sparrow M.A. (2005) Ecology and biogeochemistry of alkenone production at Station ALOHA. *Deep-Sea Res. Pt. I* **52**, 699-719.

Revesz K.M., Landwehr J.M. and Keybl J. (2001) Measurement of $\delta^{13}C$ and $\delta\ ^{18}O$ isotopic ratios of $CaCO_3$ using a Thermoquest Finnigan GasBench II Delta Plus XL continuous flow isotope ratio mass spectrometer with application to Devils Hole Core DH-11 calcite. U.S. Geological Survey Open-File Report 01-257.

Richardson T.L. and Jackson G.A. (2007) Small phytoplankton and carbon export from the surface ocean. *Science* **315**, 838-840.

Riegman R., Stolte W., Noordeloos A.A.M. and Slezak D. (2000) Nutrient uptake and alkaline phosphatase (EC 3:1:3:1) activity of *Emiliania huxleyi* (prymnesiophyceae) during growth under N and P limitation in continuous cultures. *J. Phycol.* **36**, 87-96.

Sciandra A., Harlay J., Lefevre D., Lemee R., Rimmelin P., Denis M. and Gattuso J.P. (2003) Response of coccolithophorid *Emiliania huxleyi* to elevated partial pressure of $CO_2$ under nitrogen limitation. *Mar. Ecol.-Prog. Ser.* **261**, 111-122.

Sheppard C.W. (1962) *Basic Principles of the Tracer Method: Introduction to Mathematical Tracer Kinetics*. Wiley.

Small L.F., Knauer G.A. and Tuel M.D. (1987) The role of sinking fecal pellets in stratified euphotic zones. *Deep-Sea Res. Pt. A.* **34**, 1705-1712.

Thunell R.C., Pride C., Ziveri P., Muller-Karger F., Sancetta C. and Murray D. (1996) Plankton response to the physical forcing in the Gulf of California. *J. Plankton Res.* **18**, 2017-2026.

Thunell R.C. (1998) Seasonal and annual variability in particle fluxes in the Gulf of California: A response to climate forcing. *Deep-Sea Res. Pt. I* **45**, 2059-2083.

Tozzi S., Schofield O. and Falkowski P. (2004) Historical change and ocean turbulence as selective agents for two key phytoplankton functional groups. *Mar. Eco. Prog. Ser.* **274**, 123-132.

Tyrrell T. (2008) Calcium carbonate cycling in future oceans and its influence on future climates. *J. Plankton Res.* **30**, 141-146.

Volkman J.K., Eglinton G., Corner E.D.S. and Sargent J.R. (1980) Novel unsaturated straight-chain C37-C39 methyl and ethyl ketones in marine sediments and a coccolithophore *Emiliania huxleyi*, p. 219-227. *In* A.G. Douglas and J.R. Maxwell [eds.], *Advances in organic geochemistry, 1979: Proceedings of the Ninth International Meeting on Organic Geochemistry*. Pergamon Press.

Volkman J.K., Barrerr S.M., Blackburn S.I. and Sikes E.L. (1995) Alkenones in *Gephyrocapsa oceanica*: Implications for studies of paleoclimate. *Geochim. Cosmochim. Ac.* **59**, 513-520.

Walinsky S.E., Prahl F.G., Mix A.C., Finney B.P., Jaeger J.M. and Rosen G.P. (2009) Distribution and composition of organic matter in surface sediments of coastal Southeast Alaska. *Cont. Shelf Res.* **29**, 1565-1579.

White A.E., Prahl F.G., Letelier R.M. and Popp B.N. (2007) Summer surface waters in the Gulf of California: Prime habitat for biological $N_2$ fixation. *Global Biogeochem. Cy.* **21**, doi:10.1029/2006GB002779.

White A.E., Foster R.A., Benitez-Nelson C.R., Masqué P., Verdeny E., Popp B.N., Arthur K.E. and Prahl F.G. (2013) Nitrogen fixation in the Gulf of California and the Eastern Tropical North Pacific. *Prog. Oceanogr.* **109**, 1-17.

Winter A., Jordan R. and Roth P. (1994) Biogeography of living coccolithophores in ocean waters, p. 161-167. *In* A. Winter and W. G. Siesser [eds.], *Coccolithophores*. Cambridge University Press.

Ziveri P. and Thunell R.C. (2000) Coccolithophore export production in Guaymas Basin, Gulf of California: response to climate forcing. *Deep-Sea Res. Pt. II* **47**, 2073-2100.

Zondervan I., Zeebe R.E., Rost B. and Riebesell U. (2001) Decreasing marine biogenic calcification: A negative feedback on rising atmospheric $pCO_2$. *Global Biogeochem. Cy.* **15**, 507-516.

Zondervan I. (2007) The effects of light, macronutrients, trace metals and $CO_2$ on the production of calcium carbonate and organic carbon in coccolithophores—A review. *Deep-Sea Res. Pt. II* **54**, 521-537.

# 3. Alkenone δD As an Ecological Indicator: A Culture and Field Study of Physiologically-Controlled Chemical and Hydrogen-Isotopic Variation in $C_{37}$ Alkenones

Matthew D. Wolhowe, Fredrick G. Prahl, Gerald Langer, Angela Maria Oviedo, and Patrizia Ziveri

In review for Geochimica et Cosmochimica Acta
Elsevier Inc.
225 Wyman Street
Waltham, MA 02144
www.elsevier.com/geochimica-et-cosmochimica-acta

**Abstract:** A combined culture and field study was conducted in order to 1) more firmly establish the physiological controls on hydrogen isotopic composition of $C_{37}$ alkenones produced by coccolithophores and 2) determine the degree to which these controls are manifested in a natural water column. Nutrient-limitation experiments in culture, combined with previously published data, show that net fractionation between the growth medium and alkenones ($\alpha_{K37}$) increases rapidly with increasing cellular alkenone content and production rate, and, by extension, growth phase. Previously-described controls of temperature, growth rate, and species on $\alpha_{K37}$ appear significantly less predictive. It is suggested that the relationship of $\alpha_{K37}$ with cellular alkenone content is due to increased use of catabolic NADPH in response to high rates of lipid synthesis. In contrast to previous discussions of this effect based on studies of higher plants, in which lipids become D-enriched due to increased OPP pathway activity, we hypothesize that increased OPP activity generates D-depleted values of $\delta D_{K37}$ at both high growth rates and in stationary phase. Euphotic zone profiles of $\delta D_{K37}$, measured in suspended material from the Gulf of California and Eastern Tropical North Pacific, decreased with depth and did not correlate in any expected way with previously-suggested controls on $\alpha_{K37}$. It is possible that the field data is driven by behavior in light-limited cells that is not represented by the available, nutrient-limited culture data. Relationships between $\alpha_{K37}$, cell density, and the carbon-isotopic fractionation term $\varepsilon_p$, however, suggest that $\alpha_{K37}$ is an indicator of growth rate in this setting, consistent with our interpretation of the culture data. If the former interpretation proves correct, $\delta D_{K37}$ may have utility as an indicator of production depth in settings prone to subsurface production maxima. If the latter proves correct, $\delta D_{K37}$ may prove a powerful ecological proxy specific to these climatically-important, calcifying, temperature-encoding species.

## 3.1. Introduction:

The hydrogen isotopic composition of plant and algal lipids has received considerable attention from the oceanographic and paleoclimate communities. Lipids produced by photoautotrophs encode the D/H composition of environmental water in their abundant, non-exchangeable hydrogen (Estep and Hoering 1980). This relationship

has spurred attempts to develop hydrologic proxies from these compounds (e.g. Estep and Hoering 1981; Sauer et al 2001; Huang et al. 2004). However, it has become clear that the large and variable species-specific vital effects relating water and lipid isotopic compositions make biomarkers with multiple potential sources (e.g. Zhang and Sachs 2007) problematic as climate archives. The need for a lipid with a well-defined source organism has, in turn, spurred research focus on the hydrogen isotopic systematics of $C_{37}$ alkenones, which appear to be energy storage products (Epstein et al. 2001; Eltgroth et al. 2005) specific to prymnesiophytes. They are largely produced in modern marine settings by the coccolithophores *Emiliania huxleyi* and species of the genus Gephyrocapsa (Volkman et al. 1980, 1995; Marlowe et al. 1984). These species are found throughout the world ocean (Winter et al. 1994; Bollmann 1997) and primarily produce the di- and tri-unsaturated 37-carbon methyl ketones K37:2 and K37:3. This source specificity of K37 alkenones has already led to the development of their carbon isotopic fractionation ($\varepsilon_p$) as a growth rate and/or $pCO_2$ proxy (e.g. Pagani 2014). The ratio in which these compounds are produced varies as a function of growth temperature (e.g. Prahl et al. 1988; Volkman et al. 1995), also providing these compounds utility as the $U_{37}^{K'}$ paleo-temperature proxy (e.g. Herbert 2003).

Previous development of these compounds as a temperature proxy, coupled with the potential to determine water-compound fractionation factors for the limited source species, makes alkenones an attractive target for development as a sedimentary hydrologic proxy. Attempts to relate the deuterium isotopic composition of sedimentary alkenones ($\delta D_{K37}$) to that of the overlying water ($\delta D_{H2O}$) via laboratory- or field-determined values of the apparent fractionation factor, $\alpha_{K37}$:

$$\alpha_{K37} = \frac{\delta D_{K37} + 1000}{\delta D_{H_2O} + 1000} = \frac{\frac{D}{H}_{K37}}{\frac{D}{H}_{H_2O}} \qquad \textbf{3.1.1}$$

have yielded reasonable results (Englebrecht and Sachs 2005). However, it has become clear that $\alpha_{K37}$ is highly variable, and may respond to a number of physiological influences. In addition to differences between species, such as open-ocean alkenone

producers *E. huxleyi* and *G. oceanica* (Schouten et al. 2006) and coastal species *I. galbana* (M'boule et al. 2014) and *C. lamellose* (Chivall et al. 2014b), factors suggested to control $\alpha_{K37}$ include growth rate and salinity (Schouten et al. 2006; M'boule et al. 2014), growth phase (Wolhowe et al. 2009; Chivall et al. 2014b), and temperature (Wolhowe et al. 2009; Zhang et al. 2009b). There is an additional 'temperature effect' in that an isotopic offset between K37:2 and K37:3 exists ($\alpha_{K37:3\text{-}K37:2}$), and appears to vary in magnitude with temperature (D'Andrea et al. 2007; Schwab and Sachs 2009, 2011; van der Meer et al. 2013).

The 'salinity effect', which is hypothesized to act via changes in composition of the intracellular water pool (Sachse and Sachs 2008; M'boule et al. 2014), has been the best-studied physiological influence on $\alpha_{K37}$ (e.g. Schouten et al. 2006). As salinity appears to have an amplifying effect on the association of more negative $\delta D_{K37}$ values with fresher (lower $\delta D_{H2O}$) waters (Schouten et al. 2006; Sachse and Sachs 2008), the 'salinity effect' has been a factor in multiple studies of $\delta D_{K37}$ as a hydrological proxy in high-salinity contrast, high-$\delta D_{H2O}$ contrast environments (Pahnke et al. 2007; van der Meer et al. 2008; Schwab and Sachs 2011). In these settings, other proposed physiological influences are theoretically minimized by the high dynamic range of water isotopic composition.

In locations with lower-amplitude $\delta D_{H2O}$ variations, however, the other physiological controls on $\alpha_{K37}$ potentially make $\delta D_{K37}$ a poor hydrologic proxy (Wolhowe et al. 2009). This statement, though, can be reversed and posed as a question: in places with low variability in $\delta D_{H2O}$ and salinity, can $\delta D_{K37}$, responding instead to changes in $\alpha_{K37}$, be used as a sedimentary proxy for the physiological condition of coccolithophores? A collection of purely empirical relationships between $\alpha_{K37}$ and growth rate, temperature, growth phase, etc. presents too many degrees of freedom if we are to interpret $\delta D_{K37}$ without a host of ancillary measurements. In order to answer this question, then, we must better understand how these physiological factors mechanistically impact $\delta D_{K37}$.

In the following work, we detail the two steps taken in attempting to make this determination. They are:

1) to present results of dilute batch culture experiments, in comparison with previously published data, in order to evaluate the consistency of the purported growth rate, temperature, and growth phase effects on $\alpha_{K37}$ in *G. oceanica* and *E. huxleyi* (Section 3.3.1);
2) to present novel marine, *in situ* $\delta D_{K37}$ data collected from the Gulf of California and Eastern Tropical North Pacific and evaluate whether the interpretive framework we develop can be extended to natural coccolithophore populations (Section 3.3.3).

We compare marine $\alpha_{K37}$ to both environmental (temperature, nutrients, light) and physiological parameters (alkenone production rate and cellular concentration, growth rate, species composition, $\varepsilon_p$) to determine the potential for future sedimentary proxy work employing ecology/physiology-$\alpha_{K37}$ dynamics. We hypothesize that the nutrient-depleted upper layer of the Gulf of California/ETNP water column will express low $\alpha_{K37}$ values, consistent with nutrient-stressed culture experiments, while higher values will be observed near the nitracline.

## 3.2. Methods:

### 3.2.1 Cultures:

Six calcifying strains of *E. huxleyi* isolated from the Mediterranean Sea (RCC1812, RCC1813, RCC1817, RCC1827, RCC1830 and RCC1833; Roscoff Culture Collection, http://roscoff-culture-collection.org) were batch cultured in nutrient replete (f/2, ~740 μM nitrate, ~35 μM phosphate) and low phosphate (f/2, but with ~0.2 μM phosphate) media under 400 μE $m^{-2}$ $s^{-1}$ PAR (16:8 light:dark) at 20°C and a salinity of 32 (Table 1; reported salinity values were measured individually after sampling, see Section 3.2.4.2). Low-phosphate cultures depleted their phosphate in ~5 days and were harvested after 3 or 4 days in stationary phase at a cell density of ~100,000 cells $ml^{-1}$. Nutrient-replete cultures were harvested (still in log phase) at the same density. A strain of *E. huxleyi* isolated from the Norwegian Sea (B92/11; Plymouth Marine Lab, http://www.mba.ac.uk/culture-collection) was cultured at 15°C under analogous conditions (phosphate replete and reduced-phosphate f/2 treatments) and harvested at the

same cell densities. Additionally, this strain underwent a nitrate limited treatment (f/2 with ~2 μM nitrate). Duplicate, parallel cultures were conducted for each set of conditions. Samples (300 ml filtered onto pre-combusted glass fiber filters) were oven-dried and stored at room temperature until analysis. These cultures are described in more detail, along with discussion of their calcification behavior, in Langer et al. (2013; for B92/11) and Oviedo et al. (2014; for RCC1812-1833).

**Table 3.1.** Growth parameters, quantitative alkenone parameters, and alkenone isotopic composition from the culture experiments described in Section 3.2.1. Chemical and isotopic analysis are described in Sections 3.2.3 and 3.2.4. Data from Wolhowe et al. (2009) is provided along with previously unreported carbon and uncertainty data. Note that Wolhowe et al. (2009) log- and stationary-phase data are different sampling points of the same cultures; new log- and stationary-phase samples described here are separate treatments as described in Section 3.2.1.

**Table 3.1.** Chemical and Isotopic Composition of Nutrient-Replete Exponential and Nutrient-Depleted Stationary Cultures.

| *E huxlei* Strain | Treatment[a] | Temperature (°C) | Salinity | PAR (µE $m^{-2}$ $s^{-1}$) | Day Length (h) | Growth Rate ($d^{-1}$) | Standard Error[b] | $U^{K'}_{37}$ | $q_{K37}$ (pg K37 $cell^{-1}$) | ±[c] | K37 Production Rate (pg K37 $cell^{-1}$ $d^{-1}$) | ± | Organic Carbon (pg OC $cell^{-1}$) | ±[d] | OC Production Rate (pg OC $cell^{-1}$ $d^{-1}$) | ± | K37:OC (pg K37 pg $OC^{-1}$) | ± | $\delta D_{K37}$ (‰ vs. SMOW) | σ | $\delta D_{H2O}$ (‰ vs. SMOW) | σ | $\alpha_{K37}$ | ± |
|---|---|---|---|---|---|---|---|---|---|---|---|---|---|---|---|---|---|---|---|---|---|---|---|---|
| *Wolhowe et al. 2009* E. huxleyi[e] | | | | | | | | | | | | | | | | | | | | | | | | |
| CCMP 1742 | | 15 | 32 | 70 | 12 | 0.58 | 0.02 | 0.409 | 0.44 | 0.05 | 0.35 | 0.04 | 8.1 | 0.4 | 6.3 | 0.4 | 0.054 | 0.007 | -186.4 | 0.9 | -8.7 | 1.8 | 0.821 | 0.002 |
| CCMP 1742 | | 15 | 32 | 70 | 12 | 0.56 | 0.02 | 0.413 | 0.46 | 0.05 | 0.35 | 0.04 | 8.1 | 0.4 | 6.1 | 0.4 | 0.057 | 0.007 | -191.0 | 0.1 | -9.2 | 2.7 | 0.817 | 0.002 |
| CCMP 1742 | | 15 | 32 | 70 | 12 | Stationary | | 0.304 | 1.32 | 0.16 | | | 11.7 | 0.6 | | | 0.112 | 0.015 | -215.3 | 3.5 | -7.7 | 3.4 | 0.791 | 0.004 |
| CCMP 1742 | | 15 | 32 | 70 | 12 | Stationary | | 0.302 | 1.37 | 0.17 | | | 13.3 | 0.7 | | | 0.103 | 0.014 | -212.9 | 2.1 | -7.6 | 0.8 | 0.793 | 0.002 |
| *Wolhowe et al. 2009* G. oceanica[e] | | | | | | | | | | | | | | | | | | | | | | | | |
| PZ3-1 | | 17 | 32 | 150 | 14 | 0.62 | 0.04 | 0.437 | 0.60 | 0.08 | 0.52 | 0.09 | 19.6 | 1.0 | 16.8 | 1.7 | 0.031 | 0.005 | -190.9 | 1.3 | 0 | 2 | 0.809 | 0.002 |
| PZ3-1 | | 21 | 32 | 150 | 14 | 0.92 | 0.04 | 0.744 | 0.82 | 0.12 | 1.24 | 0.20 | 26.7 | 1.3 | 40.2 | 3.6 | 0.031 | 0.005 | -204.6 | 0.2 | 0 | 2 | 0.795 | 0.002 |
| PZ3-1 | | 25 | 32 | 150 | 14 | 0.93 | 0.05 | 0.985 | 1.98 | 0.28 | 3.04 | 0.49 | 53.4 | 2.7 | 81.9 | 7.3 | 0.037 | 0.006 | -229.9 | 2.0 | 0 | 2 | 0.770 | 0.003 |
| PZ3-1 | | 17 | 32 | 150 | 14 | Stationary | | 0.384 | 0.78 | 0.11 | | | 23.7 | 1.2 | | | 0.033 | 0.005 | -213.2 | 7.6 | 0 | 2 | 0.787 | 0.008 |
| PZ3-1 | | 21 | 32 | 150 | 14 | Stationary | | 0.683 | 1.17 | 0.17 | | | 16.6 | 0.8 | | | 0.070 | 0.011 | -235.5 | 0.3 | 0 | 2 | 0.765 | 0.002 |
| PZ3-1 | | 25 | 32 | 150 | 14 | Stationary | | 0.976 | 1.08 | 0.15 | | | 17.8 | 0.9 | | | 0.061 | 0.009 | -262.6 | 0.5 | 0 | 2 | 0.737 | 0.002 |
| *Mediterranean Strains* | | | | | | | | | | | | | | | | | | | | | | | | |
| RCC1812 | P-Replete | 20 | 29.6 | 400 | 16 | 1.14 | 0.02 | 0.642 | 0.99 | 0.14 | 1.12 | 0.16 | 12.0 | 0.6 | 25.3 | 1.5 | 0.083 | 0.012 | -258.2 | 2.0 | -32.0 | 0.2 | 0.766 | 0.002 |
| RCC1812 | P-Replete | 20 | 29.6 | 400 | 16 | 1.12 | 0.02 | 0.643 | 1.19 | 0.17 | 1.33 | 0.19 | 11.2 | 0.6 | 23.1 | 1.4 | 0.106 | 0.016 | -254.0 | 0.7 | -32.8 | 0.1 | 0.771 | 0.001 |
| RCC1813 | P-Replete | 20 | 29.6 | 400 | 16 | 1.05 | 0.02 | 0.606 | 0.84 | 0.12 | 0.89 | 0.13 | 8.6 | 0.4 | 16.0 | 0.9 | 0.098 | 0.015 | -230.3 | 0.9 | -31.1 | 0.1 | 0.794 | 0.001 |
| RCC1813 | P-Replete | 20 | 29.6 | 400 | 16 | 1.05 | 0.02 | 0.611 | 1.05 | 0.15 | 1.09 | 0.16 | 8.6 | 0.4 | 15.8 | 1.0 | 0.122 | 0.018 | -229.4 | 3.0 | -33.1 | 0.1 | 0.797 | 0.003 |
| RCC1817 | P-Replete | 20 | 29.6 | 400 | 16 | 1.03 | 0.03 | 0.664 | 0.89 | 0.13 | 0.92 | 0.13 | 8.5 | 0.4 | 15.4 | 1.0 | 0.104 | 0.016 | -239.7 | 1.3 | -31.8 | 0.1 | 0.785 | 0.001 |
| RCC1817 | P-Replete | 20 | 29.6 | 400 | 16 | 1.06 | 0.03 | 0.673 | 1.00 | 0.14 | 1.07 | 0.15 | 8.4 | 0.4 | 15.9 | 1.1 | 0.120 | 0.018 | -246.0 | 0.1 | -32.2 | 0.1 | 0.779 | 0.000 |
| RCC1827 | P-Replete | 20 | 30.3 | 400 | 16 | 1.01 | 0.03 | 0.758 | 0.94 | 0.13 | 0.95 | 0.14 | 8.1 | 0.4 | 14.2 | 0.9 | 0.116 | 0.017 | -260.6 | 0.8 | -31.6 | 0.2 | 0.764 | 0.001 |
| RCC1827 | P-Replete | 20 | 29.6 | 400 | 16 | 0.99 | 0.02 | 0.760 | 0.97 | 0.14 | 0.96 | 0.14 | 8.0 | 0.4 | 13.5 | 0.8 | 0.121 | 0.018 | -262.5 | 1.7 | -30.5 | 0.1 | 0.761 | 0.002 |
| RCC1830 | P-Replete | 20 | 29.6 | 400 | 16 | 1.22 | 0.02 | 0.607 | 1.01 | 0.14 | 1.24 | 0.18 | 10.2 | 0.5 | 24.4 | 1.4 | 0.100 | 0.015 | -256.6 | 3.2 | -31.1 | 0.2 | 0.767 | 0.003 |
| RCC1830 | P-Replete | 20 | 29.6 | 400 | 16 | 1.21 | 0.03 | 0.618 | 1.10 | 0.16 | 1.33 | 0.19 | 10.8 | 0.5 | 25.4 | 1.6 | 0.102 | 0.015 | -258.7 | 3.2 | -29.4 | 0.1 | 0.764 | 0.003 |
| RCC1833 | P-Replete | 20 | 30.3 | 400 | 16 | 1.02 | 0.02 | 0.572 | 0.77 | 0.11 | 0.78 | 0.11 | 7.8 | 0.4 | 13.8 | 0.8 | 0.099 | 0.015 | -231.9 | 2.1 | -31.5 | 0.1 | 0.793 | 0.002 |
| RCC1833 | P-Replete | 20 | 29.6 | 400 | 16 | 1.02 | 0.02 | 0.557 | 0.80 | 0.11 | 0.81 | 0.12 | 8.1 | 0.4 | 14.2 | 0.8 | 0.099 | 0.015 | -229.9 | 0.3 | -30.4 | 0.1 | 0.794 | 0.000 |
| RCC1812 | P-Depleted | 20 | 29.6 | 400 | 16 | Stationary | | 0.659 | 3.08 | 0.44 | | | 33.7 | 1.7 | | | 0.091 | 0.014 | -281.3 | 2.4 | -32.8 | 0.1 | 0.743 | 0.002 |
| RCC1812 | P-Depleted | 20 | 29.6 | 400 | 16 | Stationary | | 0.649 | 4.21 | 0.60 | | | 35.8 | 1.8 | | | 0.118 | 0.018 | -282.1 | 3.4 | -32.7 | 0.2 | 0.742 | 0.004 |
| RCC1813 | P-Depleted | 20 | 29.6 | 400 | 16 | Stationary | | 0.639 | 3.88 | 0.55 | | | 22.6 | 1.1 | | | 0.172 | 0.026 | -253.6 | 2.4 | -32.0 | 0.1 | 0.771 | 0.002 |
| RCC1813 | P-Depleted | 20 | 29.6 | 400 | 16 | Stationary | | 0.633 | 5.20 | 0.74 | | | 24.5 | 1.2 | | | 0.212 | 0.032 | -252.3 | 1.1 | -32.3 | 0.1 | 0.773 | 0.001 |
| RCC1817 | P-Depleted | 20 | 28.8 | 400 | 16 | Stationary | | 0.668 | 4.09 | 0.58 | | | 31.3 | 1.6 | | | 0.131 | 0.020 | -256.7 | 4.2 | -30.8 | 0.1 | 0.767 | 0.004 |
| RCC1817 | P-Depleted | 20 | 29.6 | 400 | 16 | Stationary | | 0.671 | 3.87 | 0.55 | | | 29.4 | 1.5 | | | 0.131 | 0.020 | -260.7 | 2.0 | -30.9 | 0.1 | 0.763 | 0.002 |
| RCC1827 | P-Depleted | 20 | 29.6 | 400 | 16 | Stationary | | 0.792 | 4.52 | 0.64 | | | 24.8 | 1.2 | | | 0.182 | 0.027 | -282.1 | 2.1 | -31.4 | 0.1 | 0.741 | 0.002 |
| RCC1827 | P-Depleted | 20 | 30.3 | 400 | 16 | Stationary | | 0.786 | 3.99 | 0.56 | | | 24.2 | 1.2 | | | 0.165 | 0.025 | -282.3 | 0.4 | -29.4 | 0.1 | 0.739 | 0.000 |
| RCC1830 | P-Depleted | 20 | 29.6 | 400 | 16 | Stationary | | 0.676 | 3.67 | 0.52 | | | 34.2 | 1.7 | | | 0.107 | 0.016 | -284.6 | 0.2 | -30.6 | 0.2 | 0.738 | 0.000 |
| RCC1830 | P-Depleted | 20 | 30.3 | 400 | 16 | Stationary | | 0.690 | 3.53 | 0.50 | | | 31.8 | 1.6 | | | 0.111 | 0.017 | -283.9 | 2.6 | -29.3 | 0.1 | 0.738 | 0.003 |
| RCC1833 | P-Depleted | 20 | 30.3 | 400 | 16 | Stationary | | 0.528 | 2.74 | 0.39 | | | 20.0 | 1.0 | | | 0.136 | 0.020 | -254.7 | 1.7 | -32.0 | 0.1 | 0.770 | 0.002 |
| RCC1833 | P-Depleted | 20 | 30.3 | 400 | 16 | Stationary | | 0.526 | 3.13 | 0.44 | | | 24.5 | 1.2 | | | 0.128 | 0.019 | -260.2 | 2.3 | -29.9 | 0.1 | 0.763 | 0.002 |
| *Norwegian Strain* | | | | | 16 | | | | | | | | | | | | | | | | | | | |
| PML B92/11 | N-Replete | 15 | 31.1 | 400 | 16 | 1.32 | 0.02 | 0.455 | 0.60 | 0.09 | 0.80 | 0.11 | 8.2 | 0.4 | 22.5 | 1.2 | 0.074 | 0.011 | -227.6 | 2.0 | -38.7 | 0.1 | 0.803 | 0.002 |
| PML B92/11 | N-Replete | 15 | 31.1 | 400 | 16 | 1.32 | 0.02 | 0.459 | 0.63 | 0.09 | 0.83 | 0.12 | 8.4 | 0.4 | 23.1 | 1.3 | 0.073 | 0.011 | -230.7 | 2.0 | -36.7 | 0.1 | 0.799 | 0.002 |
| PML B92/11 | N-Depleted | 15 | 31.1 | 400 | 16 | Stationary | | 0.600 | 1.17 | 0.17 | | | 16.2 | 0.8 | | | 0.073 | 0.011 | -231.4 | 1.0 | -39.1 | 0.1 | 0.800 | 0.001 |
| PML B92/11 | N-Depleted | 15 | 30.3 | 400 | 16 | Stationary | | 0.607 | 1.35 | 0.19 | | | 15.9 | 0.8 | | | 0.085 | 0.013 | -235.2 | 0.1 | -37.1 | 0.1 | 0.794 | 0.000 |
| PML B92/11 | P-Replete | 15 | 30.3 | 400 | 16 | 1.13 | 0.04 | 0.495 | 0.32 | 0.05 | 0.36 | 0.05 | 8.2 | 0.4 | 17.1 | 1.4 | 0.039 | 0.006 | -203.4 | 6.4 | -19.2 | 0.1 | 0.812 | 0.007 |
| PML B92/11 | P-Replete | 15 | 31.1 | 400 | 16 | 1.14 | 0.04 | 0.494 | 0.28 | 0.04 | 0.32 | 0.05 | 8.6 | 0.4 | 18.2 | 1.4 | 0.033 | 0.005 | -208.9 | 0.6 | -18.4 | 0.1 | 0.806 | 0.001 |
| PML B92/11 | P-Depleted | 15 | 31.1 | 400 | 16 | Stationary | | 0.544 | 3.26 | 0.46 | | | 40.2 | 2.0 | | | 0.082 | 0.012 | -256.3 | 0.6 | -19.5 | 0.1 | 0.759 | 0.001 |
| PML B92/11 | P-Depleted | 15 | 31.1 | 400 | 16 | Stationary | | 0.538 | 2.46 | 0.35 | | | 39.5 | 2.0 | | | 0.063 | 0.009 | -263.0 | 3.7 | -16.8 | 0.1 | 0.750 | 0.004 |

[a] "Replete' treatments are stoicheometrically limited by the indicated nutrient (see Section 3.2.1).

[b] Standard error of the slope of the linear regression of ln(cells $mL^{-1}$) vs. time.

[c] Propagated from assumed 10% uncertainty in alkenone quantification and the number of cells sampled.

[d] Assumed 5% uncertainty based on typical standard deviation of replicate measurements.

[e] Alkenone abundance and isotopic data from Wolhowe et al. 2009, reproduced here for convienience with previously unreported uncertainty estimates and organic carbon quantification.

3.2.2 LVF Samples:

*In situ* large volume filters (LVFs) were collected on the 2008 'GoCal4' cruise to the Gulf of California and adjacent eastern tropical north Pacific (ETNP). Alkenone-producers *E. huxleyi* and Gephyrocapsa *spp.* are the predominant species of coccolithophores in this setting (Ziveri et al. 1995; Thunell et al. 1996; Ziveri and Thunell 2000; Malinverno et al. 2008). This cruise and the stations in question (Table 3.2) are documented fully in White et al. (2013) and Wolhowe et al. (2014).

At seven of the Gulf of California and ETNP stations (Table 3.2), Challenger *in situ* pumps were deployed by hydrowire to sample alkenones in suspended particulate matter (SPM) for $\delta D_{K37}$ analysis. Suspended alkenones were collected at two or three depths between 10 and 57m by filtering ~340-570 L onto 142 mm pre-combusted type A/E glass fiber filters (> 1 μm fraction) over the course of ~2-4 hours. Samples from other depths at these stations were acquired by using the filter material left from similar pump deployments made for U/Th analysis after twenty 20 mm punches had been removed. The additional samples were collected on pre-combusted QM-A quartz filters (~1 μm to 53 μm size fraction), but otherwise were handled identically. All filters were frozen at ~-80°C until analysis. Filter type/size cutoff did not appear to impact the resulting isotopic data.

**Table 3.2.** Ecological and isotopic field data from the Gulf of California and ETNP. In addition to the alkenone chemical and isotopic (δD and $\varepsilon_P$) data reported here, alkenone-producer species composition and abundance, temperature, light levels, estimated per-cell alkenone content, and estimated growth rate are provided (all linearly interpolated from the results of Wolhowe et al. 2014). $\varepsilon_p$ and $\varepsilon_p$-estimated growth rate are calculated as described in Section 3.3.3.2.

**Table 3.2.** Isotopic Composition and Production Rate of Alkenones in Gulf of California/ETNP SPM

| Station[a] | Lat | Lon | Occupation Date | Depth | $U^K_{37}$ | $\delta D_{K37}$ | σ | S | Modeled $\delta D_{H2O}$ | $\alpha_{K37}$ | ±[b] | Temperature | Noon PAR[c] | *E. huxleyi* + Gephy.[c,d] | ± | Fraction *E.huxleyi*[c] | $q_{K37}$[c] | ± | Per-Cell $PR_{K37}$[c] | ± | Incubation μ | ±[e] | $\varepsilon_p$[f] | $\varepsilon_p$ Esitmated μ[f] | ±[f] |
|---|---|---|---|---|---|---|---|---|---|---|---|---|---|---|---|---|---|---|---|---|---|---|---|---|---|
| | (ºN) | (ºW) | | (m) | | (‰ vs. SMOW) | | | (‰ vs. SMOW) | | | (ºC) | ($\mu E\ m^{-2}\ s^{-1}$) | (cs $L^{-1}$ x $10^3$) | | (of *E.hux* + Gephy.) | (pg K37 $cell^{-1}$) | | (pg K37 $cell^{-1}\ d^{-1}$) | | ($d^{-1}$) | | (‰ vs.PDB ± 0.15) | ($d^{-1}$) | |
| 4-1 | 26.5 | 111.5 | July 11th-13th 2008 | 30 | 0.981 | -199.7 | 5.0 | 34.8 | 12.3 | 0.791 | 0.007 | 22.6 | 107 | 44 | 5 | 0.99 | 0.4 | 0.1 | 0.39 | 0.06 | 0.56 | 0.02 | 16.2 | 0.75 | 0.17 |
| 4-1 | | | | 50 | 0.876 | -216.5 | 1.6 | 34.7 | 12.0 | 0.774 | 0.006 | 19.0 | 18 | 35 | 5 | 0.73 | 0.15 | 0.03 | 0.07 | 0.01 | 0.12 | 0.01 | | | |
| 4-2a | 24.5 | 109.0 | July 14th-16th 2008 | 10 | 0.973 | -192.7 | 1.0 | 35.0 | 13.4 | 0.797 | 0.006 | 29.0 | 1400 | 44 | 6 | 0.19 | 0.8 | 0.1 | 0.16 | 0.03 | 0.24 | 0.01 | 16.8 | 0.53 | 0.14 |
| 4-2a | | | | 20 | 0.968 | -192.9 | 4.6 | 35.0 | 13.3 | 0.796 | 0.007 | 28.5 | 581 | 43 | 6 | 0.21 | 0.8 | 0.1 | 0.15 | 0.02 | 0.24 | 0.01 | 16.7 | 0.54 | 0.14 |
| 4-2a | | | | 30 | 0.978 | -192.8 | 2.6 | 35.1 | 13.6 | 0.796 | 0.006 | 27.8 | 239 | 47 | 7 | 0.34 | 0.4 | 0.1 | 0.07 | 0.01 | 0.26 | 0.01 | 16.2 | 0.62 | 0.16 |
| 4-2a | | | | 40 | 0.979 | -202.8 | 5.0 | 35.0 | 13.4 | 0.787 | 0.007 | 26.6 | 114 | 60 | 8 | 0.53 | 0.27 | 0.05 | 0.022 | 0.004 | 0.38 | 0.01 | 15.9 | 0.75 | 0.18 |
| 4-2a | | | | 50 | 0.970 | -201.2 | 5.0 | 35.0 | 13.4 | 0.788 | 0.007 | 24.0 | 63 | 22 | 4 | 0.70 | 0.6 | 0.1 | 0.04 | 0.01 | 0.28 | 0.01 | 14.9 | 0.92 | 0.22 |
| 4-2b | 24.5 | 109.0 | July 22nd-24th 2008 | 10 | 0.992 | -191.9 | 1.1 | 34.3 | 10.4 | 0.800 | 0.006 | 29.6 | 684 | 16 | 3 | 0.08 | 1.4 | 0.3 | | | | | | | |
| 4-2b | | | | 20 | 0.992 | -195.6 | 3.3 | 34.4 | 10.6 | 0.796 | 0.006 | 29.0 | 450 | 13 | 2 | 0.16 | 1.0 | 0.2 | | | | | | | |
| 4-2b | | | | 45 | 0.992 | -200.9 | 5.0 | 34.8 | 12.5 | 0.789 | 0.007 | 27.1 | 64 | 28 | 4 | 0.45 | 0.4 | 0.1 | | | | | | | |
| 4-8 | 20.5 | 106.5 | July 18th-21st 2008 | 10 | 0.947 | -194.0 | 0.6 | 34.2 | 9.7 | 0.798 | 0.006 | 29.2 | 415 | 27 | 3 | 0.02 | 1.0 | 0.2 | 0.20 | 0.03 | 0.21 | 0.01 | 17.1 | 0.43 | 0.12 |
| 4-8 | | | | 20 | 0.967 | -190.6 | 5.1 | 34.4 | 10.7 | 0.801 | 0.008 | 28.5 | 181 | 32 | 5 | 0.07 | 0.9 | 0.2 | 0.17 | 0.03 | 0.21 | 0.01 | 17.0 | 0.48 | 0.13 |
| 4-8 | | | | 57 | 0.956 | -241.9 | 5.0 | 34.9 | 12.8 | 0.749 | 0.007 | 25.8 | 10 | 47 | 6 | 0.50 | | | 0[g] | | 0[g] | 0[g] | | | |
| 4-10 | 24.7 | 113.3 | July 28th-31st 2008 | 10 | 0.907 | -187.5 | 5.0 | 33.9 | 8.3 | 0.806 | 0.008 | 23.6 | 923 | 7 | 1 | 0.68 | 0.36 | 0.06 | | | | | | | |
| 4-10 | | | | 25 | 0.650 | -209.4 | 8.8 | 33.7 | 7.5 | 0.785 | 0.010 | 18.8 | 396 | 22 | 3 | 0.77 | 1.2 | 0.2 | | | | | | | |
| 4-10 | | | | 52 | 0.500 | -224.6 | 6.1 | 33.7 | 7.5 | 0.770 | 0.008 | 14.5 | 37 | 56 | 7 | 0.86 | 0.40 | 0.06 | | | | | | | |
| 4-10 | | | | 57 | 0.483 | -208.9 | 5.0 | 33.7 | 7.6 | 0.785 | 0.007 | 14.1 | 23 | 85 | 9 | 0.90 | 0.32 | 0.04 | | | | | | | |
| 4-11 | 27.5 | 117.5 | Aug. 1st-3rd 2008 | 20 | 0.689 | -191.6 | 5.0 | 33.6 | 7.1 | 0.803 | 0.008 | 20.8 | 232 | 17 | 2 | 0.73 | 1.7 | 0.3 | | | | | | | |
| 4-11 | | | | 50 | 0.401 | -220.6 | 0.4 | 33.5 | 6.4 | 0.774 | 0.005 | 14.8 | 15 | 78 | 11 | 0.78 | 0.43 | 0.07 | | | | | | | |
| 4-12 | 32.5 | 120.5 | Aug. 5th-7th 2008 | 10 | 0.533 | -237.2 | 0.2 | 33.6 | 7.2 | 0.757 | 0.005 | 16.9 | 344 | 62 | 7 | 0.90 | 1.0 | 0.1 | 0.35 | 0.06 | 0.48 | 0.03 | 13.5 | 0.92 | 0.21 |
| 4-12 | | | | 25 | 0.538 | -245.0 | 3.1 | 33.6 | 7.2 | 0.750 | 0.006 | 15.7 | 23 | 68 | 9 | 0.91 | 0.52 | 0.08 | 0.006 | 0.004 | 0.01 | 0.01 | 13.0 | 1.15 | 0.26 |

[a] Stations detailed in Wolhowe et al. (2014) and White et al. (2013).

[b] Propagated from standard deviation of replicate alkenone isotopic measurements and assumed 3.7‰ uncertainty in estimated water values (see Section 3.2.4.3).

[c] Mean density/property profiles of Wolhowe et al. (2014) interpolated to the density at time and depth of LVF collection.

[d] Gephyrocapsa counts include species *muellerae*, *ericsonii*, and *ornata*, but were >90% *G. oceanica* (Wolhowe et al. 2014).

[e] Propagated from $TR_{K37:2}$ and incubation time uncertainties reported in Wolhowe et al.(2014).

[f] See Appendix B for data used in calculation.

[g] The isopycnal where this LVF was collected was ~8 m below the isopycnal corresponding to the deepest incubation depth (mean density/production rate profile of Wolhowe et al. 2014). Rate extrapolates to 0 between these two depths.

3.2.3 Chemical Analysis:

Alkenone quantification followed the procedures outlined in Wolhowe et al. (2014 and references therein). Briefly, lipids were extracted from the filters using a Dionex ASE-200 automated solvent extraction system (Walinsky et al. 2009) and the resulting total extractable lipids (TEL) partitioned into hexane. In the case of the field samples, alkenone fractions were isolated from the TEL by liquid column chromatography on silica gel (Prahl and Pinto 1987). The alkenone fractions (field) or TELs (culture) were then saponified in basic ethanol to remove co-eluting alkenoates (Christie 2003) and characterized/quantified by capillary gas chromatography with flame ionization detection (GC-FID; Walinsky et al. 2009). Reported alkenone concentrations have been corrected for recovery (typically 80-90%) of hexatriacontan-2-one (K36:0), a standard added to each sample prior to ASE extraction. Due to a lack of true sample replication for the field samples, a conservative uncertainty of 10% (as per Popp et al. 2006) has been assumed in the quantification of K37:2 and K37:3.

Organic carbon was determined by acid-fuming filter cakes overnight to remove inorganic carbon, followed by standard high-temperature combustion method (Verardo et al. 1990).Typical uncertainty in cell-carbon analysis was ~5%.

3.2.4 Isotopic Analysis:

$\delta D_{K37}$ and $\delta D_{H2O}$ analysis was performed using a ThermoQuest-Finnigan Delta Plus XL isotope ratio mass spectrometer. '$H_3^+$' correction factors (Sessions et al., 1999) were determined each day within the ISODAT software using eight sequential $H_2$ reference gas injections of increasing partial pressure. $H_3^+$ factor values ranged between ~2 and ~4 ppm $nA^{-1}$. All δD values are reported in permille versus Standard Mean Ocean Water (SMOW).

*3.2.4.1 Compound-Specific δD Analysis:*

$\delta D_{K37}$ was determined by gas chromatography-thermal conversion-isotope ratio monitoring mass spectrometry (GC-TC-IRMS). Samples were dissolved in the volume of toluene necessary to analyze ~500 ng of the minor $C_{37}$ in a 2 μL GC injection (except

for those Gulf of California field samples in which there was no appreciable K37:3 due to high growth temperatures). Samples, coinjected with 1 μL of an n-alkane working standard (410 ng $nC_{37}$ $\mu L^{-1}$), were chromatographically separated using an HP6890 GC equipped with a cool on-column injector and a SGE BF5 column (30 m x 0.32 mm i.d., 1.0 μm film). The GC was operated at a constant helium carrier gas flow rate (2.5 mL $min^{-1}$). Separations were achieved by temperature programming (80-270°C at 10°C $min^{-1}$, 270-320°C at 5°C $min^{-1}$, 43 min hold at 320°C) and alkenones eluted after approximately 50 minutes. The alumina pyrolysis reactor (32 cm x 0.5 mm i.d.), installed in a Thermo-Finnigan GC-TC interface, was maintained at 1410°C. Upon initial use, 1 μL injections of isooctane were passed through the reactor for pre-conditioning (graphitization) until measured standard values stabilized. $\delta D_{K37}$ values were calculated versus the coinjected and $nC_{37}$ alkane and $C_{36}$ methyl ketone (K36:0) reference materials. 'Known' values of these working references were determined by daily standardization through co-injection with 'Mixture B', a 15 compound mixture of n-alkanes with known δD values, obtained from A. Schimmelmann (Indiana University; http://mypage.iu.edu/~aschimme/compounds.html). The standard errors of the mean (SEM) of the working reference materials (n = 68) were 0.6‰ for both. All $\delta D_{K37}$ values are reported as the mean of two or three replicate analyses of the same sample; conservative uncertainties of 5‰ were assumed for samples where replication was not possible (indicated in Tables 3.1- 3.2). The mean standard deviation for replicate analyses was 3.0‰ for the LVF samples and 1.9‰ for the culture samples.

*3.2.4.2 Water δD Analysis:*

Culture media $\delta D_{H2O}$ (Section 2.1) was determined by $H_2$ equilibration following the methods of Horita et al. (1989) and Coplen et al. (1991). For each sample, 2.5 mL of filtered media and a set of platinum "Hokko bead" catalysts (Isoprime) were placed in a 20 mL glass reservoir (manifold of 18 samples + standards in a given run) interfaced to the duel inlet of the mass spectrometer. The reservoirs were lowered into an 18°C water bath, evacuated, and the headspace filled to 250 mbar with $H_2$ 'fill gas' of $\delta D_{H2}$ ~124‰. The isotopic composition of the fill gas was determined to have no measurable effect on

the final equilibrated values due to its small contribution to the hydrogen mass balance. The samples were shaken for ten hours to allow for isotopic equilibration between $H_2O$ and $H_2$. The gas content of each reservoir was then admitted to the sample side of the duel inlet through a -90°C water trap. Each sample was measured eight times versus a monitoring gas, yielding a mean analytical precision (standard deviation) of 0.1‰. Each run contained two reservoirs each of two working standards (-0.9 and -69.1‰) which this monitoring gas was referenced to, as well as at least one sample from each previous run to monitor drift. The working standards, in turn, were calibrated against the GISP, SLAP, and VSMOW2 standards. The SEM of the working reference materials (n = 6) was 0.3 and 0.1‰, respectively. The mean standard deviation of all sets of repeated samples was 0.5‰.

Due to the presence of salinity effects on the catalyzed equilibrium fractionation between $H_2O$ and $H_2$ (Martineau et al. 2011), a salinity correction was empirically determined. A series of 15 artificial seawater standards with salinities ranging from 0 to 40 were made from distilled water of -80‰. Salinities were determined via AgCl titration (Adkins and Schrag 2003). A δD correction of ~0.06‰ relative to fresh water, per salinity unit, was determined from equilibration of these standards. The salinity of samples and isotope working standards was measured prior to equilibration to determine the necessary degree of correction. As all samples had salinities of ~32, no sample had an applied correction greater than ~2‰.

*3.2.4.3 Estimation of Environmental $\delta D_{H2O}$:*

Water samples corresponding to the LVF samples from the Gulf of California were not available. However, given the narrow range of salinity measurements in our study area and the covariation of salinity and $\delta D_{H2O}$ in marine settings (e.g. Craig and Gordon 1965; Rohling 2007), we are able to reasonably estimate water composition for the purposes of sample comparison within the LVF data set. First, a regional $\delta^{18}O$ vs. salinity relationship ($\delta^{18}O = 0.56*\text{salinity} - 19.23$; $R^2 = 0.86$) was determined from all data points in the NASA GISS $^{18}O$ database from <100 m between 15 to 35°N and 95 to 150°W with associated salinity measurements (n=19). Assuming a meteoric relationship

between $\delta^{18}O$ and $\delta D$ ($\delta D = 8*\delta^{18}O + 10$), these points generate a $\delta D$ vs. S relationship of $\delta D = 4.5*$salinity -143.8. This equation and the salinity fields reported in Wolhowe et al. (2014) were used to estimate $\delta D_{H2O}$ at the depth of each LVF. As the full range of salinity associated with the LVF data set was 33.47 to 35.05, estimated $\delta D_{H2O}$ ranged from 6.5 to 13.6‰ (Table 3.2). We assume a generous uncertainty in these values of 7.1‰, the range of the individual estimates.

## 3.3. Results and Discussion

### 3.3.1 Results of Culture Experiments

The alkenone signatures in cultured Mediterranean and Norwegian strains of *E. huxleyi* responded, both chemically and isotopically, as expected from studies of log- and stationary-phase alkenone-producers (Table 3.1). Log-phase cells (growth rates between 0.99 and 1.32 $d^{-1}$) had low per-cell alkenone quotas, $q_{K37}$, averaging 0.96 pg $cell^{-1}$ for the Mediterranean strains and 0.46 pg $cell^{-1}$ for the Norwegian strain. Stationary-phase cells, in contrast, exhibited increased quotas, averaging 3.8 pg $cell^{-1}$ for the P-limited Mediterranean strains and 2.9 and 1.3 pg $cell^{-1}$, respectively, for the P-limited and N-limited treatments of the Norwegian strain. These changes in alkenone abundance were accompanied by shifts to more D-depleted isotopic compositions (Table 3.1). The $\delta D_{K37}$ of the Mediterranean strains shifted ~20‰ lighter in stationary phase. While the $\delta D_{K37}$ of the N-limited Norwegian strain was ~4‰ lighter than in log phase, the P-limited treatment was lighter by more than 50‰.

Combining these results with previously-published culture data (Schouten et al. 2006; Wolhowe et al. 2009; M'boule et al. 2014), a body of data from experiments with the major oceanic alkenone-producers, within a narrow range of growth salinities, is available with which we may evaluate isotopic and chemical trends. The one consistent observation is that for log-phase cells, a decreasing relationship exists between $\alpha_{K37}$ values and $q_{K37}$ or alkenone production rate (where available; Figure 3.1A-B). Stationary-phase samples either fall along the log-phase $\alpha_{K37}$ vs. $q_{K37}$ trajectory or appear to lose functionality between at values higher than ~2 pg $cell^{-1}$. The trend with alkenone production rate applies over a temperature range of 15 to 25°C, to multiple

strains of both *E. huxleyi* and *G. oceanica*, and to calcifying and non-calcifying cultures; the trend with $q_{K37}$ applies additionally to log-phase, late-log 'transition phase' and stationary-phase cells. Data for the log-phase Mediterranean and Norwegian strains of *E. huxleyi* extend a relationship between $\alpha_{K37}$ and $q_{K37}$ that is observed in the previously-published results. Furthermore, stationary-phase samples from these cultures confirm that, upon entering senescence, shifts occur towards higher $q_{K37}$ (Prahl et al. 2003, Chivall et al. 2014a) and lower $\alpha_{K37}$ (Wolhowe et al. 2009 and Chivall et al. 2014b).

Other, previously-described physiological controls on $\alpha_{K37}$ do not appear to be as robust. Comparing $\alpha_{K37}$ to growth rate for all log-phase samples, weak trends are observed within individual data sets but no overall dependence on $\mu$ is seen (Figure 3.1C). Likewise, while data for the Norwegian and Mediterranean strains of *E. huxleyi* are roughly consistent with the overall relationships previously observed between $\alpha_{K37}$ and growth temperature (Wolhowe et al. 2009; Schouten et al. 2006), the range of $\alpha_{K37}$ values at individual temperatures is nearly that of the full data set (Figure 3.1D).

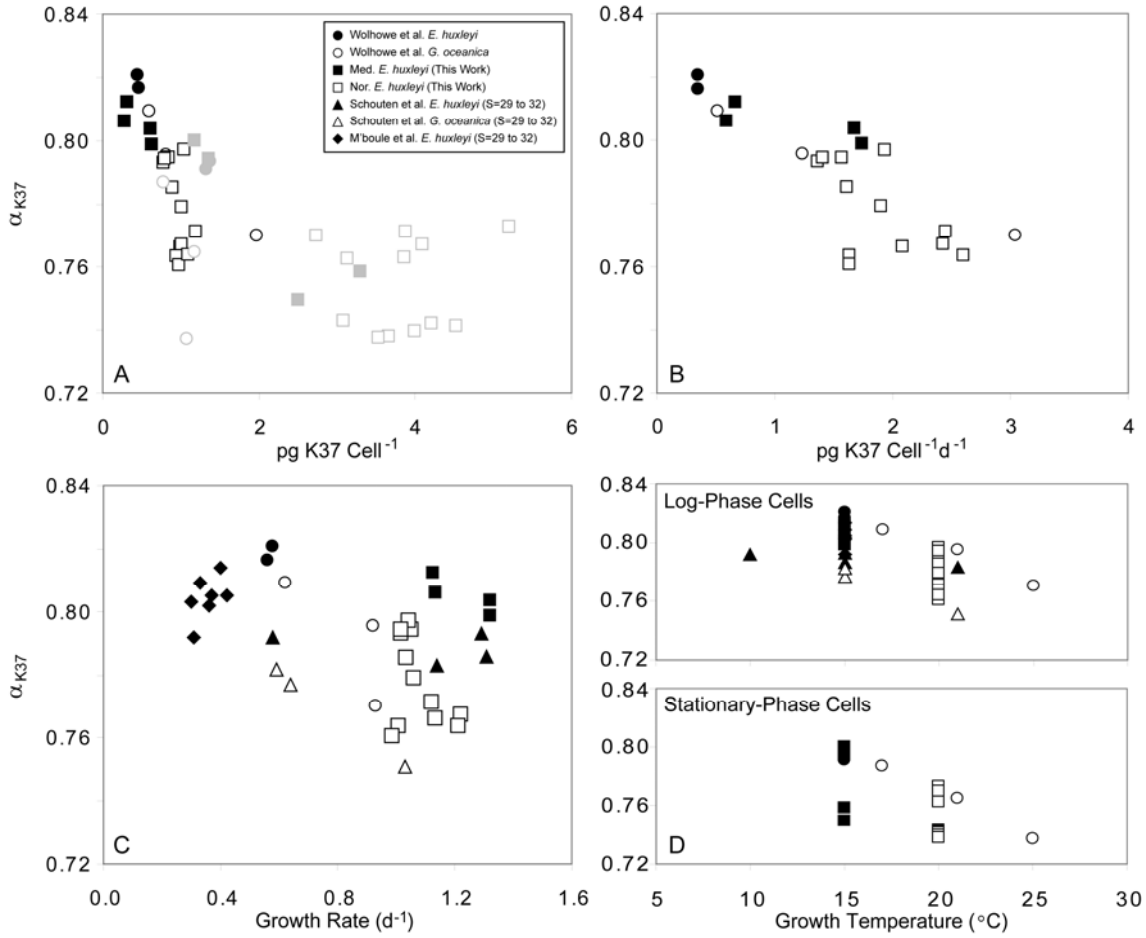


**Figure 3.1.** Compiled experimental culture results for oceanic alkenone producers. In **A**, $\alpha_{K37}$ measured in culture (Table 3.1) is plotted as a function of the alkenone cell abundance $q_{K37}$ ($q_{K37}$ not available for Schouten et al. or M'boule et al. data); black symbols represent log-phase samples and grey symbols represent stationary-phase samples or, in the case of the Wolhowe et al. 2009 *G. oceanica* data, late-log 'transition phase'. $\alpha_{K37}$ is plotted versus alkenone production rate (log-phase samples only) in **B**, versus exponential growth rate μ in **C**, and versus growth temperature in **D**. Note that only data from the salinity range of ~29-32 are displayed from Schouten et al. (2006) and M'boule et al. (2014) in **C** and **D**. Growth temperature relationships are split into log-phase (upper) and stationary-phase (lower) panels in **D**.

3.3.2 Interpretation of Culture Data

*3.3.2.1. Alkenone Production Rates and Potential Growth Rate Controls*

There are multiple potential explanations/ramifications for an overarching control of cellular alkenone abundance or production rate on $\alpha_{K37}$. If alkenone abundance, via some mechanism, controls $\alpha_{K37}$, this would tie $\alpha_{K37}$ behavior in log-phase cells to the reduction in $\alpha_{K37}$ associated with stationary growth phase (Wolhowe et al. 2009; Chivall et al. 2014b), during which $q_{K37}$ rapidly increases (Prahl et al. 2003; Wolhowe et al. 2009; Chivall et al. 2014a). This may also explain the previously-observed relationship of $\alpha_{K37}$ with growth rate. As described by Halsey et al. 2011, phytoplankton produce proportionally more lipids at higher growth rates. This has been observed explicitly for alkenone-producers *Isochrysis galbana* (Sukenik and Livine 1991) and *E. huxleyi* in culture (Fernández et al. 1996) and implicitly for *E. huxleyi* in the field (significant increase in per-cell lipid content associated with a subsurface production maximum; Fernández et al. 1994). Increased lipid loading is explained by Halsey et al. (2011) in terms of greater demand for polar membrane lipids – neutral storage lipids such as alkenones are not explicitly discussed. However, Fernández et al. (1994) reported unchanged proportions of polar and neutral lipids (predominantly alkenones in *E. huxleyi*; Eltgroth et al. 2005) despite the 2-fold change in lipids as a percent of carbon though the water column in their fjord study. Thus, it appears reasonable to extend the relationship between lipid content and growth rate to K37s.

If carbon-normalized lipid production rate, and thus lipid content, generally increase at higher growth rates, and if $\alpha_{K37}$ decreases at higher $q_{K37}$ and/or production rates (Figure 3.1A-B), this would explain both the observed dependence of net fractionation on growth rate (Schouten et al. 2006; M'boule et al 2014) and the lack of reproducibility of this response culture to culture (Figure 3.1C). There are presumably numerous factors (light intensity, nutrient availability, strain and species) that one may expect to alter the response of $q_{K37}$ to growth rate. Additionally, there are other reasons for which coccolithophore cells have been hypothesized to regulate their alkenone content, such as buoyancy control (e.g. Fernández et al. 1994). The *E. huxleyi* and *G. oceanica* cultures for which $q_{K37}$ is available, for example, express increasing $q_{K37}$ with

increasing growth rate individually (Table 3.1), but there is no overall relationship. Unfortunately, the only other $\alpha_{K37}$ literature reporting $q_{K37}$ values, that of Chivall et al. (2014b), is from coastal, low-salinity species, and not directly comparable due to the use of salinity treatments and the lack of variability in growth rate. We suggest that $q_{K37}$ values be reported in subsequent literature on this topic.

We still require an explanation, though, for why $q_{K37}$ or alkenone production rate should relate to net fractionation in the first place. Wolhowe et al. (2009) suggest that increased production of acetogenic lipids (i.e. alkenones) at the expense of significantly more-fractionated isoprenoidal structural lipids (i.e. Chikaraishi et al. 2004a) might, by mass balance, be expected to result in an isotopically-lighter acetogenic lipid pool. However, as Chikaraishi et al. (2004a) suggest the more-negative δD observed in isoprenoid lipids is due to fractionation during hydrogenation steps, this seems unlikely. An explanation that has been proposed for the phase-dependence of $\alpha_{K37}$ by Chivall et al. (2014b) is that the balance between photosynthetic rate and the exchange time of intracellular water controls internal $\delta D_{H2O}$ and, ultimately, $\delta D_{K37}$, due to the D-enriching effect of NADPH production. Thus, as photosynthetic NADPH production increases, a 'Rayleigh-like' decrease in expressed fractionation should occur as either the water pool available for reduction of NADP, or the NADPH pool itself, is more completely consumed. This is a compelling mechanism, as it would provide a way in which the well-established salinity effect (e.g. Schouten et al., 2006; Chivall et al. 2015b; M'boule et al. 2014) could impact $\alpha_{K37}$ (via changes in cell wall permeability altering the residence time of intracellular water). Furthermore, it would explain the anti-correlation of $\alpha_{K37}$ and $q_{K37}$ across growth phases (stationary phase cells have increasing $q_{K37}$ despite an overall reduction in photosynthetic rate). However, it would not explain the trend of decreasing $\alpha_{K37}$ at higher values of $q_{K37}$ or higher alkenone production rates during log-phase growth; as alkenone and/or lipid production increases in log-phase cells, more complete, fractionating utilization of the NADPH or water pools would be predicted to generate an increasing relationship, if any. Regardless of what link may exist between photosynthetic rate and $\alpha_{K37}$, no relationship is observed between $\alpha_{K37}$ and estimated cell-specific net organic carbon production or daily irradiance (Table 3.1),

suggesting any such mechanism does not play a major role in log-phase, light-saturated cells.

A more suitable explanation for a control of $q_{K37}$ on $\alpha_{K37}$ may be an increased roll of reductant (NADPH) derived from the oxidative pentose phosphate (OPP) pathway at higher rates of lipid synthesis. The hydrogen in lipids such as alkenones derives from NADPH, incorporated during both the formation of glyceraldehyde 3-phosphate and during subsequent chain elongation (Chikaraishi et al. 2004a,b). High rates of reductant (NADPH) production via increased OPP pathway activity, in order to support high rates of lipid synthesis, have been proposed as mechanism for the rapid turnover of carbohydrates in fast-growing phytoplankton (Halsey et al. 2011). The redox-active hydrogen that is abstracted from glucose and ribulose 5-phosphate to form NADPH during processing of starch in the OPP pathway (e.g. Fan et al. 2014) may have a very different isotopic composition than that in NADPH produced by the photosystem (Zhang et al. 2009a). This mechanism was invoked by Romero-Viana et al. (2013) as a reason why D-enrichment of alkenones might occur higher growth rates. This hypothesis is based, however, on studies of higher plants in which long-lived starch/cellulose pools are shown to be D-enriched, presumably as a result of heterotrophic processing (Luo and Sternberg 1991; Sessions 2006). NADPH derived from these enriched starch pools appears to lead to enriched lipid compositions in plants with high respiration rates (e.g. Sessions 2006). Alkenones, however, appear to be produced in the chloroplast (Eltgroth et al. 2005), where Luo and Sternberg (1991) observe the synthesis of highly D-depleted starch and where Sessions (2006) proposes that synthesis of light carbon products occurs due access to the D-depleted "immediate products of photosynthesis". If the substrate for the OPP pathway in the chloroplast is already highly depleted relative to cell water, then the abstraction of isotopically-light hydrogen from this starch pool via OPP activity (e.g. Hayes et al. 2001) should result in even further-depleted NADPH. Greater contributions of NADPH derived from this process, as opposed to directly from photosynthesis, should thus lead to more isotopically-light (lower $\alpha_{K37}$) lipids.

If this mechanism (broadly, changing use of NADPH pools or sources at higher rates of lipid synthesis) is indeed responsible, it may also explain the shift to lower $\alpha_{K37}$

values in nutrient-induced stationary growth phase. High catabolic losses of newly-synthesized carbon in stationary-phase plankton cells have been recognized by multiple authors (Ryther 1954; Li and Harrison 1982; Lancelot and Mathot 1985), and the high OPP pathway activity associated with high growth rates (see above) is also associated with stationary-phase cells (see Halsen and Jones 2014 for review). Lipids produced under these conditions would also, theoretically, have relatively depleted isotopic compositions. This explanation would provide mechanistic continuity for $\alpha_{K37}$ through batch-culture (or bloom) progression, in place of a bimodal 'growth-phase effect' (Wolhowe et al. 2009). Regardless of mechanism, the loss of $\alpha_{K37}$ functionality with $q_{K37}$ at high values (>2 pg cell$^{-1}$; Figure 3.1A) is presumably due to these cells not being at steady state with respect to their alkenone content, and the length of time spent in stationary phase, as opposed to production rate, thus controls $q_{K37}$.

*3.3.2.2. Potential Secondary Temperature Controls*

If growth rate impacts $\alpha_{K37}$ via changes in alkenone production rate, it is possible that what appears to be a secondary effect of temperature on $\alpha_{K37}$ (Figure 3.1D) is, in fact, related to a tendency towards higher growth rates at higher temperatures. However, the set of experiments expressing the most distinct 'temperature effect', the *G. oceanica* cultures reported in Wolhowe et al. (2009), show no appreciable difference in growth rate between the 21 and 25°C treatments (Table 3.1). Conversely, while the *E. huxleyi* temperature treatments of Schouten et al. (2006) show a large change in growth rate between 10 and 15°C degrees, very little change in $\alpha_{K37}$ is observed. Additionally, variation in $\alpha_{K37}$ with growth temperature is still evident in stationary phase cells (Figure 3.1D).

Direct dependence of $\alpha_{K37}$ on $U_{37}^{K'}$, via isotopic offsets between K37:3 (lighter) and K37:2 (heavier) (e.g. D'Andrea et al. 2007), has been ruled out as a mechanism for previously-reported $\alpha_{K37}$ vs. temperature relationships, as the $\alpha_{K37}$ vs. temperature slope is the wrong direction (Wolhowe et al. 2009) and $\delta D_{K37}$ is thought to be insensitive to changes in the relative proportions of the two compounds (van der Meer 2013). This is

presumed to be due to consumption of the K37:2 pool to create K37:3 (Popp et al. 2006; Rontani et al. 2006); 'Rayleigh-like', fractionating consumption of K37:2 to form K37:3 in a closed system would generate the observed, exponentially increasing isotopic offset between the two compounds at lower temperatures (lower $U_{37}^{K'}$, higher degrees of conversion; van der Meer 2013). The trend in K37:2-K37:3 offsets defined by previously-compiled culture data (van der Meer et al. 2013), however, converges on negative values (K37:3 isotopically heavier than K37:2), inconsistent with fractionation occurring solely during the desaturation of K37:2 to form K37:3. Another process that could A) generate variable isotopic offsets between these two K37 compounds and B) alter the K37:2 vs K37:3 mass balance, leading to 'temperature effects' on $\alpha_{K37}$, is the presence of differential consumption rates for K37:2 and K37:3. While Pan and Sun (2011) show that consumption of alkenones by *E. huxleyi* in carefully conducted, axenic cultures during extended periods of darkness appears to be a 1$^{st}$ order process that does treat the two compounds selectively, there is the possibility of preferential degradation of K37:3 by bacteria with consumption mechanisms that are dependent on degree of unsaturation (e.g. Rontani et al. 2008). This is potentially a concern in many laboratory and field settings (Rontani et al. 2013). Preferential, fractionating consumption of the more-unsaturated K37:3 could drive both increases in $\alpha_{K37}$ and sign reversals in $\delta D_{K37:2}$ - $\delta D_{K37:3}$. This mechanism could be tested by monitoring $U_{37}^{K'}$ and $\delta D_{K37}$ though the night or through extended dark periods in both axenic and non-axenic cultures, and may explain the different responses of $\alpha_{K37}$ to temperature in different culture experiments (Figure 3.1D). As a potentially simpler explanation, Zhang et al. (2009b) propose that multiple isoenzymes with different temperature tolerances and fractionation factors are employed in alkenone synthesis, though this has yet to be investigated.

*3.3.2.3. Summary*

The compiled culture data presented here shows that alkenone isotopic composition is best described by cellular alkenone abundance or production rate. A potential mechanism for this dependence is enhanced use of alternate NADPH sources at

high lipid production rates or when cells enter stationary phase. A mechanism of this sort would explain the observed, but inconsistent, dependence of $\alpha_{K37}$ on growth rate and growth stage. Future experiments will be required to determine whether the empirical relationship between $\alpha_{K37}$ and $q_{K37}$ indeed represents a dependence of $\alpha_{K37}$ on alkenone production and/or the pathway of reductant formation. For example, a carbon-labeled 'pulse-chase' experiment, of the sort conducted by Halsey et al. (2011), but analyzed on a compound-specific basis, would potentially allow one to assess this by determining whether $\alpha_{K37}$ shows a dependence on polysaccharide turnover rate.

While there is also abundant evidence for temperature dependence in the existing culture data, it appears that, in general, we should expect to observe lower $\alpha_{K37}$ values in cells that are A) growing very rapidly or B) are not growing at all due to nutrient limitation. These predictions have diametrically opposing ecological implications if we are to examine field data in this interpretive framework. We must, then, examine $\alpha_{K37}$ behavior in a natural water column.

### 3.3.3 Gulf of California/ETNP *in situ* Observations and Interpretation

#### *3.3.3.1. Response of $\alpha_{K37}$ to Proposed Physiological Controls*

Given an interpretive framework based on culture experiments, we now examine the *in situ* $\alpha_{K37}$ values from the Gulf of California and ETNP. The data show high variability (Table 3.2), and values at a given station generally decrease with depth (Figure 3.2). On the whole, the decrease with depth is remarkably robust (Figure 3.3A), with the only noticeable outliers being samples from station 4-12 in the ETNP, a station significantly cooler than the others and with a surface chlorophyll maximum rather than a DCML (White et al. 2013; Wolhowe et al. 2014). Can this pattern be explained in terms of the dynamics observed in culture? Variables that A) may be expected to change with depth in the GoCal and with distance north in the ETNP and B) have been proposed to control $\alpha_{K37}$ include temperature (Wolhowe et al. 2009; Zhang et al. 2009b, Figure 3.1D) and composition of the alkenone-producing assemblage (*E. huxleyi* vs. *G. oceanica*; Schouten et al. 2006). The composition of the alkenone-producing assemblage does vary systematically with temperature here, between ~100% *G. oceanica* at 30°C

and ~100% *E. huxleyi* at 15°C (Figure 3.3B). However, the trend of lower $\alpha_{K37}$ in colder, higher *E. huxleyi*-percentage waters opposes the report of lower $\alpha_{K37}$ values in *G. oceanica* (Schouten et al. 2006). Temperature itself is a predictive variable in this data, but, even if temperature does have a direct control on $\alpha_{K37}$ (which, as discussed above, is unclear), the direction of the relationship in Figure 3.3B (positive) opposes previously-reported temperature effects (negative).

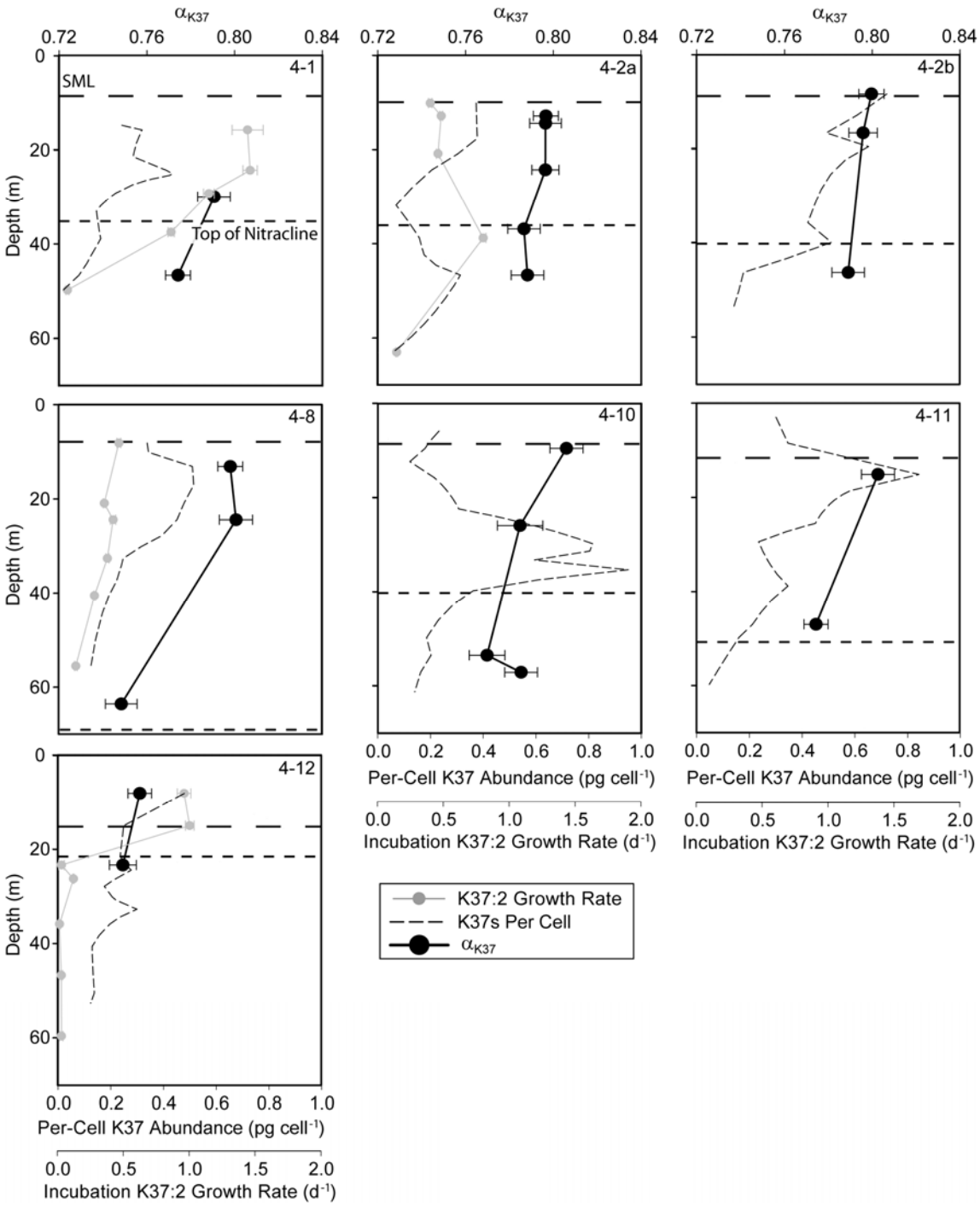
$\alpha_{K37}$
0.72
0.76
0.80
0.84
4-1
SML
Top of Nitracline
4-2a
4-2b
4-8
4-10
4-11
4-12
Depth (m)
0
20
40
60
0.0
0.2
0.4
0.6
0.8
1.0
Per-Cell K37 Abundance (pg cell$^{-1}$)
0.0
0.5
1.0
1.5
2.0
Incubation K37:2 Growth Rate (d$^{-1}$)
K37:2 Growth Rate
K37s Per Cell
$\alpha_{K37}$

**Figure 3.2.** Alkenone isotopic composition ($\alpha_{K37}$) relative to estimated *in situ* $\delta D_{H2O}$ (Section 3.2.4.3) from SPM filters taken in the Gulf of California and ETNP (Table 3.2). Per-cell K37 abundance is taken from Wolhowe et al. (2014) and is calculated from separate profiles of alkenone-producing cell abundance and suspended K37 concentration. Growth rates, estimated from K37:2 turnover in labeled incubations, are calculated via Equation 3.3.1 using turnover rate data from Wolhowe et al. (2014). Also shown are the average mixed layer (long dash) and nitracline (short dash) depths reported by Wolhowe et al. (2014).

Figure 3.1A suggests we may see a functional relationship between $\alpha_{K37}$ and $q_{K37}$. No correlation is observed, though, between $\alpha_{K37}$ and the previously-reported $q_{K37}$ values for our field samples (Figure 3.3C), though it is possible that any underlying trends are obfuscated by variations in species/size composition of the alkenone-producing assemblage. Wolhowe et al. (2014) report alkenone production rate profiles coincident with the collection of a number of these $\alpha_{K37}$ samples, providing another basis for comparison of our field and culture results. Estimates of the exponential growth rate, μ, can be calculated from the K37:2 turnover rates ($TR_{K37:2}$) reported in Wolhowe et al. (2014). Assuming cellular K37:2 concentrations are approximately at steady state (no change in $q_{K37}$) over incubation time t, μ is given by:

$$\mu = \frac{-1.025 * \ln(1 - t * TR_{K37:2})}{t} \qquad \textbf{3.3.1}$$

Weak trends are observed with both alkenone-producer growth rate and per-cell alkenone production rate (Figure 3.3C-D), but the observed functionality opposes the demonstrated dependencies on either growth rate alone (Schouten et al. 2006) or alkenone production rate (Figure 3.1B). Given the highly nutrient-stratified nature of the summertime GoCal and ETNP (Wolhowe et al. 2014), it is possible that near-surface cells were in nutrient-limited stationary phase, and thus that $q_{K37}$ was not at steady state. If this were the case, labeled growth rate estimates would be unreliable and $q_{K37}$ would theoretically lose its functionality with $\alpha_{K37}$ (i.e. Figure 3.1A). The growth-phase effects demonstrated in culture (Wolhowe et al. 2009; Chivall et al. 2014b) would lead us, in this case, to expect low $\alpha_{K37}$ values near the surface, where nutrient depletion and high light should lead to nutrient stressed physiology. Again, the trend towards lower values of $\alpha_{K37}$ at depth (Figure 3.3A) opposes this expectation.

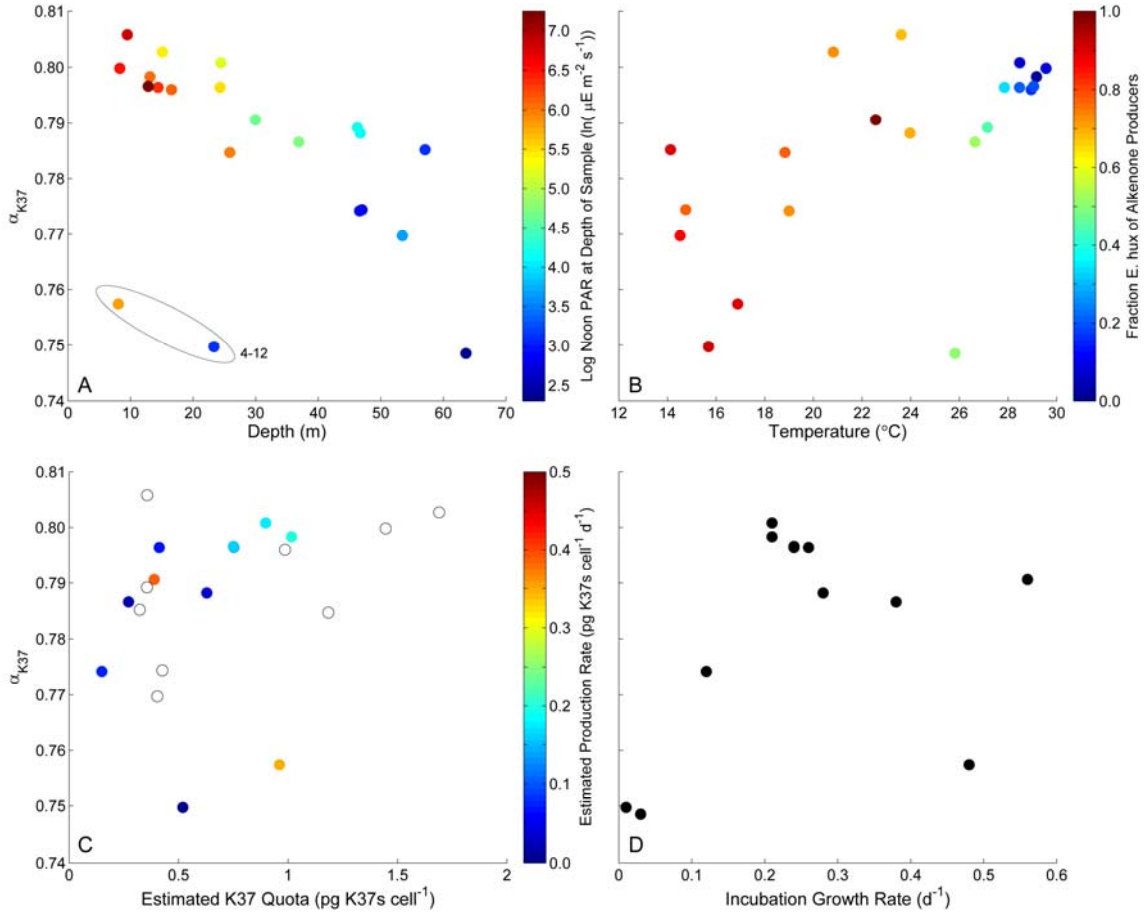


**Figure 3.3.** *In situ* $\alpha_{K37}$ from the Gulf of California and ETNP stations (Table 3.2). Data plotted as a function of **A**) collection depth and the noon PAR at that depth (natural log scale); **B**) temperature and the composition of the alkenone-producing community (fractional *E. huxleyi* abundance of *E. huxleyi* + Gephyrocapsa sp.); **C**) estimated per-cell K37 abundance ($q_{K37}$) and, where available, per-cell K37 production rate estimated from the labeled incubations of Wolhowe et al. (2014); and **D**) alkenone-producer growth rate (Section 3.3.3.1) estimated from these incubations where available. Community composition, per-cell production rate, $q_{K37}$, and growth rate profiles were linearly interpolated to the depths of the alkenone *in situ* filter samples. Uncolored symbols in plot **C** are data from all stations at which rate data is not available (4-2b, 4-10, 4-11); the 57m sample from station 4-10 is also absent from this plot as $q_{K37}$ data was not available. The data from station 4-12 is indicated in **A** as per the discussion in Section 3.3.3.1.

As described above, the hypothesis of Chivall et al. (2014b) that photosynthetic rate controls $\delta D_{K37}$ does not appear likely to explain available culture data. However, all of these data are taken from light-saturated cultures. Light is another depth-dependant parameter for our field samples, and the water-column data here appears to show a dichotomy between samples collected above and below mid-day PAR values of ~100 μE $m^{-2}$ $s^{-1}$, (Table 3.2; ln(PAR) ≈ 4.6 on Figure 3.3A color axis). *E. huxleyi* reaches its light-saturated growth rate maximum at ~70 μE $m^{-2}$ $s^{-1}$ (Bleijswijk et al. 1994). The simplest explanation for the depth-dependant decrease in $\alpha_{K37}$ in our study area may, then, be a dependence on irradiance or photosynthetic rate. If so, the implication is that there are differences in $\alpha_{K37}$ behavior between light-limited and nutrient-limited cells, and that the physiological drivers discussed in Section 3.3.2 for nutrient-limited cells have less impact in this study area. Is photosynthetic enrichment of cell water by NADPH formation a reasonable mechanism though?

Assuming an $\alpha_{K37}$ value of 0.78 (the approximate median of data in Figures 3.1 and 3.3), a ~50‰ shift in intercellular water would be required to generate the observed range of $\delta D_{K37}$ values (~-180‰ to -220‰). If we assume a fractionation factor between water and NADPH of 0.83 (estimate from *Lemna gibba* L under autotrophic growth conditions; Yakir and DeNiro 1990), 25% of the intracellular water-bound hydrogen pool would have to consumed and bound in organic matter to generate a $\delta D_{H2O}$ shift of this magnitude. This estimate does not even allow for exchange of water across the cell membrane, which would drive cell water back towards the external isotopic composition. For perspective, a cell with 5 pg of organic carbon would contain ~0.7 pmoles organic hydrogen and ~12 pmoles water-bound hydrogen, assuming empirical C:H:O ratio 1:1.7:1 for phytoplankton biomass (Hedges et al. 2002) and a cell that is ~90% water by mass. Removing 25% of this water-H pool into biomass would be sufficient to synthesize the cell ~4 times over, even assuming that every biomass-bound H in the cell is non-exchangeable (e.g. all lipids, no carbohydrates). Therefore, it seems unlikely that the $\delta D_{K37}$ shifts seen in culture and in our field samples are caused by a control of photosynthetic rate directly on $\delta D_{H2O}$.

*3.3.3.2. Alternate Assessment of $\alpha_{K37}$ Relationship to Growth Rate*

On the whole, the field data does not appear to meet our expectations, from culture, of $\alpha_{K37}$ dependence on $q_{K37}$ or alkenone production. There are potential pitfalls, however, in comparing alkenone abundance profiles collected by Nisken bottle, cell abundance profiles collected on different casts, rate estimates from 24-hour, free-floating fixed-depth incubations, and $\delta D_{K37}$ measurements from multi-hour *in situ* pump deployments, all collected at different times across ~36 hours of station occupation and with low depth-resolution (White et al. 2013; Wolhowe et al. 2014). If coccolithophore growth at these stations is balanced by grazing losses, the alkenone turnover rates reported by Wolhowe et al. (2014) (~0.1 to 0.4 $d^{-1}$ at the depths of our isotopic samples) imply the alkenone pool turns over on a time scale of 2-10 days. Thus it may be problematic to compare (relatively) instantaneous production rate measurements made at fixed water depths to isotopic information from a time-integrating alkenone standing stock with a potentially variable depth habitat and contributions from sinking, detrital material.

There is, however, a way to potentially assess growth rate on time and depth scales directly applicable to those represented by the δD of the K37 standing stock. An unexpected relationship is observed between $\alpha_{K37}$ and another physiological indicator, $\varepsilon_p$ (Figure 3.4A). This parameter, an estimate of the photosynthetic $^{13}C$ fractionation between aqueous $CO_2$ and phytoplankton biomass, is defined for coccolithophores via $\delta^{13}C_{K37:2}$ measurements as:

$$\varepsilon_p = \left( \frac{\delta^{13}C_{CO_2} + 1000}{\delta^{13}C_{K37:2} + \varepsilon_{cell-K37:2} + 1000} - 1 \right) * 1000 \qquad \textbf{3.3.2}$$

where $\varepsilon_{cell\text{-}K37:2}$ is an average offset between K37:2 alkenones and bulk cell carbon (4.2‰) proposed by Popp et al. (1998b). Natural-abundance $\delta^{13}C_{CO2}$ and $\delta^{13}C_{K37:2}$ (Appendix B) were determined in the course of Wolhowe et al.'s (2014) production rate experiments, allowing us to calculate $\varepsilon_p$ (Table 3.2). Alkenone $^{13}C$ fractionation is the subject of a considerable volume of literature concerning a relationship observed between $\varepsilon_p$ and $\mu/[CO_2]$ (see Pagani 2014 for review). While the $\varepsilon_p$ behavior has been

shown to be increasingly complicated in recent years, $\varepsilon_p$ for certain species, including *E. huxleyi*, appears to have linear functionality with $(\mu/[CO_2])$*(volume/surface area) of the form:

$$\varepsilon_p = a\frac{\mu}{[CO_2]}\frac{V}{SA} + b \qquad \textbf{3.3.3}$$

where a and b are the constants -182 and 25.3, respectively (Popp et al. 1998a). Linearity appears to be maintained within the limited range of $(\mu/[CO_2])$*(V/SA) = 0 to ~0.08 kg μm $\mu mol^{-1}$ $d^{-1}$ (Popp et al. 1998a). At the depths associated with our $\delta D_{K37}$ measurements, $[CO_2]$ values (Appendix B) and instantaneous growth rate estimates (Table 3.2) range from ~ 10 to 16 μmol $kg^{-1}$ and ~0 to 0.56 $d^{-1}$, respectively. Assuming spherical coccolithophore cells of ~5 μm diameter (see Appendix B), $(\mu/[CO_2])$*(V/SA) estimates fall in the range of 0 to ~0.04 kg μm $\mu mol^{-1}$ $d^{-1}$, a range where $\varepsilon_p$ is well-described by this model. We should therefore be able to use $\varepsilon_p$ and $[CO_2]$ measurements to estimate growth rates corresponding exactly to the time period and depth range integrated by our $\delta D_{K37}$ data.

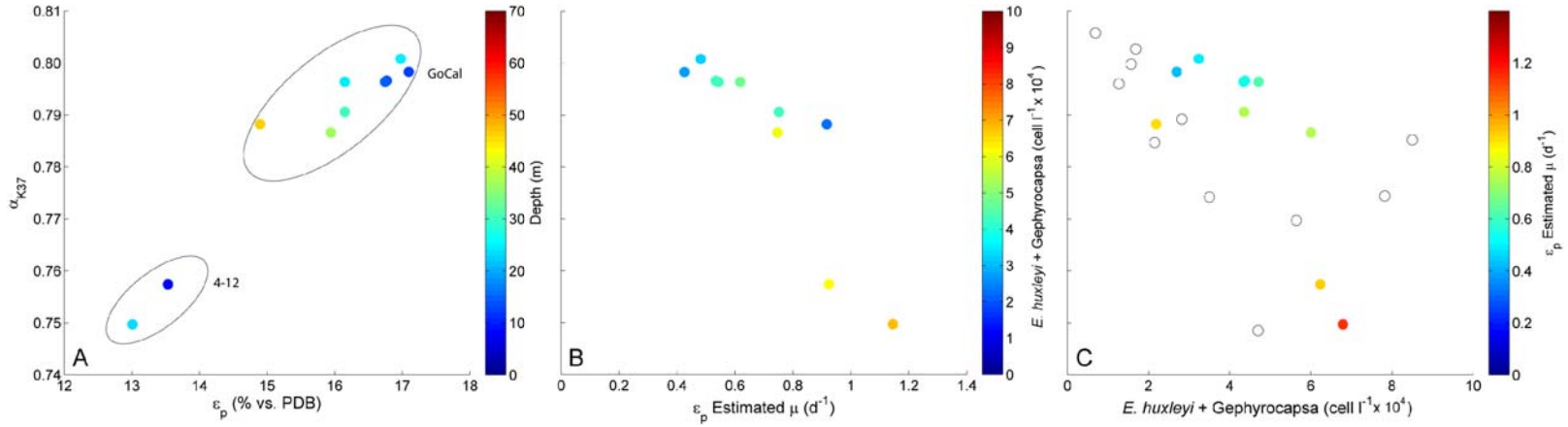


**Figure 3.4.** *In situ* $\alpha_{K37}$ from the Gulf of California and ETNP stations (Table 3.2) compared to **A**) carbon isotopic fractionation ($\varepsilon_p$, Equation 3.3.2) and depth; **B**) growth rate (μ), estimated from $\varepsilon_p$, via Equation 3.3.3 (see Section 3.3.3.2 and Appendix B); and **C**) and alkenone-producer cell abundance. The dependant variable of **B** is shown as the color axis in **C**, and vice versa. Uncolored symbols in plot **C** are data from all stations at which rate estimates are not available (4-2b, 4-10, 4-11). The annotations in **A** indicate the consistent decrease in $\varepsilon_p$ with depth in the GoCal and the offset decrease with depth at 4-12 in the ETNP.

When Equation 3.3.3 is solved for μ, estimates range from ~0.4 to 1.2 (Table 3.2). Higher growth rates are estimated for deeper (closer to the nitracline) samples; subsurface maxima in estimated $q_{K37}$ (Figure 3.2) near these depths may be consistent with the hypothesis of higher per-cell alkenone production at higher growth rates. There is, additionally, a clear negative relationship between these estimates and $\alpha_{K37}$ (Figure 3.4B), as is discussed for culture data in Section 3.3.2. This relationship in Figure 3.4B is data-sparse due to incomplete overlap of carbon-isotopic, hydrogen-isotopic, and $CO_2$ system measurements. However, cell abundance appears to be a rough indicator of growth rate here, as well; while necessarily weak because of the unquantified influence of grazing on phytoplankton standing stock, there is a broad association of higher $\varepsilon_p$-estimated growth rates with higher cell abundances (Figure 3.4C color axis). If higher cell abundances are generally indicative of higher time-integrated growth rates, the relationship observed between $\alpha_{K37}$ and cell abundance (Figure 3.4C) lends support to the relationship between $\alpha_{K37}$ and μ indicated in Figure 3.4.B.

The data presented here are sparse and from a single oceanographic setting; study of samples from other settings and production regimes (such as developing coccolithophore blooms, where growth status can be more objectively assessed) would be beneficial. Specifically, it would be informative to determine whether culture-predicted negative correlations between $\alpha_{K37}$ and $q_{K37}$ can be observed in cooler, better mixed settings like station 4-12 where the species assemblage is less variable.

## 3.4. Summary and Conclusions:

The trends observed in culture and *in situ* suspended material have indicated what physiological information environmental $\delta D_{K37}$ may convey, but not without complication. To summarize the culture component of this study:

1) We have observed that in nutrient-limited batch cultures with low narrow salinity ranges, $\alpha_{K37}$ appears to depend negatively on per-cell alkenone quota (Figure 3.1A) and associated production rate (Figure 3.1B) more than the previously-identified factors of growth rate or temperature.

2) We have proposed, as an explanation for these data, that cell quota effects on $\alpha_{K37}$ are due to increasing use of catabolic NADPH sources with increasing lipid synthetic demands. This mechanism explains the observed, but inconsistent, response of $\alpha_{K37}$ to growth rate. There is evidence that the secondary temperature effects observed in culture are not related to temperature-driven growth rate changes, though a satisfying alternate explanation is still lacking.

Field samples, limited by both nutrients and light from the summertime Gulf of California, were analyzed to determine whether the dynamics observed in culture could be observed in the natural environment. To summarize the investigation of the field samples:

1) $\alpha_{K37}$ was observed to decrease with depth, resulting in relationships with light availability (positive, Figure 3.3A), alkenone-producing cell abundance (negative, Figure 3.4C) and, unexpectedly, the carbon isotopic fractionation parameter $\varepsilon_p$ (positive, Figure 3.4A). The expected relationships with alkenone cell quota, temperature, growth rate estimated from *in situ* $^{13}C$ incubations were not observed. Using natural $^{13}C$ composition ($\varepsilon_p$) as an alternate means to assess coccolithophore growth rate on time- and depth-scales directly corresponding to our $\delta D_{K37}$ data, we observe a negative relationship of $\alpha_{K37}$ with growth rate (Figure 3.4B).
2) We have proposed two possible explanations for the observed $\alpha_{K37}$ data. First, there is a possibility that changes in light availability with depth control $\alpha_{K37}$, and that differences between the isotopic dynamics of light- and nutrient-limited cells trump the dynamics observed solely for nutrient-limited cells in culture. Alternately, we suggest that the $\varepsilon_p$-derived estimates of growth rate correspond better to the time- and depth-integrated physiological signals recorded in the alkenone standing stock than instantaneous, fixed-depth production rate measurements. If true, this implies that the depth-dependant decrease in $\alpha_{K37}$ is related to increased growth rates in proximity to the nitracline, and is consistent with the $\alpha_{K37}/\mu$ dynamics hypothesized to explain the culture data.

In the open ocean, salinity effects are minimal and the isotopic composition of water is relatively constrained. If alkenone-producer physiology exerts a control on $\alpha_{K37}$ such that its values provide information about light availability or growth rate in these settings, then $\delta D_{K37}$ may prove a powerful tool. If light truly does control $\alpha_{K37}$ in the field, then paleoceanographic assessment of $\alpha_{K37}$ may provide information about changes in surface vs. DCML production of coccolithophores in oceanographic settings susceptible to changes in stratification regime – information of use both in reconstructions of temperature (via $U_{37}^{K'}$) and of the marine carbon cycle. If $\alpha_{K37}$ is predictive of alkenone-producer growth rate, then $\alpha_{K37}$ estimates may allow us to overcome the major hurdle in alkenone-based paleo-$pCO_2$ reconstructions (the inability to constrain $\mu$) in addition to providing a coccolithophore-specific productivity proxy. Further work comparing $\alpha_{K37}$ to coccolithophore growth rate in the field may revitalize a paleoceanographic technique that has appeared unreliable (e.g. Pagani 2014) when constrained only by global scale, correlative estimates of growth rate (i.e. geochemical macronutrient proxies).

## 3.5. References


Adkins J.F. and Schrag D.P. (2003) Reconstructing Last Glacial Maximum bottom water salinities from deep-sea sediment pore fluid profiles. *Earth Plan. Sci. Lett.* **216**, 109-123.

Bleijswijk J.D.L.v., Kempers R.S., Veldhuis M.J. and Westbroek P. (1994) Cell and growth characteristics of type A and B of *Emiliania huxleyi* (Prymnesiophyceae) as determined by flow cytometry and chemical analyses. *J. Phycol.* **30**, 230-241.

Bollmann J. (1997) Morphology and biogeography of *Gephyrocapsa* coccoliths in Holocene sediments. *Mar. Micropaleontol.* **29**, 319-350.

Chikaraishi Y., Naraoka H. and Poulson S. R. (2004a) Carbon and hydrogen isotopic fractionation during lipid biosynthesis in a higher plant (*Cryptomeria japonica*). *Phytochem.* **65**, 323-330.

Chikaraishi Y., Suzuki Y. and Naroaka H. (2004b) Hydrogen isotopic fractionations during desaturation and elongation associated with polyunsaturated fatty acid biosynthesis in marine macroalgae. *Phytochem.* **65**, 2293-2300.

Chivall D., M'Boule D., Sinke-Schoen D., Sinninghe Damsté J.S., Schouten S. and van der Meer M.T.J. (2014a) Impact of salinity and growth phase on alkenone distributions in coastal haptophytes. *Org. Geochem.* **67**, 31-34.

Chivall D., M'Boule D., Sinke-Schoen D., Sinninghe Damsté J.S., Schouten S. and van der Meer M.T.J. (2014b) The effects of growth phase and salinity on the hydrogen isotopic composition of alkenones produced by coastal haptophyte algae. *Geochim. Cosmochim. Ac.* **140**, 381-390.

Christie W.W. (2003) *Lipid Analysis: Isolation, Separation, Identification and Structural Analysis of Lipids*. The Oily Press.

Coplen T.B., Wildman J.D. and Chen J. (1991) Improvements in the gaseous hydrogen-water equilibration technique for hydrogen isotope ratio analysis. *Anal. Chem.* **63**, 910-912.

Craig H. and Gordon L.I. (1965) Deuterium and oxygen 18 variations in the ocean and marine atmosphere. *In* E. Tongiorgi [ed.] *Stable Isotopes in Oceanographic Studies and Paleotemperatures*. Laboratorio di Geologia Nucleare, Pisa, Italy.

D'Andrea W.J., Liu Z., Alexandre M.D., Wattley S., Herbert T.D. and Huang Y. (2007) An efficient method for isolating individual long-chain alkenones for compound-specific hydrogen isotope analysis. *Anal. Chem.* **79**, 3430-3435.

Eltgroth M.L., Watwood R.L. and Wolfe G.V. (2005) Production and cellular localization of neutral long-chain lipids in the haptophyte algae *Isochrisis galbana* and *Emiliania huxleyi*. *J. Phycol.* **41**, 1000-1009.

Englebrecht A.C. and Sachs J.P. (2005) Determination of sediment provenance at drift sites using hydrogen isotopes and unsaturation ratios in alkenones. *Geochim. Cosmochim. Ac.* **69**, 4253-4265.

Epstein B.L., D'Hondt S. and Hargraves P.E. (2001) The possible metabolic role of $C_{37}$ alkenones in *Emiliania huxleyi*. *Org. Geochem.* **32**, 867-875.

Estep M.F. and Hoering T.C. (1980) Biogeochemistry of the stable hydrogen isotopes. *Geochim. Cosmochim. Ac.* **44**, 1197-1206.

Estep M.F. and Hoering T.C. (1981) Stable hydrogen isotope fractionations during autotrophic and mixotrophic growth in microalgae. *Plant. Physiol.* **67**, 474-477.

Fan J., Ye J., Kamphorst J.J., Shlomi T., Thompson C.B. and Rabinowitz J.D. (2014) Quantitative flux analysis reveals folate-dependent NADPH production. *Nature* **510**, 298-302.

Fernández E., Balch W.M., Marañón E. And Holligan P.M. (1994) High rates of lipid biosynthesis in cultured, mesocosm and coastal populations of the coccolithophore *Emiliania huxleyi*. *Mar. Ecol. Prog. Ser.* **114**, 13-22.

Fernández E., Fritz J.J. and Balch W.M. (1996) Chemical composition of the coccolithophorid *Emiliania huxleyi* under light-limited steady-state growth. *J. Exp. Mar. Bio. Ecol.* **207**, 149-160.

Halsey K.H. and Jones B.M. (2014) Phytoplankton strategies for photosynthetic energy allocation. *Annu. Rev. Mar. Sci.* **7**, 5.1-5.33.

Halsey K.H., Milligan A.J. and Behrenfeld M.J. (2011) Linking time-dependant carbon-fixation efficiencies in *Dunalielia tertiolecta* (Chlorophyceae) to underlying metabolic pathways. *J. Phycol.* **47**, 66-76.

Hayes J.M. (2001) Fractionation of the isotopes of carbon and hydrogen in biosynthetic processes, p. 225-227. *In* J.W. Valley and D.R. Cole [eds.], *Reviews in Mineralogy and Geochemistry 43, Stable Isotope Geochemistry.* The Mineralogical Society of America, Washington.

Hedges J.I., Baldock J.A., Gélinas Y., Lee C., Peterson M.L. and Wakeham S.G. (2002) The biochemical and elemental compositions of marine plankton: A NMR perspective. *Mar. Chem.* **78**, 47-63.

Herbert T.D. (2003) Alkenone paleotemperature determinations, p. 391-342. *In* K.K. Turekian and H.D. Holland [eds.], *Treatise on Geochemistry*, Vol. 6. Elsevier.

Horita J., Ueda A., Mizukami K. and Takatori I. (1989) Automatic δD and $\delta^{18}O$ analyses of multi-water samples using $H_2$- and $CO_2$-water equilibration methods with a common equilibration set-up. *Appl. Radiat. Isot.* **40**, 801-805.

Huang Y., Shuman B., Wang Y. and Webb III T. (2004) Hydrogen isotope ratios of individual lipids in lake sediments as novel tracers of climatic and environmental change: A surface sediment test. *J. Paleolimmol.* **31**, 363-375.

Lancelot C. and Mathot S. (1985) Biochemical fractionation of primary production by phytoplankton in Belgian coastal waters during short- and long-term incubations with $^{14}C$-bicarbonate I. Mixed diatom population. *Mar. Biol.* **86**, 219-226.

Langer G., Oetjen K. and Brenneis T. (2013) Coccolithophores do not increase particulate carbon production under nutrient limitation: A case study using *Emiliania huxleyi* (PML B92/11). *J. Exp. Mar. Bio. Eco.* **443**, 155-161.

Laws E.A., Popp B.N., Bidigare R.R., Kennicut M.C. and Macko S.A. (1995) Dependence of phytoplankton carbon isotopic composition on growth rate and $[CO_2]_{aq}$: Theoretical considerations and experimental results. *Geochim. Cosmochim. Ac.* **59**, 1131-1138.

Li W.K.W. and Harrison W.G. (1982) Carbon flow into the end-products of photosynthesis in short and long incubations of a natural phytoplankton population. *Mar. Biol.* **72**, 175-182.

Luo Y. and Sternberg L. (1991) Deuterium heterogeneity in starth and cellulose nitrate of CAM and C3 plants. *Phytochem.* **30**, 1095-1098.

Malinverno E., Prahl F.G., Popp B.N. and Ziveri P. (2008) Alkenone abundance and its relationship to the coccolithophore assemblage in Gulf of California surface waters. *Deep-Sea Res. Pt. I* **55**, 1118-1130.

Marlowe I.T., Green J.C., Neal A.C., Brassell S.C., Eglinton G. and Course P.A. (1984) Long chain (n-$C_{37}$-$C_{39}$) alkenones in the Prymnesiophyceae. Distribution of alkenones and other lipids and their taxonomic significance. *Brit. Phycol. J.* **19**, 203-216.

Martineau F., Fourel F., Bodergat A.-M. and Lécuyer C. (2011) D/H equilibrium fractionation between $H_2O$ and $H_2$ as a function of the salinity of aqueous solutions. *Chem. Geo.* **291**, 236-240.

M'boule D., Chivall D., Sinke-Schoen D., Sinninghe Damsté J.S., Schouten S. and van der Meer M.T.J. (2014) Salinity dependent hydrogen isotope fractionation in alkenones produced by coastal and open ocean haptophyte algae. *Geochim. Cosmochim. Ac.* **130**, 126-135.

Oviedo A.M., Langer G. and Ziveri P. (2014) Effect of phosphorus limitation on coccolith morphology and element ratios in Mediterranean strains of the coccolithophore *Emiliania huxleyi*. *J. Exp. Mar. Bio. Eco.* **449**, 105-113.

Pagani M. (2014). Biomarker-based inferences of past climate: The alkenone *p*CO2 proxy, p. 361-378. *In* H.D. Holland and K.K. Turekian and [eds.], *Treatise on Geochemistry*. 2nd Ed., Vol. 12. Elsevier.

Pahnke K., Sachs J. P., Keigwin L., Timmermann A. and Xie S. (2007) Eastern tropical Pacific hydrologic changes during the past 27,000 years from D/H ratios in alkenones. *Paleoceanography* **22**, doi:10.1029/2007PA001468.

Popp B.N., Bidigare R.R., Deschenes B., Laws E.A., Prahl F.G., Tanimoto J.K. and Wallsgrove R.J. (2006) A new method for estimating growth rates of alkenone producing haptophytes. *Limnol. Oceanogr.-Meth.* **4**, 114-129.

Popp B.N., Laws E.A., Bidigare R.R., Dore J.E., Hanson K.L. and Wakeham S.G. (1998a) Effect of phytoplankton cell geometry on carbon isotopic fractionation. *Geochim. Cosmochim. Ac.* **62**, 69-77.

Popp B.N., Kenig F., Wakeham S.G., Laws E.A. and Bidigare R.R. (1998b) Does growth rate affect ketone unsaturation and intracellular carbon isotopic variability in *Emiliania huxleyi*? *Paleoceanography* **13**, 35-41.

Prahl F.G., Muehlhausen L.A. and Zahnle D.L. (1988) Further evaluation of long-chain alkenones as indicators of paleoceanographic conditions. *Geochim. Cosmochim. Ac.* **52**, 2303-2310.

Prahl F.G. and Pinto L.A. (1987) A geochemical study of long-chain n-aldehydes in Washington coastal sediments. *Geochim. Cosmochim. Ac.* **51**, 1573-1582.

Prahl F.G., Wolfe G.V. and Sparrow M.A. (2003) Physiological impacts on alkenone paleothermometry. *Paleoceanography* **18**, doi:10.1029/2002PA000803.

Rohling E.J. (2007) Progress in paleosalinity: Overview and presentation of a new approach. *Paleoceanography* **22**, doi: 10.1029/2007PA001437.

Romero-Viana L., Kienel U., Wilkes H. and Sachse D. (2013) Growth-dependent hydrogen isotopic fractionation of algal lipid biomarkers in hypersaline Isabel Lake (México). *Geochim. Cosmochim. Ac*. **106**, 490-500.

Rontani J.-F., Prahl F.G. and Volkman J.K. (2006) Re-examination of the double bond positions in alkenones and derivatives: Biosynthetic implications. *J. Phycol.* **42**, 800-813.

Rontani J.-F., Harji R., Guasco S., Prahl F.G., Volkman J.K., Bhosle N.B. and Bonin P. (1998) Degradation of alkenones by aerobic heterotrophic bacteria: Selective or not? *Org. Geochem.* **39**, 34-51.

Rontani J.-F., Volkman J.K., Prahl F.G. and Wakeham S.G. (2013) Biotic and abiotic degradation of alkenones and implications for UK'37 paleoproxy applications: A review. *Org. Geochem.* **59**, 95-113.

Ryther J.H. (1954) The ratio of photosynthesis to respiration in marine plankton algae and its effect upon the measurement of productivity. *Deep-Sea Res.* **2**, 134-139.

Sachse D. and Sachs J.P. (2008) Inverse relationship between D/H fractionation in cyanobacterial lipids and salinity in Christmas Island saline ponds. *Geochim. Cosmochim. Ac.* **72**, 793-806.

Sauer P.E., Eglinton T.I., Hayes J.M., Schimmelmann A. and Sessions A. L. (2001) Compound-specific D/H ratios of lipid biomarkers from sediments as a proxy for environmental and climatic conditions. *Geochim. Cosmochim. Ac.* **65**, 213-222.

Schouten S., Ossebaar K., Schreiber K., Kienhuis M. V. M., Langer G., Benthien A. and Bijma J. (2006) The effect of temperature, salinity and growth rate on the stable hydrogen isotopic composition of long chain alkenones produced by *Emiliania huxleyi* and *Gephyrocapsa oceanica*. *Biogeosci.* **3**, 113-119.

Schwab V.F. and Sachs J.P. (2009) The measurement of D/H ratio in alkenones and their isotopic heterogeneity. *Org. Geochem.* **40**, 111-118.

Schwab V.F. and Sachs J.P. (2011) Hydrogen isotopes in individual alkenones from the Chesapeake Bay estuary. *Geochim. Cosmochim. Ac.* **75**, 7552-7565.

Sessions A. L., Burgoyne T. W., Schimmelmann A. and Hayes J. M. (1999) Fractionation of hydrogen isotopes in lipid biosynthesis. *Org. Geochem.* **30**, 1193-1200.

Sessions A.L. (2006) Seasonal changes in D/H fractionation accompanying lipid biosynthesis in *Spartina alterniflora*. *Geochim. Cosmochim. Ac.* **70**, 2153-2162.

Sukenik A. and Livine A. (1991) Variations in lipid and fatty-acid content in relation to acetyl CoA carboxylase in the marine prymnesiophyte *Isochrysis galbana*. *Plant Cell Physiol.* **32**, 371-378.

Thunell R.C., Pride C., Ziveri P., Muller-Karger F., Sancetta C. and Murray D. (1996) Plankton response to the physical forcing in the Gulf of California. *J. Plankton Res.* **18**, 2017-2026.

van der Meer M.T.J., Benthien A., Bijma J., Schouten S. and Sinninghe Damsté J.S. (2013) Alkenone distribution impacts the hydrogen isotopic composition of the $C_{37:2}$ and $C_{37:3}$ alkan-2-ones in *Emiliania huxleyi*. *Geochim. Cosmochim. Ac.* **111**, 162-166.

van der Meer M.T.J., Sangiorgi F., Baas M., Brinkhuis H., Sinninghe Damsté J.S. and Schoutan S. (2008) Molecular isotopic and dinoflagellate evidence for Late Holocene freshening of the Black Sea. *Earth Planet. Sc. Lett.* **267**, 426-434.

Verardo D.J., Froelich P.N. and McIntyre A. (1990) Determination of organic carbon and nitrogen in marine sediments using the Carlo Erba NA-1500 analyzer. *Deep Sea Res. Pt. I.* **37**, 157-165.

Volkman J.K., Barrett S.M., Blackburn S.I. and Sikes E.L. (1995) Alkenones in *Gephyrocapsa oceanica*: Implications for studies of paleoclimate. *Geochim. Cosmochim. Ac.* **59**, 513-520.

Volkman J.K., Eglinton G., Corner E.D.S. and Sargent J.R. (1980) Novel unsaturated straight-chain C37-C39 methyl and ethyl ketones in marine sediments and a coccolithophore *Emiliania huxleyi*, p. 219-227. *In* A.G. Douglas and J.R. Maxwell [eds.], *Advances in organic geochemistry, 1979: Proceedings of the Ninth International Meeting on Organic Geochemistry*. Pergamon Press.

Walinsky S.E., Prahl F.G., Mix A.C., Finney B.P., Jaeger J.M. and Rosen G.P. (2009) Distribution and composition of organic matter in surface sediments of coastal Southeast Alaska. *Cont. Shelf Res.* **29**, 1565-1579.

White A.E., Foster R.A., Benitez-Nelson C.R., Masqué P., Verdeny E., Popp B.N., Arthur K.E. and Prahl F.G. (2013) Nitrogen fixation in the Gulf of California and the Eastern Tropical North Pacific. *Prog. Oceanogr.* **109**, 1-17.

Winter A., Jordan R. and Roth P. (1994) Biogeography of living coccolithophores in ocean waters, p. 161-167. *In* A. Winter and W. G. Siesser [eds.], *Coccolithophores*. Cambridge University Press.

Wolhowe M.D., Prahl F.G., Probert I. and Maldonado M. (2009) Growth phase dependent hydrogen isotopic fractionation in alkenone-producing haptophytes. *Biogeosci.* **8**, 1681-1694.

Wolhowe M.D., Prahl F.G., White A.E., Popp B.N. and Rosas-Navarro A. (2014) A biomarker perspective on coccolithophorid growth and export in a stratified sea. *Prog. Oceanogr.* **122**, 65-76.

Yakir D. and DeNiro M.J. (1990) Oxygen and hydrogen isotope fractionation during cellulose metabolism in *Lemna gibba* L. *Plant Physiol.* **93**, 325-332.

Zhang Z. and Sachs J.P. (2007) Hydrogen isotope fractionation in freshwater algae: 1. Variations among lipids and species. *Org. Geochem.* **38**, 582-608.

Zhang X., Gillespie A.L. and Sessions A.L. (2009a) Large D/H variations in bacterial lipids reflect central metabolic pathways. *Proc. Nat. Acad. Sci.* **106**, 12580-12586.

Zhang Z., Sachs J.P. and Marchetti A. (2009b) Hydrogen isotope fractionation in freshwater and marine algae: II. Temperature and nitrogen limited growth rate effects. *Org. Geochem.* **40**, 428-439.

Ziveri P. and Thunell R.C. (2000) Coccolithophore export production in Guaymas Basin, Gulf of California: response to climate forcing. *Deep-Sea Res. II* **47**, 2073-2100.

Ziveri P., Thunell R.C. and Rio D. (1995) Seasonal changes in coccolithophore densities in the Southern California Bight during 1991-1992. *Deep-Sea Res. I* **42**, 1881-1903.

# 4. Core-Top and LGM Covariation of $U_{37}^{K'}$ and Alkenone D/H Fractionation in Sediments: Implications for Paleohydrology and the Study of Coccolithophore Ecology

Matthew D. Wolhowe, Fredrick G. Prahl, Alan C. Mix

Target journal identification pending.

**Abstract:** The chemical and hydrogen-isotopic composition of $C_{37}$ alkenones were measured in sediment samples along a transect of the North-American Pacific margin from ~42°N to the tip of Baja California. Both core-top and LGM intervals expressed a strong relationship between the temperature proxy $U_{37}^{K'}$ and the estimated alkenone D/H fractionation factor $\alpha_{K37}$. This relationship stands in opposition to previous work stating that temperature should have only a minor effect on $\alpha_{K37}$, and appears to be the dominant source of variability in $\alpha_{K37}$ in this marine setting. If $U_{37}^{K'}$ is a robust indicator of $\alpha_{K37}$ in areas of low salinity contrast, then $\delta D_{K37}$ may prove a more reliable hydrologic proxy in marine settings than previously suggested. It is argued, however, that in the absence of a theoretical mechanism for direct temperature dependence it is cellular growth rate, via mechanisms described in Chapter 3, that controls $\alpha_{K37}$ in these sediment samples; growth rate, in turn, may be controlled by temperature on these time scales. Regional deviations from the overall $\alpha_{K37}$ vs. $U_{37}^{K'}$ relationship are observed in core-tops at the northern and southern edges of the California/Oregon upwelling zone, and are tentatively identified as corresponding to locations where alkenone producers are subjected to nutrient deprivation before sedimentation due to the dominance of event-scale production. Disappearance of these deviations at the LGM is consistent with previous reconstructions of a northward retreat of the California Current and reduction in upwelling at this time. We propose that future pairing of $U_{37}^{K'}$ measurements with estimates of $\alpha_{K37}$ may provide valuable physiological context to studies of paleoecology.

## 4.1. Introduction

The hydrogen isotopic composition (δD) of $C_{37}$ alkenones, lipid biomarkers of the dominant species of coccolithophorid, prymnesiophyte algae in the modern ocean (Volkman et al. 1980, 1995; Marlowe et al. 1984), has been the subject of considerable recent research. With limited source organisms, a net fractionation factor, $\alpha_{K37}$, can theoretically be constrained by laboratory experiments (e.g. Englebrecht and Sachs 2005) and used to relate measured alkenone composition ($\delta D_{K37}$) with the composition of the water ($\delta D_{H2O}$) from which the compounds were synthesized (Equation 4.4.1).

Coupled with the paleotemperature proxy $U_{37}^{K'}$, an index defining the relative abundance of the dominant alkenone compounds K37:2 and K37:3 (see Herbert et al. 2003 for review; Equation 4.4.2), $\delta D_{K37}$ has been put forward as a paleoenvironmental proxy. It has been employed in inland seas (van der Meer et al. 2008; Vasiliev et al. 2014), estuarine systems (Schwab and Sachs 2011), and areas of high freshwater discharge (Pahnke et al. 2007) to reconstruct salinity and/or $\delta D_{H2O}$. The fractionation factor $\alpha_{K37}$ is not a constant, however, and in settings where changes in water composition are relatively small (i.e. most marine settings), physiological levers on $\alpha_{K37}$ are thought to dominate variability in $\delta D_{K37}$ (Wolhowe et al. 2009; Chapter 3).

$$\alpha_{K37} = \frac{\delta D_{K37} + 1000}{\delta D_{H2O} + 1000} \quad \textbf{4.4.1}$$

$$U_{37}^{K'} = \frac{[K37:2]}{[K37:2] + [K37:3]} \quad \textbf{4.4.2}$$

Factors that have been empirically or theoretically suggested to control $\alpha_{K37}$ include growth rate, growth phase, temperature, salinity, species and strain of alkenone producer, and light intensity (Schouten et al. 2006; Wolhowe et al. 2009; Zhang et al. 2009; Romero-Viana et al. 2013; Chivall et al. 2014; M'boule et al. 2014). In Chapter 3, we have proposed that, in the absence of strong changes in salinity, $\alpha_{K37}$ is primarily controlled by alkenone production rate, and that its response to these other variables is either minor (temperature) or due to their effects on this rate itself (growth rate and phase, light). It is argued that, in the field, this dependence manifests as a relationship between $\alpha_{K37}$ and growth rate; growth on the time- and depth-scales recorded by the alkenone standing stock, in turn, appears to be controlled by nutrient availability (Chapter 3). Greater net fractionation (smaller values of $\alpha_{K37}$ and more negative values of $\delta D_{K37}$) is observed for samples closer to the nitracline, which are suggested to be more productive, while less apparent fractionation (larger values of $\alpha_{K37}$ and less negative values of $\delta D_{K37}$) is observed for near-surface, low-nutrient samples. If this dynamic holds true across greater spatial and temporal scales, then $\delta D_{K37}$ has potential

utility as a proxy for mean ecological conditions, specific to coccolithophores, in the sedimentary record.

We predict, then, that sedimentary $\delta D_{K37}$ will vary with overlying nutrient availability and record changes in mean coccolithophore growth rate. Knowledge of coccolithophore growth rate could be of use for interpretation of the $U_{37}^{K'}$ proxy temperature record (which has been suggested to respond to nutrient stress effects; Prahl et al. 2003), for understanding particulate inorganic carbon (PIC) production and export (providing contextual information to measured accumulation rates in sediments), and for constraining the alkenone $^{13}C$ $pCO_2$ proxy (currently complicated by the inability to resolve growth rate effects; Pagani 2014).

To test whether $\alpha_{K37}$ varies in the sediment record in response to ecological changes, we must analyze $\delta D_{K37}$ in sediments where the isotopic signal is not driven by salinity gradients. A promising natural laboratory for work of this sort is the western margin of North America outside the influence of the Columbia River plume (Figure 4.1). Coccolithophore export appears tied to the spring transition and the onset of coastal upwelling in the northern portion of this region (Prahl et al. 1993), where upwelling of cold, nutrient-rich waters is associated with the California current system (CCS; Figure 4.1). Export is more year-round south of Point Conception (Thunell 1998), where upwelling is less seasonal. Year-round export is likely also the case in the warm, stratified waters of the Eastern Tropical North Pacific (ETNP) off of Baja (Figure 4.1), where coccolithophore production has been associated with subsurface chlorophyll maxima (Wolhowe et al. 2014), features that have been observed in all seasons (Espinosa-Carreón et al. 2012).

The gradient in upwelling behavior from the Oregon/California upwelling zone, through the complex oceanography of the southern California bight (SCB), to southern Baja and the eastern tropical north Pacific (ETNP) thus presents a range of alkenone production and export regimes. This area has also been subject to both core-top (Doose et al. 1997; Herbert et al. 1998) and down-core (Manglesdorf et al. 2000; Herbert et al. 2001) $U_{37}^{K'}$ surveys. At the last glacial maximum (LGM), a weakening of the CCS,

forced by changes in the North-Pacific High (Yamamoto et al. 2007) is argued to have reduced upwelling off the SCB and Baja and allowed warm, open-ocean waters to push inwards towards the coast (Herbert et al. 2001). This oceanographic shift, furthermore, is defined directly by $U_{37}^{K'}$ records, and is believed to be responsible for marked changes in the export of organic matter (Manglesdorf et al. 2000). Thus, there are potentially production/export contrasts with both space (north vs. south) and time (Holocene vs. LGM) against which we may compare $\alpha_{K37}$.

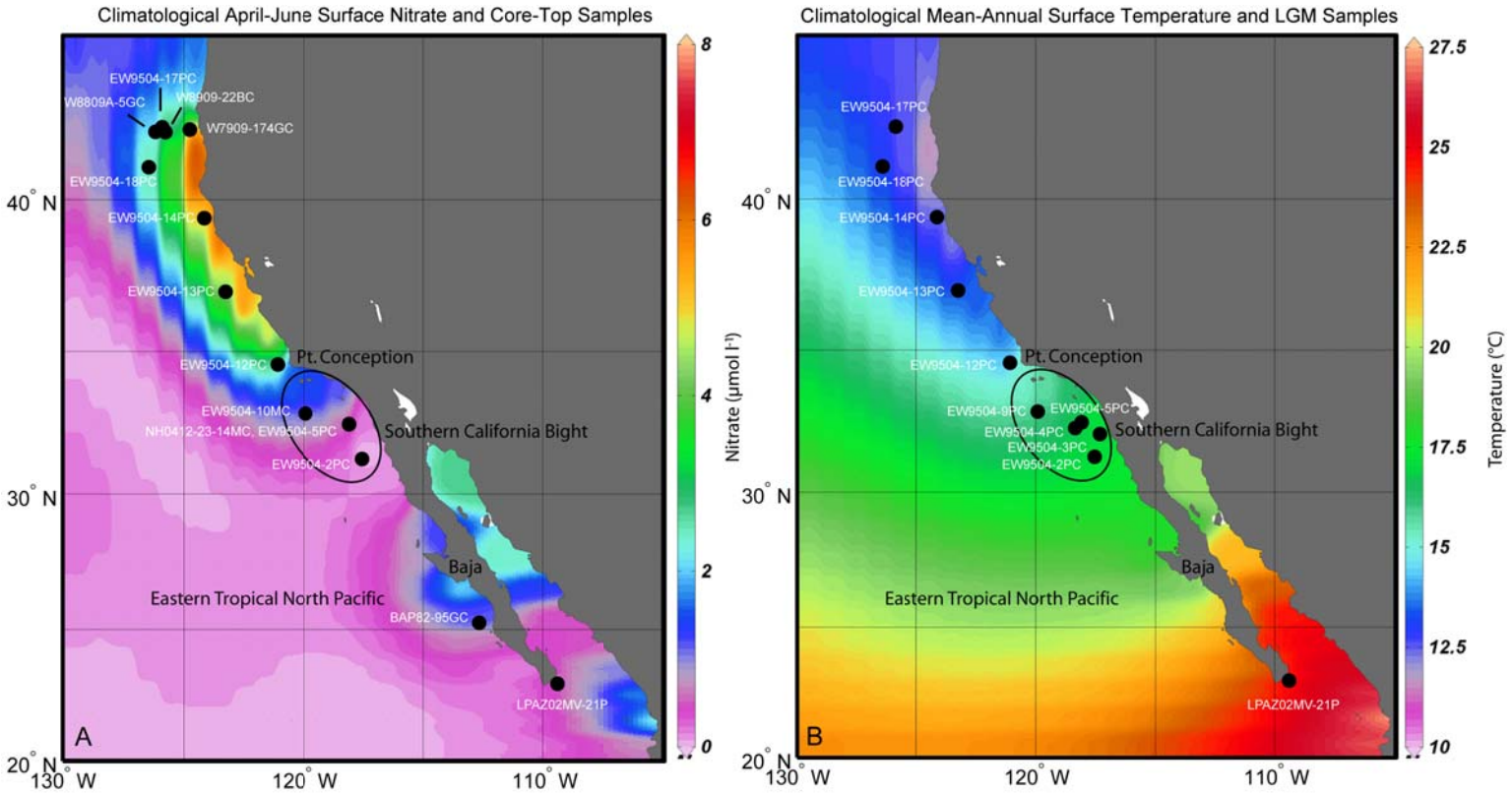


**Figure 4.1.** The study area, showing the locations of the core-top (**A**) and LGM (**B**) samples. Plot **A** (World Ocean Atlas 2013 climatological April-June surface nitrate concentration for the 1955-2012 period; Garcia et al. 2013) illustrates the difference in spring/summer upwelling behavior between the CCS, north of Point Conception, and the ETNP/Baja Coast. Plot **B** (WOA13 climatological 1955-2012 mean-annual surface temperature; Zweng et al. 2013) illustrates the oceanographic contrast between the CCS and waters to the south.

We predict that we will observe low $\alpha_{K37}$ values in core-top sediments under the northern portion of the modern North American margin, where mean-annual nutrient concentrations are higher and production is driven by large Spring/Summer upwelling events. Conversely, we hypothesize that higher values will be observed in the south, where summer stratification prevails and upwelling is much more spatially restricted. If this contrast appears, we hypothesize that the pattern will shift northward at the LGM, as upwelling weakened in SCB (Herbert et al. 2001). Alternately, we may see onshore-offshore gradients between more coastal (upwelling dominated) and open ocean (stratified) sites. To test these hypotheses, we have collected surface sediments along the margin (Figure 4.1), as well as LGM samples from a select number of these sites. By measuring $\delta D_{K37}$ and estimating surface-water isotopic composition using salinity (core-top) and planktonic foraminiferal $\delta^{18}O$ (glacial), we are able to present a first-of-its-kind survey of core-top and LGM $\alpha_{K37}$ data.

## 4.2. Methods

### 4.2.1 Cores, Sampling, and Existing Data

All cores sampled (Figure 4.1; Table 4.1 and Table 4.3) were stored at the Oregon State University core repository with the exception of LPAZ02MV-21P, samples of which were provided by Scripps Institute of Oceanography. Sampling and processing for determination of benthic (*Cibicides mckannai*) and planktonic (*Globigerina bulloides*) foraminiferal $\delta^{18}O$ for EW9504-2PC, -3PC, -4PC, -5PC, and -9PC are described in Stott et al. (2000). Previously-unpublished benthic $\delta^{18}O$ values from cores EW9504-12PC, -13PC, -14PC, -17PC, and -18PC (*Cibides wuellerstorfi* and *Uvigerina sp*.) and planktonic values from 17PC (*Neogloboquadrina pachyderma* L) were determined during the analysis of material associated with IODP leg 167 (Lyle et al. 2000) using the methods described in Mix et al. (1999), and are provided in Appendix C. Benthic values for LPAZ02MV-21P (mixed benthic species) were taken from Herbert et al. (2001). Sediment samples for alkenone quantification and isotopic analysis (~10 $cm^3$) were collected at ~1 cm core-top and down-core (Table 4.3) intervals and freeze dried prior to analysis.

**Table 4.1.** Core locations, alkenone compositional properties (Section 4.2.4), climatological hydrographic data (World Ocean Atlas 2013), estimated water isotopic composition (Section 4.2.5), and alkenone isotopic composition for the core-top transect.

**Table 4.1.** Surface Sediment Samples

| Core | Lat (°N) | Lon (°W) | Water Depth (m) | UK'37 | ± | K37s (μg $g^{-1}$ dry) | ± | UK'37 Temperature[a] (°C) | ± | maSST[b] (°C) | maSSS[b] | Estimated $\delta D_{H2O}$[c] (‰ vs. SMOW, ± 2) | $\delta D_{K37}$ (‰ vs. SMOW) | ± | $\alpha_{K37}$ | ± |
|---|---|---|---|---|---|---|---|---|---|---|---|---|---|---|---|---|
| LPAZ02MV-21P | 22.98 | 109.47 | 624 | 0.886 | 0.008 | 21.76 | 1.00 | 24.92 | 0.2 | 24.61 | 34.53 | 0.81 | -221.3 | 4.8 | 0.778 | 0.005 |
| BAP82-95GC | 25.29 | 112.72 | 410 | 0.735 | 0.015 | 28.82 | 1.17 | 20.46 | 0.4 | 20.77 | 34.03 | -0.71 | -215.9 | 5.0 | 0.785 | 0.005 |
| EW9504-2PC | 31.26 | 117.59 | 2042 | 0.618 | 0.018 | 3.54 | 0.14 | 17.03 | 0.5 | 17.07 | 33.52 | -2.24 | -201.1 | 2.3 | 0.801 | 0.003 |
| EW9504-5PC | 32.48 | 118.13 | 1818 | 0.606 | 0.019 | 11.21 | 0.44 | 16.69 | 0.5 | 16.71 | 33.53 | -2.21 | -208.5 | 5.0[e] | 0.793 | 0.005 |
| NH0412-23-14MC | 32.49 | 118.13 | 2012 | 0.606 | 0.019 | 7.92 | 0.31 | 16.67 | 0.5 | 16.71 | 33.53 | -2.21 | -215.6 | 0.9 | 0.786 | 0.002 |
| EW9504-10MC[d] | 32.86 | 119.96 | 1194 | 0.559 | 0.021 | 18.84 | 0.80 | 15.28 | 0.6 | 15.88 | 33.42 | -2.53 | -212.4 | 5.7 | 0.790 | 0.006 |
| EW9504-12PC | 34.55 | 121.11 | 938 | 0.548 | 0.020 | 3.96 | 0.16 | 14.97 | 0.6 | 14.47 | 33.34 | -2.77 | -203.0 | 3.7 | 0.799 | 0.004 |
| EW9504-13PC | 36.99 | 123.27 | 2510 | 0.498 | 0.020 | 3.72 | 0.14 | 13.49 | 0.6 | 13.30 | 33.17 | -3.27 | -200.6 | 3.9 | 0.802 | 0.004 |
| EW9504-14PC | 39.39 | 124.15 | 889 | 0.475 | 0.021 | 1.24 | 0.05 | 12.83 | 0.6 | 12.39 | 32.91 | -4.05 | -200.8 | 5.0[e] | 0.802 | 0.005 |
| EW9504-18PC | 41.00 | 126.44 | 3075 | 0.431 | 0.018 | 2.05 | 0.08 | 11.53 | 0.5 | 13.09 | 32.64 | -4.89 | -200.4 | 3.5 | 0.804 | 0.004 |
| W8909 22BC | 42.09 | 125.76 | 2750 | 0.415 | 0.019 | 2.12 | 0.08 | 11.07 | 0.6 | 12.51 | 32.55 | -5.13 | -208.4 | 5.0[e] | 0.796 | 0.005 |
| W8809A-5GC | 42.10 | 126.17 | 2764 | 0.408 | 0.019 | 2.36 | 0.09 | 10.87 | 0.6 | 12.85 | 32.54 | -5.18 | -210.6 | 0.5 | 0.793 | 0.002 |
| W7909-174GC | 42.17 | 124.75 | 616 | 0.416 | 0.020 | 1.66 | 0.07 | 11.09 | 0.6 | 11.81 | 32.60 | -4.99 | -198.4 | 5.0[e] | 0.806 | 0.005 |
| EW9504-17PC | 42.24 | 125.89 | 2671 | 0.434 | 0.018 | 2.29 | 0.09 | 11.61 | 0.5 | 12.57 | 32.53 | -5.21 | -201.6 | 2.3 | 0.803 | 0.003 |

[a] Using calibration of Prahl et al. (1988).

[b] From 2013 World Ocean Atlas gridded climatology.

[c] See Section 4.2.5.

[d] Same location as down-core samples from EW9504-9PC, Table 4.3.

[e] Non-replicated, assumed uncertainty, see Section 4.2.4.

4.2.2 Age Models

Depth-age models were constructed or taken from existing literature to identify ~19, 21, and 23 kya sampling intervals in the EW9504 and LPAZ02MV cores. These ages were selected in accordance with the sea-level defined 'Chronozone 1' of the EPILOG LGM assessment (Mix et al. 2001). For the previously-unpublished records from EW9504 cores 12PC to 18PC, four to five $\delta^{18}O$ tie points were selected corresponding to ~17-25 kya interval of the well-developed W8709A-13PC chronology for the NE Pacific (Mix et al. 1999), as indicated in Appendix C. The depth-age models for EW9504 cores 2PC, 4PC, and 5PC were taken from Stott et al. (2000), who based them on $^{14}C$-derived accumulation rates and tuning to the SPECMAP chronology. While the relative ages of each $\delta^{18}O$ measurement were retained from Stott et al. (2000), the records were shifted ~700-2200 years to assign the isotopic 'turning point' at the end of the glacial period to 17.2 kya in accordance with the updated W8709A-13PC chronology. More recent, ice-core tuned age models for EW9504-3PC, -9PC, and LPAZ02MV-21P were taken from Herbert et al. (2001). These models were similarly adjusted (200-1200 yr) to match the 17.2 kya 'turning point' on the W8709A-13PC chronology. The resulting $\delta^{18}O$ depth-age models for the glacial portions of these cores are provided in Appendix C.

4.2.3 Additional Planktonic Foraminiferal $\delta^{18}O$

Planktonic foraminifera were collected, at the depth intervals listed in Table 4.2, from the same material previously sampled for benthic species during analysis for IODP leg 167 (Lyle et al. 2000). *Globigerina bulloides* (10-15 individuals, 250-355 μm fraction) were sonicated with methanol, followed by water, and dried overnight. The samples were acidified in a Kiel III carbonate device (70°C) and the resulting $CO_{2(g)}$ analyzed in Thermo-Finnigan MAT-252 mass spectrometer via duel-inlet injection. The standard deviation of replicate analyses of a local carbonate standard was 0.04‰ vs. PDB. Calibration to the PDB scale was accomplished via analysis of the NBS-19 standard.

**Table 4.2.** Additional planktonic foraminiferal (*G. bulloides*) $\delta^{18}O$ (Section 4.2.3) for cores EW9504-12PC through -18PC.

**Table 4.2**. Planktonic (*G. bulloides* ) $\delta^{18}O$

| Core | Interval (cm) | $\delta^{18}O$ (‰ vs. PDB, ± 0.04) |
|---|---|---|
| EW9504-12PC | 71 | 2.63 |
| | 151 | 2.31 |
| | 221 | 2.72 |
| | 231 | 2.69 |
| EW9504-13PC | 139 | 2.79 |
| | 154 | 2.69 |
| | 241 | 2.40 |
| | 311 | 2.79 |
| EW9504-14PC | 261 | 2.76 |
| | 271 | 2.66 |
| | 291 | 2.47 |
| | 306 | 2.56 |
| | 351 | 2.67 |
| | 361 | 2.59 |
| EW9504-18PC | 201 | 2.60 |
| | 251 | 2.35 |
| | 301 | 2.29 |
| | 351 | 2.87 |
| | 401 | 2.38 |
| | 151 | 1.98 |

4.2.4 Alkenone Extraction, Quantification, and Isotopic Analysis

Freeze-dried sediments were pulverized, and total lipids extracted with 3:1 dichloromethane:methanol using an ASE-200 solvent extractor following the methods outlined in Walinsky et al. (2009). Total lipid extracts were partitioned into hexane, and alkenone/alkenoate fractions isolated via silica gel chromatography (Prahl and Pinto 1987). Branched compounds were removed from these fractions via urea adduction (Christie 2003), and the purified alkenone/alkenoate fractions quantified via gas chromatography with flame ionization detection (GC-FID). Samples were then saponified in basic methanol to remove the alkenoates (Christie 2003), and the resulting neutral alkenone fractions were then quantified again via GC-FID. Alkenone concentrations were recovery-corrected via quantification of hexatriacontan-2-one (K36:0), an alkenone analogue added to each sample prior to extraction. Alkenone abundance and $U_{37}^{K'}$ were determined from the saponified samples; alkenone temperature estimates were made using the standard temperature calibration of Prahl et al. (1988), $T = 29.41(U_{37}^{K'}) - 1.15$.

Internal precision of alkenone properties were determined by conservatively treating the uncertainty in each chromatographic peak area as the sum of an average baseline variability component (dominates error in low-abundance samples) and an average percent uncertainty (5%) in the integrated area (dominates in high-abundance samples). These uncertainties were then propagated into calculation of alkenone concentration and the temperature index (from 0.008 to 0.021 $U_{37}^{K'}$ units), corresponding to temperature estimate uncertainty of ~0.2 to 0.6°C.

Following chemical analysis, the δD of combined K37 alkenones ($\delta D_{K37}$, integrating K37:2, K37:3, and K37:4 where present; in accordance with the recommendations of van der Meer, 2013) was determined via gas chromatography-thermal conversion-isotope ratio monitoring mass spectrometry (GC-TC-IRMS) using the methods detailed in Chapter 3. $\delta D_{K37}$ values are reported as the mean of two or three replicate analyses of the same sample, and external precision given as the standard deviation (average of 3.1‰ vs. SMOW for repeated core-top samples, to 3.5‰ for

LGM). Samples for which multiple analyses were not possible were assigned an assumed uncertainty of 5.0‰.

4.2.5 Estimation of Water δD

Surface $\delta D_{H2O}$ estimates for calculation of $\alpha_{K37}$ in core-top sediments were made using a $\delta D_{H2O}$-salinity relationship ($\delta D_{H2O} = 3.00*S - 102.90$, $R^2 = 0.84$) determined from the 60 Pacific Ocean GEOSECS (Ostlund et al. 1987) measurements shallower than 200 m. Climatological, mean-annual surface salinity estimates were made for the location of each core-top sample using two-dimensional interpolation of the gridded 2013 World Ocean Atlas data set (Zweng et al. 2013) using the Ocean Data View 4.6.2 software. These salinity estimates (range of 32.5 to 34.5) and the above relationship were used to estimate climatological $\delta D_{H2O}$ for each core location (0.81 to -5.21‰ vs. SMOW). Uncertainty in these estimates (2.04‰) was defined as the RMS of 1) an assumed uncertainty of 0.76 in salinity (the standard deviation of all individual estimates) multiplied by the $\delta D_{H2O}$-salinity slope and 2) the standard error of the y-estimate for the $\delta D_{H2O}$-salinity regression (0.94‰).

$\delta^{18}O_{H2O}$ estimates corresponding to the down-core alkenone samples were made using planktonic foraminiferal $\delta^{18}O$ and $U_{37}^{K'}$ temperature estimates. $\delta^{18}O_{foram} - \delta^{18}O_{H2O}$ offsets (vs. PDB) for all cores but EW9504-17PC were determined using the *G. bulloides* paleotemperature equation of Mulitza et al. (2003), $\delta^{18}O_{foram} - \delta^{18}O_{H2O} = -0.206(T) + 3.03$. Uncertainty in water-calcite offsets (~0.42 to 0.50‰) was estimated as the RMS of 1) the uncertainty in $U_{37}^{K'}$ temperature (discussed above) multiplied by the slope of the paleotemperature equation and 2) the standard error of the y-estimate for this relationship (0.26 ‰). Offset estimates and uncertainties for EW9504-17PC were made in the same way, but used the *N. pachyderma* paleotemperature equation of Mulitza et al. (2003), $\delta^{18}O_{foram} - \delta^{18}O_{H2O} = -0.247(T) + 3.53$, with a y-estimate standard error of 0.31‰. Planktonic $\delta^{18}O_{foram}$ values were linearly interpolated to the depth interval of the alkenone samples (indicated in Table 4.3). Uncertainty in these interpolated values is taken as the range between bracketing measurements (up to

1.19‰) or the analytical precision of 0.04‰, whichever was larger. $\delta^{18}O_{H2O}$ values were then calculated from the foraminiferal values and offsets, and adjusted to the SMOW scale by adding 0.27‰ (Hut 1987). Uncertainty in calculated $\delta^{18}O_{H2O}$ was ~0.3 to 1.2‰.

$\delta D_{H2O}$ was derived from these $\delta^{18}O_{H2O}$ estimates using the modern, surface Pacific Ocean $\delta D_{H2O}$ vs $\delta^{18}O_{H2O}$ relationship defined by the same 60 GEOSECS samples described above, $\delta D_{H2O} = 7.01(\delta^{18}O_{H2O}) - 0.56$ ($R^2 = 0.91$). These final estimates ranged from ~5 to 22‰ (Table 4.3). Uncertainty in $\delta D_{H2O}$ estimates (~2 to 8‰) was defined as the RMS of 1) the uncertainty in $\delta^{18}O_{H2O}$ estimates multiplied by the slope of the $\delta D_{H2O}$ vs. $\delta^{18}O_{H2O}$ relationship and 2) the standard error of the y-estimate for this relationship (0.68‰).

Planktonic $\delta^{18}O_{foram}$ data was not available for core LPAZ02MV-21P. Due to the rough co-variation of temperature and the isotopic composition of surface water in this study area (LeGrand and Schmidt 2006), estimates for $\delta D_{H2O}$ were made using $U_{37}^{K'}$ values and a linear regression of estimated $\delta D_{H2O}$ onto $U_{37}^{K'}$ temperature for the other sites ($R^2 = 0.45$; Appendix C). Accordingly, large uncertainties (10‰) were assumed for these values.

**Table 4.3.** Core locations, sample depths, and modeled ages (Section 4.2.2); alkenone compositional properties (Section 4.2.4); interpolated planktonic foraminiferal $\delta^{18}O$ and estimated water isotopic composition (Section 4.2.5); and alkenone isotopic composition for the LGM transect. Mean LGM values for each core are shown in bold under each set of samples.

**Table 4.3.** LGM Sediment Samples

| Core | Interval (cm) | Modeled Age[a] (kya) | UK'37 | ± | K37s ($\mu g\ g^{-1}$ dry) | ± | UK'37 Temperature (°C) | ± | Planktonic $\delta^{18}O_{calcite}$[b] (‰ vs. PDB) | ± | Estimated $\delta^{18}O_{H2O}$ (‰ vs. SMOW) | ± | Estimated $\delta D_{H2O}$ (‰ vs. SMOW) | ± | $\delta D_{K37}$ (‰ vs. SMOW) | ± | $\alpha_{K37}$ | ± |
|---|---|---|---|---|---|---|---|---|---|---|---|---|---|---|---|---|---|---|
| EW9504-2PC | 53-54 | 19.1 | 0.433 | 0.022 | 4.13 | 0.18 | 11.6 | 1.6 | 1.45 | 0.35 | 1.1 | 0.5 | 7.0 | 4.0 | -191.5 | 4.5 | 0.803 | 0.005 |
| | 70-71 | 23.0 | 0.396 | 0.021 | 4.01 | 0.17 | 10.5 | 1.6 | 1.70 | 0.06 | 1.1 | 0.4 | 7.1 | 3.1 | -191.5 | 5.0[f] | 0.803 | 0.005 |
| | | **mean** | **0.414** | **0.012** | **3.95** | **0.10** | **11.0** | **0.9** | **1.62** | **0.12** | **1.1** | **0.3** | **7.4** | **2.0** | **-191.5** | **2.2** | **0.803** | **0.002** |
| EW9504-3PC[c] | 102-103 | 21.0 | 0.468 | 0.020 | 4.49 | 0.17 | 12.6 | 1.6 | 2.04 | 0.34 | 1.9 | 0.5 | 12.6 | 3.9 | -189.9 | 5.0[f] | 0.800 | 0.006 |
| | 108-109 | 22.9 | 0.451 | 0.020 | 3.86 | 0.15 | 12.1 | 1.6 | 2.31 | 0.51 | 2.0 | 0.7 | 13.8 | 4.7 | -185.1 | 0.8 | 0.804 | 0.003 |
| | | **mean** | **0.471** | **0.011** | **4.08** | **0.09** | **12.7** | **0.9** | **2.21** | **0.23** | **2.1** | **0.3** | **13.9** | **2.4** | **-187.5** | **1.7** | **0.802** | **0.002** |
| EW9504-4PC[c] | 152-153 | 19.0 | 0.621 | 0.021 | 14.47 | 0.65 | 17.1 | 1.6 | 1.70 | 0.45 | 2.5 | 0.6 | 16.7 | 4.4 | -199.2 | 7.0 | 0.788 | 0.007 |
| | 170-171 | 21.0 | 0.596 | 0.019 | 10.87 | 0.42 | 16.4 | 1.6 | 1.80 | 0.33 | 2.4 | 0.5 | 16.3 | 3.9 | -201.8 | 1.5 | 0.785 | 0.003 |
| | 188-189 | 23.0 | 0.561 | 0.020 | 8.78 | 0.34 | 15.3 | 1.6 | 1.48 | 0.33 | 1.9 | 0.5 | 12.6 | 3.9 | -196.3 | 1.6 | 0.794 | 0.003 |
| | | **mean** | **0.592** | **0.011** | **11.38** | **0.28** | **16.3** | **0.9** | **1.66** | **0.22** | **2.3** | **0.3** | **15.2** | **2.3** | **-199.1** | **2.4** | **0.789** | **0.003** |
| EW9504-5PC | 129-130 | 19.0 | 0.595 | 0.020 | 6.42 | 0.26 | 16.4 | 1.6 | 2.55 | 0.08 | 3.2 | 0.4 | 21.6 | 3.1 | -196.8 | 3.2 | 0.786 | 0.004 |
| | 144-145 | 21.1 | 0.549 | 0.021 | 4.50 | 0.19 | 15.0 | 1.6 | 2.54 | 0.15 | 2.9 | 0.4 | 19.6 | 3.3 | -194.3 | 5.0[f] | 0.790 | 0.005 |
| | 158-159 | 23.0 | 0.507 | 0.022 | 3.95 | 0.17 | 13.8 | 1.6 | 1.98 | 0.04 | 2.1 | 0.4 | 13.8 | 3.1 | -193.0 | 6.0 | 0.796 | 0.006 |
| | | **mean** | **0.550** | **0.012** | **4.96** | **0.12** | **15.0** | **0.9** | **2.36** | **0.06** | **2.7** | **0.3** | **18.3** | **1.8** | **-194.7** | **2.8** | **0.791** | **0.003** |
| EW9504-9PC[d] | 176-177 | 19.0 | 0.542 | 0.019 | 11.94 | 0.44 | 14.8 | 1.6 | 0.64 | 1.19 | 0.9 | 1.3 | 6.0 | 8.9 | -195.2 | 4.4 | 0.800 | 0.008 |
| | 203-204 | 21.0 | 0.499 | 0.019 | 9.89 | 0.36 | 13.5 | 1.6 | 1.78 | 0.04 | 1.8 | 0.4 | 12.1 | 3.1 | -189.8 | 4.7 | 0.801 | 0.005 |
| | 232-233 | 23.0 | 0.493 | 0.020 | 7.62 | 0.29 | 13.3 | 1.6 | 1.45 | 0.04 | 1.4 | 0.4 | 9.5 | 3.1 | -191.2 | 3.4 | 0.801 | 0.004 |
| | | **mean** | **0.511** | **0.011** | **9.82** | **0.21** | **13.9** | **0.9** | **1.29** | **0.40** | **1.4** | **0.5** | **9.2** | **3.3** | **-192.1** | **2.4** | **0.801** | **0.003** |
| EW9504-12PC | 71-72 | 19.0 | 0.483 | 0.023 | 1.22 | 0.05 | 13.1 | 1.6 | 2.63 | 0.04 | 2.6 | 0.4 | 17.4 | 3.1 | -184.9 | 4.9 | 0.801 | 0.005 |
| | 224-225 | 23.0 | 0.410 | 0.023 | 1.02 | 0.05 | 10.9 | 1.6 | 2.71 | 0.04 | 2.2 | 0.4 | 14.8 | 3.1 | -176.1 | 1.8 | 0.812 | 0.003 |
| | | **mean** | **0.450** | **0.013** | **1.07** | **0.03** | **12.1** | **0.9** | **2.55** | **0.02** | **2.3** | **0.2** | **15.4** | **1.8** | **-180.5** | **2.6** | **0.806** | **0.003** |
| EW9504-13PC | 144-145 | 19.0 | 0.348 | 0.020 | 1.50 | 0.06 | 9.1 | 1.6 | 2.76 | 0.10 | 1.9 | 0.4 | 12.5 | 3.2 | -179.0 | 5.0[f] | 0.811 | 0.005 |
| | 241-242 | 21.0 | 0.318 | 0.017 | 1.23 | 0.05 | 8.2 | 1.6 | 2.40 | 0.04 | 1.3 | 0.4 | 8.8 | 3.1 | -182.5 | 5.0[f] | 0.810 | 0.005 |
| | 311-312 | 22.9 | 0.316 | 0.018 | 0.78 | 0.03 | 8.2 | 1.6 | 2.79 | 0.04 | 1.7 | 0.4 | 11.4 | 3.1 | -179.1 | 0.9 | 0.812 | 0.002 |
| | | **mean** | **0.327** | **0.011** | **1.17** | **0.03** | **8.5** | **0.9** | **2.65** | **0.04** | **1.6** | **0.2** | **10.9** | **1.8** | **-180.2** | **2.4** | **0.811** | **0.003** |
| EW9504-14PC | 265-266 | 19.0 | 0.353 | 0.018 | 1.52 | 0.06 | 9.2 | 1.6 | 2.72 | 0.09 | 1.9 | 0.4 | 12.5 | 3.1 | -174.7 | 5.0[f] | 0.815 | 0.005 |
| | 302-303 | 20.6 | 0.360 | 0.020 | 0.32 | 0.01 | 9.4 | 1.6 | 2.54 | 0.09 | 1.7 | 0.4 | 11.5 | 3.2 | -181.2 | 8.5 | 0.809 | 0.009 |
| | 354-355 | 23.0 | 0.340 | 0.018 | 1.56 | 0.06 | 8.8 | 1.6 | 2.65 | 0.08 | 1.7 | 0.4 | 11.4 | 3.1 | -181.3 | 5.0[f] | 0.809 | 0.005 |
| | | **mean** | **0.351** | **0.011** | **1.13** | **0.03** | **9.2** | **0.9** | **2.63** | **0.05** | **1.8** | **0.2** | **11.8** | **1.8** | **-179.1** | **3.7** | **0.811** | **0.004** |
| EW9504-17PC | 355-356 | 19.0 | 0.306 | 0.016 | 1.13 | 0.04 | 7.9 | 1.6 | 2.13 | 0.04 | 0.8 | 0.5 | 5.1 | 3.6 | -190.7 | 5.0[f] | 0.805 | 0.005 |
| | 398-399 | 21.0 | 0.286 | 0.016 | 0.86 | 0.03 | 7.3 | 1.6 | 2.22 | 0.27 | 0.7 | 0.6 | 4.7 | 4.1 | -187.5 | 5.0[f] | 0.809 | 0.006 |
| | 438-439 | 22.9 | 0.279 | 0.018 | 0.44 | 0.02 | 7.1 | 1.6 | 2.69 | 0.08 | 1.2 | 0.5 | 7.6 | 3.7 | -175.8 | 5.0[f] | 0.818 | 0.005 |
| | | **mean** | **0.290** | **0.010** | **0.81** | **0.02** | **7.4** | **0.9** | **2.35** | **0.09** | **0.9** | **0.3** | **5.8** | **2.2** | **-184.7** | **2.9** | **0.811** | **0.003** |
| EW9504-18PC | 311-312 | 21.0 | 0.327 | 0.018 | 0.72 | 0.03 | 8.5 | 1.6 | 2.41 | 0.58 | 1.4 | 0.7 | 9.2 | 5.1 | -182.6 | 4.1 | 0.810 | 0.005 |
| | 423-424 | 23.0 | 0.352 | 0.019 | 1.20 | 0.05 | 9.2 | 1.6 | 2.20 | 0.40 | 1.3 | 0.6 | 8.8 | 4.2 | -192.7 | 0.3 | 0.800 | 0.003 |
| | | **mean** | **0.328** | **0.010** | **0.87** | **0.02** | **8.5** | **0.9** | **2.39** | **0.25** | **1.4** | **0.3** | **9.1** | **2.5** | **-187.6** | **1.4** | **0.805** | **0.002** |
| LPAZ02MV-21P[e] | 88-89 | 19.0 | 0.772 | 0.014 | 9.89 | 0.42 | 21.6 | 1.6 | | | | | 20.8 | 10.0 | -192.2 | 2.5 | 0.791 | 0.008 |
| | 96-97 | 21.1 | 0.770 | 0.014 | 6.96 | 0.30 | 21.5 | 1.6 | | | | | 20.8 | 10.0 | -196.9 | 5.0[f] | 0.787 | 0.009 |
| | 103-104 | 23.2 | 0.800 | 0.013 | 5.14 | 0.23 | 22.4 | 1.6 | | | | | 21.6 | 10.0 | -196.2 | 5.0[f] | 0.787 | 0.009 |
| | | **mean** | **0.781** | **0.008** | **7.33** | **0.19** | **21.8** | **0.9** | | | | | **21.1** | **5.8** | **-195.1** | **2.5** | **0.788** | **0.005** |

[a] Linear interpolation of depth-age models in Appendix C.

[b] Linear interpolation of *G. bulloides* and *N. pachyderma* L (17PC only) records in Table 4.2 and Appendix C.

[c] No core-top equivalent. Locations are 32.07°N x 117.37°W (3PC) and 32.28°N x 118.40°W (4PC).

[d] Same location as core-top samples from EW9504-10MC.

[e] LPAZ-21P planktonic $\delta^{18}O$ predicted based on benthic $\delta^{18}O$ and multiple linear regression of benthic-planktonic difference on water depth and temperature, see Appendix C.

[f] Non-replicated, assumed uncertainty, see Section 4.2.4.

## 4.3. Results

$U_{37}^{K'}$ indices in the core-top transect closely followed overlying, modern climatological maSST (Table 4.1; Figure 4.2A). Only cores in the 40-42°N cluster yielded temperature estimates that were outside uncertainty of maSST, appearing to be systematically 'cold' (Figure 4.2B). This is consistent with previous observations (Doose et al. 1997) and the conclusions of Prahl et al. (2010), who suggest that cold-biased alkenone production away from the coast at this latitude is due to the offshore advection of cold 'upwelling filaments' which are a persistent feature near Cape Blanco, Oregon (Barth et al. 2002).

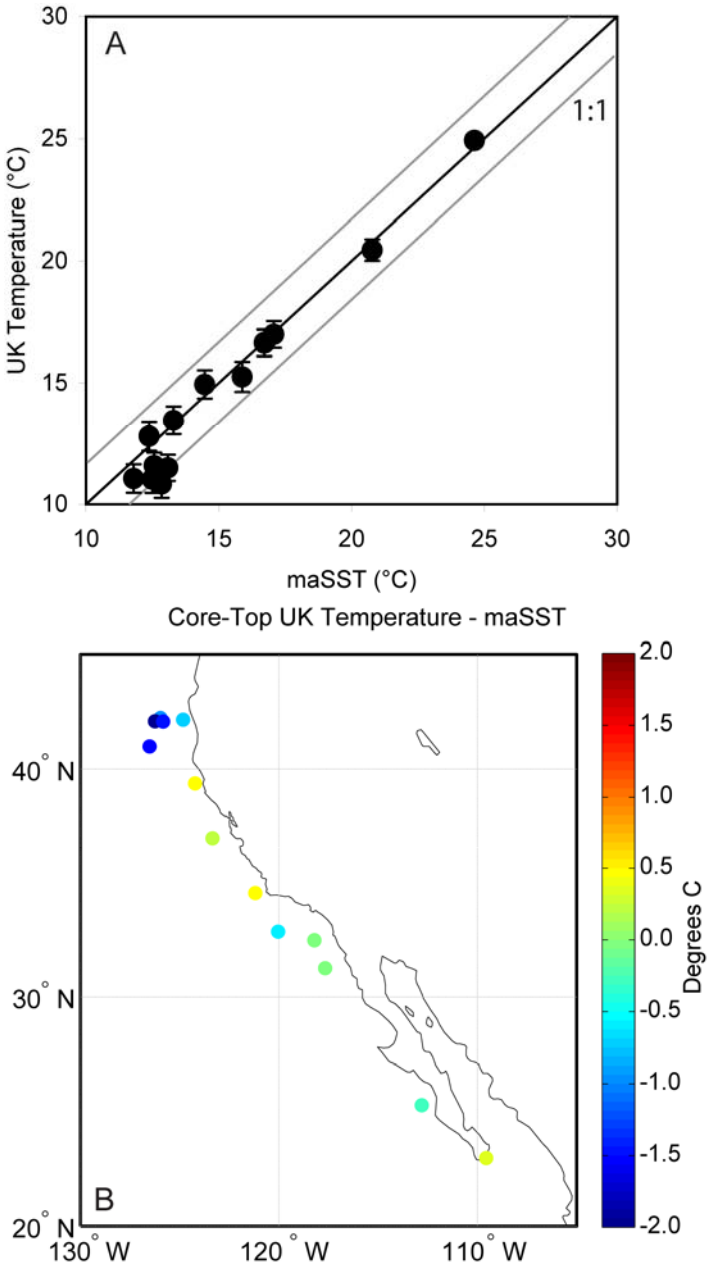


**Figure 4.2.** Core-top $U_{37}^{K'}$ temperature (via Prahl et al. 1988 calibration) versus maSST (**A**) showing deviations from the 1:1 line (black) within a 1.5°C envelope (grey), the standard error of the global core-top $U_{37}^{K'}$ vs. maSST calibration (Müller et al. 1998). A map of the residuals from maSST is shown in **B**.

Among the fourteen core-top samples, there are three gravity cores and eight piston cores. Loss of surface sediment may be a concern for these samples, particularly for the piston cores. Three of the piston cores (EW9504-12PC, -13PC, and -18PC) show clear signs of having lost recent portions of the Holocene record via inspection of their associated $\delta^{18}O$ stratrigraphy (Appendix C). The fact that $U_{37}^{K'}$ temperature estimates from even the cores with obvious loss agree so well (Figure 4.2A) with modern maSST (or with expected deviations from it, in the case of the 42°N samples), as well as with nearby multi- or box-cores, suggests that our samples are sufficiently indicative of modern/Holocene oceanographic conditions to discuss in the context of observed ecology below.

$\delta D_{K37}$ in the core-top samples (Table 4.1) ranged from ~-198‰ to -221‰. Estimates of surface water $\delta D_{H2O}$ only ranged from ~-5‰ to 1‰ and, rather than a positive correlation between water and alkenone isotopic values, there was a weak negative correlation ($R^2 = 0.46$). Thus, variability in $\delta D_{K37}$ is driven by fractionation ($\alpha_{K37}$) and not water composition itself. $\alpha_{K37}$ in the core-top samples fell between ~0.77 and 0.81, squarely in the range expected from previous estimates from cultures (~0.74 to 0.82; Chapter 3). These values exhibited an increasing trend with latitude, closely following the decrease in maSST over this transect (Figure 4.3A). Negative deviations from this trend occur in some, but not all, of the SCB samples (EW9504-5PC, -10MC, and NH0412-23-14MC) and the 42°N samples (W8808A-5GC, W8909-22BC). Note that if $\delta D_{K37}$ is used in Figure 4.3, rather than $\alpha_{K37}$, the forms of the plots are essentially unchanged, demonstrating that the patterns in $\alpha_{K37}$ we discuss below are not driven by spatial biases in our estimates of water composition.

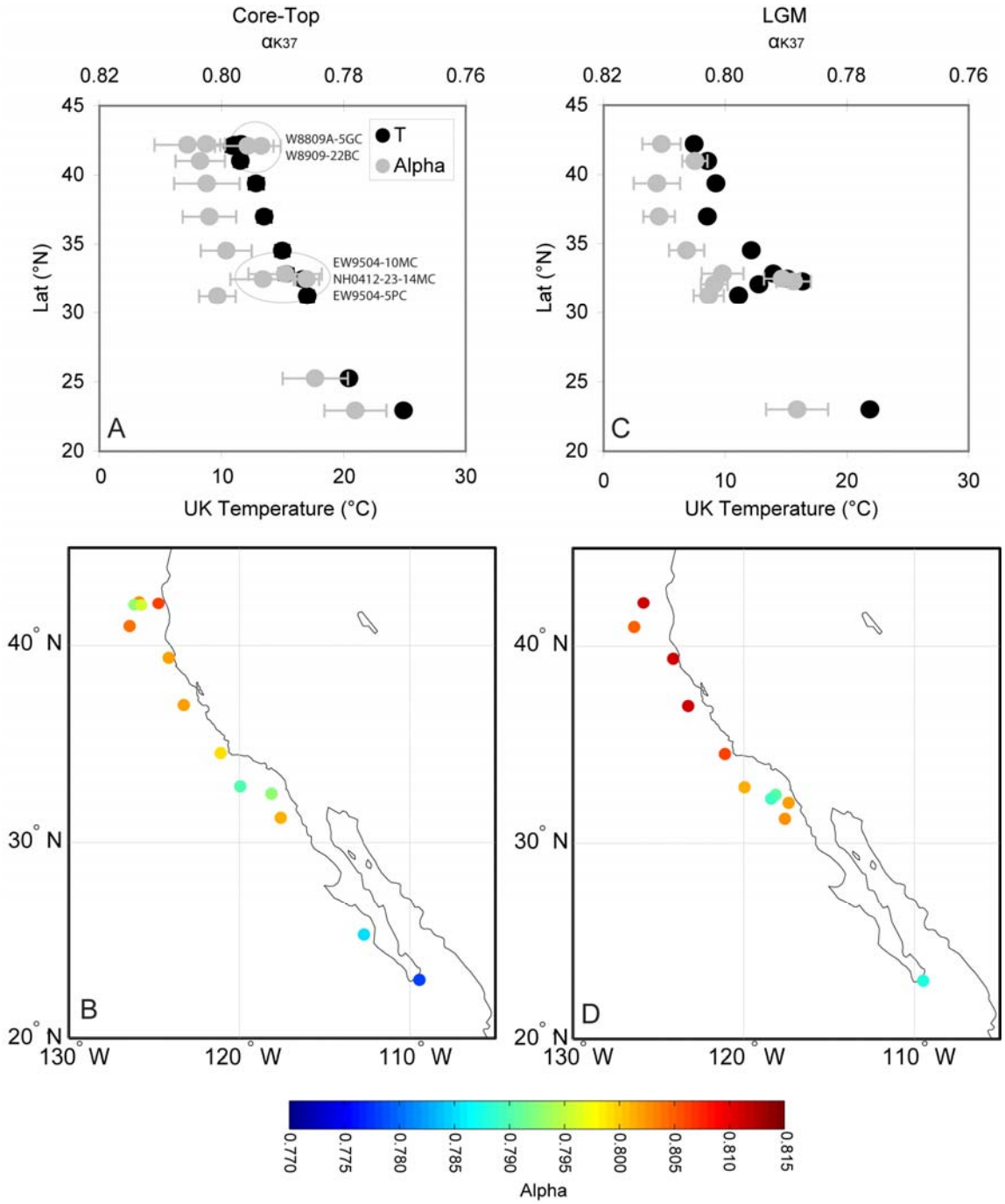


**Figure 4.3.** Trends in $\alpha_{K37}$ with latitude and $U_{37}^{K'}$ temperature in the core-top samples (**A**), with the spatial trend mapped below (**B**). Subsets of the 40-42°N cores and SCB cores discussed in Section 4.4.2 are indicated. Analogous plots for the LGM samples are shown in **C** and **D**.

The overall pattern of mean LGM $U_{37}^{K'}$ temperature estimates (Table 4.3) with latitude is that of the modern distribution (Figure 4.3A), shifted by ~-3.3°C (Figure 4.3C). A wide range of $U_{37}^{K'}$ anomalies are observed in the borderlands, however, with shifts as small as ~-1.7 °C (EW9504-5PC) and as large as to ~-6.0°C (EW9504-2PC). The proxy estimates are in general agreement with the broad-scale MARGO reconstruction for the 19-23kya time period (~-2 to -4°C anomalies of increasing magnitude moving north along the North American margin; MARGO Project Members 2009) and the estimates of glacial cooling along the N-S CCS transect of Doose et al. (1997). $U_{37}^{K'}$ records are also available from Herbert et al. (2001) for the cores EW9504-2PC, -3PC, and LPAZ02MV-21P. These records, interpolated to our sampling depths, all agree with our estimates to within 1.3°C, inside the ~1.5°C standard error of the global core-top $U_{37}^{K'}$ vs. maSST comparison of Müller et al. (1998).

The mean LGM $\alpha_{K37}$ estimates follow north-south trend similar to the modern data, also exhibiting a wide range of values in the SCB, and follow $U_{37}^{K'}$ temperature even more closely (Figure 4.3C). Values range from ~0.79 to 0.82, slightly higher than modern estimates. While the magnitude of glacial $\alpha_{K37}$ is dependant on our estimates of water composition, the same spatial pattern is observed if $\delta D_{K37}$ is mapped. This indicates that the latitude/temperature functionality of $\alpha_{K37}$ is not an artifact of the use of temperature data in the estimation of $\delta D_{H2O}$ (see Section 4.2.5).

The decreasing relationship with temperature and latitude displayed by core-top $\alpha_{K37}$ (Figure 4.3A) stands in contrast to the hypothesized, increasing north-south (or onshore-offshore) relationship with upwelling regime (Section 4.1). The change in upwelling behavior north and south of Point Conception does not manifest as a clear step in the core-top $\alpha_{K37}$ data (Figure 4.3B). Including the LGM data strengthens the relationship between $\alpha_{K37}$ and $U_{37}^{K'}$ (Figure 4.4A; $R^2$ improves from 0.63 to 0.73) and shows it to be linear. The fact that, with the exception of one sample from the SCB (EW9504-5PC; discussed below), the available LGM/core-top sample pairs show

decreasing $U_{37}^{K'}$ accompanied by increasing $\alpha_{K37}$ (Figure 4.4B) indicates that, whatever the link between the two measures, it is robust through time as well as space.

There is a small north-to-south range of overlying salinities in this study area (~2, Table 4.1) which may potentially affect a latitude-driven pattern in $\alpha_{K37}$. Previously-reported sensitivity to salinity (Schouten et al. 2006) would only shift $\alpha_{K37}$ ~0.006 units along this gradient, however, approximately the same scale as typical uncertainty (e.g. Wolhowe et al. 2009) and only slightly larger than the uncertainty reported here.

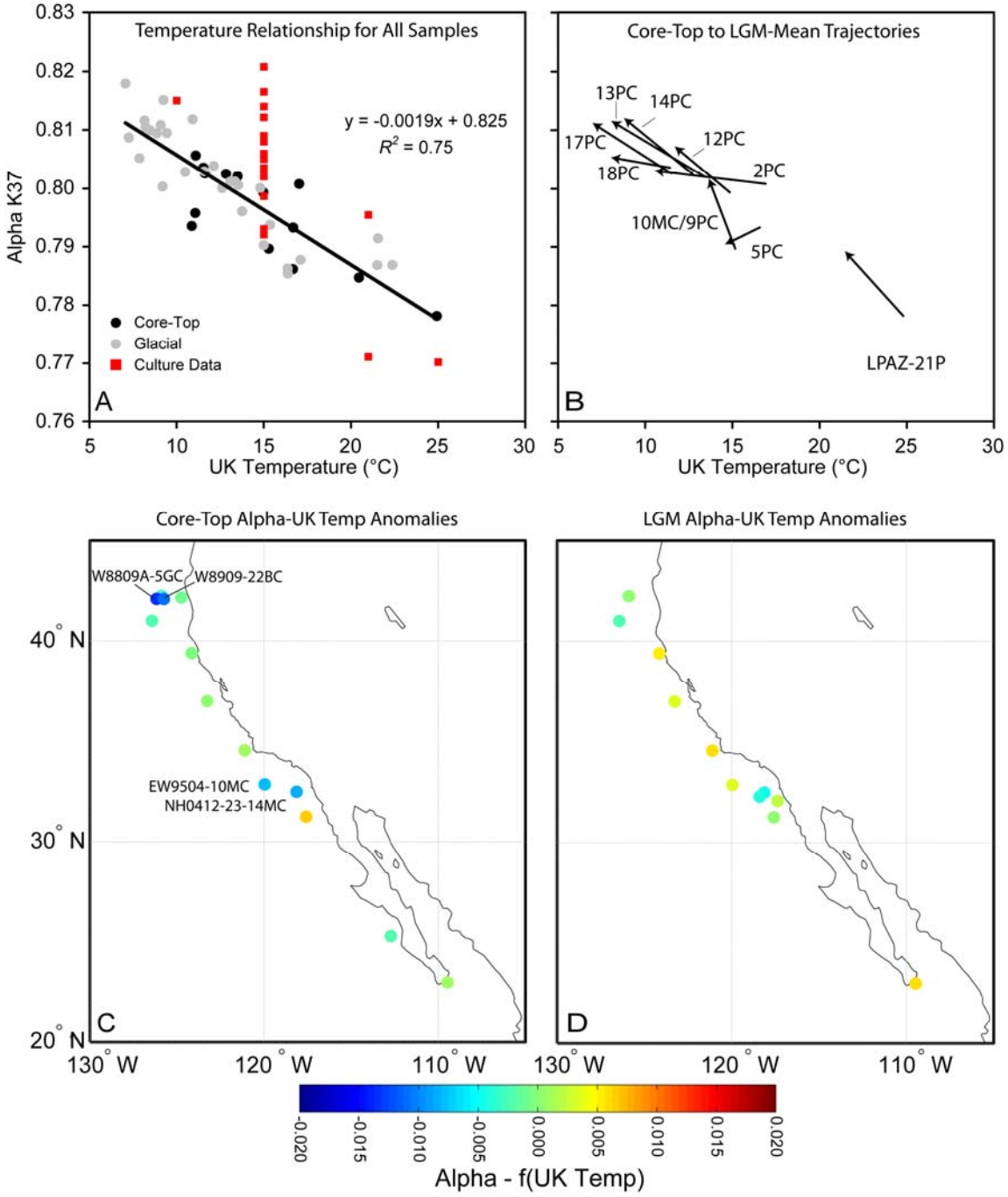
Temperature Relationship for All Samples
y = -0.0019x + 0.825
$R^2$ = 0.75
Core-Top
Glacial
Culture Data
Alpha K37
UK Temperature (°C)
A
Core-Top to LGM-Mean Trajectories
13PC
14PC
17PC
12PC
18PC
2PC
10MC/9PC
5PC
LPAZ-21P
UK Temperature (°C)
B
Core-Top Alpha-UK Temp Anomalies
W8809A-5GC
W8909-22BC
EW9504-10MC
NH0412-23-14MC
40° N
30° N
20° N
130° W
120° W
110° W
C
LGM Alpha-UK Temp Anomalies
D
-0.020
-0.015
-0.010
-0.005
0.000
0.005
0.010
0.015
0.020
Alpha - f(UK Temp)

**Figure 4.4.** The relationship between $\alpha_{K37}$ and $U_{37}^{K'}$ temperature for all sedimentary data (Section 4.4). **A** shows the overall relationship for both modern (black) and down-core (grey) samples (error bars omitted for clarity). Red symbols are the available culture data for *E. huxleyi* grown at 20°C or lower and *G. oceanica* at 20°C or higher (see Section 4.4.1). Culture data is taken from Chapter 3, Wolhowe et al. (2009), M'boule et al. (2014), and Schouten et al. (2006). For M'boule et al. (2014) and Schouten et al. (2006) data, only samples grown between salinities of 30 and 35 are shown. The regression shown is for all core-top and LGM samples. **B** shows the trajectories, in $\alpha_{K37}$ vs. $U_{37}^{K'}$ space, taken by each core-top/LGM pair from Holocene to mean-LGM values. In the lower panels, $\alpha_{K37}$ residuals, relative to the regression versus $U_{37}^{K'}$ shown in **A**, are mapped for the core-top (**C**) and mean LGM (**D**) samples. Specific locations discussed in Section 4.4.2 are indicated in **C**. Note that EW9504-5PC is at approximately the same location as NH0412-23-14MC; the color value shown in **C** corresponds to the latter core.

**4.4. Discussion:**

One possible explanation for the N-S trend is that, as hypothesized in Section 4.1, $\alpha_{K37}$ is indeed driven by coccolithophore productivity and that the relationship with temperature is corollary, not causal. Temperature correlates with many oceanographic variables in this region, particularly nitrate and chlorophyll abundance (Figure 4.5), due to the influence of upwelling. Relationships are observed between core-top $\alpha_{K37}$ and potential abundance proxies such as climatological surface nitrate (Garcia et al. 2013) or satellite derived sea-surface chlorophyll and PIC abundance (AquaMODIS 9km level 3 data; all $R^2 < 0.4$; Figure 4.5). The stronger relationship with maSST ($R^2 = 0.63$) than with these three parameters may simply be due to the significantly greater temporal coverage of the WOA13 temperature climatology; the available satellite-based ecological estimates (from satellites that were not active until after all the cores in our dataset were collected) integrate a much shorter time frame and may not compare well to the time-integrated sedimentary $\alpha_{K37}$ values. However, on a 1-month (July/August) time scale and regional (Gulf of California) spatial scale, Chapter 3 illustrates a negative relationship between $\alpha_{K37}$ and alkenone-producer abundance, and suggest that conditions that favor high productivity (represented there by proximity to the nitracline and chlorophyll maximum) are associated with lower, not higher, values of $\alpha_{K37}$. This fact, taken with the stronger dependence of $\alpha_{K37}$ on temperature, suggests that any weak correlation of $\alpha_{K37}$ with these abundance proxies is due to their own dependence on temperature in this area.

As for temperature, a positive, rather than negative, relationship between $\alpha_{K37}$ and temperature is shown for suspended material in the Gulf of California euphotic zone (Chapter 3). The authors, however, ascribe this to either higher growth rates (closer to the nitracline) or lower light levels (further from the surface) driving lower values of $\alpha_{K37}$, rather than actual dependence on temperature. Negative dependence of $\alpha_{K37}$ on growth temperature has previously been suggested for individual culture experiments (Wolhowe et al. 2009; Zhang et al. 2009), and the available culture data, when taken as a whole, suggests that temperature does play a role in controlling $\alpha_{K37}$ (Chapter 3). It is unclear, however, to what degree this is due to higher temperatures driving higher

growth rates. Growth rate is proposed to, in part, control $\alpha_{K37}$ due its control of lipid production rate (Chapter 3); this is the explanation the authors provide for the relationship of $\alpha_{K37}$ and cell abundance in the field. Furthermore, the $\alpha_{K37}$ shifts associated with the full experimental temperature range (10-25°C) are on a similar scale to those associated with both strain- and species-specific differences and growth phase changes (Chapter 3). The apparently robust link between $U_{37}^{K'}$ and $\alpha_{K37}$ is, thus, surprising.

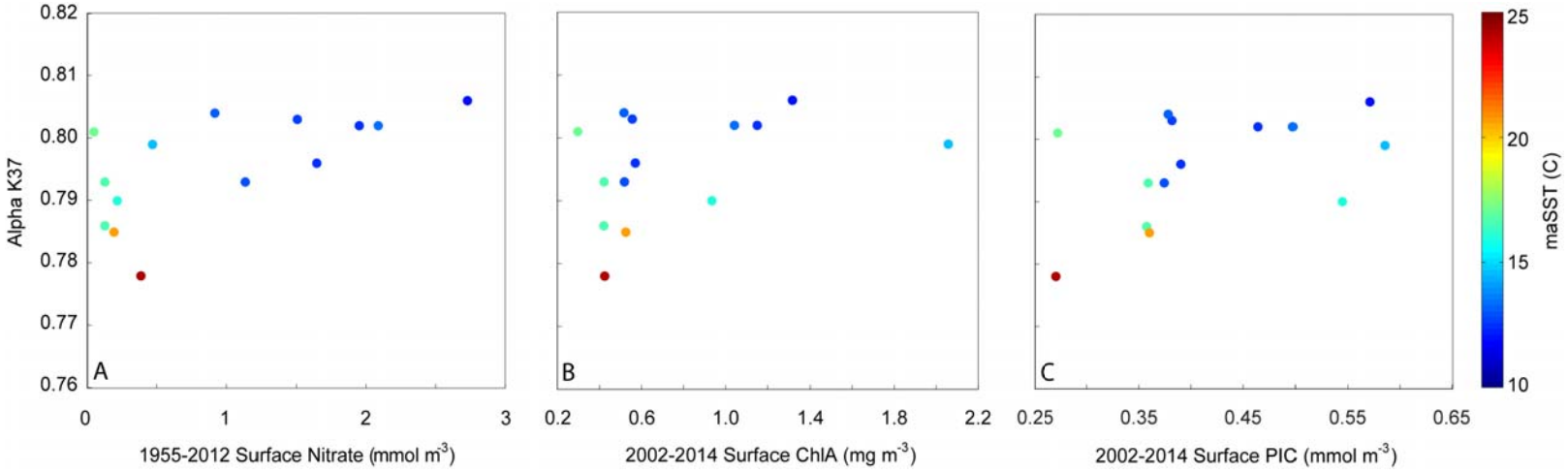


**Figure 4.5.** Relationships for core-top $\alpha_{K37}$ versus **A**) mean-annual surface nitrate concentration (WOA13 climatology for 1955-2012; Garcia et al. 2013), **B**) satellite-derived mean-annual surface chlorophyll and **C**) satellite-derived mean-annual PIC concentration. Chlorophyll and PIC data are taken from the MODIS-Aqua 9km level 3 climatology for 2002-2014 (data from NASA Giovanni portal), linearly interpolated to the core locations. Mean-annual SST is shown as the color bar for all three plots.

4.4.1. Potential Mechanisms Behind the North-South $\alpha_{K37}$ Gradient

Given the conclusions of Chapter 3 (that lower $\alpha_{K37}$ may associated with either production deeper in the water column due to the influence of light, with greater growth rate, or, to a lesser degree, higher temperature), there are three possible explanations for the N-S, apparently temperature-driven trend in $\alpha_{K37}$. One is that production in the subsurface becomes more prominent to the south. It has been shown that low surface nutrients in ETNP can drive production into subsurface chlorophyll features (Espinosa-Carreón et al. 2012; Wolhowe et al. 2014), and Chapter 3 illustrates a trend of lower $\alpha_{K37}$ values deeper in the water column, correlating with mid-day PAR. The authors attribute this to depth-variable growth rate effects independent of light, but allow that the effects of light limitation on photosystem activity may be the simplest explanation for their water-column data if a compelling mechanism can be described in the future. Unfortunately, all current experimental data comes from nutrient-limited cultures, and light cannot be deconvolved from other growth variables in the available field data (Chapter 3). Should light limitation prove to be a driver of $\alpha_{K37}$ in the field, the North-South core-top 'temperature' trend may represent an increased tendency towards subsurface production as the water column warms and becomes more stratified at lower latitudes. Note that this hypothetical effect of average production depth must necessarily outweigh latitude-dependant day-length controls on light availability in this study area, as lower values of $\alpha_{K37}$ (observed in the south, where day-length is increased) are associated with lower light in Chapter 3. Likewise, a control of production seasonality on light (more summer-biased production in the north, and thus higher average light conditions; see section 4.1) seems unlikely, as no distinct step in $\alpha_{K37}$ between samples in and out of the OR/CA upwelling zone (Figure 4.3B).

An indicator of coccolithophore production depth would be of use both in studies of paleoecology and in interpretation of alkenone paleotemperature records, which may be biased by subsurface production (Prahl et al. 2010). The fact that $\alpha_{K37}$ almost universally shifts to higher values at the LGM, however (Figure 4.4B), suggests that light is not the primary controlling factor. The movement of 'gyre like' conditions

towards the coast and a reduction of upwelling are hypothesized at the LGM from the SCB southward (Herbert et al. 2001). A reduction in average mixed layer depth, which would increase average light exposure, might be expected here if a net warming relative to modern conditions occurred; this oceanographic shift appears to have only muted the glacial-interglacial temperature contrast at the LGM though, not fully counteracted it (Herbert et al. 2001). If anything, the reduction in upwelling might be expected to make subsurface production more prominent from the SCB southward. As for the rest of the study area, glacial cooling would be expected to have increased the average mixed layer depth, which would also lead to decreased light exposure. Values of $\alpha_{K37}$ at the LGM would thus be expected to decrease, rather than increase, if the field data described in Chapter 3 indeed indicates a positive effect of light on $\alpha_{K37}$. The LGM $\alpha_{K37}$ values are thus inconsistent with this mechanism.

A second possible explanation for the N-S trend is that temperature alone is driving $\alpha_{K37}$ along this transect. It has been argued in a previous core-top study of the western North American margin that the averaging nature of sediments smoothes the $U_{37}^{K'}$ signal to a close approximation of mean-annual surface temperature, despite the observation of seasonally-variable production and flux intensity and of subsurface production maxima in the region (Herbert et al. 1998). Only along a transect of the 40-42°N region (e.g. Figure 4.2B), where high offshore primary production appears to consistently derive from cold, advected, upwelling filaments (Abbott and Zion 1985; Barth et al. 2002), are anomalous temperature and nutrient conditions suggested to lead to systematic $U_{37}^{K'}$/maSST biases (Prahl et al. 2010). It is likely that, in a similar fashion, many of the sources of variability in $\alpha_{K37}$, observed instantaneously in culture and in the water column, are averaged out when considering core samples integrating tens to hundreds of years of alkenone sedimentation. A signal of temperature, a more constant growth parameter with time, may be retained.

A robust $\alpha_{K37}$ vs. temperature relationship would have significant ramifications for the paleoceanographic utility of $\delta D_{K37}$ measurements. It has been argued extensively (Wolhowe et al. 2009; Chapter 3) that $\delta D_{K37}$ cannot serve as a hydrologic proxy in

settings without strong salinity/isotopic contrasts due to unconstrained variability in $\alpha_{K37}$. These results suggest that this is not true, and that $\alpha_{K37}$ can be calibrated versus $U_{37}^{K'}$ for use in locations where foraminiferal calcite estimates of water composition are not available or where there are questions about the temporal or spatial correspondence of alkenone and foraminiferal records. Currently, this relationship (Figure 4.4A) is insufficiently precise. The standard error of the y-estimate for the regression, 0.005, is large enough that a single $\delta D_{K37}$ value, paired with a single $\alpha_{K37}$ value (for example, -188‰ and 0.801, the mean of the LGM samples), could yield $\delta D_{H2O}$ estimates ranging from 19.4 to 6.8‰ (if $\alpha_{K37}$ were shifted by -0.005 or +0.005, respectively). This range (12.6‰) is ~50% larger than the full range of foram-derived LGM $\delta D_{H2O}$ estimates (8.2‰). However, the fact that the standard error estimate is approximately the same as estimates of uncertainty in $\alpha_{K37}$ (Table 4.1) means that much of this 'scatter' could potentially be analytical in nature, and thus there is the potential that it may be resolved by improvements in the precision and accuracy of $\delta D_{K37}$ measurements. Additionally, future data from properly age-controlled, explicitly 'modern' core-top sediments (see Section 4.3) may be more accurately compared to overlying temperature and $\delta D_{H2O}$ measurements.

A mechanism for direct temperature control of $\alpha_{K37}$, however, has not yet been described. Analogously to the case made above for an association of maSST with light conditions, it is possible that the association of higher temperatures with lower nutrient availability (Figure 4.1) increases the contribution of stationary-phase cells (which exhibit low values of $\alpha_{K37}$; Wolhowe et al. 2009; Chivall et at. 2014b) to the sedimentary record at the southern core locations. If this were the case, though, one might expect a bimodal distribution of high- and low-$\alpha_{K37}$ sites in and out of the northern upwelling region, which we do not. Furthermore, as described above, low surface nutrients in this region are known to drive production into the shallow subsurface where nutrients are more available (Espinosa-Carreón et al. 2012; Wolhowe et al. 2014).

In the absence of an experimentally determined mechanism for direct control of temperature on $\alpha_{K37}$, the third and simplest explanation for a temperature-driven trend is

a control of temperature itself on growth rate. All else being equal, *E. huxleyi* growth rate increases with temperature up to ~20°C (Mjaaland 1956), while the optimal growth temperature for *G. oceanica* is at least 25°C and, given its geographic distribution, likely higher (Buitenhuis et al. 2008). Wolhowe et al. (2014) show significant contributions of *G. oceanica*, relative to *E. huxleyi*, in the summertime ETNP and GoCal occurring at temperatures greater than ~20-25 degrees (Appendix A), consistent with the two species' optimal growth temperatures. If we consider the laboratory data for *E. huxleyi* at <20°C and *G. oceanica* at >20°C, we can see that the sedimentary $\alpha_{K37}$ data falls along approximately the same trajectory in $\alpha_{K37}$ vs. temperature space (Figure 4.4A).

On the time scale of sediment integration, the most important factor controlling coccolithophorid growth rate (not production rate) may indeed be temperature, rather than nutrient or light availability. Variation of light availability due to changes in cloud cover or production depth should, theotetically, not be resolved by samples containing tens to hundreds of years of sedimentation. Nutrient input does control the rate of net algal production on time scales of days and longer (e.g. Marañón et al. 2014), but the 'Michaelis-Menten' paradigm of a microscopic growth rate ($d^{-1}$) response to 'rate limiting' nutrients in the natural environment is known to be greatly complicated by non-steady state nutrient uptake and nutrient regeneration in the surface ocean (e.g. Harris 1980). Furthermore, coccolithophores occupy a mid-low nutrient niche that has been associated either intermediate depth ranges in stratified conditions (Wolhowe et al. 2014) or decreasing (in time) nutrient concentration in locations where production is dominated by surface blooms (Iglesias-Rodríguez et al. 2002). Variations in mean-annual nutrient levels along the CCS (Figure 4.1A) are due to upwelling events with an approximately day-week frequency (e.g. Huyer et al. 1983); at their onset these events would theoretically favor the production of more rapidly-growing species such as diatoms. Changes in the mean surface nutrient field along this transect, then, may only change how *often* conditions are favorable to coccolithophore growth, not the nutrient levels under which they are growing. Temperature may be the most consistent driver of coccolithophore growth rate represented in these sediments. If this is the case, the $\alpha_{K37}$ vs. temperature curve in Figure 4.4A would represent increasing growth rates at higher

temperatures, with *E. huxleyi* growing more rapidly with decreasing latitude to ~25°N (~20°C waters; Figure 4.1B) and *G. oceanica* growing more rapidly with moving south of this point. A growth rate control on $\alpha_{K37}$, which happens to be temperature driven, would be consistent with the mechanisms proposed in Chapter 3 (control of $\alpha_{K37}$ by lipid production rate, correlating with growth rate).

4.4.2 Regional Variation About the $\alpha_{K37}$ vs. Temperature Relationship

As described above, it is possible that the 'scatter' about the relationship shown in Figure 4.4A is analytical. However, if the core-top data are taken at face value, there appear to be significant controls on $\alpha_{K37}$ besides whatever is driving the overall north-south trend (be it light availability, temperature, or temperature-driven growth rate). Deviation from the overall $\alpha_{K37}$ vs. $U_{37}^{K'}$ trend can be described by a residual analysis, subtracting each data point from the linear fit in Figure 4.4A. Given the large uncertainty in $\alpha_{K37}$, the only points in the core-top data set that we can say are statistically different from the linear model come from the northern and southern terminuses of the OR/CA upwelling zone; two points at 42°N and two points in the northern SCB (Figure 4.4.C). Are there oceanographic explanations for why these samples deviate?

The 'offset' 42°N cores occur where sedimentary $U_{37}^{K'}$ temperatures consistently underestimate maSST (Figure 4.2B). Advection of upwelling filaments off of Cape Blanco has been invoked to explain the $U_{37}^{K'}$ biases (see Section 4.3). These features result in the observation of particularly high-productivity waters, with high carbon-exporting potential, much further offshore than is typical in the OR/CA upwelling zone (Barth et al. 2002). Alkenone export at this latitude is predominantly associated with the onset of upwelling, coincident with the advent of these high-productivity features (Prahl et al. 1993). Low $\alpha_{K37}$ values at these locations make sense, then, in the context of the influence of growth dynamics put forth in Chapter 3. If production at these locations is persistently derived from these high-nutrient bloom features, then higher average growth rates, and thus lower values of $\alpha_{K37}$, may be represented by the exported alkenone signal. As discussed above, it is unclear whether these conditions would actually lead to

unusually high coccolithophore growth rates; prototypical bloom-succession dynamics would hold 'r-strategists', such as diatoms, as the predominant beneficiary, with the bulk of production by prymnesiophytes occurring after nutrients had been significantly reduced (e.g. Sieracki et al. 1993). Alternately, however, short, spatially- and temporally-isolated blooms should necessarily be lagged by grazing pressure (see Legendre 1990 for review), potentially exposing phytoplankton to nutrient stress prior to sedimentation (Figure 4.6). Alkenones exported to the seabed after filament events, then, may represent an a higher proportion of stationary-phase cells (which exhibit low $\alpha_{K37}$; Wolhowe et al. 2009; Chivall et al. 2014b) if rapid plankton growth depletes the limited nitrate pool before the grazer community can respond. Nutrient-stress effects are suggested to be partially responsible for the $U_{37}^{K'}$ biases in this area, in addition to the SST-anomalies exhibited by the filament waters themselves (Prahl et al. 2010).

The apparent lack of consistency core-to-core in this region may, in part, represent real spatial variability; W7909-174GC, which does not appear offset in $\alpha_{K37}$, is near shore (Figure 4.1A), where alkenone sedimentation has been shown to be much less associated with the onset of upwelling (Prahl et al. 1993). The fact that EW9504-17PC differs markedly in $\alpha_{K37}$ from proximal W8809A-5GC and W8909-22BC, however, may suggest a temporal bias in the piston core due to sediment loss. High sedimentation rates in this area (Mix et al. 1999, Appendix C) mean that these cores have the potential to resolve decadal-scale variability in upwelling conditions, such as that driven by the different regimes of the Pacific Decadal Oscillation. While surface sediments from W8809A-5GC and W8909-22BC (collected in 1988 and 1989, respectively) would theoretically integrate primarily sediments from the 1947-1977 negative PDO phase (Mantua et al. 1997), a bias on the order of decades for 'core-top' sediments in EW9504-17PC could mean sediments from the previous positive phase (1925-1947) were sampled. Positive PDO phases have been associated with weaker upwelling in the CCS (Narayan et al. 2010), and would presumably correspond to lower filament activity.

The second area of deviation from the $\alpha_{K37}$ vs. SST relationship is in the northern SCB (EW9504-10MC and NH0412-23-14MC), another location on the edge of the

OR/CA upwelling zone (Figure 4.1). It is possible that alkenone sedimentation over these sites derives from a production regime similar to the 42°N cores. Intense, summertime primary production occurs over the northwestern SCB (Figure 4.7), coincident with movement of water from the area of Point Conception, along the Santa Rosa Ridge, before curving to the west around the Catalina Eddy, as the California current in this area strengthens to a jet and moves inshore (Bray et al. 1999). This feature is host to extensive mesoscale eddy and meander activity (Lynn and Simpson 1987), and the wind events driving southward movement of California Current waters vary strongly on ~5 day time scales (e.g. Caldwell et al. 1986; Münchow 2000). Like the 42°N cores, export derived primarily from intermittent, patchy, nutrient-rich surface waters could drive alkenone sedimentation representative of abnormally high average growth rates. Again like 42°N, an alternate explanation could come in the form of growth-phase effects. The ~5 or 10 days it would take water to reach the locations of EW9504-10MC or NH0412-23-14MC, respectively, from Point Conception at the speed of spring and summer surface currents here (Bray et al. 1999) is an appropriate time-scale for phytoplankton blooms to consume ~2.5 μM nitrate (typical of surface water from the CCS near Point Conception during the upwelling season) and enter stationary phase if growth is lagged by grazing pressure (Figure 4.6). This mechanism may be more likely, as high primary productivity rates do not appear to be maintained as far as NH0412-23-14MC, potentially indicative of complete nutrient consumption at this distance from the water source (Figure 4.7). While not biased to the degree of the 42°N cores, EW9504-10MC does show a 'cold' $U_{37}^{K'}$ signal, potentially indicative of nutrient stress effects (Prahl et al. 2003). The lower magnitude of the $U_{37}^{K'}$ residual is likely due to the fact that, unlike the upwelling filaments discussed above, these summertime production features do not manifest as a SST anomaly (Bray et al. 1999). Significant warming has presumably occurred by the time water reaches NH0412-23-14MC.

The fact that NH0412-23-14MC and EW9504-5PC show such different $\alpha_{K37}$ vs. $U_{37}^{K'}$ residuals (5PC has a residual of 0) while being essentially co-located is difficult to explain. While this may be attributable to temporal biasing due to sediment loss,

similarly to what is suggested for EW9504-17PC above, sedimentation rates here are on the order of 1 cm $kyr^{-1}$, too low to resolve decadal-scale variability (Stott et al. 2000). The cores' location, the sediment-focusing San Clemente Basin, however, is prone to slope failures and turbidite deposits, meaning surface sediments collected nine years apart (1995 and 2004) may be sampling different material. Note that while EW9504-5PC does not show a low $\alpha_{K37}$ value relative to the overall trend with temperature, it is still low with respect to the $\alpha_{K37}$ trend with latitude (Figure 4.3A). This may be evidence that the north-south trend is not driven by temperature directly, but by growth rate (see Section 4.4.1), which relates to temperature in a potentially-variable way depending on species composition and other environmental factors.

Thus, there are two regions where low $\alpha_{K37}$ values, as per the mechanisms described in Chapter 3, may derive either from event-scale production with rapid growth (high lipid production rates) or from the termination that occurs afterwards (growth phase/nutrient stress effects). Upwelling-driven production at the CCS sites in the core the OR/CA upwelling zone, in contrast to the highly-dynamic terminuses at 42°N and in the northern SCB, appears predominantly as chlorophyll features that persist near frontal boundaries (Traganza et al. 1987). It is unclear whether or not this would result in lower average growth rates for coccolithophores. However, if post-bloom nutrient-stress effects are responsible for the $\alpha_{K37}$ residuals at the sites detailed above, different behavior in the core of the upwelling zone can be explained. It has been suggested that these more-typical upwelling blooms can be maintained in a band near the coastal nutrient source by microzooplankton grazing that is spatially and temporarily coincident with nutrient uptake by phytoplankton (Edwards et al. 2000). As microzooplankton are a size class thought to prey particularly efficiently on coccolithophores (e.g. Marañón et al. 1996), regulation of coccolithophore growth by grazing could explain the lack of 'stressed' signatures throughout most of the northern upwelling zone (Figure 4.6).

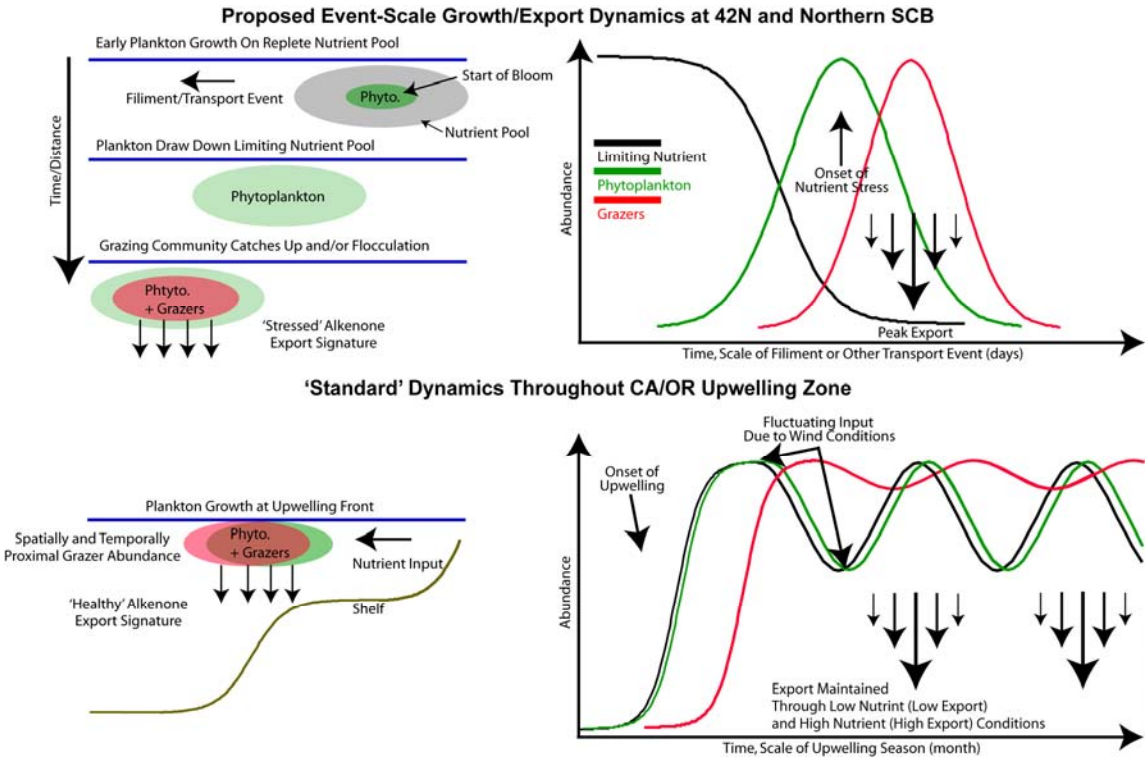


**Figure 4.6.** Schematic of the production and export regimes proposed in Section 4.4.2 for the modern CCS. The upper panels correspond to the event-scale, adjective, high-production regimes proposed for sedimentation offshore at 42°N (driven by upwelling filaments) and in the northern SCB (driven by intermittent transport of water from Pt. Conception southeast along the Santa Rosa Ridge). Here, isolated patches of advected nutrients are depleted prior to alkenone sedimentation, potentially leading to an impact of growth-phase effects on $\alpha_{K37}$ through nutrient stress. The lower panels correspond to more-typical export regimes throughout the core of the core of the OR/CA upwelling zone. Here, more temporally-consistent upwelling-driven coccolithophore productivity and export are maintained near the coast due to microzooplankton grazing.

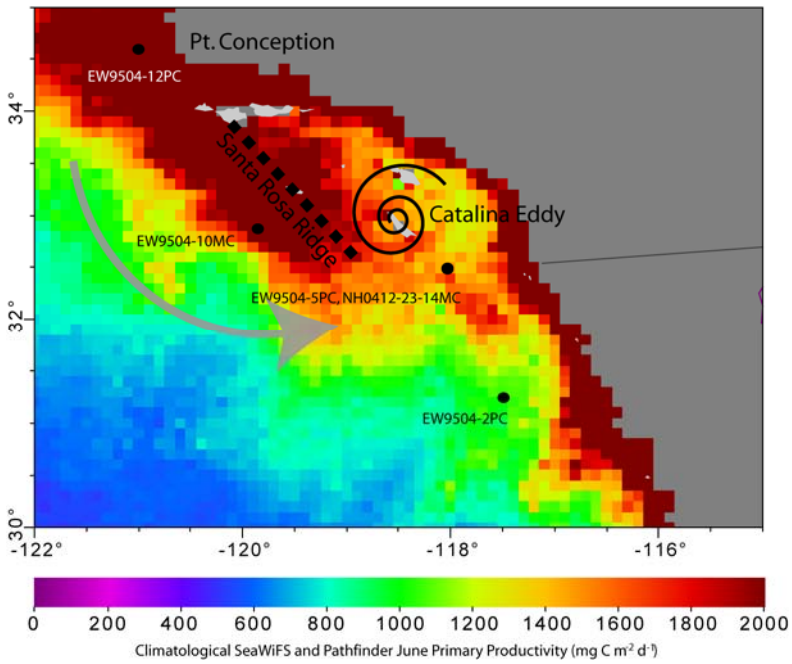


**Figure 4.7.** Satellite-derived, climatological, June primary productivity estimates in the SCB, illustrating the tongue of upwelled water transported southeast from Point Conception by the California Current. Productivity estimates are an experimental data set provided by NOAA CoastWatch, derived from SeaWiFS chlorophyll and Pathfinder SST (http://coastwatch.pfeg.noaa.gov/infog/PP_bfp1_las.html).

The core-top data, then, appear to illustrate a system where:

1) $U_{37}^{K'}$ generally reproduces maSST.
2) $\alpha_{K37}$ generally follows maSST and $U_{37}^{K'}$.
3) Deviations of $\alpha_{K37}$ from the maSST/$U_{37}^{K'}$ pattern may be tied to locations where alkenone sedimentation consistently derives from coccolithophores with abnormally high growth rates or which are subject to nutrient-stressed conditions prior to sedimentation.

Thus, while pairing $U_{37}^{K'}$ with $\delta D_{K37}$ measurements shows the potential to allow rough $\delta D_{H2O}$ estimates due to the overall relationship of $U_{37}^{K'}$ and $\alpha_{K37}$ shown here, pairing $U_{37}^{K'}$ with estimates of $\alpha_{K37}$ (possible in locations where independent estimates of $\delta D_{H2O}$ can be made) may serve as a useful ecological indicator.

If this is true, $\alpha_{K37}$ vs. $U_{37}^{K'}$ behavior at the LGM should reflect ecological changes known to have occurred at that time. Coincident with the margin-wide reduction in CCS activity and upwelling suggested to occur at this time, we see that no sites in the down-core data set possess $\alpha_{K37}$ vs. $U_{37}^{K'}$ residuals greater than uncertainty in $\alpha_{K37}$ (Figure 4.4D). Sample coverage at 42°N is admittedly less robust at the LGM; only EW9604-17PC is represented down core, which shows no modern anomaly (in contrast to the proximal cores box and gravity cores; Figure 4.4.C). Averaging three age-controlled samples across the LGM (Table 4.3) should negate the sampling concerns suggested above for EW9604-17PC, however. We may tentatively, then, interpret the 'disappearance' of anomalies in this area at the LGM as indicative as a reduction in the upwelling-driven filaments. The core-top $\alpha_{K37}$ anomaly observed in the SCB at EW9504-10MC (represented at the LGM by co-located EW9504-9PC) also disappears at the LGM (Figure 4.4D). This is consistent with a northward retreat of the California Current at this time (Herbert et al. 2001) and a cessation of alkenone export derived from the southward-transported, high-nutrient waters that drive modern production over the northwest borderlands.

**4.5. Conclusions:**

Analysis of paired $U_{37}^{K'}$ and $\delta D_{K37}$ values in sediments from the eastern margin of the North Pacific has revealed patterns in the isotopic composition of coccolithophorid biomarkers. Spatial variability in alkenone isotopic composition in this marine setting appears, as expected, to relate almost entirely to changes in $\alpha_{K37}$ as opposed to variability in the salinity or isotopic composition of surface water. This allows for analysis of controls on $\alpha_{K37}$. In opposition to previous field observations that would lead us to expect no, or even a positive, relationship between $\alpha_{K37}$ and temperature, core-top and LGM alkenone samples show a strong, inverse functionality between $\alpha_{K37}$ and maSST and/or $U_{37}^{K'}$. While it is possible that this relationship is due to light effects on $\alpha_{K37}$ and a correlation of maSST and average production depth, this is argued to be unlikely. It appears, instead, that the averaging nature of sediments reveals control of $\alpha_{K37}$ by either temperature directly or by the growth-rate controls proposed in Chapter 3, which may in turn be driven by temperature on these time scales. This co-variation of $\alpha_{K37}$ and a separate, co-eval molecular signal ($U_{37}^{K'}$) illustrates three potential uses for $\delta D_{K37}$ as a sedimentary proxy, depending on the mechanism behind the apparent temperature dependence and whether our preliminary identification of regional variability about the $\alpha_{K37}$ vs. $U_{37}^{K'}$ relationship is accurate:

1) If the 'scatter' about the $\alpha_{K37}$ vs. $U_{37}^{K'}$ relationship proves to be analytical in nature and temperature itself controls $\alpha_{K37}$, then $U_{37}^{K'}$ is the dominant predictor of marine $\alpha_{K37}$. $\delta D_{K37}$, in this case, may serve as a hydrologic proxy outside of the high salinity-contrast, high isotopic-contrast areas to which it previously appeared to be restricted.
2) If the dependence of $\alpha_{K37}$ on $U_{37}^{K'}$ is due to temperature control of growth rate on sufficiently long time scales, then $\alpha_{K37}$ may serve as a proxy for alkenone-producer growth rate as discussed in Chapter 3. While useful as a paleoecological measure in its own right, alkenone-producer specific growth rate estimates would enable

the use of alkenones as a paleo-$pCO_2$ proxy, a tool currently complicated by the inability to constrain growth rate in the past (see Pagani et al. 2014; Chapter 3).

3) If regional deviation from the $\alpha_{K37}$ vs. $U_{37}^{K'}$ relationship is correctly interpreted in terms of previously-described physiological and ecological impacts on $\alpha_{K37}$, then this term may serve as an indicator of coccolithophore export derived primarily from more or less temporally-patchy production. Sedimentary alkenones at the highly-dynamic terminuses of the California/Oregon upwelling zone, for example, exhibit negative $\alpha_{K37}$ vs. $U_{37}^{K'}$ anomalies that may represent the impact of post-bloom nutrient stress associated with transient, short time-scale growth events lagged by grazing pressure. This would illustrate the potential for $\alpha_{K37}$ to lend valuable ecological context to $U_{37}^{K'}$ data and reconstructions of PIC production and export.

A thorough understanding of local oceanography, such as what an indication of 'bloom/stressed' or 'normal' alkenone sedimentation might mean for the fidelity of the $U_{37}^{K'}$ record, will clearly be necessary to interpret paired analyses of $U_{37}^{K'}$ and $\delta D_{K37}$ in the future. However, the data presented here shows, regardless of cause, a systematic trend in $\alpha_{K37}$ in sediments independent of salinity variation. The potential of $\delta D_{K37}$ in paleoecological/paleoclimatological studies will be clear if future analysis of this property in sediments from other marine settings, with better core-top age controls or in sediment traps (to enable more precise comparison to overlying ecological conditions), can reveal which of the mechanisms proposed above is responsible for these observations.

## 4.6. References:


Abbott M.R. and Zion P.M. (1987) Spatial and temporal variability of phytoplankton pigment off northern California during Coastal Ocean Dynamics Experiment 1. *J. Geophys. Res.* **92**, 10.1029/JC092IC02P01745.

Barth J.A., Cowles T.J., Kosro M., Shearman R.K., Huyer A. and Smith R.L. (2002) Injection of carbon from the shelf to offshore beneath the euphotic zone in the California Current. *J. Geophys. Res.* **106**, 3057.

Bray N.A., Keyes A. and Morawitz W.M.L. (1999) The California Current system in the Southern California Bight and the Santa Barbara Channel. *J. Geophys. Res.* **104**, 7695-7714.

Buitenhuis E.T., Pangerc T., Franklin D.J., Le Quéré C. and Malin G. (2008) Growth rates of six coccolithophorid strains as a function of temperature. *Limnol. Oceanogr.* **53**, 1181-1185.

Caldwell P.C., Stuart D.W. and Brink K.H. (1986) Mesoscale wind variability near Point Conception, California during spring 1983. *J. Clim. Appl. Meteorol.* **25**, 1241-1254.

Chivall D., M'Boule D., Sinke-Schoen D., Sinninghe Damsté J.S., Schouten S. and van der Meer M.T.J. (2014b) The effects of growth phase and salinity on the hydrogen isotopic composition of alkenones produced by coastal haptophyte algae. *Geochim. Cosmochim. Ac.* **140**, 381-390.

Christie W.W. (2003) *Lipid Analysis: Isolation, Separation, Identification and Structural Analysis of Lipids*. The Oily Press.

D'Andrea W.J., Liu Z., Alexandre M.D., Wattley S., Herbert T.D. and Huang Y. (2007) An efficient method for isolating individual long-chain alkenones for compound-specific hydrogen isotope analysis. *Anal. Chem.* **79**, 3430-3435.

Doose H., Prahl F.G. and Lyle M. (1997) Biomarker temperature estimates for modern and last glacial surface waters of the California Current system between 33º and 42ºN. *Paleoceanography* **12,** 615-622.

Edwards C.A., Batchelder H.P. and Powell T.M. (2000) Modeling microzooplankton and macrozooplankton dynamics within a coastal upwelling system. *J. Plankton Res.* **22**, 1619-1648.

Englebrecht A.C. and Sachs J.P. (2005) Determination of sediment provenance at drift sites using hydrogen isotopes and unsaturation ratios in alkenones. *Geochim. Cosmochim. Ac.* **69**, 4253-4265.

Espinosa-Carreón T.L., Gaxiola-Castro G., Beier E., Strub P.T. and Kurczyn J.A. (2012) Effects of mesoscale processes on phytoplankton chlorophyll off Baja California. *J. Geophys. Res.* **117**, 10.1029/2011JC007604.

Garcia, H.E., Locarnini R.A., Boyer T.P., Antonov J.I., Baranova O.K., Zweng M.M., Reagan J.R. and Johnson D.R. (2014) World Ocean Atlas 2013, Volume 4: Dissolved Inorganic Nutrients (phosphate, nitrate, silicate). [Ed] S. Levitus, A. Mishonov; NOAA Atlas NESDIS 76, 25 pp.

Harris G.P. (1980) Temporal and spatial scales in phytoplankton ecology. Mechanisms, methods, models, and management. *Can. J. Fish. Aquat. Sci.* **37**, 877-900.

Herbert T.D., Schuffert J.D. and Thomas D. (1998) Depth and seasonality of alkenone production along the California margin inferred from a core top transect. *Paleoceanography* **13,** 263-271.

Herbert T.D., Schuffert J.D., Andreasen D., Heusser L., Lyle M., Mix A., Ravelo A.C. Stott L.D. and Herguera J.C. (2001) Collapse of the California Current during glacial maxima linked to climate change on land. *Science* **293**, 71-76.

Herbert T.D. (2003) Alkenone paleotemperature determinations, p. 391-342. *In* K.K. Turekian and H.D. Holland [eds.], *Treatise on Geochemistry*, Vol. 6. Elsevier.

Hut G. (1987) Consultants group meeting on stable isotope reference samples for geochemical and hydrological investigations. Report to the Director General, International Atomic Energy Agency, Vienna, 42 pp.

Huyer A. (1983) Coastal upwelling in the California current system. *Prog. Oceanogr.* **12**, 259-284.

Iglesias-Rodríguez M.D., Brown C.W., Doney S.C., Kleypas J., Kolber D., Hayes P.K. and Falkowski P.G. (2002) Representing key phytoplankton functional groups in ocean carbon cycle models: Coccolithophorids. *Global Biogeochem. Cy.* **16**, doi:10.1029/2001GB001454.

Legendre L. (1990) The significance of microalgal blooms for fisheries and for the export of particulate organic carbon in oceans. *J. Plankton Res.* **12**, 681-699.

LeGrande A.N. and Schmidt G.A. (2006) Global gridded data set of the oxygen isotopic composition in seawater. *Geophys. Res. Lett.* **33**, 10.1029/2006GL026011.

Lyle M., Koizumi I., Richter C. and Moore Jr. T.C. (2000) Proc. ODP, Sci. Results, 167: College Station, TX (Ocean Drilling Program). doi:10.2973/odp.proc.sr.167.2000.

Lynn R.J. and Simpson J.J. (1987) The California Current system: the seasonal variability of its physical characteristics. *J. Geophys. Res.* **92**, 12947-12966.

Mangelsdorf K., Guntner U. and Rullkötter J. (2000) Climatic and oceanographic variations on the California continental margin during the last 160 kyr. *Org. Geochem.* **31**, 829-846.

Mantua N.J., Hare S.R., Zhang Y., Wallace J.M. and Francis R.C. (1997) A Pacific interdecadal climate oscillation with impacts on salmon production. *Bul. Am. Meteorolg. Soc.* **78**, 1069-1079.

Marañón E., Fernández E., Harris R.P. and Harbour D.S. (1996) Effects of the diatom-*Emiliania huxleyi* succession on photosynthesis, calcification and carbon metabolism bu size-fractionated phytoplankton. *Hydrobiolog.* **317**, 189-199.

Marañón E., Cermeño P., Huete-Ortega M., López-Sandoval D.C., Mouriño-Carballido B. and Rodríguez-Ramos T. (2014) Resource supply overrides temperature as a controlling factor of marine phytoplankton growth. *PLoS ONE* **9**, doi:10.1371/journal.pone.0099312.

MARGO Project Members (2009) Constraints on the magnitude and patters of ocean cooling at the Last Glacial Maximum. *Nature Geosci.* **2**, 127-132.

Marlowe I.T., Green J.C., Neal A.C., Brassell S.C., Eglinton G. and Course P.A. (1984) Long chain (n-$C_{37}$-$C_{39}$) alkenones in the Prymnesiophyceae. Distribution of alkenones and other lipids and their taxonomic significance. *Brit. Phycol. J.* **19**, 203-216.

M'boule D., Chivall D., Sinke-Schoen D., Sinninghe Damsté J.S., Schouten S. and van der Meer M.T.J. (2014) Salinity dependent hydrogen isotope fractionation in alkenones produced by coastal and open ocean haptophyte algae. *Geochim. Cosmochim. Ac.* **130**, 126-135.

Mix A.C., Lund D.C., Pisias N.G., Bodén P., Bornmalm L., Lyle M. and Pike J. (1999) Rapid climate oscillations in the Northeast Pacific during the last deglaciation reflect northern and southern hemisphere sources. *In* [Eds] P.U. Clark, R.S. Webb and L.D. Keigwin, Geophysical Monograph Series Vol 112: Mechanisms of Global Climate Change at Millennial Time Scales. American Geophysical Union.

Mix A.C., Bard E. and Schneider R. (2001) Environmental processes of the ice age: land, oceans, glaciers (EPILOG). *Quat. Sci. Rev.* **20**, 627-657.

Mjaaland, G. (1956) Some laboratory experiments on the coccolithophorid *Coccolithus huxleyi*. *Oikos* **7**, 251-255.

Mulitza S., Boltovskoy D., Donner B., Meggers H., Paul A. and Wefer G. (2003) Temperature:$\delta^{18}O$ relationships of planktonic foraminifera collected from surface waters. *Paleogeo. Paleoclim. Paleoecol.* **202**, 143-152.

Müller P.J., Kirst G., Ruhland G., von Storch I. and Rosell-Melé A. (1998) Calibration of the alkenone paleotemperature index UK'37 based on core-tops from the eastern South Atlantic and the global ocean (60°N-60°S). *Geochim. Cosmochim. Ac.* **62**, 1757-1772.

Münchow A. (2000) Wind stress curl forcing of the coastal ocean near Point Conception, California. *J. Phys. Oce.* **30**, 1265-1280.

Narayan N., Paul A., Mulitza S. and Schulz M. (2010) Trends in coastal upwelling intensity during the late 20$^{th}$ century. *Ocean Sci.* **6**, 815-823.

Ostlund H.G., Craig H., Broecker W.S. and Spenser D. (1987) GEOSECS Atlantic, Pacific, and Indian Ocean expeditions. *In* Shore-based Data and Graphics, Vol 7, pp. 1-200, Natl. Sci. Found., Washington D.C.

Pagani M. (2014). Biomarker-based inferences of past climate: The alkenone *p*CO2 proxy, p. 361-378. *In* H.D. Holland and K.K. Turekian and [eds.], *Treatise on Geochemistry*. 2$^{nd}$ Ed., Vol. 12. Elsevier.

Pahnke K., Sachs J.P., Keigwin L., Timmermann A. and Xie S. (2007) Eastern tropical Pacific hydrologic changes during the past 27,000 years from D/H ratios in alkenones. *Paleoceanography* **22,** 10.1029/2007PA001468.

Prahl F.G. and Pinto L.A. (1987) A geochemical study of long-chain n-aldehydes in Washington coastal sediments. *Geochim. Cosmochim. Ac.* **51**, 1573-1582.

Prahl F.G., Muehlhausen L.A. and Zahnle D.L. (1988) Further evaluation of long-chain alkenones as indicators of paleoceanographic conditions. *Geochim. Cosmochim. Ac.* **52**, 2303-2310.

Prahl F.G., Collier R.B., Dymond J., Lyle M. and Sparrow M.A. (1993). A biomarker perspective on prymnesiophyte productivity in the northeast Pacific Ocean. *Deep-Sea Res. Pt. I* **40**, 2061-2076.

Prahl F. G., Rontani J., Zabeti N., Walinsky S. E., and Sparrow M. A. (2010) Systematic pattern in UK'37-Temperature residuals for surface sediments from high latitude and other oceanographic settings. *Geochimica et Cosmochimica Acta* **74**, 131-143.

Romero-Viana L., Kienel U., Wilkes H. and Sachse D. (2013) Growth-dependent hydrogen isotopic fractionation of algal lipid biomarkers in hypersaline Isabel Lake (México). *Geochim. Cosmochim. Ac*. **106**, 490-500.

Schwab V.F. and Sachs J.P. (2011) Hydrogen isotopes in individual alkenones from the Chesapeake Bay estuary. *Geochim. Cosmochim. Ac.* **75**, 7552-7565.

Sieracki M.E., Verity P.G. and Stoecker D.K. (1993) Plankton community response to sequential silicate and nitrate depletion during the 1989 North Atlantic spring bloom. *Deep Sea Res II* **40**, 213-225.

Stott L.D., Neumann M. and Hammond D. (2000) Intermediate water ventilation on the northeastern Pacific margin during the late Pleistocene inferred from benthic foraminiferal δ13C. *Paleoceanography* **15**, 161-169.

Thunell R.C. (1998) Particle fluxes in a coastal upwelling zone: sediment trap results from Santa Barbara Basin, California. *Deep-Sea Res. Pt. II* **45**, 1863-1884.

Traganza E.D., Redalije D.G. and Garwood R.W. (1987) Chemical flux, mixed layer entrainment and phytoplankton blooms at upwelling fronts in the California coastal zone. *Cont. Shelf. Res*. **7**, 89-105.

van der Meer M.T.J., Sangiorgi F., Baas M., Brinkhuis H., Sinninghe Damsté J.S. and Schoutan S. (2008) Molecular isotopic and dinoflagellate evidence for Late Holocene freshening of the Black Sea. *Earth Planet. Sc. Lett.* **267**, 426-434.

van der Meer M.T.J., Benthien A., Bijma J., Schouten S. and Sinninghe Damsté J.S. (2013) Alkenone distribution impacts the hydrogen isotopic composition of the $C_{37:2}$ and $C_{37:3}$ alkan-2-ones in *Emiliania huxleyi*. *Geochim. Cosmochim. Ac.* **111**, 162-166.

Vasiliev I., Reichart G.-J. and Krijgsman W. (2013) Impact of the Messinian Salinity Crisis on Black Sea hydrology – Insights from hydrogen isotopes analysis on biomarkers. *Earth Plan. Sci. Lett.* **362**, 272-282.

Volkman J.K., Eglinton G., Corner E.D.S. and Sargent J.R. (1980) Novel unsaturated straight-chain C37-C39 methyl and ethyl ketones in marine sediments and a coccolithophore *Emiliania huxleyi*, p. 219-227. *In* A.G. Douglas and J.R. Maxwell [eds.], *Advances in organic geochemistry, 1979: Proceedings of the Ninth International Meeting on Organic Geochemistry*. Pergamon Press.

Volkman J.K., Barrett S.M., Blackburn S.I. and Sikes E.L. (1995) Alkenones in *Gephyrocapsa oceanica*: Implications for studies of paleoclimate. *Geochim. Cosmochim. Ac.* **59**, 513-520.

Walinsky S.E., Prahl F.G., Mix A.C., Finney B.P., Jaeger J.M. and Rosen G.P. (2009) Distribution and composition of organic matter in surface sediments of coastal Southeast Alaska. *Cont. Shelf Res.* **29**, 1565-1579.

Wolhowe M.D., Prahl F.G., Probert I. and Maldonado M. (2009) Growth phase dependent hydrogen isotopic fractionation in alkenone-producing haptophytes. *Biogeosci.* **8**, 1681-1694.

Wolhowe M.D., Prahl F.G., White A.E., Popp B.N. and Rosas-Navarro A. (2014) A biomarker perspective on coccolithophorid growth and export in a stratified sea. *Prog. Oceanog.* **122**, 65-76.

Yamamoto M., Yamamuro M., and Tanaka Y. (2007) The California current system during the last 136,000 years: response of the North Pacific High to precessional forcing. *Quaternary Science Reviews* **26**, 405-414.

Zhang Z., Sachs J.P. and Marchetti A. (2009) Hydrogen isotope fractionation in freshwater and marine algae: II. Temperature and nitrogen limited growth rate effects. *Org. Geochem.* **40**, 428-439.

Zweng, M.M, J.R. Reagan, J.I. Antonov, R.A. Locarnini, A.V. Mishonov, T.P. Boyer, H.E. Garcia, O.K. Baranova, D.R. Johnson, D.Seidov, M.M. Biddle, 2013. World Ocean Atlas 2013, Volume 2: Salinity. S. Levitus, Ed., A. Mishonov Technical Ed.; NOAA Atlas NESDIS 74, 39 pp.

# V. General Conclusions

The work detailed in the previous chapters had three primary goals: A) to gain insight into the response of coccolithophores to strong thermal and nutrient stratification, B) to determine what, and how, physiological factors control $\alpha_{K37}$, and C) to test whether $\delta D_{K37}$ varies in the marine sedimentary record in a manner useful to the paleoclimatological or paleoecological communities. While the systems under consideration are complex, analytically challenging, and often data-sparse, these goals were met. There is, as is typical of most studies of natural systems, abundant room for future work to confirm or disprove many of the tentative conclusions reached above. The results of this work are promising, nonetheless.

With regards to the characterization of coccolithophore production and export in a thermally-stratified water column, we can state unambiguously that:

- While production of alkenone biomarkers is a more important component of overall carbon fixation in the summertime GoCal and ETNP under more nutrient-stratified conditions, integrated production rates of coccolithophorid cells, relative to bulk carbon fixation, do not vary with nutrient conditions.
- Patterns in alkenone:POC export or estimated coccolithophorid cell:POC export are decoupled from patterns these components' relative production rates. Instead, the controlling factor appears to be variations in the export efficiency of bulk organic carbon.

With regards to the determination of the factors controlling $\alpha_{K37}$, we can with certainty state that:

- In culture, $\alpha_{K37}$ covaries with per-cell alkenone quota, and by extension growth phase, more than previously-identified physiological or environmental.
- In the summertime GoCal/ETNP study area, $\alpha_{K37}$ varies negatively with alkenone-producing cell abundance, decreasing towards the productive nitracline, and positively with the carbon isotopic fractionation parameter $\varepsilon_p$.

With regards to the sedimentary application of $\delta D_{K37}$ values, it has been made clear that:

- Core-top and LGM alkenone samples along the Pacific margin of North America show a strong, inverse functionality between $\alpha_{K37}$ and maSST and/or $U_{37}^{K'}$. If

$U_{37}^{K'}$ truly serves as the primary predictor of sedimentary $\alpha_{K37}$ in areas of low salinity contrast, then paired measurements of $U_{37}^{K'}$ and $\delta D_{K37}$ should enable the estimation of paleoceanographic $\delta D_{H2O}$.

Many of these findings are surprising. One would expect coccolithophore production to be increasingly favored under increasingly nutrient-poor conditions; this work, in contrast, shows that under sufficiently stratified conditions, this functionality may be absent. Based on previous culture work, one would expect $\alpha_{K37}$ in culture to primarily be controlled by temperature and growth phase, and in the field to have higher values closer to the source of limiting nutrients; this work shows strong variability independent of both these properties, and the opposite trend in the water column. In light of existing knowledge of $\alpha_{K37}$ dynamics, one would expect sedimentary $\alpha_{K37}$ along the Baja/California/Oregon margin to vary with overlying upwelling conditions; instead, temperature appears to be a dominant control. To place these unexpected findings in broader conceptual frameworks, a number of more speculative conclusions were reached. While assuredly subject to future revision, they have broad oceanographic and climatological implications.

- A threshold of temporal stability may exist beyond which the euphotic zone may lose its low- to mid-nutrient, coccolithophore-favorable niche. In these settings, coccolithophore production, relative to bulk production, may depend on decoupling of the nutricline and the euphotic depth, as opposed to nutricline depth itself. As such, coccolithophore export may serve as a weaker feedback on atmospheric $CO_2$ levels than previously expected from theoretical warming- and stratification-driven enhancement.
- A control of lipid production rate on $\alpha_{K37}$ can be explained by increased use of the OPP pathway to generate reductant at higher lipid demand. Dependence on the relative importance of the OPP pathway to lipid synthesis would explain A) the previously-observed dependence of $\alpha_{K37}$ on growth rate (faster growing cells express increased lipid synthesis and OPP activity), B) the inconsistent nature of this growth-rate response (different changes in photosynthetic energy allocation

will be observed in response to changes in growth rate for different strains, environmental conditions, etc.) and C) the growth-phase response (high catabolic rates are observed for nutrient-limited stationary phase cells). While depth-dependence of $\alpha_{K37}$ in the *in situ* samples may show a dependence of light that is not represented in our nutrient-limited cultures, the proposed lipid-production mechanism can explain the relationship between $\alpha_{K37}$ and $\varepsilon_p$, which appears to indicate lower values of $\alpha_{K37}$ at higher growth rates associated with the nitracline.

• In light of the conclusions above regarding the functionality of $\alpha_{K37}$, we suggest that the sedimentary $\alpha_{K37}$ vs. temperature relationship in eastern North Pacific margin may be driven by a control of temperature on alkenone-producer growth rates on long time scales, rather than temperature itself. If true, this would mean that $\alpha_{K37}$, estimates would allow more-effective application of $\varepsilon_p$ as a paleo-$pCO_2$ proxy, as this tool has previously been hampered by the inability to constrain growth rate. Local variation about the $\alpha_{K37}$ vs. temperature relationship in core-tops may relate to samples whose alkenone inputs derive primarily from transient, bloom-like event scale production where cells deplete available nutrients prior to sedimentation, resulting in exposure to nutrient stress. Changes in the pattern of deviations at the LGM are potentially consistent with a retreat of the California Current and reduction of upwelling at this time. If true, estimates of $\alpha_{K37}$ may lend valuable context to $U_{37}^{K'}$ data and reconstructions of PIC production and export.

There are a number of straightforward steps that may be taken in the future to reduce the ambiguity surrounding these 'bigger-picture' conclusions. For the case of a disappearing coccolithophore niche in sufficiently stratified conditions, production and abundance studies similar to those detailed in Chapter 2, conducted in other warm, low-nutrient settings, and with explicit determination if PIC fluxes, would help determine the wider applicability of the conclusions from this regional study. Chapter 3 suggests many experiments that could improve/confirm our understanding of physiological controls on $\alpha_{K37}$, including pairing δD analysis with $^{13}C$ pulse-chase experiments, in order to observe dependence of $\alpha_{K37}$ on carbon processing, and monitoring the isotopic composition of

alkenones in over periods of darkness in both axenic and non-axenic cultures to better determine the mechanism of any temperature control on $\alpha_{K37}$. Comparison of the *in situ* samples described in Chapter 3 to similar measurements made in other oceanographic settings (developing coccolithophore blooms, for example) would help determine whether the conclusions regarding the relative importance of growth rate and light are valid or have applicability to the wider ocean. The three potential interpretations of the sedimentary data in Chapter 4 may also be resolved with greater data coverage, in addition to improved temporal controls compound-specific analytical capability. Should future work of this sort more fully resolve the cause for the observed sedimentary $\alpha_{K37}$ dynamics, $\delta D_{K37}$ would possess strong utility as an ecological and/or physiological proxy.

# Bibliography

Adkins J.F. and Schrag D.P. (2003) Reconstructing Last Glacial Maximum bottom water salinities from deep-sea sediment pore fluid profiles. *Earth Plan. Sci. Lett.* **216**, 109-123.

Abbott M.R. and Zion P.M. (1987) Spatial and temporal variability of phytoplankton pigment off northern California during Coastal Ocean Dynamics Experiment 1. *J. Geophys. Res.* **92**, 10.1029/JC092IC02P01745.

Balch W.M. and Utgoff P.E. (2009) Potential interactions among ocean acidification, coccolithophores, and the optical properties of seawater. *Oceanogr*. **22**, 146-159.

Barth J.A., Cowles T.J., Kosro M., Shearman R.K., Huyer A. and Smith R.L. (2002) Injection of carbon from the shelf to offshore beneath the euphotic zone in the California Current. *J. Geophys. Res.* **106**, 3057.

Baumann K.-H., Backel B. and Frenz M. (2004) Coccolith contribution to South Atlantic carbonate sedimentation, p. 368-402. *In* H.R. Thierstein and J.R. Young [eds.], *Coccolithophores*. Springer.

Beaufort L., Probert I., de Garidel-Thoron T., Bendif E.M., Ruiz-Pino D., Metzl N., Goyet C., Buchet N., Coupel P., Grelaud M., Rost B., Rickaby R.E.M. and de Vargas C. (2011) Sensitivity of coccolithophores to carbonate chemistry and ocean acidification. *Nature* **476**, 80-83.

Bleijswijk J.D.L.v., Kempers R.S., Veldhuis M.J. and Westbroek P. (1994) Cell and growth characteristics of type A and B of *Emiliania huxleyi* (Prymnesiophyceae) as determined by flow cytometry and chemical analyses. *J. Phycol.* **30**, 230-241.

Bollmann J. (1997) Morphology and biogeography of *Gephyrocapsa* coccoliths in Holocene sediments. *Mar. Micropaleontol.* **29**, 319-350.

Bray N.A., Keyes A. and Morawitz W.M.L. (1999) The California Current system in the Southern California Bight and the Santa Barbara Channel. *J. Geophys. Res.* **104**, 7695-7714.

Brown C.W. and Yoder J.A. (1994) Coccolithophorid blooms in the global ocean. *J. Geophys. Res.* **99**, 7467-7482.

Buesseler K.O., Antia A.N., Chen M., Fowler S.W., Gardner W.D., Gustafsson O., Harada K., Michaels A.F., van der Loeff M.R., Sarin M., Steinberg D.K. and Trull T. (2007) An assessment of the use of sediment traps for estimating upper ocean particle fluxes. *J. Mar. Res.* **65,** 345-416.

Buitenhuis E.T., Pangerc T., Franklin D.J., Le Quéré C. and Malin G. (2008) Growth rates of six coccolithophorid strains as a function of temperature. *Limnol. Oceanogr.* **53**, 1181-1185.

Burd A.B. and Jackson G.A. (2009) Particle aggregation. *Annu. Rev. Mar. Sci.* **1**, 65-90.

Caldwell P.C., Stuart D.W. and Brink K.H. (1986) Mesoscale wind variability near Point Conception, California during spring 1983. *J. Clim. Appl. Meteorol.* **25**, 1241-1254.

Cermeño P., Dutkiewicz S., Harris R.P., Follows M., Schofield O. and Falkowski P.G. (2008) The role of nutricline depth in regulating the ocean carbon cycle. *P. Natl. Acad. Sci. USA* **105**, 20344-20349.

Chikaraishi Y., Naraoka H. and Poulson S. R. (2004a) Carbon and hydrogen isotopic fractionation during lipid biosynthesis in a higher plant (*Cryptomeria japonica*). *Phytochem.* **65**, 323-330.

Chikaraishi Y., Suzuki Y. and Naroaka H. (2004b) Hydrogen isotopic fractionations during desaturation and elongation associated with polyunsaturated fatty acid biosynthesis in marine macroalgae. *Phytochem.* **65**, 2293-2300.

Chivall D., M'Boule D., Sinke-Schoen D., Sinninghe Damsté J.S., Schouten S. and van der Meer M.T.J. (2014a) Impact of salinity and growth phase on alkenone distributions in coastal haptophytes. *Org. Geochem.* **67**, 31-34.

Chivall D., M'Boule D., Sinke-Schoen D., Sinninghe Damsté J.S., Schouten S. and van der Meer M.T.J. (2014b) The effects of growth phase and salinity on the hydrogen isotopic composition of alkenones produced by coastal haptophyte algae. *Geochim. Cosmochim. Ac.* **140**, 381-390.

Christie W.W. (2003) *Lipid Analysis: Isolation, Separation, Identification and Structural Analysis of Lipids*. The Oily Press.

Coale K.H. and Bruland K.W. (1987) Oceanic stratified euphotic zone as elucidated by $^{234}Th$:$^{238}U$ disequilibria. *Limnol. Oceanogr.* **32**, 189-200.

Conte M.H., Thompson A., Lesley D. and Harris R.P. (1998) Genetic and physiological influences on the alkenone/alkenoate versus growth temperature relationship in *Emiliania huxleyi* and *Gephyrocapsa oceanica*. *Geochim. Cosmochim. Ac.* **62**, 51-68.

Coplen T.B., Wildman J.D. and Chen J. (1991) Improvements in the gaseous hydrogen-water equilibration technique for hydrogen isotope ratio analysis. *Anal. Chem.* **63**, 910-912.

Craig H. and Gordon L.I. (1965) Deuterium and oxygen 18 variations in the ocean and marine atmosphere. *In* E. Tongiorgi [ed.] *Stable Isotopes in Oceanographic Studies and Paleotemperatures*. Laboratorio di Geologia Nucleare, Pisa, Italy.

D'Andrea W.J., Liu Z., Alexandre M.D., Wattley S., Herbert T.D. and Huang Y. (2007) An efficient method for isolating individual long-chain alkenones for compound-specific hydrogen isotope analysis. *Anal. Chem.* **79**, 3430-3435.

De Bernardi B., Ziveri P., Erba E. and Thunell R.C. (2005) Coccolithophore export production during the 1997-1998 El Nino event in Santa Barbara Basin (California). *Mar. Micropaleo.* **55**, 107-125.

de Vargas C. and Probert I. (2004) New keys to the past: current and future DNA studies in Coccolithophores. *Micropaleontol.* **50**, 45-54.

Doose H., Prahl F.G. and Lyle M. (1997) Biomarker temperature estimates for modern and last glacial surface waters of the California Current system between 33º and 42ºN. *Paleoceanography* **12,** 615-622.

Edwards C.A., Batchelder H.P. and Powell T.M. (2000) Modeling microzooplankton and macrozooplankton dynamics within a coastal upwelling system. *J. Plankton Res.* **22**, 1619-1648.

Eltgroth M.L., Watwood R.L. and Wolfe G.V. (2005) Production and cellular localization of neutral long-chain lipids in the haptophyte algae *Isochrisis galbana* and *Emiliania huxleyi*. *J. Phycol.* **41**, 1000-1009.

Englebrecht A.C. and Sachs J.P. (2005) Determination of sediment provenance at drift sites using hydrogen isotopes and unsaturation ratios in alkenones. *Geochim. Cosmochim. Ac.* **69**, 4253-4265.

Epstein B.L., D'Hondt S. and Hargraves P.E. (2001) The possible metabolic role of $C_{37}$ alkenones in *Emiliania huxleyi*. *Org. Geochem.* **32**, 867-875.

Espinosa-Carreón T.L., Gaxiola-Castro G., Beier E., Strub P.T. and Kurczyn J.A. (2012) Effects of mesoscale processes on phytoplankton chlorophyll off Baja California. *J. Geophys. Res.* **117**, 10.1029/2011JC007604.

Estep M.F. and Hoering T.C. (1980) Biogeochemistry of the stable hydrogen isotopes. *Geochim. Cosmochim. Ac.* **44**, 1197-1206.

Estep M.F. and Hoering T.C. (1981) Stable hydrogen isotope fractionations during autotrophic and mixotrophic growth in microalgae. *Plant. Physiol.* **67**, 474-477.

Fan J., Ye J., Kamphorst J.J., Shlomi T., Thompson C.B. and Rabinowitz J.D. (2014) Quantitative flux analysis reveals folate-dependent NADPH production. *Nature* **510**, 298-302.

Fernández E., Boyd P., Holligan P.M. and Harbour D.S. (1993) Production of organic and inorganic carbon within a large-scale coccolithophore bloom in the northeast Atlantic Ocean. *Mar. Ecol.-Prog. Ser*. **97**, 271-285.

Fernández E., Balch W.M., Marañón E. And Holligan P.M. (1994) High rates of lipid biosynthesis in cultured, mesocosm and coastal populations of the coccolithophore *Emiliania huxleyi*. *Mar. Ecol. Prog. Ser.* **114**, 13-22.

Fernández E., Fritz J.J. and Balch W.M. (1996) Chemical composition of the coccolithophorid *Emiliania huxleyi* under light-limited steady state growth. *J. Exp. Mar. Biol. Ecol.* **207**, 149-160.

Garcia, H.E., Locarnini R.A., Boyer T.P., Antonov J.I., Baranova O.K., Zweng M.M., Reagan J.R. and Johnson D.R. (2014) World Ocean Atlas 2013, Volume 4: Dissolved Inorganic Nutrients (phosphate, nitrate, silicate). [Ed] S. Levitus, A. Mishonov; NOAA Atlas NESDIS 76, 25 pp.

Goñi M.A., Hartz D.M., Thunell R.C. and Tappa E. (2001) Oceanographic considerations for the application of the alkenone-based paleotemperature $U_{37}^{K'}$ index in the Gulf of California. *Geochim. Cosmochim. Ac.* **65**, 545-557.

Halsey K.H. and Jones B.M. (2014) Phytoplankton strategies for photosynthetic energy allocation. *Annu. Rev. Mar. Sci.* **7**, 5.1-5.33.

Halsey K.H., Milligan A.J. and Behrenfeld M.J. (2011) Linking time-dependant carbon-fixation efficiencies in *Dunalielia tertiolecta* (Chlorophyceae) to underlying metabolic pathways. *J. Phycol.* **47**, 66-76.

Hama T., Miyazaki T., Ogawa Y., Iwakuma T., Takahashi M., Otsuki A. and Ichimura S. (1983) Measurement of photosynthetic production of a marine phytoplankton population using a stable $^{13}C$ isotope. *Mar. Bio.* **73**, 31-36.

Hama T., Hama J. and Handa N. (1993) $^{13}C$ Tracer methodology in microbial ecology with special reference to primary production processes in aquatic environments, p. 39-83. In J. Gwynfryn [ed.], *Advances in Microbial Ecology*, Springer.

Hamanaka J., Sawada K. and Tanoue E. (2000) Production rates of $C_{37}$ alkenones determined by $^{13}C$-labeling technique in the euphotic zone of Sagami Bay, Japan. *Org. Geochem.* **31**, 1095-1102.

Harris G.P. (1980) Temporal and spatial scales in phytoplankton ecology. Mechanisms, methods, models, and management. *Can. J. Fish. Aquat. Sci.* **37**, 877-900.

Hay W.W. (2004) Carbonate fluxes and calcareous phytoplankton, p. 509-528. *In* H.R. Thierstein and J.R. Young [eds.], *Coccolithophores*. Springer.

Hayes J.M., Freeman K.H., Popp B.N. and Hoham C.H. (1990) Compound-specific isotopic analyses: A novel tool for reconstruction of ancient biogeochemical processes. *Org. Geochem.* **16**, 1115-1128.

Hayes J.M. (2001) Fractionation of the isotopes of carbon and hydrogen in biosynthetic processes, p. 225-227. *In* J.W. Valley and D.R. Cole [eds.], *Reviews in Mineralogy and Geochemistry 43, Stable Isotope Geochemistry.* The Mineralogical Society of America, Washington.

Head R.N., Crawford D.W., Egge J.K., Harris R.P., Kristiansen S., Lesley D.J., Marañón E., Pond D. and Purdie D.A. (1998) The hydrography and biology of a bloom of the coccolithophorid *Emiliania huxleyi* in the northern North Sea. *J. Sea Res.* **39**, 255-266.

Hedges J.I., Baldock J.A., Gélinas Y., Lee C., Peterson M.L. and Wakeham S.G. (2002) The biochemical and elemental compositions of marine plankton: A NMR perspective. *Mar. Chem.* **78**, 47-63.

Helmke P., Neuer S., Lomas M.W., Conte M. and Freudenthal T. (2010) Cross-Basin differences in particulate organic carbon export and flux attenuation in the subtropical North Atlantic gyre. *Deep-Sea Res. Pt. I* **57**, 213-227.

Herbert T.D., Schuffert J.D. and Thomas D. (1998) Depth and seasonality of alkenone production along the California margin inferred from a core top transect. *Paleoceanography* **13,** 263-271.

Herbert T.D., Schuffert J.D., Andreasen D., Heusser L., Lyle M., Mix A., Ravelo A.C. Stott L.D. and Herguera J.C. (2001) Collapse of the California Current during glacial maxima linked to climate change on land. *Science* **293**, 71-76.

Herbert T.D. (2003) Alkenone paleotemperature determinations, p. 391-342. *In* K.K. Turekian and H.D. Holland [eds.], *Treatise on Geochemistry*, Vol. 6. Elsevier.

Hernández-Becerril D.U. (1987) Vertical distribution of phytoplankton in the central and northern part of the Gulf of California (June 1982). *Mar. Ecol.* **8**, 237-251.

Holligan P.M. and Robertson J.E. (1996) Significance of ocean carbonate budgets for the global carbon cycle. *Glob. Change Biol.* **2**, 85-95.

Horita J., Ueda A., Mizukami K. and Takatori I. (1989) Automatic δD and $\delta^{18}O$ analyses of multi-water samples using $H_2$- and $CO_2$-water equilibration methods with a common equilibration set-up. *Appl. Radiat. Isot.* **40**, 801-805.

Huang Y., Shuman B., Wang Y. and Webb III T. (2004) Hydrogen isotope ratios of individual lipids in lake sediments as novel tracers of climatic and environmental change: A surface sediment test. *J. Paleolimmol.* **31**, 363-375.

Hut G. (1987) Consultants group meeting on stable isotope reference samples for geochemical and hydrological investigations. Report to the Director General, International Atomic Energy Agency, Vienna, 42 pp.

Huyer A. (1983) Coastal upwelling in the California current system. *Prog. Oceanogr.* **12**, 259-284.

Iglesias-Rodríguez M.D., Brown C.W., Doney S.C., Kleypas J., Kolber D., Hayes P.K. and Falkowski P.G. (2002) Representing key phytoplankton functional groups in ocean carbon cycle models: Coccolithophorids. *Global Biogeochem. Cy.* **16**, doi:10.1029/2001GB001454.

Kara A.B., Rochford P.A. and Hurlburt H.E. (2000) An optimal definition for ocean mixed layer depth. *J. Geophys. Res.* **105**, 16803-16821.

Knauer G.A., Karl D.M., Martin J. and Hunter C. (1984) In situ effects of selected preservatives on total carbon, nitrogen and metals collected in sediment traps. *J. Mar. Res.* **42**: 445-462.

Lancelot C. and Mathot S. (1985) Biochemical fractionation of primary production by phytoplankton in Belgian coastal waters during short- and long-term incubations with $^{14}$C-bicarbonate I. Mixed diatom population. *Mar. Biol.* **86**, 219-226.

Langer G., Probert I., Nehrke G. and Ziveri P. (2011) The morphological response of *Emiliania huxleyi* to seawater carbonate chemistry changes: an inter-strain comparison. *J. Nanoplankton Res*. **32**, 29-34.

Langer G., Oetjen K. and Brenneis T. (2013) Coccolithophores do not increase particulate carbon production under nutrient limitation: A case study using *Emiliania huxleyi* (PML B92/11). *J. Exp. Mar. Bio. Eco.* **443**, 155-161.

Laws E. A. (1984) Improved estimates of phytoplankton carbon based on $^{14}$C incorporation into chlorophyll a. *J. Theor. Biol.* **110**, 425-434.

Laws E.A., Popp B.N., Bidigare R.R., Kennicut M.C. and Macko S.A. (1995) Dependence of phytoplankton carbon isotopic composition on growth rate and $[CO_2]_{aq}$: Theoretical considerations and experimental results. *Geochim. Cosmochim. Ac.* **59**, 1131-1138.

Legendre L. (1990) The significance of microalgal blooms for fisheries and for the export of particulate organic carbon in oceans. *J. Plankton Res.* **12**, 681-699.

LeGrande A.N. and Schmidt G.A. (2006) Global gridded data set of the oxygen isotopic composition in seawater. *Geophys. Res. Lett.* **33**, 10.1029/2006GL026011.

Leonardos N. and Geider R.J. (2005) Elevated atmospheric carbon dioxide increases organic carbon fixation by *Emiliania huxleyi* (Haptophyta), under nutrient-limited high-light conditions. *J. Phycol* **41**, 1196-1203.

Li W.K.W. and Harrison W.G. (1982) Carbon flow into the end-products of photosynthesis in short and long incubations of a natural phytoplankton population. *Mar. Biol.* **72**, 175-182.

Litchman E., Klausmeier C.A., Schofield O.M. and Falkowski P.G. (2007) The role of functional traits and trade-offs in structuring phytoplankton communities: scaling from cellular to ecosystem level. *Ecol. Lett.* **10**, 1170-1181.

Lochte K., Ducklow H.W., Fasham M.J.R. and Stienen C. (1993) Plankton succession and carbon cycling at 47°N 20°W during the JGOFS North Atlantic Bloom Experiment. *Deep-Sea Res. Pt. II* **40**, 91-114.

Lomas M. and Moran S. (2011) Evidence for aggregation and export of cyanobacteria and nano-eukaryotes from the Sargasso Sea euphotic zone. *Biogeosci.* **8**, 203-216.

Luo Y. and Sternberg L. (1991) Deuterium heterogeneity in starth and cellulose nitrate of CAM and C3 plants. *Phytochem.* **30**, 1095-1098.

Lyle M., Koizumi I., Richter C. and Moore Jr. T.C. (2000) Proc. ODP, Sci. Results, 167: College Station, TX (Ocean Drilling Program). doi:10.2973/odp.proc.sr.167.2000.

Lynn R.J. and Simpson J.J. (1987) The California Current system: the seasonal variability of its physical characteristics. *J. Geophys. Res.* **92**, 12947-12966.

Malinverno E., Prahl F.G., Popp B.N. and Ziveri P. (2008) Alkenone abundance and its relationship to the coccolithophore assemblage in Gulf of California surface waters. *Deep-Sea Res. Pt. I* **55**, 1118-1130.

Mangelsdorf K., Guntner U. and Rullkötter J. (2000) Climatic and oceanographic variations on the California continental margin during the last 160 kyr. *Org. Geochem.* **31**, 829-846.

Mantua N.J., Hare S.R., Zhang Y., Wallace J.M. and Francis R.C. (1997) A Pacific interdecadal climate oscillation with impacts on salmon production. *Bul. Am. Meteorolg. Soc.* **78**, 1069-1079.

Marañón E., Fernández E., Harris R.P. and Harbour D.S. (1996) Effects of the diatom-*Emiliania huxleyi* succession on photosynthesis, calcification and carbon metabolism bu size-fractionated phytoplankton. *Hydrobiolog.* **317**, 189-199.

Marañón E., Cermeño P., Huete-Ortega M., López-Sandoval D.C., Mouriño-Carballido B. and Rodríguez-Ramos T. (2014) Resource supply overrides temperature as a controlling factor of marine phytoplankton growth. *PLoS ONE* **9**, doi:10.1371/journal.pone.0099312.

MARGO Project Members (2009) Constraints on the magnitude and patters of ocean cooling at the Last Glacial Maximum. *Nature Geosci.* **2**, 127-132.

Marlowe I.T., Green J.C., Neal A.C., Brassell S.C., Eglinton G. and Course P.A. (1984) Long chain (n-$C_{37}$-$C_{39}$) alkenones in the Prymnesiophyceae. Distribution of alkenones and other lipids and their taxonomic significance. *Brit. Phycol. J.* **19**, 203-216.

Martineau F., Fourel F., Bodergat A.-M. and Lécuyer C. (2011) D/H equilibrium fractionation between $H_2O$ and $H_2$ as a function of the salinity of aqueous solutions. *Chem. Geo.* **291**, 236-240.

M'boule D., Chivall D., Sinke-Schoen D., Sinninghe Damsté J.S., Schouten S. and van der Meer M.T.J. (2014) Salinity dependent hydrogen isotope fractionation in alkenones produced by coastal and open ocean haptophyte algae. *Geochim. Cosmochim. Ac.* **130**, 126-135.

Mix A.C., Lund D.C., Pisias N.G., Bodén P., Bornmalm L., Lyle M. and Pike J. (1999) Rapid climate oscillations in the Northeast Pacific during the last deglaciation reflect northern and southern hemisphere sources. *In* [Eds] P.U. Clark, R.S. Webb

and L.D. Keigwin, Geophysical Monograph Series Vol 112: Mechanisms of Global Climate Change at Millennial Time Scales. American Geophysical Union.

Mix A.C., Bard E. and Schneider R. (2001) Environmental processes of the ice age: land, oceans, glaciers (EPILOG). *Quat. Sci. Rev.* **20**, 627-657.

Mjaaland, G. (1956) Some laboratory experiments on the coccolithophorid *Coccolithus huxleyi*. *Oikos* **7**, 251-255.

Mulitza S., Boltovskoy D., Donner B., Meggers H., Paul A. and Wefer G. (2003) Temperature:$\delta^{18}$O relationships of planktonic foraminifera collected from surface waters. *Paleogeo. Paleoclim. Paleoecol.* **202**, 143-152.

Müller P.J., Kirst G., Ruhland G., von Storch I. and Rosell-Melé A. (1998) Calibration of the alkenone paleotemperature index UK'37 based on core-tops from the eastern South Atlantic and the global ocean (60°N-60°S). *Geochim. Cosmochim. Ac.* **62**, 1757-1772.

Müller M.N., Antia A.N. and LaRoche J. (2008) Influence of cell cycle phase on calcification in the coccolithophore *Emiliania huxleyi*. *Limnol. Oceanogr.* **53**, 506-512.

Münchow A. (2000) Wind stress curl forcing of the coastal ocean near Point Conception, California. *J. Phys. Oce.* **30**, 1265-1280.

Narayan N., Paul A., Mulitza S. and Schulz M. (2010) Trends in coastal upwelling intensity during the late 20$^{th}$ century. *Ocean Sci.* **6**, 815-823.

Ostlund H.G., Craig H., Broecker W.S. and Spenser D. (1987) GEOSECS Atlantic, Pacific, and Indian Ocean expeditions. *In* Shore-based Data and Graphics, Vol 7, pp. 1-200, Natl. Sci. Found., Washington D.C.

Oviedo A.M., Langer G. and Ziveri P. (2014) Effect of phosphorus limitation on coccolith morphology and element ratios in Mediterranean strains of the coccolithophore *Emiliania huxleyi*. *J. Exp. Mar. Bio. Eco.* **449**, 105-113.

Pagani M. (2014) Biomarker-based inferences of past climate: The alkenone *p*CO2 proxy, p. 361-378. *In* H.D. Holland and K.K. Turekian and [eds.], *Treatise on Geochemistry*. 2$^{nd}$ Ed., Vol. 12. Elsevier.

Pahnke K., Sachs J. P., Keigwin L., Timmermann A. and Xie S. (2007) Eastern tropical Pacific hydrologic changes during the past 27,000 years from D/H ratios in alkenones. *Paleoceanography* **22**, doi:10.1029/2007PA001468.

Popp B.N., Laws E.A., Bidigare R.R., Dore J.E., Hanson K.L. and Wakeham S.G. (1998a) Effect of phytoplankton cell geometry on carbon isotopic fractionation. *Geochim. Cosmochim. Ac.* **62**, 69-77.

Popp B.N., Kenig F., Wakeham S.G., Laws E.A. and Bidigare R.R. (1998b) Does growth rate affect ketone unsaturation and intracellular carbon isotopic variability in *Emiliania huxleyi*? *Paleoceanography* **13**, 35-41.

Popp B.N., Bidigare R.R., Deschenes B., Laws E.A., Prahl F.G., Tanimoto J.K. and Wallsgrove R.J. (2006) A new method for estimating growth rates of alkenone producing haptophytes. *Limnol. Oceanogr.-Meth.* **4**, 114-129.

Popp B.N., Prahl F.G., Wallsgrove R.J. and Tanimoto J. (2006) Seasonal patterns of alkenone production in the subtropical oligotrophic North Pacific. *Paleoceanogr.* **21**, doi:10.1029/2005PA001165.

Prahl F.G. and Pinto L.A. (1987) A geochemical study of long-chain n-aldehydes in Washington coastal sediments. *Geochim. Cosmochim. Ac.* **51**, 1573-1582.

Prahl F.G., Muehlhausen L.A. and Zahnle D.L. (1988) Further evaluation of long-chain alkenones as indicators of paleoceanographic conditions. *Geochim. Cosmochim. Ac.* **52**, 2303-2310.

Prahl F.G., Collier R.B., Dymond J., Lyle M. and Sparrow M.A. (1993) A biomarker perspective on prymnesiophyte productivity in the northeast Pacific Ocean. *Deep-sea Res. Pt. I* **40**, 2061-2076.

Prahl F.G., Wolfe G.V. and Sparrow M.A. (2003) Physiological impacts on alkenone paleothermometry. *Paleoceanography* **18**, doi:10.1029/2002PA000803.

Prahl F. G., Rontani J., Zabeti N., Walinsky S. E., and Sparrow M. A. (2010) Systematic pattern in UK'37-Temperature residuals for surface sediments from high latitude and other oceanographic settings. *Geochimica et Cosmochimica Acta* **74**, 131-143.

Prahl F.G., Popp B.N., Karl D.M. and Sparrow M.A. (2005) Ecology and biogeochemistry of alkenone production at Station ALOHA. *Deep-Sea Res. Pt. I* **52**, 699-719.

Revesz K.M., Landwehr J.M. and Keybl J. (2001) Measurement of $\delta^{13}C$ and $\delta\ ^{18}O$ isotopic ratios of $CaCO_3$ using a Thermoquest Finnigan GasBench II Delta Plus XL continuous flow isotope ratio mass spectrometer with application to Devils Hole Core DH-11 calcite. U.S. Geological Survey Open-File Report 01-257.

Richardson T.L. and Jackson G.A. (2007) Small phytoplankton and carbon export from the surface ocean. *Science* **315**, 838-840.

Riegman R., Stolte W., Noordeloos A.A.M. and Slezak D. (2000) Nutrient uptake and alkaline phosphatase (EC 3:1:3:1) activity of *Emiliania huxleyi* (prymnesiophyceae) during growth under N and P limitation in continuous cultures. *J. Phycol.* **36**, 87-96.

Rohling E.J. (2007) Progress in paleosalinity: Overview and presentation of a new approach. *Paleoceanography* **22**, doi: 10.1029/2007PA001437.

Romero-Viana L., Kienel U., Wilkes H. and Sachse D. Growth-dependent hydrogen isotopic fractionation of algal lipid biomarkers in hypersaline Isabel Lake (México). *Geochim. Cosmochim. Ac*. **106**, 490-500.

Rontani J.-F., Harji R., Guasco S., Prahl F.G., Volkman J.K., Bhosle N.B. and Bonin P. (1998) Degradation of alkenones by aerobic heterotrophic bacteria: Selective or not? *Org. Geochem.* **39**, 34-51.

Rontani J.-F., Prahl F.G. and Volkman J.K. (2006) Re-examination of the double bond positions in alkenones and derivatives: Biosynthetic implications. *J. Phycol.* **42**, 800-813.

Rontani J.-F., Volkman J.K., Prahl F.G. and Wakeham S.G. (2013) Biotic and abiotic degradation of alkenones and implications for UK'37 paleoproxy applications: A review. *Org. Geochem.* **59**, 95-113.

Rühl M., Le Coq D., Aymerich S. and Sauer U. (2012) $^{13}C$-flux analysis reveals NADPH-balancing transhydrogenation cycles in the stationary phase of nitrogen-starving *Bacillus subtilis*. *J. Biol. Chem.* **287**, 27959-27970.

Ryther J.H. (1954) The ratio of photosynthesis to respiration in marine plankton algae and its effect upon the measurement of productivity. *Deep-Sea Res.* **2**, 134-139.

Sachse D. and Sachs J.P. (2008) Inverse relationship between D/H fractionation in cyanobacterial lipids and salinity in Christmas Island saline ponds. *Geochim. Cosmochim. Ac.* **72**, 793-806.

Sauer P.E., Eglinton T.I., Hayes J.M., Schimmelmann A. and Sessions A. L. (2001) Compound-specific D/H ratios of lipid biomarkers from sediments as a proxy for environmental and climatic conditions. *Geochim. Cosmochim. Ac.* **65**, 213-222.

Schouten S., Ossebaar K., Schreiber K., Kienhuis M. V. M., Langer G., Benthien A. and Bijma J. (2006) The effect of temperature, salinity and growth rate on the stable hydrogen isotopic composition of long chain alkenones produced by *Emiliania huxleyi* and *Gephyrocapsa oceanica*. *Biogeosci.* **3**, 113-119.

Schwab V.F. and Sachs J.P. (2009) The measurement of D/H ratio in alkenones and their isotopic heterogeneity. *Org. Geochem.* **40**, 111-118.

Schwab V.F. and Sachs J.P. (2011) Hydrogen isotopes in individual alkenones from the Chesapeake Bay estuary. *Geochim. Cosmochim. Ac.* **75**, 7552-7565.

Sciandra A., Harlay J., Lefevre D., Lemee R., Rimmelin P., Denis M. and Gattuso J.P. (2003) Response of coccolithophorid *Emiliania huxleyi* to elevated partial pressure of $CO_2$ under nitrogen limitation. *Mar. Ecol.-Prog. Ser.* **261**, 111-122.

Sessions A. L., Burgoyne T. W., Schimmelmann A. and Hayes J. M. (1999) Fractionation of hydrogen isotopes in lipid biosynthesis. *Org. Geochem.* **30**, 1193-1200.

Sessions A.L. (2006) Seasonal changes in D/H fractionation accompanying lipid biosynthesis in *Spartina alterniflora*. *Geochim. Cosmochim. Ac.* **70**, 2153-2162.

Sheppard C.W. (1962) *Basic Principles of the Tracer Method: Introduction to Mathematical Tracer Kinetics*. Wiley.

Sieracki M.E., Verity P.G. and Stoecker D.K. (1993) Plankton community response to sequential silicate and nitrate depletion during the 1989 North Atlantic spring bloom. *Deep Sea Res II* **40**, 213-225.

Small L.F., Knauer G.A. and Tuel M.D. (1987) The role of sinking fecal pellets in stratified euphotic zones. *Deep-Sea Res. Pt. A.* **34**, 1705-1712.

Stott L.D., Neumann M. and Hammond D. (2000) Intermediate water ventilation on the northeastern Pacific margin during the late Pleistocene inferred from benthic foraminiferal δ13C. *Paleoceanography* **15**, 161-169.

Sukenik A. and Livine A. (1991) Variations in lipid and fatty-acid content in relation to acetyl CoA carboxylase in the marine prymnesiophyte *Isochrysis galbana*. *Plant Cell Physiol.* **32**, 371-378.

Thunell R.C., Pride C., Ziveri P., Muller-Karger F., Sancetta C. and Murray D. (1996) Plankton response to the physical forcing in the Gulf of California. *J. Plankton Res.* **18**, 2017-2026.

Thunell R.C. (1998) Particle fluxes in a coastal upwelling zone: sediment trap results from Santa Barbara Basin, California. *Deep-Sea Res. Pt. II* **45**, 1863-1884.

Thunell R.C. (1998). Seasonal and annual variability in particle fluxes in the Gulf of California: A response to climate forcing. *Deep-Sea Res. Pt. I* **45**, 2059-2083.

Tozzi S., Schofield O. and Falkowski P. (2004) Historical change and ocean turbulence as selective agents for two key phytoplankton functional groups. *Mar. Eco. Prog. Ser.* **274**, 123-132.

Traganza E.D., Redalije D.G. and Garwood R.W. (1987) Chemical flux, mixed layer entrainment and phytoplankton blooms at upwelling fronts in the California coastal zone. *Cont. Shelf. Res*. **7**, 89-105.

Tyrrell T. (2008) Calcium carbonate cycling in future oceans and its influence on future climates. *J. Plankton Res.* **30**, 141-146.

van der Meer M.T.J., Sangiorgi F., Baas M., Brinkhuis H., Sinninghe Damsté J.S. and Schoutan S. (2008) Molecular isotopic and dinoflagellate evidence for Late Holocene freshening of the Black Sea. *Earth Planet. Sc. Lett.* **267**, 426-434.

van der Meer M.T.J., Benthien A., Bijma J., Schouten S. and Sinninghe Damsté J.S. (2013) Alkenone distribution impacts the hydrogen isotopic composition of the $C_{37:2}$ and $C_{37:3}$ alkan-2-ones in *Emiliania huxleyi*. *Geochim. Cosmochim. Ac.* **111**, 162-166.

Vasiliev I., Reichart G.-J. and Krijgsman W. (2013) Impact of the Messinian Salinity Crisis on Black Sea hydrology – Insights from hydrogen isotopes analysis on biomarkers. *Earth Plan. Sci. Lett.* **362**, 272-282.

Verardo D.J., Froelich P.N. and McIntyre A. (1990) Determination of organic carbon and nitrogen in marine sediments using the Carlo Erba NA-1500 analyzer. *Deep Sea Res. Pt. I.* **37**, 157-165.

Volkman J.K., Eglinton G., Corner E.D.S. and Sargent J.R. (1980) Novel unsaturated straight-chain C37-C39 methyl and ethyl ketones in marine sediments and a coccolithophore *Emiliania huxleyi*, p. 219-227. *In* A.G. Douglas and J.R. Maxwell [eds.], *Advances in organic geochemistry, 1979: Proceedings of the Ninth International Meeting on Organic Geochemistry*. Pergamon Press.

Volkman J.K., Barrett S.M., Blackburn S.I. and Sikes E.L. (1995) Alkenones in *Gephyrocapsa oceanica*: Implications for studies of paleoclimate. *Geochim. Cosmochim. Ac.* **59**, 513-520.

Walinsky S.E., Prahl F.G., Mix A.C., Finney B.P., Jaeger J.M. and Rosen G.P. (2009) Distribution and composition of organic matter in surface sediments of coastal Southeast Alaska. *Cont. Shelf Res.* **29**, 1565-1579.

White A.E., Prahl F.G., Letelier R.M. and Popp B.N. (2007) Summer surface waters in the Gulf of California: Prime habitat for biological $N_2$ fixation. *Global Biogeochem. Cy.* **21**, doi:10.1029/2006GB002779.

White A.E., Foster R.A., Benitez-Nelson C.R., Masqué P., Verdeny E., Popp B.N., Arthur K.E. and Prahl F.G. (2013) Nitrogen fixation in the Gulf of California and the Eastern Tropical North Pacific. *Prog. Oceanogr.* **109**, 1-17.

Winter A., Jordan R. and Roth P. (1994) Biogeography of living coccolithophores in ocean waters, p. 161-167. *In* A. Winter and W. G. Siesser [eds.], *Coccolithophores*. Cambridge University Press.

Wolhowe M.D., Prahl F.G., Probert I. and Maldonado M. (2009) Growth phase dependent hydrogen isotopic fractionation in alkenone-producing haptophytes. *Biogeosci.* **8**, 1681-1694.

Wolhowe M.D., Prahl F.G., White A.E., Popp B.N. and Rosas-Navarro A. (2014) A biomarker perspective on coccolithophorid growth and export in a stratified sea. *Prog. Oceanogr.* **122**, 65-76.

Yakir D. and DeNiro M.J. (1990) Oxygen and hydrogen isotope fractionation during cellulose metabolism in *Lemna gibba* L. *Plant Physiol.* **93**, 325-332.

Yamamoto M., Yamamuro M., and Tanaka Y. (2007) The California current system during the last 136,000 years: response of the North Pacific High to precessional forcing. *Quaternary Science Reviews* **26**, 405-414.

Zhang Z. and Sachs J.P. (2007) Hydrogen isotope fractionation in freshwater algae: 1. Variations among lipids and species. *Org. Geochem.* **38**, 582-608.

Zhang X., Gillespie A.L. and Sessions A.L. (2009a) Large D/H variations in bacterial lipids reflect central metabolic pathways. *Proc. Nat. Acad. Sci.* **106**, 12580-12586.

Zhang Z., Sachs J.P. and Marchetti A. (2009b) Hydrogen isotope fractionation in freshwater and marine algae: II. Temperature and nitrogen limited growth rate effects. *Org. Geochem.* **40**, 428-439.

Ziveri P., Thunell R.C. and Rio D. (1995) Seasonal changes in coccolithophore densities in the Southern California Bight during 1991-1992. *Deep-Sea Res. I* **42**, 1881-1903.

Ziveri P. and Thunell R.C. (2000) Coccolithophore export production in Guaymas Basin, Gulf of California: response to climate forcing. *Deep-Sea Res. II* **47**, 2073-2100.

Zondervan I., Zeebe R.E., Rost B. and Riebesell U. (2001) Decreasing marine biogenic calcification: A negative feedback on rising atmospheric $pCO_2$. *Global Biogeochem. Cy.* **15**, 507-516.

Zondervan I. (2007) The effects of light, macronutrients, trace metals and $CO_2$ on the production of calcium carbonate and organic carbon in coccolithophores—A review. *Deep-Sea Res. Pt. II* **54**, 521-537.

Zweng, M.M, J.R. Reagan, J.I. Antonov, R.A. Locarnini, A.V. Mishonov, T.P. Boyer, H.E. Garcia, O.K. Baranova, D.R. Johnson, D.Seidov, M.M. Biddle, 2013. World Ocean Atlas 2013, Volume 2: Salinity. S. Levitus, Ed., A. Mishonov Technical Ed.; NOAA Atlas NESDIS 74, 39 pp.

# Appendices

**Appendix A. Gulf of California and ETNP Supplementary Data Tables:**

Below are the collected physical, chemical, and biological properties for the GoCal and ETNP stations addressed in Chapter 2. Much of this data (physical properties, Table A.1; nutrient profiles, Table A.4; chlorophyll A profiles, Table A.5; POC data, Table A.5; NPP profiles, Table A.7; alkenone producer cell abundance for years 2004-2005, Table A.8) has been addressed elsewhere (White et al. 2007, 2013; Malinverno et al. 2005). It has not been explicitly reported, however, and as such it is included below. New data included here are alkenone compositional profiles (Table A.2), alkenone production rates (Table A.3), alkenone-producer cell abundance from 2008 (Table A.8), and the estimated alkenone-producer cellular production rates (Table A.9). All properties have been binned and adjusted to common density vs. depth profiles (Table A.I) as described in Section 2.2.2.

**Table A.1.** Mean density, temperature, and percent PAR profiles for the upper 100m of the water column. Depths are provided as the mean depth of the isopycnals included in a given density bin (see Section 2.2.2), and uncertainty given as the standard deviation of the values in that bin. Profiles are the average of 8 to 32 casts over ~48 hours depending on station (see Table 2.1). Percent PAR is given as the 400-700nm spherical irradiance relative to simultaneous surface irradiance. Table continued onto subsequent pages.

**Table A.1 Physical Property Profiles**

| Station | Depth[a] (m) | σ[b] | Density (kg m$^{-3}$) | T (ºC) | σ | S | σ | % PAR[c] | σ | Station | Depth[a] (m) | σ[b] | Density (kg m$^{-3}$) | T (ºC) | σ | S | σ | % PAR[c] | σ |
|---|---|---|---|---|---|---|---|---|---|---|---|---|---|---|---|---|---|---|---|
| *Gulf of California* | | | | | | | | | | 3-1 | 53.3 | 6.9 | 1024.57 | 21.49 | 0.3 | 35.0 | 0.13 | 0.4 | 0.2 |
| 1-1 | 5.0 | 3.5 | 1022.33 | 28.55 | 0.1 | 35.2 | 0.05 | 19.5 | 14.8 | 3-1 | 56.3 | 6.9 | 1024.69 | 21.30 | 0.2 | 35.0 | 0.10 | 0.3 | 0.2 |
| 1-1 | 5.8 | 1.1 | 1022.44 | 28.32 | 0.1 | 35.2 | 0.02 | 14.1 | 9.6 | 3-1 | 59.3 | 6.3 | 1024.80 | 21.03 | 0.2 | 35.1 | 0.06 | 0.3 | 0.1 |
| 1-1 | 9.6 | 2.3 | 1022.54 | 28.09 | 0.1 | 35.2 | 0.01 | 7.0 | 6.7 | 3-1 | 62.0 | 5.9 | 1024.92 | 20.61 | 0.2 | 35.1 | 0.05 | 0.2 | 0.1 |
| 1-1 | 11.1 | 2.0 | 1022.65 | 27.79 | 0.1 | 35.2 | 0.01 | 4.1 | 3.9 | 3-1 | 65.0 | 5.6 | 1025.03 | 20.05 | 0.4 | 35.0 | 0.11 | 0.2 | 0.1 |
| 1-1 | 12.5 | 2.0 | 1022.76 | 27.41 | 0.1 | 35.2 | 0.02 | 3.9 | 3.8 | 3-1 | 68.0 | 5.2 | 1025.15 | 19.77 | 0.3 | 35.0 | 0.10 | 0.2 | 0.1 |
| 1-1 | 13.1 | 1.4 | 1022.87 | 27.10 | 0.1 | 35.2 | 0.03 | 3.5 | 3.8 | 3-1 | 71.2 | 5.1 | 1025.26 | 19.71 | 0.1 | 35.1 | 0.04 | 0.2 | 0.1 |
| 1-1 | 14.1 | 1.7 | 1022.97 | 26.75 | 0.2 | 35.2 | 0.04 | 2.3 | 1.9 | 3-1 | 76.1 | 5.0 | 1025.38 | 19.38 | 0.1 | 35.2 | 0.05 | 0.1 | 0.1 |
| 1-1 | 14.4 | 2.1 | 1023.08 | 26.42 | 0.2 | 35.1 | 0.04 | 3.0 | 2.8 | 3-1 | 81.9 | 3.6 | 1025.49 | 19.07 | 0.1 | 35.2 | 0.05 | 0.1 | 0.1 |
| 1-1 | 15.6 | 2.3 | 1023.30 | 25.68 | 0.1 | 35.1 | 0.04 | 1.8 | 2.3 | 3-1 | 87.9 | 2.0 | 1025.61 | 18.71 | 0.1 | 35.2 | 0.05 | 0.1 | 0.1 |
| 1-1 | 15.7 | 1.6 | 1023.19 | 26.05 | 0.1 | 35.1 | 0.03 | 2.2 | 2.5 | 3-1 | 94.1 | 3.0 | 1025.72 | 18.36 | 0.2 | 35.2 | 0.04 | 0.1 | 0.1 |
| 1-1 | 16.2 | 2.7 | 1023.40 | 25.23 | 0.1 | 35.1 | 0.03 | 2.1 | 2.0 | 3-1 | 99.9 | 4.0 | 1025.84 | 17.97 | 0.2 | 35.1 | 0.04 | 0.1 | 0.1 |
| 1-1 | 16.9 | 2.4 | 1023.51 | 24.91 | 0.1 | 35.1 | 0.04 | 2.0 | 2.0 | 3-2 | 3.7 | 1.8 | 1021.95 | 29.37 | 0.1 | 35.0 | 0.01 | 23.0 | 9.3 |
| 1-1 | 17.6 | 2.7 | 1023.62 | 24.47 | 0.2 | 35.1 | 0.04 | 1.3 | 1.4 | 3-2 | 7.0 | 1.4 | 1022.06 | 29.22 | 0.1 | 35.0 | 0.01 | 11.5 | 11.7 |
| 1-1 | 18.4 | 2.2 | 1023.73 | 24.20 | 0.2 | 35.1 | 0.07 | 1.2 | 1.2 | 3-2 | 9.9 | 2.8 | 1022.16 | 29.00 | 0.1 | 35.1 | 0.01 | 5.9 | 5.8 |
| 1-1 | 19.8 | 2.1 | 1023.83 | 23.82 | 0.1 | 35.1 | 0.03 | 0.6 | 0.7 | 3-2 | 11.9 | 2.9 | 1022.27 | 28.66 | 0.1 | 35.1 | 0.01 | 2.6 | 3.0 |
| 1-1 | 21.2 | 2.0 | 1023.94 | 23.47 | 0.2 | 35.1 | 0.06 | 0.7 | 0.8 | 3-2 | 14.2 | 2.9 | 1022.37 | 28.37 | 0.1 | 35.1 | 0.01 | 3.6 | 4.7 |
| 1-1 | 23.0 | 2.2 | 1024.05 | 23.10 | 0.2 | 35.1 | 0.06 | 0.6 | 0.7 | 3-2 | 15.4 | 3.0 | 1022.48 | 27.99 | 0.2 | 35.0 | 0.05 | 3.5 | 5.3 |
| 1-1 | 24.3 | 2.5 | 1024.16 | 22.74 | 0.2 | 35.1 | 0.05 | 0.4 | 0.6 | 3-2 | 15.6 | 3.7 | 1022.79 | 26.87 | 0.3 | 34.9 | 0.10 | 4.1 | 4.3 |
| 1-1 | 26.0 | 2.3 | 1024.26 | 22.43 | 0.2 | 35.1 | 0.05 | 0.4 | 0.5 | 3-2 | 16.5 | 3.1 | 1022.58 | 27.72 | 0.1 | 35.0 | 0.05 | 4.3 | 4.8 |
| 1-1 | 27.9 | 2.5 | 1024.37 | 22.02 | 0.2 | 35.0 | 0.05 | 0.3 | 0.4 | 3-2 | 18.1 | 4.3 | 1023.00 | 25.85 | 0.2 | 34.8 | 0.06 | 2.9 | 3.5 |
| 1-1 | 28.9 | 1.7 | 1024.48 | 21.67 | 0.2 | 35.0 | 0.06 | 0.3 | 0.3 | 3-2 | 18.9 | 1.0 | 1022.69 | 27.20 | 0.0 | 34.9 | 0.01 | 0.5 | 0.1 |
| 1-1 | 30.9 | 2.2 | 1024.59 | 21.31 | 0.1 | 35.0 | 0.05 | 0.2 | 0.3 | 3-2 | 20.2 | 0.5 | 1022.90 | 26.50 | 0.2 | 34.9 | 0.09 | 2.5 | 4.2 |
| 1-1 | 32.3 | 2.3 | 1024.69 | 20.97 | 0.1 | 35.1 | 0.03 | 0.2 | 0.2 | 3-2 | 21.0 | 4.2 | 1023.21 | 25.08 | 0.1 | 34.7 | 0.05 | 1.3 | 2.0 |
| 1-1 | 33.6 | 2.1 | 1024.80 | 20.53 | 0.1 | 35.1 | 0.03 | 0.2 | 0.2 | 3-2 | 21.0 | 4.9 | 1023.32 | 24.63 | 0.2 | 34.7 | 0.05 | 2.1 | 2.8 |
| 1-1 | 35.0 | 2.2 | 1024.91 | 20.18 | 0.1 | 35.1 | 0.03 | 0.2 | 0.2 | 3-2 | 22.1 | 6.1 | 1023.53 | 23.86 | 0.2 | 34.7 | 0.05 | 1.1 | 1.4 |
| 1-1 | 36.4 | 2.3 | 1025.01 | 19.84 | 0.2 | 35.1 | 0.04 | 0.1 | 0.1 | 3-2 | 22.2 | 0.6 | 1023.11 | 25.53 | 0.0 | 34.8 | 0.02 | 2.8 | 4.1 |
| 1-1 | 38.1 | 2.2 | 1025.12 | 19.45 | 0.1 | 35.1 | 0.03 | 0.1 | 0.1 | 3-2 | 22.8 | 4.0 | 1023.42 | 24.32 | 0.2 | 34.7 | 0.06 | 2.6 | 2.9 |
| 1-1 | 40.5 | 2.0 | 1025.23 | 19.11 | 0.1 | 35.1 | 0.02 | 0.1 | 0.1 | 3-2 | 23.5 | 5.0 | 1023.63 | 23.60 | 0.3 | 34.7 | 0.07 | 2.0 | 2.5 |
| 1-1 | 43.1 | 2.0 | 1025.34 | 18.74 | 0.1 | 35.1 | 0.02 | 0.1 | 0.1 | 3-2 | 25.5 | 1.6 | 1023.84 | 22.98 | 0.2 | 34.7 | 0.06 | 2.2 | 2.3 |
| 1-1 | 45.6 | 2.1 | 1025.44 | 18.29 | 0.1 | 35.1 | 0.03 | 0.1 | 0.1 | 3-2 | 25.8 | 4.1 | 1023.74 | 23.28 | 0.2 | 34.7 | 0.08 | 1.5 | 2.1 |
| 1-1 | 48.5 | 2.5 | 1025.55 | 17.93 | 0.1 | 35.1 | 0.03 | 0.0 | 0.0 | 3-2 | 28.6 | 2.7 | 1023.95 | 22.65 | 0.0 | 34.7 | 0.04 | 1.3 | 1.6 |
| 1-1 | 51.7 | 3.2 | 1025.66 | 17.46 | 0.1 | 35.0 | 0.02 | 0.0 | 0.0 | 3-2 | 29.3 | 3.1 | 1024.05 | 22.27 | 0.2 | 34.7 | 0.03 | 0.5 | 0.5 |
| 1-1 | 55.5 | 3.2 | 1025.77 | 17.03 | 0.1 | 35.0 | 0.02 | 0.0 | 0.0 | 3-2 | 29.3 | 1.1 | 1024.16 | 21.94 | 0.0 | 34.7 | 0.01 | 1.3 | 1.5 |
| 1-1 | 61.2 | 3.3 | 1025.87 | 16.74 | 0.1 | 35.0 | 0.02 | 0.0 | 0.0 | 3-2 | 31.3 | 2.0 | 1024.26 | 21.70 | 0.1 | 34.8 | 0.04 | 0.8 | 1.0 |
| 1-1 | 68.6 | 3.6 | 1025.98 | 16.42 | 0.1 | 35.0 | 0.02 | 0.0 | 0.0 | 3-2 | 32.1 | 1.8 | 1024.37 | 21.37 | 0.1 | 34.8 | 0.02 | 0.8 | 0.8 |
| 1-1 | 75.8 | 4.1 | 1026.09 | 16.05 | 0.1 | 35.0 | 0.03 | 0.0 | 0.0 | 3-2 | 34.0 | 2.3 | 1024.47 | 21.10 | 0.1 | 34.8 | 0.01 | 0.6 | 0.5 |
| 1-1 | 82.8 | 4.0 | 1026.20 | 15.64 | 0.1 | 35.0 | 0.03 | 0.0 | 0.0 | 3-2 | 36.3 | 2.3 | 1024.58 | 20.82 | 0.1 | 34.8 | 0.02 | 0.4 | 0.3 |
| 1-1 | 91.1 | 3.1 | 1026.30 | 15.40 | 0.1 | 35.0 | 0.01 | 0.0 | 0.0 | 3-2 | 39.1 | 2.3 | 1024.69 | 20.52 | 0.1 | 34.9 | 0.03 | 0.4 | 0.2 |
| 1-1 | 99.2 | 2.9 | 1026.41 | 15.06 | 0.1 | 35.0 | 0.01 | 0.0 | 0.0 | 3-2 | 40.0 | 1.8 | 1024.79 | 20.28 | 0.1 | 34.9 | 0.04 | 0.3 | 0.0 |
| 3-1 | 2.7 | 0.4 | 1021.35 | 30.89 | 0.1 | 34.9 | 0.02 | 66.2 | 35.3 | 3-2 | 42.0 | 2.1 | 1024.90 | 20.10 | 0.1 | 35.0 | 0.04 | 0.3 | 0.2 |
| 3-1 | 4.0 | 0.0 | 1021.47 | 30.62 | 0.1 | 35.0 | 0.08 | 53.2 | 31.2 | 3-2 | 43.1 | 2.1 | 1025.00 | 19.90 | 0.2 | 35.0 | 0.06 | 0.3 | 0.2 |
| 3-1 | 4.0 | 1.4 | 1021.58 | 30.36 | 0.2 | 35.0 | 0.05 | 42.6 | 23.1 | 3-2 | 45.1 | 1.8 | 1025.11 | 19.64 | 0.2 | 35.1 | 0.04 | 0.3 | 0.1 |
| 3-1 | 7.5 | 1.2 | 1021.70 | 30.06 | 0.2 | 34.9 | 0.06 | 26.3 | 17.2 | 3-2 | 48.1 | 1.9 | 1025.21 | 19.34 | 0.2 | 35.1 | 0.04 | 0.2 | 0.1 |
| 3-1 | 11.1 | 1.6 | 1021.81 | 29.73 | 0.1 | 34.9 | 0.05 | 19.1 | 13.6 | 3-2 | 51.5 | 2.4 | 1025.32 | 19.02 | 0.1 | 35.1 | 0.04 | 0.2 | 0.1 |
| 3-1 | 14.3 | 1.7 | 1021.93 | 29.44 | 0.2 | 34.9 | 0.07 | 14.9 | 11.3 | 3-2 | 55.8 | 1.7 | 1025.42 | 18.63 | 0.1 | 35.1 | 0.05 | 0.2 | 0.1 |
| 3-1 | 16.0 | 2.0 | 1022.04 | 29.08 | 0.2 | 34.9 | 0.05 | 14.4 | 11.3 | 3-2 | 60.8 | 2.3 | 1025.53 | 18.28 | 0.2 | 35.1 | 0.05 | 0.2 | 0.0 |
| 3-1 | 17.6 | 2.3 | 1022.16 | 28.73 | 0.2 | 34.9 | 0.06 | 15.5 | 10.0 | 3-2 | 65.1 | 2.5 | 1025.63 | 17.92 | 0.1 | 35.1 | 0.02 | 0.2 | 0.0 |
| 3-1 | 19.9 | 2.3 | 1022.27 | 28.35 | 0.2 | 34.9 | 0.05 | 10.9 | 8.4 | 3-2 | 68.4 | 3.2 | 1025.74 | 17.58 | 0.1 | 35.1 | 0.02 | 0.2 | 0.0 |
| 3-1 | 21.0 | 3.1 | 1022.39 | 27.93 | 0.1 | 34.8 | 0.05 | 11.3 | 8.7 | 3-2 | 72.1 | 3.1 | 1025.84 | 17.15 | 0.0 | 35.1 | 0.01 | 0.2 | 0.0 |
| 3-1 | 23.3 | 3.1 | 1022.50 | 27.59 | 0.1 | 34.8 | 0.05 | 9.8 | 7.7 | 3-2 | 76.9 | 3.0 | 1025.95 | 16.78 | 0.1 | 35.1 | 0.03 | 0.1 | 0.0 |
| 3-1 | 24.6 | 3.7 | 1022.62 | 27.22 | 0.1 | 34.8 | 0.03 | 8.4 | 6.2 | 3-2 | 82.3 | 3.1 | 1026.05 | 16.44 | 0.2 | 35.1 | 0.04 | 0.1 | 0.0 |
| 3-1 | 26.1 | 3.5 | 1022.73 | 26.84 | 0.1 | 34.8 | 0.03 | 7.5 | 5.4 | 3-2 | 89.3 | 2.7 | 1026.16 | 16.20 | 0.1 | 35.1 | 0.01 | 0.1 | 0.0 |
| 3-1 | 27.6 | 3.8 | 1022.85 | 26.46 | 0.1 | 34.8 | 0.04 | 5.6 | 4.6 | 3-2 | 97.6 | 1.6 | 1026.26 | 15.88 | 0.0 | 35.1 | 0.01 | 0.1 | 0.0 |
| 3-1 | 29.0 | 3.7 | 1022.96 | 26.08 | 0.1 | 34.8 | 0.05 | 6.4 | 3.9 | 3-3 | 3.8 | 1.4 | 1022.18 | 30.15 | 0.1 | 35.7 | 0.01 | 55.0 | 27.7 |
| 3-1 | 30.4 | 3.8 | 1023.08 | 25.76 | 0.1 | 34.8 | 0.04 | 4.8 | 3.6 | 3-3 | 4.5 | 1.0 | 1022.29 | 29.88 | 0.1 | 35.7 | 0.00 | 57.5 | 36.9 |
| 3-1 | 32.2 | 4.4 | 1023.19 | 25.39 | 0.1 | 34.8 | 0.04 | 3.7 | 2.8 | 3-3 | 6.5 | 2.5 | 1022.39 | 29.61 | 0.0 | 35.7 | 0.01 | 20.8 | 10.8 |
| 3-1 | 33.5 | 4.8 | 1023.31 | 25.03 | 0.2 | 34.8 | 0.07 | 3.0 | 2.4 | 3-3 | 8.7 | 2.3 | 1022.49 | 29.31 | 0.1 | 35.7 | 0.01 | 21.0 | 18.0 |
| 3-1 | 35.0 | 4.3 | 1023.42 | 24.65 | 0.2 | 34.8 | 0.09 | 2.9 | 2.2 | 3-3 | 8.9 | 2.4 | 1022.59 | 28.99 | 0.1 | 35.7 | 0.01 | 21.2 | 19.9 |
| 3-1 | 37.1 | 3.9 | 1023.54 | 24.34 | 0.3 | 34.8 | 0.12 | 2.3 | 1.7 | 3-3 | 11.1 | 2.6 | 1022.70 | 28.64 | 0.1 | 35.6 | 0.01 | 22.0 | 14.2 |
| 3-1 | 39.5 | 3.8 | 1023.65 | 23.96 | 0.3 | 34.8 | 0.12 | 1.7 | 1.2 | 3-3 | 11.6 | 2.1 | 1022.80 | 28.42 | 0.1 | 35.6 | 0.00 | 16.6 | 15.5 |
| 3-1 | 41.9 | 3.6 | 1023.77 | 23.65 | 0.3 | 34.8 | 0.12 | 1.2 | 0.7 | 3-3 | 12.7 | 1.5 | 1022.90 | 28.05 | 0.1 | 35.6 | 0.01 | 14.5 | 12.1 |
| 3-1 | 43.9 | 3.6 | 1023.88 | 23.31 | 0.3 | 34.8 | 0.13 | 0.9 | 0.5 | 3-3 | 13.7 | 2.0 | 1023.01 | 27.75 | 0.1 | 35.6 | 0.01 | 18.0 | 13.3 |
| 3-1 | 45.9 | 4.1 | 1024.00 | 22.87 | 0.3 | 34.8 | 0.12 | 0.8 | 0.3 | 3-3 | 13.8 | 3.2 | 1023.21 | 27.03 | 0.1 | 35.6 | 0.01 | 18.2 | 12.0 |
| 3-1 | 47.5 | 4.8 | 1024.11 | 22.52 | 0.3 | 34.8 | 0.12 | 0.7 | 0.3 | 3-3 | 14.2 | 5.0 | 1023.42 | 26.29 | 0.1 | 35.6 | 0.01 | 27.3 | 4.5 |
| 3-1 | 48.5 | 5.3 | 1024.23 | 22.22 | 0.2 | 34.8 | 0.11 | 0.5 | 0.2 | 3-3 | 15.2 | 3.2 | 1023.52 | 26.08 | 0.1 | 35.5 | 0.01 | 14.6 | 12.1 |
| 3-1 | 50.8 | 5.6 | 1024.34 | 21.92 | 0.2 | 34.8 | 0.10 | 0.5 | 0.2 | 3-3 | 15.6 | 2.8 | 1023.62 | 25.61 | 0.1 | 35.5 | 0.01 | 13.4 | 10.1 |
| 3-1 | 51.1 | 6.2 | 1024.46 | 21.70 | 0.3 | 34.9 | 0.14 | 0.5 | 0.2 | 3-3 | 17.1 | 3.5 | 1023.83 | 24.95 | 0.1 | 35.5 | 0.01 | 8.3 | 12.9 |

[a] Mean depth of isopycnals included in density bin (see Section 2.2.2 of text).

[b] Uncertainty given as 1σ of measurements within density bin from all averaged casts (see Section 2.2.2 of text).

[c] 400-700 nm spherical irradiance, versus simultaneous surface irradiance.

**Table A.1 Physical Property Profiles Continued**

| Station | Depth[a] (m) | σ[b] | Density (kg m$^{-3}$) | T (ºC) | σ | S | σ | % PAR[c] | σ | Station | Depth[a] (m) | σ[b] | Density (kg m$^{-3}$) | T (ºC) | σ | S | σ | % PAR[c] | σ |
|---|---|---|---|---|---|---|---|---|---|---|---|---|---|---|---|---|---|---|---|
| 3-3 | 17.2 | 3.5 | 1023.72 | 25.31 | 0.1 | 35.5 | 0.01 | 14.1 | 12.0 | 4-1 | 6.5 | 2.0 | 1022.31 | 28.76 | 0.0 | 35.2 | 0.01 | 30.3 | 24.8 |
| 3-3 | 17.7 | 2.0 | 1024.03 | 24.11 | 0.1 | 35.5 | 0.01 | 8.5 | 8.5 | 4-1 | 11.4 | 7.8 | 1022.60 | 27.96 | 0.1 | 35.2 | 0.04 | 16.6 | 19.6 |
| 3-3 | 19.1 | 3.2 | 1023.93 | 24.59 | 0.1 | 35.5 | 0.01 | 11.0 | 8.6 | 4-1 | 12.8 | 4.7 | 1022.41 | 28.66 | 0.1 | 35.2 | 0.01 | 18.1 | 18.5 |
| 3-3 | 21.3 | 3.6 | 1024.14 | 23.87 | 0.1 | 35.5 | 0.01 | 14.6 | 4.5 | 4-1 | 14.8 | 6.4 | 1022.70 | 27.71 | 0.1 | 35.2 | 0.06 | 12.9 | 14.2 |
| 3-3 | 21.3 | 3.1 | 1024.34 | 23.06 | 0.1 | 35.4 | 0.01 | 8.9 | 7.1 | 4-1 | 15.8 | 3.3 | 1022.80 | 27.43 | 0.2 | 35.2 | 0.08 | 12.9 | 12.5 |
| 3-3 | 21.7 | 2.7 | 1024.24 | 23.50 | 0.1 | 35.5 | 0.01 | 7.6 | 7.7 | 4-1 | 16.1 | 6.7 | 1022.51 | 28.34 | 0.2 | 35.2 | 0.02 | 16.8 | 15.7 |
| 3-3 | 22.7 | 2.5 | 1024.44 | 22.75 | 0.2 | 35.4 | 0.01 | 6.8 | 6.7 | 4-1 | 18.6 | 4.1 | 1022.90 | 27.12 | 0.1 | 35.2 | 0.05 | 8.5 | 8.1 |
| 3-3 | 24.3 | 2.9 | 1024.55 | 22.44 | 0.1 | 35.4 | 0.01 | 7.3 | 5.8 | 4-1 | 20.7 | 4.6 | 1022.99 | 26.68 | 0.2 | 35.1 | 0.11 | 8.8 | 9.5 |
| 3-3 | 25.7 | 2.8 | 1024.65 | 22.00 | 0.1 | 35.4 | 0.01 | 5.0 | 4.9 | 4-1 | 21.4 | 4.8 | 1023.09 | 26.31 | 0.3 | 35.1 | 0.10 | 8.1 | 7.7 |
| 3-3 | 25.8 | 2.7 | 1024.75 | 21.62 | 0.1 | 35.4 | 0.01 | 5.4 | 4.3 | 4-1 | 24.3 | 5.7 | 1023.39 | 25.20 | 0.3 | 35.0 | 0.13 | 7.6 | 8.0 |
| 3-3 | 28.5 | 3.3 | 1024.96 | 20.91 | 0.1 | 35.4 | 0.01 | 4.7 | 3.4 | 4-1 | 24.3 | 5.4 | 1023.29 | 25.64 | 0.3 | 35.0 | 0.11 | 6.0 | 5.1 |
| 3-3 | 28.6 | 2.6 | 1024.86 | 21.21 | 0.1 | 35.4 | 0.01 | 3.4 | 3.5 | 4-1 | 25.0 | 5.5 | 1023.48 | 24.84 | 0.3 | 35.0 | 0.12 | 7.4 | 7.0 |
| 3-3 | 29.6 | 3.1 | 1025.06 | 20.47 | 0.1 | 35.4 | 0.01 | 2.4 | 1.8 | 4-1 | 25.4 | 5.1 | 1023.19 | 25.84 | 0.3 | 35.0 | 0.11 | 5.9 | 5.4 |
| 3-3 | 30.3 | 2.7 | 1025.16 | 20.11 | 0.1 | 35.4 | 0.01 | 3.4 | 3.1 | 4-1 | 26.2 | 5.5 | 1023.68 | 24.07 | 0.4 | 34.9 | 0.14 | 6.0 | 7.1 |
| 3-3 | 32.5 | 2.6 | 1025.27 | 19.67 | 0.1 | 35.4 | 0.01 | 2.2 | 2.2 | 4-1 | 26.6 | 5.5 | 1023.58 | 24.48 | 0.3 | 35.0 | 0.13 | 6.0 | 4.2 |
| 3-3 | 34.2 | 2.3 | 1025.37 | 19.29 | 0.1 | 35.4 | 0.01 | 1.0 | 0.8 | 4-1 | 27.5 | 5.9 | 1023.78 | 23.72 | 0.4 | 34.9 | 0.13 | 4.8 | 5.6 |
| 3-3 | 37.1 | 2.8 | 1025.47 | 18.94 | 0.1 | 35.3 | 0.01 | 0.4 | 0.2 | 4-1 | 29.2 | 6.2 | 1023.97 | 22.94 | 0.4 | 34.9 | 0.13 | 4.6 | 6.0 |
| 3-3 | 39.5 | 2.9 | 1025.58 | 18.51 | 0.1 | 35.3 | 0.01 | 0.2 | 0.1 | 4-1 | 29.3 | 5.9 | 1023.87 | 23.30 | 0.3 | 34.9 | 0.12 | 3.1 | 3.0 |
| 3-3 | 41.5 | 3.1 | 1025.68 | 18.11 | 0.1 | 35.3 | 0.01 | 0.2 | 0.2 | 4-1 | 30.0 | 4.5 | 1024.07 | 22.70 | 0.4 | 34.9 | 0.14 | 3.6 | 4.7 |
| 3-3 | 45.4 | 3.8 | 1025.78 | 17.73 | 0.1 | 35.3 | 0.01 | 0.1 | 0.1 | 4-1 | 31.8 | 5.7 | 1024.17 | 22.32 | 0.3 | 34.9 | 0.12 | 3.2 | 3.8 |
| 3-3 | 49.4 | 4.8 | 1025.88 | 17.30 | 0.2 | 35.3 | 0.01 | 0.1 | 0.1 | 4-1 | 33.0 | 6.1 | 1024.27 | 21.95 | 0.3 | 34.9 | 0.11 | 2.8 | 3.5 |
| 3-3 | 53.0 | 3.8 | 1025.99 | 16.91 | 0.1 | 35.3 | 0.01 | 0.1 | 0.1 | 4-1 | 34.5 | 6.1 | 1024.36 | 21.64 | 0.2 | 34.9 | 0.10 | 2.2 | 2.9 |
| 3-3 | 58.1 | 2.8 | 1026.09 | 16.46 | 0.0 | 35.3 | 0.01 | 0.1 | 0.1 | 4-1 | 36.5 | 6.3 | 1024.46 | 21.16 | 0.3 | 34.8 | 0.09 | 1.8 | 2.2 |
| 3-3 | 64.4 | 3.2 | 1026.19 | 16.09 | 0.1 | 35.2 | 0.01 | 0.1 | 0.1 | 4-1 | 37.5 | 6.4 | 1024.56 | 20.78 | 0.3 | 34.8 | 0.08 | 1.5 | 2.0 |
| 3-3 | 71.5 | 3.4 | 1026.29 | 15.67 | 0.1 | 35.2 | 0.01 | 0.1 | 0.1 | 4-1 | 38.8 | 6.4 | 1024.66 | 20.48 | 0.3 | 34.8 | 0.09 | 1.3 | 1.6 |
| 3-3 | 80.6 | 2.9 | 1026.40 | 15.37 | 0.1 | 35.2 | 0.01 | 0.1 | 0.1 | 4-1 | 40.4 | 6.5 | 1024.76 | 20.13 | 0.3 | 34.8 | 0.10 | 1.1 | 1.5 |
| 3-3 | 91.7 | 2.3 | 1026.50 | 15.03 | 0.1 | 35.2 | 0.01 | 0.1 | 0.1 | 4-1 | 42.6 | 6.2 | 1024.85 | 19.84 | 0.4 | 34.8 | 0.11 | 0.9 | 1.3 |
| 3-3 | 104.5 | 1.1 | 1026.60 | 14.73 | 0.1 | 35.1 | 0.01 | 0.1 | 0.1 | 4-1 | 44.0 | 6.9 | 1024.95 | 19.39 | 0.4 | 34.8 | 0.12 | 0.8 | 1.1 |
| 3-4 | 6.5 | 2.6 | 1021.92 | 29.76 | 0.1 | 35.1 | 0.02 | 36.6 | 30.6 | 4-1 | 46.6 | 6.9 | 1025.05 | 19.05 | 0.4 | 34.8 | 0.11 | 0.5 | 0.8 |
| 3-4 | 13.9 | 3.1 | 1022.04 | 29.59 | 0.0 | 35.1 | 0.02 | 18.5 | 18.6 | 4-1 | 49.8 | 6.6 | 1025.15 | 18.70 | 0.4 | 34.8 | 0.11 | 0.4 | 0.5 |
| 3-4 | 19.3 | 2.8 | 1022.15 | 29.21 | 0.1 | 35.1 | 0.04 | 11.0 | 11.0 | 4-1 | 53.3 | 6.8 | 1025.24 | 18.45 | 0.4 | 34.8 | 0.11 | 0.3 | 0.3 |
| 3-4 | 21.6 | 3.2 | 1022.27 | 28.79 | 0.2 | 35.1 | 0.05 | 8.3 | 8.9 | 4-1 | 57.3 | 7.5 | 1025.34 | 18.11 | 0.4 | 34.8 | 0.10 | 0.2 | 0.3 |
| 3-4 | 23.0 | 2.9 | 1022.38 | 28.34 | 0.2 | 35.0 | 0.05 | 7.7 | 8.9 | 4-1 | 61.1 | 8.1 | 1025.44 | 17.78 | 0.4 | 34.8 | 0.09 | 0.1 | 0.2 |
| 3-4 | 24.6 | 2.6 | 1022.50 | 27.94 | 0.1 | 35.0 | 0.03 | 6.5 | 7.2 | 4-1 | 64.9 | 8.1 | 1025.54 | 17.51 | 0.4 | 34.8 | 0.09 | 0.1 | 0.1 |
| 3-4 | 26.3 | 2.2 | 1022.61 | 27.64 | 0.0 | 35.0 | 0.03 | 5.8 | 6.8 | 4-1 | 69.2 | 7.8 | 1025.64 | 17.24 | 0.4 | 34.8 | 0.08 | 0.1 | 0.1 |
| 3-4 | 27.6 | 2.0 | 1022.73 | 27.35 | 0.1 | 35.0 | 0.02 | 4.7 | 4.2 | 4-1 | 74.0 | 7.3 | 1025.73 | 16.97 | 0.4 | 34.9 | 0.10 | 0.0 | 0.1 |
| 3-4 | 29.0 | 2.5 | 1022.84 | 26.98 | 0.1 | 35.0 | 0.03 | 4.8 | 6.0 | 4-1 | 79.3 | 6.7 | 1025.83 | 16.79 | 0.3 | 34.9 | 0.08 | 0.0 | 0.0 |
| 3-4 | 29.9 | 2.8 | 1022.96 | 26.52 | 0.1 | 35.0 | 0.04 | 5.2 | 5.6 | 4-1 | 84.3 | 6.7 | 1025.93 | 16.50 | 0.3 | 34.9 | 0.06 | 0.0 | 0.0 |
| 3-4 | 30.1 | 2.0 | 1023.07 | 26.18 | 0.2 | 35.0 | 0.04 | 6.0 | 5.3 | 4-1 | 89.5 | 7.2 | 1026.03 | 16.18 | 0.3 | 34.9 | 0.06 | 0.0 | 0.0 |
| 3-4 | 31.8 | 2.2 | 1023.19 | 25.90 | 0.1 | 35.0 | 0.04 | 3.9 | 4.4 | 4-1 | 94.8 | 7.4 | 1026.12 | 15.84 | 0.3 | 34.9 | 0.05 | 0.0 | 0.0 |
| 3-4 | 32.9 | 2.0 | 1023.30 | 25.44 | 0.2 | 34.9 | 0.03 | 3.4 | 3.7 | 4-1 | 100.3 | 7.6 | 1026.22 | 15.49 | 0.3 | 34.9 | 0.04 | 0.0 | 0.0 |
| 3-4 | 34.5 | 2.2 | 1023.42 | 25.05 | 0.1 | 34.9 | 0.02 | 4.3 | 3.5 | 4-2a | 6.1 | 3.9 | 1021.75 | 29.42 | 0.1 | 34.8 | 0.07 | 31.6 | 20.4 |
| 3-4 | 34.9 | 2.1 | 1023.53 | 24.70 | 0.2 | 34.9 | 0.03 | 3.1 | 2.6 | 4-2a | 9.5 | 5.3 | 1021.86 | 29.31 | 0.1 | 34.8 | 0.05 | 33.4 | 17.7 |
| 3-4 | 36.4 | 1.8 | 1023.65 | 24.28 | 0.1 | 34.9 | 0.03 | 2.5 | 1.9 | 4-2a | 10.1 | 5.4 | 1022.07 | 28.98 | 0.1 | 34.9 | 0.06 | 19.0 | 22.3 |
| 3-4 | 37.5 | 1.9 | 1023.76 | 23.84 | 0.1 | 34.9 | 0.02 | 1.7 | 1.5 | 4-2a | 10.8 | 6.0 | 1021.96 | 29.14 | 0.0 | 34.9 | 0.07 | 12.5 | 15.4 |
| 3-4 | 39.0 | 2.2 | 1023.88 | 23.43 | 0.1 | 34.9 | 0.04 | 1.4 | 1.2 | 4-2a | 12.8 | 5.0 | 1022.18 | 28.75 | 0.1 | 35.0 | 0.05 | 13.6 | 16.2 |
| 3-4 | 40.2 | 2.4 | 1023.99 | 23.04 | 0.2 | 34.9 | 0.05 | 1.2 | 1.1 | 4-2a | 14.4 | 6.0 | 1022.28 | 28.49 | 0.1 | 35.0 | 0.05 | 20.1 | 22.6 |
| 3-4 | 42.0 | 2.3 | 1024.11 | 22.79 | 0.2 | 34.9 | 0.05 | 1.0 | 0.8 | 4-2a | 17.6 | 6.8 | 1022.39 | 28.25 | 0.1 | 35.0 | 0.07 | 14.6 | 17.3 |
| 3-4 | 43.6 | 2.6 | 1024.22 | 22.47 | 0.2 | 34.9 | 0.07 | 0.8 | 0.6 | 4-2a | 20.9 | 7.0 | 1022.49 | 28.01 | 0.1 | 35.0 | 0.08 | 11.9 | 13.6 |
| 3-4 | 45.2 | 2.9 | 1024.34 | 21.96 | 0.2 | 34.9 | 0.07 | 0.7 | 0.5 | 4-2a | 24.3 | 7.5 | 1022.60 | 27.76 | 0.2 | 35.0 | 0.09 | 9.8 | 11.6 |
| 3-4 | 45.9 | 2.4 | 1024.45 | 21.58 | 0.3 | 34.9 | 0.08 | 0.4 | 0.4 | 4-2a | 28.2 | 7.8 | 1022.71 | 27.52 | 0.2 | 35.0 | 0.10 | 8.1 | 9.9 |
| 3-4 | 47.5 | 3.2 | 1024.56 | 21.21 | 0.3 | 34.9 | 0.08 | 0.5 | 0.3 | 4-2a | 31.8 | 7.4 | 1022.81 | 27.21 | 0.3 | 35.0 | 0.12 | 6.4 | 7.7 |
| 3-4 | 48.5 | 2.9 | 1024.68 | 20.73 | 0.3 | 34.9 | 0.09 | 0.4 | 0.3 | 4-2a | 34.7 | 6.8 | 1022.92 | 26.84 | 0.3 | 35.0 | 0.12 | 5.1 | 6.0 |
| 3-4 | 50.7 | 2.7 | 1024.79 | 20.40 | 0.3 | 34.9 | 0.09 | 0.4 | 0.2 | 4-2a | 36.9 | 6.0 | 1023.03 | 26.42 | 0.4 | 35.0 | 0.14 | 4.2 | 4.8 |
| 3-4 | 52.9 | 2.6 | 1024.91 | 20.00 | 0.2 | 34.9 | 0.09 | 0.3 | 0.2 | 4-2a | 38.8 | 5.7 | 1023.13 | 26.01 | 0.3 | 34.9 | 0.12 | 3.5 | 3.9 |
| 3-4 | 55.1 | 2.2 | 1025.02 | 19.69 | 0.3 | 34.9 | 0.09 | 0.3 | 0.1 | 4-2a | 40.7 | 5.5 | 1023.24 | 25.64 | 0.3 | 34.9 | 0.11 | 3.0 | 3.3 |
| 3-4 | 57.4 | 1.9 | 1025.14 | 19.34 | 0.2 | 34.9 | 0.10 | 0.2 | 0.1 | 4-2a | 42.4 | 5.3 | 1023.35 | 25.21 | 0.2 | 34.8 | 0.10 | 2.6 | 2.9 |
| 3-4 | 59.6 | 1.8 | 1025.25 | 18.95 | 0.3 | 35.0 | 0.09 | 0.2 | 0.1 | 4-2a | 44.6 | 5.6 | 1023.45 | 24.79 | 0.2 | 34.8 | 0.11 | 2.1 | 2.4 |
| 3-4 | 61.9 | 1.6 | 1025.37 | 18.60 | 0.2 | 35.0 | 0.07 | 0.2 | 0.1 | 4-2a | 46.7 | 5.8 | 1023.56 | 24.38 | 0.3 | 34.8 | 0.13 | 1.8 | 1.9 |
| 3-4 | 64.7 | 1.9 | 1025.48 | 18.30 | 0.3 | 35.0 | 0.07 | 0.2 | 0.1 | 4-2a | 48.9 | 6.4 | 1023.67 | 24.02 | 0.3 | 34.8 | 0.12 | 1.5 | 1.6 |
| 3-4 | 67.9 | 2.6 | 1025.60 | 17.87 | 0.2 | 35.0 | 0.06 | 0.1 | 0.1 | 4-2a | 51.6 | 7.4 | 1023.77 | 23.70 | 0.2 | 34.7 | 0.10 | 1.2 | 1.5 |
| 3-4 | 71.2 | 2.7 | 1025.71 | 17.40 | 0.2 | 35.0 | 0.06 | 0.1 | 0.1 | 4-2a | 54.3 | 8.7 | 1023.88 | 23.23 | 0.2 | 34.7 | 0.09 | 1.1 | 1.4 |
| 3-4 | 74.8 | 2.2 | 1025.83 | 16.98 | 0.2 | 35.0 | 0.06 | 0.1 | 0.1 | 4-2a | 55.2 | 9.7 | 1023.98 | 22.86 | 0.2 | 34.7 | 0.07 | 0.9 | 1.2 |
| 3-4 | 78.8 | 1.6 | 1025.94 | 16.55 | 0.1 | 35.0 | 0.05 | 0.1 | 0.1 | 4-2a | 57.1 | 10.4 | 1024.09 | 22.51 | 0.2 | 34.7 | 0.06 | 0.8 | 1.1 |
| 3-4 | 83.8 | 1.4 | 1026.06 | 16.28 | 0.1 | 35.0 | 0.04 | 0.1 | 0.1 | 4-2a | 59.6 | 11.2 | 1024.20 | 22.07 | 0.2 | 34.7 | 0.04 | 0.8 | 1.0 |
| 3-4 | 89.6 | 2.1 | 1026.17 | 15.89 | 0.1 | 35.0 | 0.04 | 0.1 | 0.1 | 4-2a | 61.0 | 10.4 | 1024.30 | 21.73 | 0.1 | 34.7 | 0.03 | 0.6 | 0.8 |
| 3-4 | 97.2 | 2.7 | 1026.29 | 15.55 | 0.1 | 35.0 | 0.03 | 0.1 | 0.1 | 4-2a | 63.1 | 9.9 | 1024.41 | 21.38 | 0.2 | 34.7 | 0.03 | 0.4 | 0.6 |
| 3-4 | 105.9 | 2.4 | 1026.40 | 15.21 | 0.1 | 35.0 | 0.02 | 0.0 | 0.1 | 4-2a | 65.2 | 9.5 | 1024.52 | 20.97 | 0.2 | 34.6 | 0.02 | 0.3 | 0.4 |

[a] Mean depth of isopycnals included in density bin (see Section 2.2.2 of text).

[b] Uncertainty given as 1σ of measurements within density bin from all averaged casts (see Section 2.2.2 of text).

[c] 400-700 nm spherical irradiance, versus simultaneous surface irradiance.

**Table A.1 Physical Property Profiles Continued**

| Station | Depth[a] (m) | σ[b] | Density (kg m$^{-3}$) | T (ºC) | σ | S | σ | % PAR[c] | σ |
|---|---|---|---|---|---|---|---|---|---|
| 4-2a | 67.3 | 9.3 | 1024.62 | 20.60 | 0.1 | 34.6 | 0.01 | 0.3 | 0.3 |
| 4-2a | 70.0 | 9.1 | 1024.73 | 20.21 | 0.2 | 34.6 | 0.01 | 0.2 | 0.2 |
| 4-2a | 73.0 | 8.9 | 1024.84 | 19.87 | 0.2 | 34.6 | 0.01 | 0.1 | 0.2 |
| 4-2a | 76.1 | 8.8 | 1024.94 | 19.55 | 0.2 | 34.6 | 0.01 | 0.1 | 0.1 |
| 4-2a | 79.2 | 8.9 | 1025.05 | 19.15 | 0.2 | 34.6 | 0.01 | 0.1 | 0.1 |
| 4-2a | 82.2 | 8.6 | 1025.15 | 18.82 | 0.2 | 34.6 | 0.00 | 0.1 | 0.1 |
| 4-2a | 85.8 | 7.9 | 1025.26 | 18.49 | 0.1 | 34.6 | 0.01 | 0.0 | 0.0 |
| 4-2a | 91.4 | 7.2 | 1025.37 | 18.16 | 0.1 | 34.7 | 0.01 | 0.0 | 0.0 |
| 4-2a | 97.3 | 7.3 | 1025.47 | 17.87 | 0.1 | 34.7 | 0.00 | 0.0 | 0.0 |
| 4-2a | 102.6 | 7.6 | 1025.58 | 17.54 | 0.1 | 34.7 | 0.00 | 0.0 | 0.0 |
| 4-2b | 6.2 | 0.5 | 1021.35 | 29.69 | 0.1 | 34.4 | 0.03 | 15.8 | 15.1 |
| 4-2b | 8.3 | 1.9 | 1021.47 | 29.47 | 0.1 | 34.4 | 0.02 | 10.2 | 10.5 |
| 4-2b | 12.8 | 1.6 | 1021.59 | 29.16 | 0.1 | 34.4 | 0.02 | 8.3 | 9.3 |
| 4-2b | 16.5 | 1.8 | 1021.71 | 29.01 | 0.1 | 34.4 | 0.04 | 7.2 | 7.9 |
| 4-2b | 19.5 | 2.2 | 1021.83 | 28.84 | 0.1 | 34.5 | 0.04 | 6.2 | 6.5 |
| 4-2b | 22.2 | 2.7 | 1021.95 | 28.66 | 0.1 | 34.6 | 0.03 | 5.5 | 5.6 |
| 4-2b | 25.4 | 3.0 | 1022.07 | 28.44 | 0.1 | 34.6 | 0.05 | 4.6 | 4.6 |
| 4-2b | 28.7 | 3.4 | 1022.19 | 28.19 | 0.1 | 34.6 | 0.05 | 3.7 | 3.6 |
| 4-2b | 31.8 | 3.2 | 1022.31 | 28.02 | 0.1 | 34.7 | 0.06 | 3.0 | 2.8 |
| 4-2b | 35.7 | 2.4 | 1022.43 | 27.87 | 0.1 | 34.8 | 0.06 | 2.2 | 2.0 |
| 4-2b | 39.9 | 1.6 | 1022.55 | 27.67 | 0.1 | 34.8 | 0.05 | 1.6 | 1.5 |
| 4-2b | 43.3 | 1.3 | 1022.67 | 27.39 | 0.1 | 34.8 | 0.03 | 1.2 | 1.2 |
| 4-2b | 46.3 | 1.3 | 1022.79 | 27.05 | 0.1 | 34.8 | 0.03 | 0.9 | 0.9 |
| 4-2b | 50.1 | 1.7 | 1022.90 | 26.68 | 0.1 | 34.8 | 0.04 | 0.6 | 0.5 |
| 4-2b | 53.8 | 2.7 | 1023.02 | 26.27 | 0.1 | 34.8 | 0.04 | 0.4 | 0.3 |
| 4-2b | 57.2 | 3.7 | 1023.14 | 25.99 | 0.1 | 34.8 | 0.03 | 0.3 | 0.2 |
| 4-2b | 59.7 | 4.0 | 1023.26 | 25.64 | 0.1 | 34.8 | 0.02 | 0.2 | 0.2 |
| 4-2b | 62.4 | 3.8 | 1023.38 | 25.26 | 0.1 | 34.8 | 0.02 | 0.2 | 0.1 |
| 4-2b | 65.3 | 3.7 | 1023.50 | 24.81 | 0.1 | 34.8 | 0.04 | 0.1 | 0.1 |
| 4-2b | 68.3 | 3.6 | 1023.62 | 24.39 | 0.1 | 34.7 | 0.03 | 0.1 | 0.1 |
| 4-2b | 72.6 | 3.5 | 1023.74 | 23.95 | 0.1 | 34.7 | 0.02 | 0.1 | 0.0 |
| 4-2b | 76.6 | 3.5 | 1023.86 | 23.72 | 0.1 | 34.7 | 0.01 | 0.1 | 0.0 |
| 4-2b | 79.2 | 3.1 | 1023.98 | 23.29 | 0.1 | 34.7 | 0.02 | 0.0 | 0.0 |
| 4-2b | 82.2 | 2.9 | 1024.10 | 22.95 | 0.1 | 34.7 | 0.03 | 0.0 | 0.0 |
| 4-2b | 85.2 | 3.3 | 1024.22 | 22.50 | 0.1 | 34.7 | 0.02 | 0.0 | 0.0 |
| 4-2b | 87.7 | 3.4 | 1024.34 | 22.02 | 0.1 | 34.7 | 0.02 | 0.0 | 0.0 |
| 4-2b | 90.5 | 3.5 | 1024.46 | 21.63 | 0.1 | 34.7 | 0.02 | 0.0 | 0.0 |
| 4-2b | 94.0 | 3.3 | 1024.58 | 21.19 | 0.1 | 34.6 | 0.01 | 0.0 | 0.0 |
| 4-2b | 97.3 | 3.7 | 1024.70 | 20.80 | 0.1 | 34.6 | 0.01 | 0.0 | 0.0 |
| 4-2b | 100.0 | 4.0 | 1024.82 | 20.37 | 0.1 | 34.6 | 0.01 | 0.0 | 0.0 |
| 4-2b | 102.5 | 4.2 | 1024.94 | 19.91 | 0.1 | 34.6 | 0.00 | 0.0 | 0.0 |
| *Entrance Zone* | | | | | | | | | |
| 4-8 | 7.5 | 1.2 | 1021.07 | 29.46 | 0.1 | 33.9 | 0.03 | | |
| 4-8 | 8.2 | 2.9 | 1021.19 | 29.37 | 0.1 | 34.0 | 0.04 | 35.1 | 23.7 |
| 4-8 | 10.1 | 2.4 | 1021.32 | 29.28 | 0.1 | 34.1 | 0.05 | 24.9 | 17.6 |
| 4-8 | 13.1 | 2.9 | 1021.44 | 29.15 | 0.1 | 34.2 | 0.04 | 20.7 | 14.5 |
| 4-8 | 17.0 | 3.0 | 1021.56 | 29.00 | 0.1 | 34.2 | 0.04 | 15.8 | 9.6 |
| 4-8 | 20.9 | 3.4 | 1021.69 | 28.82 | 0.1 | 34.3 | 0.05 | 13.1 | 7.6 |
| 4-8 | 24.4 | 3.8 | 1021.81 | 28.64 | 0.1 | 34.4 | 0.07 | 10.7 | 6.0 |
| 4-8 | 27.8 | 4.0 | 1021.94 | 28.47 | 0.1 | 34.4 | 0.07 | 10.0 | 4.7 |
| 4-8 | 30.2 | 4.5 | 1022.06 | 28.31 | 0.1 | 34.5 | 0.08 | 7.7 | 4.8 |
| 4-8 | 32.6 | 4.4 | 1022.18 | 28.03 | 0.1 | 34.6 | 0.08 | 6.4 | 4.1 |
| 4-8 | 34.1 | 8.2 | 1022.31 | 27.86 | 0.2 | 34.6 | 0.13 | 9.1 | 14.1 |
| 4-8 | 37.4 | 8.0 | 1022.43 | 27.59 | 0.2 | 34.7 | 0.12 | 6.9 | 9.9 |
| 4-8 | 40.6 | 7.8 | 1022.55 | 27.42 | 0.2 | 34.7 | 0.12 | 5.6 | 8.1 |
| 4-8 | 44.2 | 7.9 | 1022.68 | 27.20 | 0.1 | 34.8 | 0.10 | 4.6 | 7.4 |
| 4-8 | 49.6 | 7.8 | 1022.80 | 26.98 | 0.1 | 34.8 | 0.09 | 3.4 | 5.5 |
| 4-8 | 55.6 | 7.7 | 1022.92 | 26.76 | 0.1 | 34.9 | 0.09 | 2.3 | 3.7 |
| 4-8 | 60.1 | 8.2 | 1023.05 | 26.51 | 0.1 | 34.9 | 0.08 | 1.9 | 3.1 |
| 4-8 | 62.6 | 8.8 | 1023.17 | 26.08 | 0.2 | 34.9 | 0.10 | 1.5 | 2.7 |
| 4-8 | 63.6 | 8.9 | 1023.29 | 25.66 | 0.2 | 34.8 | 0.10 | 1.4 | 2.3 |
| 4-8 | 67.0 | 7.8 | 1023.42 | 25.09 | 0.2 | 34.8 | 0.09 | 1.0 | 1.7 |
| 4-8 | 68.6 | 7.5 | 1023.54 | 24.66 | 0.2 | 34.7 | 0.10 | 0.8 | 1.4 |
| 4-8 | 70.6 | 8.8 | 1023.79 | 23.80 | 0.2 | 34.7 | 0.08 | 0.8 | 1.2 |
| 4-8 | 70.7 | 7.7 | 1023.67 | 24.21 | 0.2 | 34.7 | 0.09 | 0.8 | 1.2 |
| 4-8 | 72.9 | 7.7 | 1023.91 | 23.27 | 0.1 | 34.7 | 0.06 | 0.7 | 1.0 |
| 4-8 | 74.7 | 7.5 | 1024.04 | 22.85 | 0.1 | 34.6 | 0.05 | 0.5 | 0.8 |
| 4-8 | 77.8 | 8.3 | 1024.28 | 21.90 | 0.2 | 34.6 | 0.03 | 0.4 | 0.7 |
| 4-8 | 78.1 | 2.7 | 1024.16 | 22.36 | 0.2 | 34.6 | 0.02 | 0.3 | 0.2 |
| 4-8 | 80.0 | 8.5 | 1024.41 | 21.43 | 0.1 | 34.6 | 0.02 | 0.4 | 0.5 |
| 4-8 | 81.4 | 7.5 | 1024.53 | 20.97 | 0.2 | 34.6 | 0.02 | 0.3 | 0.3 |
| 4-8 | 83.0 | 7.3 | 1024.65 | 20.51 | 0.1 | 34.6 | 0.03 | 0.2 | 0.2 |
| 4-8 | 83.6 | 7.0 | 1024.78 | 19.99 | 0.1 | 34.5 | 0.04 | 0.2 | 0.2 |
| 4-8 | 86.0 | 6.5 | 1024.90 | 19.57 | 0.1 | 34.5 | 0.04 | 0.2 | 0.1 |
| 4-8 | 86.9 | 5.9 | 1025.03 | 19.11 | 0.1 | 34.6 | 0.05 | 0.1 | 0.1 |
| 4-8 | 89.2 | 5.2 | 1025.15 | 18.70 | 0.1 | 34.6 | 0.05 | 0.1 | 0.1 |
| 4-8 | 90.8 | 4.6 | 1025.27 | 18.25 | 0.1 | 34.6 | 0.04 | 0.1 | 0.1 |
| 4-8 | 93.4 | 4.0 | 1025.40 | 17.79 | 0.1 | 34.6 | 0.03 | 0.1 | 0.0 |
| 4-8 | 96.2 | 3.3 | 1025.52 | 17.34 | 0.1 | 34.6 | 0.03 | 0.1 | 0.0 |
| 4-8 | 99.3 | 3.0 | 1025.64 | 16.87 | 0.1 | 34.6 | 0.04 | 0.1 | 0.0 |
| 4-8 | 102.8 | 3.1 | 1025.77 | 16.45 | 0.2 | 34.6 | 0.04 | 0.0 | 0.0 |
| 4-9 | 5.9 | 1.2 | 1022.04 | 28.77 | 0.1 | 34.8 | 0.08 | 29.0 | 17.7 |
| 4-9 | 6.5 | 1.3 | 1021.93 | 28.72 | 0.1 | 34.7 | 0.05 | 14.1 | 12.8 |
| 4-9 | 7.6 | 1.2 | 1022.15 | 28.67 | 0.1 | 34.9 | 0.05 | 13.7 | 15.0 |
| 4-9 | 10.3 | 1.3 | 1022.27 | 28.28 | 0.2 | 34.9 | 0.10 | 9.9 | 12.3 |
| 4-9 | 12.6 | 1.6 | 1022.38 | 28.07 | 0.2 | 34.9 | 0.09 | 9.4 | 10.6 |
| 4-9 | 15.3 | 2.2 | 1022.49 | 27.71 | 0.2 | 34.9 | 0.10 | 8.1 | 9.3 |
| 4-9 | 17.4 | 2.6 | 1022.61 | 27.35 | 0.2 | 34.9 | 0.08 | 7.3 | 8.6 |
| 4-9 | 18.8 | 2.9 | 1022.72 | 26.99 | 0.2 | 34.9 | 0.05 | 6.9 | 8.0 |
| 4-9 | 19.5 | 2.6 | 1022.83 | 26.72 | 0.2 | 34.9 | 0.03 | 8.7 | 8.0 |
| 4-9 | 20.8 | 2.6 | 1022.95 | 26.25 | 0.2 | 34.9 | 0.05 | 5.9 | 6.6 |
| 4-9 | 22.1 | 2.6 | 1023.06 | 25.88 | 0.2 | 34.9 | 0.06 | 4.4 | 4.8 |
| 4-9 | 23.8 | 2.5 | 1023.17 | 25.57 | 0.1 | 34.9 | 0.04 | 4.9 | 5.7 |
| 4-9 | 25.8 | 2.3 | 1023.28 | 25.27 | 0.1 | 34.9 | 0.02 | 4.2 | 5.5 |
| 4-9 | 27.0 | 2.5 | 1023.40 | 24.84 | 0.1 | 34.9 | 0.02 | 4.3 | 4.5 |
| 4-9 | 28.8 | 2.2 | 1023.51 | 24.43 | 0.1 | 34.8 | 0.03 | 3.6 | 4.1 |
| 4-9 | 30.6 | 2.4 | 1023.62 | 24.04 | 0.1 | 34.8 | 0.03 | 3.3 | 3.8 |
| 4-9 | 32.7 | 2.5 | 1023.74 | 23.65 | 0.1 | 34.8 | 0.03 | 2.7 | 3.4 |
| 4-9 | 33.4 | 3.1 | 1023.96 | 22.70 | 0.1 | 34.7 | 0.03 | 3.4 | 2.7 |
| 4-9 | 34.3 | 2.6 | 1023.85 | 23.21 | 0.1 | 34.8 | 0.01 | 2.1 | 3.4 |
| 4-9 | 35.8 | 2.8 | 1024.08 | 22.24 | 0.2 | 34.7 | 0.04 | 1.6 | 1.9 |
| 4-9 | 37.4 | 2.6 | 1024.19 | 21.88 | 0.1 | 34.7 | 0.04 | 1.7 | 2.4 |
| 4-9 | 38.5 | 3.3 | 1024.30 | 21.44 | 0.2 | 34.7 | 0.05 | 1.8 | 2.0 |
| 4-9 | 40.0 | 3.6 | 1024.42 | 20.92 | 0.2 | 34.6 | 0.06 | 1.5 | 1.7 |
| 4-9 | 41.4 | 3.7 | 1024.53 | 20.46 | 0.2 | 34.6 | 0.07 | 1.3 | 1.4 |
| 4-9 | 43.0 | 4.0 | 1024.64 | 20.07 | 0.2 | 34.6 | 0.06 | 1.1 | 1.3 |
| 4-9 | 44.5 | 3.9 | 1024.76 | 19.71 | 0.1 | 34.6 | 0.05 | 1.0 | 1.0 |
| 4-9 | 46.9 | 3.6 | 1024.87 | 19.32 | 0.1 | 34.6 | 0.04 | 0.6 | 0.7 |
| 4-9 | 49.2 | 3.3 | 1024.98 | 18.87 | 0.2 | 34.6 | 0.05 | 0.5 | 0.5 |
| 4-9 | 51.3 | 3.4 | 1025.10 | 18.40 | 0.3 | 34.6 | 0.07 | 0.4 | 0.4 |
| 4-9 | 53.8 | 3.7 | 1025.21 | 17.93 | 0.2 | 34.6 | 0.07 | 0.3 | 0.3 |
| 4-9 | 56.1 | 3.7 | 1025.32 | 17.49 | 0.2 | 34.6 | 0.05 | 0.2 | 0.2 |
| 4-9 | 58.2 | 3.9 | 1025.44 | 16.92 | 0.2 | 34.5 | 0.06 | 0.2 | 0.2 |
| 4-9 | 60.7 | 3.7 | 1025.55 | 16.56 | 0.1 | 34.6 | 0.05 | 0.2 | 0.2 |
| 4-9 | 64.0 | 3.5 | 1025.66 | 15.98 | 0.1 | 34.5 | 0.03 | 0.1 | 0.1 |
| 4-9 | 67.7 | 3.6 | 1025.78 | 15.44 | 0.2 | 34.5 | 0.02 | 0.1 | 0.1 |
| 4-9 | 72.2 | 3.8 | 1025.89 | 15.02 | 0.2 | 34.5 | 0.03 | 0.1 | 0.1 |
| 4-9 | 78.3 | 3.8 | 1026.00 | 14.66 | 0.2 | 34.5 | 0.04 | 0.0 | 0.0 |
| 4-9 | 85.0 | 4.3 | 1026.11 | 14.20 | 0.2 | 34.5 | 0.05 | 0.0 | 0.0 |
| 4-9 | 90.9 | 4.2 | 1026.23 | 13.80 | 0.2 | 34.5 | 0.04 | 0.0 | 0.0 |
| 4-9 | 97.8 | 4.4 | 1026.34 | 13.49 | 0.1 | 34.5 | 0.03 | 0.0 | 0.0 |
| *Eastern Tropical North Pacific* | | | | | | | | | |
| 4-10 | 5.8 | 0.5 | 1022.75 | 24.17 | 0.0 | 33.9 | 0.00 | 20.1 | 24.4 |
| 4-10 | 8.0 | 1.8 | 1022.84 | 23.97 | 0.1 | 33.9 | 0.01 | 18.7 | 20.5 |
| 4-10 | 9.5 | 3.0 | 1022.93 | 23.57 | 0.1 | 33.9 | 0.01 | 17.0 | 19.0 |
| 4-10 | 12.3 | 2.7 | 1023.03 | 23.36 | 0.1 | 33.9 | 0.01 | 11.2 | 12.9 |
| 4-10 | 15.6 | 3.1 | 1023.21 | 22.50 | 0.3 | 33.8 | 0.07 | 7.7 | 11.9 |
| 4-10 | 16.1 | 2.2 | 1023.12 | 23.01 | 0.1 | 33.8 | 0.03 | 9.5 | 10.7 |
| 4-10 | 17.1 | 2.9 | 1023.30 | 22.11 | 0.3 | 33.7 | 0.07 | 6.3 | 8.8 |
| 4-10 | 17.1 | 2.2 | 1023.40 | 21.66 | 0.3 | 33.7 | 0.08 | 5.4 | 9.2 |
| 4-10 | 18.2 | 2.2 | 1023.58 | 20.96 | 0.2 | 33.7 | 0.05 | 10.4 | 11.4 |
| 4-10 | 18.5 | 2.8 | 1023.49 | 21.38 | 0.3 | 33.7 | 0.07 | 6.3 | 9.0 |
| 4-10 | 20.2 | 1.9 | 1023.67 | 20.74 | 0.2 | 33.7 | 0.06 | 9.2 | 9.4 |
| 4-10 | 21.3 | 2.3 | 1023.76 | 20.35 | 0.2 | 33.7 | 0.05 | 6.8 | 8.3 |
| 4-10 | 21.7 | 2.2 | 1023.86 | 20.06 | 0.2 | 33.7 | 0.05 | 10.0 | 8.7 |
| 4-10 | 22.3 | 2.7 | 1023.95 | 19.65 | 0.2 | 33.7 | 0.05 | 5.4 | 6.6 |

[a] Mean depth of isopycnals included in density bin (see Section 2.2.2 of text).

[b] Uncertainty given as 1σ of measurements within density bin from all averaged casts (see Section 2.2.2 of text).

[c] 400-700 nm spherical irradiance, versus simultaneous surface irradiance.

**Table A.1 Physical Property Profiles Continued**

| Station | Depth[a] (m) | σ[b] | Density (kg m$^{-3}$) | T (ºC) | σ | S | σ | % PAR[c] | σ |
|---|---|---|---|---|---|---|---|---|---|
| 4-10 | 23.7 | 2.1 | 1024.04 | 19.25 | 0.2 | 33.7 | 0.05 | 6.5 | 6.9 |
| 4-10 | 24.4 | 2.7 | 1024.13 | 18.85 | 0.2 | 33.7 | 0.04 | 4.7 | 6.0 |
| 4-10 | 25.9 | 2.6 | 1024.23 | 18.52 | 0.1 | 33.7 | 0.03 | 5.1 | 5.8 |
| 4-10 | 27.1 | 2.5 | 1024.32 | 18.19 | 0.2 | 33.7 | 0.03 | 3.4 | 5.1 |
| 4-10 | 28.7 | 2.3 | 1024.41 | 17.80 | 0.1 | 33.6 | 0.02 | 4.4 | 4.8 |
| 4-10 | 29.7 | 2.6 | 1024.50 | 17.40 | 0.1 | 33.6 | 0.03 | 3.7 | 4.3 |
| 4-10 | 31.3 | 2.7 | 1024.59 | 17.00 | 0.2 | 33.6 | 0.03 | 3.3 | 3.9 |
| 4-10 | 33.2 | 2.7 | 1024.69 | 16.56 | 0.2 | 33.6 | 0.04 | 2.9 | 3.4 |
| 4-10 | 35.2 | 2.8 | 1024.78 | 16.23 | 0.2 | 33.6 | 0.05 | 2.5 | 2.9 |
| 4-10 | 37.4 | 2.5 | 1024.87 | 15.89 | 0.2 | 33.6 | 0.04 | 2.1 | 2.6 |
| 4-10 | 39.7 | 2.2 | 1024.96 | 15.63 | 0.1 | 33.6 | 0.04 | 1.8 | 2.1 |
| 4-10 | 42.7 | 2.5 | 1025.06 | 15.29 | 0.1 | 33.6 | 0.04 | 1.5 | 1.7 |
| 4-10 | 46.0 | 3.0 | 1025.15 | 14.92 | 0.1 | 33.6 | 0.04 | 1.1 | 1.3 |
| 4-10 | 49.7 | 3.3 | 1025.24 | 14.64 | 0.1 | 33.7 | 0.02 | 0.8 | 0.9 |
| 4-10 | 53.5 | 3.2 | 1025.33 | 14.29 | 0.1 | 33.7 | 0.02 | 0.5 | 0.6 |
| 4-10 | 57.1 | 3.2 | 1025.42 | 13.97 | 0.1 | 33.7 | 0.02 | 0.4 | 0.4 |
| 4-10 | 61.2 | 3.5 | 1025.52 | 13.65 | 0.1 | 33.7 | 0.02 | 0.3 | 0.3 |
| 4-10 | 65.6 | 4.0 | 1025.61 | 13.32 | 0.1 | 33.7 | 0.03 | 0.2 | 0.2 |
| 4-10 | 70.1 | 4.2 | 1025.70 | 13.02 | 0.2 | 33.7 | 0.03 | 0.1 | 0.1 |
| 4-10 | 74.9 | 4.2 | 1025.79 | 12.80 | 0.2 | 33.7 | 0.04 | 0.1 | 0.1 |
| 4-10 | 79.9 | 4.1 | 1025.88 | 12.58 | 0.2 | 33.8 | 0.05 | 0.1 | 0.1 |
| 4-10 | 84.4 | 3.9 | 1025.98 | 12.27 | 0.2 | 33.8 | 0.04 | 0.0 | 0.1 |
| 4-10 | 88.9 | 3.7 | 1026.07 | 12.16 | 0.2 | 33.9 | 0.05 | 0.0 | 0.0 |
| 4-10 | 93.8 | 3.3 | 1026.16 | 12.03 | 0.2 | 33.9 | 0.05 | 0.0 | 0.0 |
| 4-10 | 99.4 | 3.4 | 1026.25 | 11.92 | 0.2 | 34.0 | 0.04 | 0.0 | 0.0 |
| 4-10 | 105.4 | 3.8 | 1026.35 | 11.79 | 0.1 | 34.0 | 0.04 | 0.0 | 0.0 |
| 4-11 | 3.0 | 2.8 | 1023.43 | 21.00 | 0.1 | 33.6 | 0.01 | 91.3 | 92.1 |
| 4-11 | 8.5 | 1.5 | 1023.51 | 20.85 | 0.1 | 33.6 | 0.00 | 12.5 | 11.8 |
| 4-11 | 15.1 | 2.0 | 1023.59 | 20.78 | 0.0 | 33.6 | 0.01 | 7.1 | 6.9 |
| 4-11 | 18.6 | 2.3 | 1023.66 | 20.38 | 0.2 | 33.6 | 0.02 | 6.4 | 5.8 |
| 4-11 | 19.4 | 2.9 | 1023.74 | 19.94 | 0.1 | 33.5 | 0.01 | 5.0 | 5.4 |
| 4-11 | 19.4 | 2.2 | 1023.82 | 19.56 | 0.1 | 33.5 | 0.02 | 6.4 | 5.3 |
| 4-11 | 20.5 | 2.4 | 1023.90 | 19.22 | 0.1 | 33.5 | 0.02 | 4.9 | 5.4 |
| 4-11 | 21.4 | 2.3 | 1023.98 | 18.85 | 0.1 | 33.5 | 0.02 | 5.2 | 5.1 |
| 4-11 | 23.2 | 2.2 | 1024.05 | 18.58 | 0.1 | 33.5 | 0.02 | 5.5 | 4.9 |
| 4-11 | 23.9 | 2.7 | 1024.13 | 18.30 | 0.1 | 33.5 | 0.02 | 4.9 | 4.5 |
| 4-11 | 25.5 | 2.9 | 1024.21 | 18.00 | 0.1 | 33.5 | 0.03 | 4.2 | 3.7 |
| 4-11 | 26.1 | 3.3 | 1024.29 | 17.62 | 0.2 | 33.5 | 0.04 | 3.3 | 3.9 |
| 4-11 | 27.3 | 2.4 | 1024.37 | 17.31 | 0.2 | 33.4 | 0.05 | 3.2 | 3.4 |
| 4-11 | 29.4 | 2.8 | 1024.44 | 17.08 | 0.2 | 33.5 | 0.05 | 3.1 | 2.8 |
| 4-11 | 31.5 | 2.7 | 1024.52 | 16.78 | 0.1 | 33.5 | 0.03 | 2.7 | 2.5 |
| 4-11 | 33.4 | 3.6 | 1024.60 | 16.54 | 0.1 | 33.5 | 0.02 | 2.5 | 2.2 |
| 4-11 | 34.4 | 3.9 | 1024.68 | 16.17 | 0.1 | 33.5 | 0.02 | 2.0 | 1.9 |
| 4-11 | 36.3 | 4.1 | 1024.76 | 15.86 | 0.1 | 33.5 | 0.01 | 1.7 | 1.7 |
| 4-11 | 38.8 | 4.4 | 1024.83 | 15.48 | 0.2 | 33.4 | 0.03 | 1.4 | 1.4 |
| 4-11 | 41.8 | 4.8 | 1024.91 | 15.10 | 0.2 | 33.4 | 0.04 | 1.0 | 1.0 |
| 4-11 | 44.4 | 5.3 | 1024.99 | 14.73 | 0.3 | 33.4 | 0.06 | 0.8 | 0.8 |
| 4-11 | 47.0 | 5.6 | 1025.07 | 14.43 | 0.3 | 33.4 | 0.06 | 0.6 | 0.6 |
| 4-11 | 49.8 | 5.5 | 1025.15 | 14.05 | 0.4 | 33.4 | 0.10 | 0.5 | 0.5 |
| 4-11 | 53.2 | 5.0 | 1025.22 | 13.68 | 0.5 | 33.4 | 0.11 | 0.3 | 0.4 |
| 4-11 | 56.7 | 4.8 | 1025.30 | 13.34 | 0.3 | 33.4 | 0.09 | 0.2 | 0.3 |
| 4-11 | 59.8 | 5.2 | 1025.38 | 13.00 | 0.3 | 33.3 | 0.07 | 0.2 | 0.2 |
| 4-11 | 62.8 | 5.1 | 1025.46 | 12.80 | 0.3 | 33.4 | 0.06 | 0.1 | 0.1 |
| 4-11 | 66.9 | 5.1 | 1025.54 | 12.62 | 0.3 | 33.4 | 0.06 | 0.1 | 0.1 |
| 4-11 | 71.3 | 5.2 | 1025.61 | 12.46 | 0.3 | 33.4 | 0.07 | 0.1 | 0.1 |
| 4-11 | 75.1 | 5.0 | 1025.69 | 12.28 | 0.3 | 33.5 | 0.07 | 0.1 | 0.1 |
| 4-11 | 78.7 | 5.1 | 1025.77 | 12.08 | 0.3 | 33.5 | 0.05 | 0.0 | 0.0 |
| 4-11 | 82.2 | 5.0 | 1025.85 | 11.90 | 0.3 | 33.5 | 0.05 | 0.0 | 0.0 |
| 4-11 | 86.0 | 5.1 | 1025.93 | 11.64 | 0.2 | 33.6 | 0.03 | 0.0 | 0.0 |
| 4-11 | 90.1 | 5.5 | 1026.00 | 11.47 | 0.1 | 33.6 | 0.03 | 0.0 | 0.0 |
| 4-11 | 94.2 | 5.3 | 1026.08 | 11.28 | 0.1 | 33.6 | 0.03 | 0.0 | 0.0 |
| 4-11 | 98.3 | 4.7 | 1026.16 | 11.09 | 0.2 | 33.7 | 0.04 | 0.0 | 0.0 |
| 4-11 | 102.2 | 4.8 | 1026.24 | 10.97 | 0.2 | 33.7 | 0.05 | 0.0 | 0.0 |
| 4-12 | 7.0 | 0.9 | 1024.48 | 16.93 | 0.1 | 33.6 | 0.02 | 24.4 | 20.0 |
| 4-12 | 8.1 | 3.8 | 1024.54 | 16.81 | 0.1 | 33.6 | 0.02 | 11.8 | 9.8 |
| 4-12 | 15.0 | 4.4 | 1024.60 | 16.75 | 0.0 | 33.6 | 0.02 | 5.0 | 4.1 |
| 4-12 | 21.5 | 3.6 | 1024.66 | 16.65 | 0.1 | 33.6 | 0.02 | 2.6 | 2.1 |
| 4-12 | 23.3 | 4.4 | 1024.85 | 15.82 | 0.1 | 33.6 | 0.02 | 2.2 | 1.9 |
| 4-12 | 24.4 | 3.8 | 1024.72 | 16.40 | 0.1 | 33.6 | 0.02 | 1.9 | 2.0 |
| 4-12 | 26.2 | 4.0 | 1024.79 | 16.19 | 0.1 | 33.6 | 0.01 | 1.2 | 1.6 |
| 4-12 | 26.6 | 3.1 | 1024.91 | 15.68 | 0.1 | 33.7 | 0.02 | 1.7 | 1.5 |
| 4-12 | 27.4 | 4.4 | 1025.15 | 14.57 | 0.1 | 33.7 | 0.01 | 1.7 | 1.1 |
| 4-12 | 27.7 | 3.9 | 1025.09 | 14.84 | 0.1 | 33.7 | 0.02 | 1.8 | 1.4 |
| 4-12 | 27.7 | 5.4 | 1024.97 | 15.37 | 0.2 | 33.6 | 0.02 | 1.5 | 1.6 |
| 4-12 | 27.8 | 4.6 | 1025.03 | 15.07 | 0.1 | 33.7 | 0.02 | 1.3 | 1.3 |
| 4-12 | 30.1 | 3.9 | 1025.21 | 14.39 | 0.1 | 33.7 | 0.01 | 1.1 | 1.1 |
| 4-12 | 30.8 | 4.2 | 1025.28 | 14.14 | 0.1 | 33.7 | 0.01 | 1.1 | 1.0 |
| 4-12 | 32.7 | 4.1 | 1025.34 | 13.95 | 0.1 | 33.7 | 0.01 | 0.9 | 0.8 |
| 4-12 | 34.4 | 3.9 | 1025.40 | 13.72 | 0.1 | 33.7 | 0.01 | 0.8 | 0.6 |
| 4-12 | 35.9 | 3.3 | 1025.46 | 13.52 | 0.1 | 33.7 | 0.02 | 0.6 | 0.5 |
| 4-12 | 38.3 | 3.0 | 1025.52 | 13.24 | 0.2 | 33.7 | 0.04 | 0.4 | 0.4 |
| 4-12 | 40.6 | 3.1 | 1025.58 | 12.95 | 0.2 | 33.7 | 0.05 | 0.4 | 0.3 |
| 4-12 | 42.6 | 3.4 | 1025.64 | 12.71 | 0.2 | 33.7 | 0.06 | 0.3 | 0.3 |
| 4-12 | 44.5 | 3.4 | 1025.70 | 12.50 | 0.2 | 33.7 | 0.06 | 0.3 | 0.2 |
| 4-12 | 46.7 | 3.6 | 1025.77 | 12.29 | 0.2 | 33.7 | 0.06 | 0.2 | 0.2 |
| 4-12 | 48.9 | 4.1 | 1025.83 | 12.11 | 0.1 | 33.8 | 0.03 | 0.2 | 0.2 |
| 4-12 | 50.5 | 4.2 | 1025.89 | 11.83 | 0.2 | 33.8 | 0.03 | 0.2 | 0.2 |
| 4-12 | 52.7 | 3.9 | 1025.95 | 11.62 | 0.2 | 33.8 | 0.03 | 0.1 | 0.1 |
| 4-12 | 55.1 | 3.6 | 1026.01 | 11.34 | 0.1 | 33.8 | 0.02 | 0.1 | 0.1 |
| 4-12 | 57.4 | 3.5 | 1026.07 | 11.09 | 0.1 | 33.8 | 0.02 | 0.1 | 0.1 |
| 4-12 | 59.7 | 3.7 | 1026.13 | 10.85 | 0.1 | 33.8 | 0.02 | 0.1 | 0.1 |
| 4-12 | 62.2 | 3.9 | 1026.19 | 10.63 | 0.1 | 33.8 | 0.02 | 0.1 | 0.1 |
| 4-12 | 65.2 | 4.2 | 1026.25 | 10.39 | 0.1 | 33.8 | 0.01 | 0.1 | 0.1 |
| 4-12 | 68.4 | 4.2 | 1026.32 | 10.23 | 0.1 | 33.8 | 0.01 | 0.0 | 0.0 |
| 4-12 | 72.1 | 4.0 | 1026.38 | 10.08 | 0.1 | 33.9 | 0.01 | 0.0 | 0.0 |
| 4-12 | 76.5 | 3.8 | 1026.44 | 9.93 | 0.1 | 33.9 | 0.02 | 0.0 | 0.0 |
| 4-12 | 81.3 | 3.7 | 1026.50 | 9.72 | 0.1 | 33.9 | 0.02 | 0.0 | 0.0 |
| 4-12 | 85.9 | 3.7 | 1026.56 | 9.54 | 0.1 | 33.9 | 0.01 | 0.0 | 0.0 |
| 4-12 | 90.9 | 3.5 | 1026.62 | 9.40 | 0.1 | 33.9 | 0.01 | 0.0 | 0.0 |
| 4-12 | 97.1 | 3.5 | 1026.68 | 9.30 | 0.1 | 33.9 | 0.01 | 0.0 | 0.0 |
| 4-12 | 103.8 | 3.4 | 1026.74 | 9.18 | 0.1 | 34.0 | 0.02 | 0.0 | 0.0 |

[a] Mean depth of isopycnals included in density bin (see Section 2.2.2 of text).

[b] Uncertainty given as 1σ of measurements within density bin from all averaged casts (see Section 2.2.2 of text).

[c] 400-700 nm spherical irradiance, versus simultaneous surface irradiance.

**Table A.2.** Profiles of suspended K37 alkenone concentration and molecular ($U_{37}^{K'}$) composition (see Section 2.2.4). Samples have been binned by density according to mean density profiles (Table A.1) as described in Section 2.2.2. Uncertainty in both terms is calculated assuming 10% uncertainty in the quantification of K37:2 and K37:3. Also included are profiles of the estimated per-cell K37 quota, $q_{K37}$. Uncertainty is derived from the 10% alkenone quantification uncertainty and the 95% confidence intervals of the alkenone-producer cell counts (Table A.8).

**Table A.2. Suspended Alkenone Abundance and Composition Profiles**

| Station | Depth (m) | σ | [K37][a] (ng L$^{-1}$) | ±[b] | $U^{K'}_{37}$[a] | ±[b] | Estimated K37 Cell Quota[c] (pg K37 Cell$^{-1}$) | ±[d] |
|---|---|---|---|---|---|---|---|---|
| *Gulf of California* | | | | | | | | |
| 1-1 | 9.6 | 2.3 | 48.1 | 4.8 | 0.989 | 0.002 | 2.7 | 1.1 |
| 1-1 | 11.1 | 2.0 | 54.2 | 5.4 | 0.992 | 0.001 | 2.1 | 0.7 |
| 1-1 | 15.6 | 2.3 | 53.3 | 5.1 | 0.963 | 0.005 | 1.1 | 0.3 |
| 1-1 | 21.2 | 2.0 | 35.8 | 3.3 | 0.925 | 0.010 | 0.4 | 0.2 |
| 1-1 | 24.3 | 2.5 | 10.1 | 0.9 | 0.931 | 0.009 | 0.1 | 0.1 |
| 1-1 | 26.0 | 2.3 | 13.0 | 1.2 | 0.910 | 0.011 | 0.2 | 0.1 |
| 1-1 | 27.9 | 2.5 | 17.9 | 1.6 | 0.890 | 0.014 | 0.3 | 0.1 |
| 1-1 | 28.9 | 1.7 | 25.6 | 2.2 | 0.844 | 0.019 | 0.5 | 0.2 |
| 1-1 | 35.0 | 2.2 | 10.2 | 0.9 | 0.830 | 0.020 | 0.6 | 0.3 |
| 1-1 | 40.5 | 2.0 | 8.5 | 0.7 | 0.846 | 0.018 | 0.9 | 0.5 |
| 1-1 | 48.5 | 2.5 | 3.8 | 0.3 | 0.807 | 0.022 | 0.7 | 0.5 |
| 3-1 | 7.5 | 1.2 | 27.7 | 2.7 | 0.992 | 0.001 | 1.1 | 0.3 |
| 3-1 | 11.1 | 1.6 | 24.9 | 2.5 | 0.992 | 0.001 | 1.0 | 0.3 |
| 3-1 | 16.0 | 2.0 | 61.9 | 6.2 | 0.994 | 0.001 | 1.9 | 0.4 |
| 3-1 | 21.0 | 3.1 | 40.3 | 4.0 | 0.985 | 0.002 | 1.9 | 0.5 |
| 3-1 | 23.3 | 3.1 | 32.5 | 3.2 | 0.997 | 0.000 | 2.0 | 0.6 |
| 3-1 | 27.6 | 3.8 | 63.3 | 6.3 | 0.992 | 0.001 | 1.7 | 0.3 |
| 3-1 | 29.0 | 3.7 | 26.6 | 2.7 | 0.996 | 0.001 | 1.2 | 0.3 |
| 3-1 | 30.4 | 3.8 | 57.9 | 5.7 | 0.984 | 0.002 | 2.0 | 0.4 |
| 3-1 | 33.5 | 4.8 | 23.2 | 2.3 | 0.989 | 0.002 | 0.6 | 0.1 |
| 3-1 | 39.5 | 3.8 | 16.7 | 1.6 | 0.979 | 0.003 | 0.4 | 0.1 |
| 3-1 | 45.9 | 4.1 | 15.8 | 1.5 | 0.973 | 0.004 | 0.4 | 0.1 |
| 3-2 | 7.0 | 1.4 | 11.8 | 1.2 | 0.990 | 0.001 | 2.0 | 0.71 |
| 3-2 | 22.2 | 0.6 | 39.3 | 3.8 | 0.976 | 0.003 | 2.8 | 0.66 |
| 3-2 | 25.5 | 1.6 | 78.3 | 7.3 | 0.936 | 0.008 | 2.5 | 0.53 |
| 3-2 | 25.8 | 4.1 | 90.2 | 8.6 | 0.948 | 0.007 | 3.5 | 0.82 |
| 3-2 | 36.3 | 2.3 | 36.1 | 3.1 | 0.859 | 0.017 | | |
| 3-2 | 42.0 | 2.1 | 15.4 | 1.3 | 0.857 | 0.017 | | |
| 3-3 | 3.8 | 1.4 | 20.0 | 2.0 | 0.999 | 0.000 | 1.5 | 0.4 |
| 3-3 | 13.7 | 2.0 | 47.1 | 4.7 | 0.997 | 0.000 | 2.1 | 0.5 |
| 3-3 | 19.1 | 3.2 | 77.9 | 7.6 | 0.972 | 0.004 | 1.7 | 0.3 |
| 3-3 | 21.7 | 2.7 | 106.8 | 10.3 | 0.965 | 0.005 | 3.0 | 0.6 |
| 3-3 | 28.5 | 3.3 | 137.9 | 11.9 | 0.854 | 0.018 | 1.2 | 0.2 |
| 3-3 | 28.6 | 2.6 | 86.5 | 7.9 | 0.902 | 0.012 | 0.8 | 0.1 |
| 3-3 | 37.1 | 2.8 | 45.0 | 3.9 | 0.843 | 0.019 | 1.5 | 0.4 |
| 3-3 | 39.5 | 2.9 | 19.9 | 1.7 | 0.841 | 0.019 | 0.9 | 0.3 |
| 3-4 | 6.5 | 2.6 | 6.8 | 0.7 | 0.986 | 0.002 | 1.2 | 0.5 |
| 3-4 | 13.9 | 3.1 | 10.3 | 1.0 | 0.997 | 0.000 | 3.2 | 1.4 |
| 3-4 | 21.6 | 3.2 | 20.6 | 2.1 | 0.998 | 0.000 | 4.4 | 1.5 |
| 3-4 | 26.3 | 2.2 | 37.1 | 3.7 | 0.997 | 0.000 | 2.0 | 0.4 |
| 3-4 | 31.8 | 2.2 | 33.8 | 3.3 | 0.987 | 0.002 | 1.2 | 0.3 |
| 3-4 | 34.5 | 2.2 | 55.6 | 5.5 | 0.981 | 0.003 | 2.6 | 0.6 |
| 3-4 | 39.0 | 2.2 | 17.8 | 1.7 | 0.960 | 0.005 | 0.4 | 0.1 |
| 4-1 | 14.8 | 6.4 | 4.2 | 0.4 | 0.949 | 0.007 | 0.5 | 0.1 |
| 4-1 | 15.8 | 3.3 | 5.5 | 0.5 | 0.943 | 0.008 | 0.6 | 0.1 |
| 4-1 | 21.4 | 4.8 | 8.9 | 0.9 | 0.964 | 0.005 | 0.6 | 0.1 |
| 4-1 | 25.0 | 5.5 | 17.6 | 1.7 | 0.960 | 0.005 | 0.9 | 0.2 |
| 4-1 | 38.8 | 6.4 | 15.8 | 1.3 | 0.806 | 0.022 | 0.3 | 0.0 |
| 4-1 | 44.0 | 6.9 | 8.8 | 0.7 | 0.805 | 0.022 | 0.2 | 0.0 |
| 4-2a | 17.6 | 6.8 | 32.7 | 3.3 | 0.998 | 0.000 | 0.8 | 0.1 |
| 4-2a | 24.3 | 7.5 | 19.4 | 1.9 | 0.982 | 0.003 | 0.4 | 0.1 |
| 4-2a | 38.8 | 5.7 | 19.6 | 1.9 | 0.965 | 0.005 | 0.3 | 0.1 |
| 4-2a | 61.0 | 10.4 | 3.3 | 0.3 | 0.840 | 0.019 | 0.2 | 0.0 |
| 4-2b | 8.3 | 1.9 | 22.7 | 2.2 | 0.989 | 0.001 | 1.4 | 0.3 |
| 4-2b | 16.5 | 1.8 | 12.49 | 1.23 | 0.98 | 0.003 | 1.0 | 0.2 |
| 4-2b | 31.8 | 3.2 | 26.46 | 2.62 | 0.99 | 0.002 | 0.9 | 0.2 |
| 4-2b | 39.9 | 1.6 | 33.13 | 3.27 | 0.99 | 0.002 | 1.0 | 0.2 |
| 4-2b | 46.3 | 1.3 | 10.04 | 0.96 | 0.95 | 0.006 | 0.4 | 0.1 |
| 4-2b | 53.8 | 2.7 | 6.54 | 0.61 | 0.92 | 0.010 | 0.3 | 0.1 |
| *Entrance Zone* | | | | | | | | |
| 4-8 | 10.1 | 2.4 | 18.8 | 1.8 | 0.98 | 0.003 | 0.7 | 0.1 |
| 4-8 | 13.1 | 2.9 | 27.3 | 2.7 | 0.98 | 0.003 | 1.0 | 0.2 |
| 4-8 | 17.0 | 3.0 | 26.8 | 2.6 | 0.99 | 0.002 | 1.0 | 0.2 |
| 4-8 | 27.8 | 4.0 | 30.1 | 3.0 | 0.98 | 0.003 | 0.8 | 0.1 |
| 4-8 | 37.4 | 8.0 | 16.1 | 1.6 | 0.98 | 0.003 | 0.4 | 0.1 |
| 4-8 | 55.6 | 7.7 | 17.9 | 1.7 | 0.97 | 0.004 | 0.2 | 0.0 |
| 4-9 | 10.3 | 1.3 | 2.3 | 0.2 | 0.933 | 0.009 | 0.6 | 0.3 |
| 4-9 | 18.8 | 2.9 | 3.0 | 0.3 | 0.849 | 0.018 | 0.6 | 0.1 |
| 4-9 | 27.0 | 2.5 | 8.8 | 0.8 | 0.923 | 0.010 | 0.7 | 0.1 |
| 4-9 | 32.7 | 2.5 | 9.8 | 0.9 | 0.910 | 0.012 | 0.3 | 0.1 |
| 4-9 | 35.8 | 2.8 | 7.2 | 0.7 | 0.894 | 0.013 | 0.1 | 0.0 |
| 4-9 | 51.3 | 3.4 | 1.4 | 0.1 | 0.708 | 0.029 | 0.0 | 0.0 |
| 4-9 | 56.1 | 3.7 | 6.1 | 0.5 | 0.747 | 0.027 | 0.1 | 0.0 |
| *Eastern Tropical North Pacific* | | | | | | | | |
| 4-10 | 9.5 | 3.0 | 2.5 | 0.2 | 0.813 | 0.022 | 0.4 | 0.1 |
| 4-10 | 12.3 | 2.7 | 2.3 | 0.2 | 0.822 | 0.021 | 0.2 | 0.0 |
| 4-10 | 22.3 | 2.7 | 11.1 | 0.9 | 0.750 | 0.027 | 0.6 | 0.1 |
| 4-10 | 31.3 | 2.7 | 47.4 | 3.4 | 0.517 | 0.035 | 1.6 | 0.3 |
| 4-10 | 39.7 | 2.2 | 19.9 | 1.4 | 0.479 | 0.035 | 0.7 | 0.1 |
| 4-10 | 49.7 | 3.3 | 17.9 | 1.3 | 0.508 | 0.035 | 0.4 | 0.1 |
| 4-10 | 61.2 | 3.5 | 32.7 | 2.4 | 0.380 | 0.033 | 0.3 | 0.0 |
| 4-11 | 3.0 | 2.8 | 9.1 | 0.7 | 0.725 | 0.028 | 0.6 | 0.1 |
| 4-11 | 8.5 | 1.5 | 8.0 | 0.6 | 0.735 | 0.028 | 0.7 | 0.1 |
| 4-11 | 25.5 | 2.9 | 60.4 | 4.3 | 0.589 | 0.034 | 0.9 | 0.1 |
| 4-11 | 29.4 | 2.8 | 40.5 | 2.9 | 0.530 | 0.035 | 0.5 | 0.1 |
| 4-11 | 38.8 | 4.4 | 36.9 | 2.6 | 0.431 | 0.035 | 0.7 | 0.1 |
| 4-11 | 47.0 | 5.6 | 33.3 | 2.4 | 0.438 | 0.035 | 0.4 | 0.1 |
| 4-11 | 59.8 | 5.2 | 8.8 | 0.6 | 0.402 | 0.034 | 0.1 | 0.0 |
| 4-12 | 8.1 | 3.8 | 59.9 | 4.2 | 0.542 | 0.035 | 1.0 | 0.1 |
| 4-12 | 15.0 | 4.4 | 52.4 | 3.7 | 0.529 | 0.035 | 0.5 | 0.1 |
| 4-12 | 26.2 | 4.0 | 29.4 | 2.1 | 0.572 | 0.035 | 0.4 | 0.1 |
| 4-12 | 32.7 | 4.1 | 15.8 | 1.1 | 0.495 | 0.035 | 0.6 | 0.1 |
| 4-12 | 40.6 | 3.1 | 15.8 | 1.1 | 0.476 | 0.035 | 0.3 | 0.0 |
| 4-12 | 52.7 | 3.9 | 9.9 | 0.7 | 0.501 | 0.035 | 0.2 | 0.0 |

[a] Samples binned by density according to mean density profiles (Table A.1, see Section 2.2.2 of text).
[b] Assuming 10% uncertainty in K37:2 and K37:3 quantification.
[c] [K37] over *E. hux* + *Gephyrocapsa spp.* abundance (Table A.8) interpolated to each bin.
[d] Propagated from uncertainty in alkenone quantification and *E. hux* + *G.oce* 95% confidence interval.

**Table A.3.** Measured K37:2 turnover and production rate profiles (Section 2.2.5) from *in situ* incubation arrays (Section 2.2.3). For each array depth, the resulting data have been associated with the depth of the density bin (from Table A.1; see Section 2.2.2) whose density corresponds closest to the *in situ* density when water for the incubation was initially collected. Uncertainty is calculated assuming a 10% uncertainty in alkenone quantification, the standard deviation of replicate isotopic measurements, and a 0.5 hr uncertainty in incubation time. Total K37 production rate estimates are calculated from $PR_{K37:2}$ and $U_{37}^{K'}$ (Table A.2) as per Section 2.2.5.

**Table A.3. K37:2 Alkenone Production Rate Profiles**

| Station | Depth (m) | σ | K37:2 Turnover Rate[a] ($day^{-1}$) | ±[b] | K37:2 Production Rate, $PR_{K37:2}$ ($ng\ L^{-1}\ d^{-1}$) | ± | Estimated $PR_{K37}$[c] ($ng\ L^{-1}\ d^{-1}$) | ± |
|---|---|---|---|---|---|---|---|---|
| *Gulf of California* | | | | | | | | |
| 1-1 | 9.6 | 2.3 | 0.127 | 0.004 | 2.5 | 0.3 | 2.5 | 0.3 |
| 1-1 | 24.3 | 2.5 | 0.111 | 0.003 | 1.7 | 0.2 | 1.8 | 0.2 |
| 1-1 | 35.0 | 2.2 | 0.054 | 0.003 | 0.4 | 0.0 | 0.5 | 0.1 |
| 3-1 | 11.1 | 1.6 | 0.20 | 0.00 | 11.5 | 1.2 | 11.5 | 1.2 |
| 3-1 | 16.0 | 2.0 | 0.17 | 0.00 | 8.4 | 0.9 | 8.5 | 0.9 |
| 3-1 | 27.6 | 3.8 | 0.14 | 0.00 | 4.6 | 0.5 | 4.6 | 0.5 |
| 3-1 | 35.0 | 4.3 | 0.38 | 0.01 | 10.6 | 1.1 | 10.8 | 1.1 |
| 3-1 | 39.5 | 3.8 | 0.10 | 0.00 | 1.3 | 0.1 | 1.3 | 0.1 |
| 3-2 | 9.9 | 2.8 | 0.25 | 0.01 | 1.2 | 0.1 | 1.2 | 0.1 |
| 3-2 | 20.2 | 0.5 | 0.11 | 0.01 | 0.4 | 0.0 | 0.4 | 0.0 |
| 3-2 | 32.1 | 1.8 | 0.29 | 0.01 | 3.2 | 0.3 | 3.6 | 0.4 |
| 3-3 | 8.9 | 2.4 | 0.19 | 0.00 | 3.6 | 0.4 | 3.6 | 0.4 |
| 3-3 | 14.2 | 5.0 | 0.14 | 0.00 | 3.9 | 0.4 | 3.9 | 0.4 |
| 3-3 | 24.3 | 2.9 | 0.12 | 0.00 | 7.5 | 0.8 | 8.1 | 0.8 |
| 3-3 | 29.6 | 3.1 | 0.08 | 0.00 | 2.1 | 0.2 | 2.3 | 0.3 |
| 3-3 | 39.5 | 2.9 | 0.00 | 0.00 | 0.0 | 0.0 | 0.1 | 0.0 |
| 3-4 | 6.5 | 2.6 | 0.24 | 0.01 | 1.6 | 0.2 | 1.6 | 0.2 |
| 3-4 | 13.9 | 3.1 | 0.26 | 0.01 | 2.1 | 0.2 | 2.1 | 0.2 |
| 3-4 | 21.6 | 3.2 | 0.23 | 0.01 | 3.9 | 0.4 | 3.9 | 0.4 |
| 3-4 | 34.5 | 2.2 | 0.35 | 0.01 | 10.6 | 1.1 | 10.8 | 1.1 |
| 3-4 | 43.6 | 2.6 | 0.33 | 0.01 | 4.7 | 0.5 | 5.0 | 0.5 |
| 4-1 | 15.8 | 3.3 | 0.50 | 0.03 | 6.0 | 0.7 | 6.4 | 0.7 |
| 4-1 | 24.3 | 5.4 | 0.51 | 0.01 | 12.7 | 1.3 | 13.2 | 1.4 |
| 4-1 | 29.3 | 5.9 | 0.43 | 0.01 | 15.8 | 1.6 | 17.3 | 1.8 |
| 4-1 | 37.5 | 6.4 | 0.34 | 0.01 | 6.4 | 0.7 | 7.8 | 0.8 |
| 4-1 | 49.8 | 6.6 | 0.03 | 0.01 | 0.5 | 0.1 | 0.6 | 0.1 |
| 4-2a | 10.1 | 5.4 | 0.18 | 0.01 | 3.5 | 0.4 | 3.5 | 0.4 |
| 4-2a | 12.8 | 5.0 | 0.21 | 0.01 | 6.9 | 0.7 | 6.9 | 0.7 |
| 4-2a | 20.9 | 7.0 | 0.200 | 0.004 | 3.5 | 0.4 | 3.5 | 0.4 |
| 4-2a | 38.8 | 5.7 | 0.32 | 0.01 | 1.0 | 0.1 | 1.0 | 0.1 |
| 4-2a | 63.1 | 9.9 | 0.068 | 0.003 | 0.0 | 0.0 | 0.1 | 0.0 |
| *Entrance Zone* | | | | | | | | |
| 4-8 | 8.2 | 2.9 | 0.20 | 0.01 | 4.2 | 0.4 | 4.3 | 0.4 |
| 4-8 | 20.9 | 3.4 | 0.16 | 0.00 | 6.6 | 0.7 | 6.7 | 0.7 |
| 4-8 | 24.4 | 3.8 | 0.183 | 0.008 | 5.4 | 0.6 | 5.5 | 0.6 |
| 4-8 | 32.6 | 4.4 | 0.17 | 0.01 | 4.9 | 0.5 | 5.0 | 0.5 |
| 4-8 | 40.6 | 7.8 | 0.12 | 0.00 | 3.0 | 0.3 | 3.1 | 0.3 |
| 4-8 | 55.6 | 7.7 | 0.062 | 0.004 | 0.5 | 0.1 | 0.5 | 0.1 |
| *Eastern Tropical North Pacific* | | | | | | | | |
| 4-12 | 8.1 | 3.8 | 0.37 | 0.02 | 11.4 | 1.2 | 21.0 | 2.7 |
| 4-12 | 15.0 | 4.4 | 0.39 | 0.01 | 9.9 | 1.0 | 18.8 | 2.3 |
| 4-12 | 23.3 | 4.4 | 0.014 | 0.010 | 0.2 | 0.1 | 0.4 | 0.3 |
| 4-12 | 26.2 | 4.0 | 0.06 | 0.00 | 0.6 | 0.1 | 1.1 | 0.1 |
| 4-12 | 35.9 | 3.3 | 0.007 | 0.004 | 0.04 | 0.02 | 0.1 | 0.0 |
| 4-12 | 46.7 | 3.6 | 0.01 | 0.00 | 0.06 | 0.02 | 0.1 | 0.0 |
| 4-12 | 59.7 | 3.7 | 0.01 | 0.01 | 0.05 | 0.02 | 0.1 | 0.0 |

[a] Sample depths assigned by placing isopycal of water collection on mean density profiles (Table A.1, see Section 2.2.2 of text).

[b] Propagated uncertainty, assuming 10% uncertainty in alkenone quantification, standard deviation of replicate isotopic measurements, 0.5hr uncertainty in incubation time.

[c] From $PR_{K37:2}$ and $U^{K'}_{37}$ (Table A.2), interpolated to each bin, via Equation 2.2.8.

**Table A.4.** Dissolved phosphate, nitrate, nitrite, and silicate concentration profiles; analysis described in White et al. (2007, 2013). Discrete samples have binned by density according to mean density profiles (Table A.1) as described in Section 2.2.2.

**Table A.4. Dissolved Macronutrient Concentrations**

| Station | Depth (m) | σ | Phosphate[a] (µM) | Nitrite (µM) | Nitrate (µM) | Silicate (µM) |
|---|---|---|---|---|---|---|
| *Gulf of California* | | | | | | |
| 1-1 | 5.8 | 1.1 | 0.46 | 0.02 | 0.01 | 1.64 |
| 1-1 | 9.6 | 2.3 | 0.45 | 0.00 | 0.00 | 1.29 |
| 1-1 | 11.1 | 2.0 | 0.39 | 0.02 | 0.00 | 1.12 |
| 1-1 | 14.1 | 1.7 | 0.58 | 0.00 | 0.02 | 6.42 |
| 1-1 | 19.8 | 2.1 | 0.75 | 0.11 | 0.42 | 3.59 |
| 1-1 | 23.0 | 2.2 | 0.82 | 0.22 | 0.79 | 4.32 |
| 1-1 | 24.3 | 2.5 | 0.95 | 0.22 | 1.06 | 3.80 |
| 1-1 | 26.0 | 2.3 | 0.93 | 0.26 | 1.34 | 4.32 |
| 1-1 | 27.9 | 2.5 | 1.15 | 0.85 | 4.20 | 11.36 |
| 1-1 | 32.3 | 2.3 | 1.36 | 0.68 | 6.94 | 15.56 |
| 1-1 | 38.1 | 2.2 | 1.67 | 0.17 | 10.71 | 22.08 |
| 1-1 | 48.5 | 2.5 | 2.00 | 0.05 | 14.86 | 29.64 |
| 1-1 | 68.6 | 3.6 | 2.24 | 0.02 | 18.02 | 34.90 |
| 1-1 | 99.2 | 2.9 | 2.23 | 0.00 | 19.21 | 28.59 |
| 3-1 | 11.1 | 1.6 | 0.44 | 0.00 | 0.03 | 1.71 |
| 3-1 | 14.3 | 1.7 | 0.43 | 0.01 | 0.07 | 1.63 |
| 3-1 | 21.0 | 3.1 | 0.47 | 0.00 | 0.10 | 2.17 |
| 3-1 | 27.6 | 3.8 | 0.55 | 0.02 | 0.08 | 3.34 |
| 3-1 | 32.2 | 4.4 | 0.69 | 0.11 | 0.08 | 4.43 |
| 3-1 | 37.1 | 3.9 | 0.77 | 0.04 | 0.00 | 4.42 |
| 3-1 | 41.9 | 3.6 | 0.81 | 0.09 | 0.00 | 4.58 |
| 3-1 | 45.9 | 4.1 | 0.89 | 0.30 | 0.23 | 4.92 |
| 3-1 | 59.3 | 6.3 | 1.62 | 0.21 | 10.30 | 21.57 |
| 3-1 | 94.1 | 3.0 | 1.90 | 0.10 | 13.75 | 30.38 |
| 3-2 | 7.0 | 1.4 | 0.57 | 0.01 | 0.04 | 0.52 |
| 3-2 | 9.9 | 2.8 | 0.58 | 0.02 | 0.07 | 0.52 |
| 3-2 | 18.1 | 4.3 | 0.65 | 0.02 | 0.04 | 1.54 |
| 3-2 | 22.1 | 6.1 | 0.72 | 0.00 | 0.12 | 2.86 |
| 3-2 | 22.2 | 0.6 | 0.60 | 0.03 | 0.03 | 1.81 |
| 3-2 | 25.5 | 1.6 | 0.76 | 0.01 | 0.11 | 3.69 |
| 3-2 | 29.3 | 3.1 | 0.78 | 0.00 | 0.11 | 3.20 |
| 3-2 | 36.3 | 2.3 | 1.08 | 0.40 | 1.97 | 6.66 |
| 3-2 | 39.1 | 2.3 | 1.10 | 0.39 | 1.40 | 5.94 |
| 3-2 | 42.0 | 2.1 | 1.36 | 0.40 | 5.08 | 9.84 |
| 3-2 | 51.5 | 2.4 | 1.72 | 0.09 | 10.95 | 17.31 |
| 3-2 | 76.9 | 3.0 | 2.25 | 0.03 | 18.15 | 34.95 |
| 3-2 | 97.6 | 1.6 | 2.49 | 0.00 | 22.59 | 35.02 |
| 3-3 | 8.9 | 2.4 | 0.93 | 0.01 | 0.04 | 6.66 |
| 3-3 | 13.8 | 3.2 | 0.94 | 0.01 | 0.01 | 5.53 |
| 3-3 | 19.1 | 3.2 | 0.93 | 0.00 | 0.01 | 3.22 |
| 3-3 | 21.7 | 2.7 | 0.96 | 0.02 | 0.02 | 1.75 |
| 3-3 | 25.7 | 2.8 | 0.99 | 0.03 | 0.05 | 1.11 |
| 3-3 | 25.8 | 2.7 | 1.04 | 0.00 | 0.04 | 0.94 |
| 3-3 | 32.5 | 2.6 | 1.42 | 0.14 | 0.65 | 4.85 |
| 3-3 | 37.1 | 2.8 | 1.90 | 0.48 | 9.17 | 22.56 |
| 3-3 | 41.5 | 3.1 | 2.07 | 0.56 | 12.65 | 29.67 |
| 3-3 | 53.0 | 3.8 | 2.31 | 0.22 | 17.37 | 39.63 |
| 3-3 | 71.5 | 3.4 | 2.57 | 0.14 | 21.32 | 50.66 |
| 3-3 | 104.5 | 1.1 | 2.69 | 0.09 | 23.25 | 58.40 |
| 3-4 | 6.5 | 2.6 | 0.62 | 0.04 | 0.00 | 0.89 |
| 3-4 | 13.9 | 3.1 | 0.64 | 0.04 | 0.00 | 1.22 |
| 3-4 | 19.3 | 2.8 | 0.65 | 0.04 | 0.00 | 1.20 |
| 3-4 | 26.3 | 2.2 | 0.51 | 0.07 | 0.00 | 0.98 |
| 3-4 | 30.1 | 2.0 | 0.71 | 0.08 | 0.00 | 2.80 |
| 3-4 | 37.5 | 1.9 | 0.81 | 0.08 | 0.00 | 4.12 |
| 3-4 | 42.0 | 2.3 | 0.87 | 0.11 | 0.01 | 4.10 |
| 3-4 | 47.5 | 3.2 | 1.09 | 0.38 | 1.47 | 6.32 |
| 3-4 | 71.2 | 2.7 | 2.14 | 0.11 | 17.64 | 23.67 |
| 3-4 | 97.2 | 2.7 | 2.52 | 0.06 | 22.84 | 36.56 |
| 4-1 | 15.8 | 3.3 | 0.65 | 0.05 | 0.00 | 1.48 |
| 4-1 | 25.4 | 5.1 | 0.80 | 0.04 | 0.00 | 2.00 |
| 4-1 | 27.5 | 5.9 | 0.87 | 0.04 | 0.03 | 2.40 |
| 4-1 | 33.0 | 6.1 | 1.00 | 0.08 | 0.30 | 3.17 |
| 4-1 | 42.6 | 6.2 | 1.28 | 0.38 | 4.45 | 5.19 |
| 4-1 | 46.6 | 6.9 | 1.63 | 0.67 | 9.39 | 7.93 |
| 4-1 | 61.1 | 8.1 | 2.26 | 0.08 | 19.72 | 16.06 |
| 4-1 | 79.3 | 6.7 | 2.38 | 0.07 | 19.19 | 20.24 |
| 4-1 | 94.8 | 7.4 | 2.43 | 0.15 | 18.84 | 22.23 |
| 4-2a | 6.1 | 3.9 | 0.44 | 0.02 | 0.05 | 1.28 |
| 4-2a | 10.1 | 5.4 | 0.45 | 0.02 | 0.00 | 1.38 |
| 4-2a | 10.8 | 6.0 | 0.41 | 0.00 | 0.06 | 0.91 |
| 4-2a | 12.8 | 5.0 | 0.46 | 0.00 | 0.02 | 1.11 |
| 4-2a | 17.6 | 6.8 | 0.50 | 0.01 | -0.01 | 1.79 |
| 4-2a | 20.9 | 7.0 | 0.53 | 0.00 | 0.02 | 1.30 |
| 4-2a | 24.3 | 7.5 | 0.56 | 0.01 | 0.09 | 1.97 |
| 4-2a | 28.2 | 7.8 | 0.47 | 0.00 | 0.05 | 1.42 |
| 4-2a | 31.8 | 7.4 | 0.54 | 0.03 | 0.17 | 1.36 |
| 4-2a | 34.7 | 6.8 | 0.57 | 0.15 | 0.57 | 1.53 |
| 4-2a | 40.7 | 5.5 | 0.83 | 0.35 | 3.49 | 2.59 |
| 4-2a | 42.4 | 5.3 | 0.65 | 0.51 | 0.80 | 2.06 |
| 4-2a | 44.6 | 5.6 | 0.93 | 0.22 | 4.88 | 3.92 |
| 4-2a | 46.7 | 5.8 | 0.74 | 0.55 | 1.85 | 2.50 |
| 4-2a | 48.9 | 6.4 | 1.16 | 0.09 | 7.94 | 5.17 |
| 4-2a | 59.6 | 11.2 | 1.43 | 0.17 | 10.54 | 7.40 |
| 4-2a | 73.0 | 8.9 | 2.01 | 0.07 | 20.23 | 11.63 |
| 4-2a | 76.1 | 8.8 | 1.76 | 0.27 | 14.82 | 10.14 |
| 4-2a | 91.4 | 7.2 | 2.42 | 0.10 | 22.35 | 15.61 |
| 4-2a | 97.3 | 7.3 | 2.33 | 0.04 | 21.67 | 15.51 |
| 4-2b | 8.3 | 1.9 | 0.32 | 0.02 | 0.09 | 1.04 |
| 4-2b | 12.8 | 1.6 | 0.34 | 0.01 | 0.00 | 0.82 |
| 4-2b | 22.2 | 2.7 | 0.28 | 0.03 | 0.00 | 0.98 |
| 4-2b | 25.4 | 3.0 | 0.45 | 0.02 | 0.00 | 2.41 |
| 4-2b | 28.7 | 3.4 | 0.48 | 0.02 | 0.00 | 2.21 |
| 4-2b | 35.7 | 2.4 | 0.58 | 0.38 | 0.17 | 3.18 |
| 4-2b | 53.8 | 2.7 | 0.83 | 0.23 | 3.52 | 3.97 |
| 4-2b | 68.3 | 3.6 | 0.96 | 0.17 | 4.89 | 3.94 |
| 4-2b | 94.0 | 3.3 | 1.41 | 0.10 | 11.22 | 8.11 |
| *Entrance Zone* | | | | | | |
| 4-8 | 7.5 | 1.2 | 0.25 | 0.02 | 0.04 | 1.12 |
| 4-8 | 10.1 | 2.4 | 0.30 | 0.04 | 0.05 | 1.22 |
| 4-8 | 13.1 | 2.9 | 0.30 | 0.05 | 0.00 | 1.18 |
| 4-8 | 17.0 | 3.0 | 0.31 | 0.03 | 0.02 | 1.14 |
| 4-8 | 20.9 | 3.4 | 0.31 | 0.05 | 0.06 | 1.13 |
| 4-8 | 24.4 | 3.8 | 0.32 | 0.02 | 0.00 | 1.20 |
| 4-8 | 27.8 | 4.0 | 0.34 | 0.04 | 0.04 | 1.24 |
| 4-8 | 30.2 | 4.5 | 0.38 | 0.05 | 0.06 | 1.40 |
| 4-8 | 32.6 | 4.4 | 0.40 | 0.02 | 0.07 | 1.42 |
| 4-8 | 34.1 | 8.2 | 0.42 | 0.04 | 0.05 | 1.94 |
| 4-8 | 37.4 | 8.0 | 0.37 | 0.03 | 0.01 | 1.47 |
| 4-8 | 44.2 | 7.9 | 0.45 | 0.05 | 0.07 | 1.48 |
| 4-8 | 55.6 | 7.7 | 0.50 | 0.04 | 0.09 | 1.64 |
| 4-8 | 68.6 | 7.5 | 0.52 | 0.13 | 0.27 | 1.82 |
| 4-8 | 70.7 | 7.7 | 0.81 | 0.94 | 2.57 | 2.78 |
| 4-8 | 74.7 | 7.5 | 0.89 | 0.80 | 3.40 | 3.50 |
| 4-8 | 78.1 | 2.7 | 0.74 | 0.29 | 1.59 | 3.00 |
| 4-8 | 80.0 | 8.5 | 0.77 | 0.20 | 1.81 | 3.68 |
| 4-8 | 86.0 | 6.5 | 1.12 | 0.34 | 6.00 | 5.49 |
| 4-8 | 86.9 | 5.9 | 1.57 | 0.13 | 12.56 | 8.64 |
| 4-8 | 90.8 | 4.6 | 1.58 | 0.25 | 12.38 | 9.47 |
| 4-8 | 96.2 | 3.3 | 1.74 | 0.47 | 14.21 | 11.19 |
| 4-8 | 99.3 | 3.0 | 2.06 | 0.06 | 19.60 | 15.24 |
| 4-8 | 102.8 | 3.1 | 2.16 | 0.07 | 21.07 | 16.29 |
| 4-9 | 5.9 | 1.2 | 0.57 | 0.03 | 0.00 | 4.34 |
| 4-9 | 12.6 | 1.6 | 0.63 | 0.01 | 0.03 | 1.59 |
| 4-9 | 15.3 | 2.2 | 0.62 | 0.03 | 0.00 | 4.66 |
| 4-9 | 22.1 | 2.6 | 0.74 | 0.01 | 0.02 | 5.92 |
| 4-9 | 27.0 | 2.5 | 0.70 | 0.04 | 0.00 | 5.17 |
| 4-9 | 34.3 | 2.6 | 0.90 | 0.12 | 0.94 | 3.32 |
| 4-9 | 40.0 | 3.6 | 1.23 | 0.48 | 5.23 | 6.03 |
| 4-9 | 44.5 | 3.9 | 1.67 | 0.82 | 10.86 | 8.20 |
| 4-9 | 53.8 | 3.7 | 1.76 | 0.49 | 14.29 | 12.91 |
| 4-9 | 72.2 | 3.8 | 2.16 | 0.10 | 21.46 | 19.81 |
| 4-9 | 85.0 | 4.3 | 2.45 | 0.09 | 24.08 | 22.93 |
| 4-9 | 97.8 | 4.4 | 2.55 | 0.06 | 25.54 | 26.12 |
| *Eastern Tropical North Pacific* | | | | | | |
| 4-10 | 12.3 | 2.7 | 0.36 | 0.01 | 0.09 | 2.19 |
| 4-10 | 20.2 | 1.9 | 0.35 | 0.00 | 0.05 | 2.43 |
| 4-10 | 25.9 | 2.6 | 0.32 | 0.00 | 0.00 | 3.48 |
| 4-10 | 29.7 | 2.6 | 0.36 | 0.00 | 0.01 | 2.21 |
| 4-10 | 31.3 | 2.7 | 0.42 | 0.00 | 0.01 | 2.37 |
| 4-10 | 37.4 | 2.5 | 0.49 | 0.01 | 0.03 | 4.30 |
| 4-10 | 57.1 | 3.2 | 0.82 | 0.37 | 6.66 | 7.12 |
| 4-10 | 61.2 | 3.5 | 0.98 | 0.35 | 7.89 | 7.29 |
| 4-10 | 70.1 | 4.2 | 0.98 | 0.09 | 9.79 | 9.40 |
| 4-10 | 74.9 | 4.2 | 1.11 | 0.13 | 11.23 | 9.81 |
| 4-10 | 79.9 | 4.1 | 1.37 | 0.07 | 14.83 | 14.02 |
| 4-10 | 99.4 | 3.4 | 1.93 | 0.06 | 21.67 | 20.90 |
| 4-10 | 105.4 | 3.8 | 1.96 | 0.01 | 22.32 | 23.05 |
| 4-11 | 8.5 | 1.5 | 0.29 | 0.03 | 0.08 | 2.70 |
| 4-11 | 21.4 | 2.3 | 0.27 | 0.02 | 0.01 | 2.29 |
| 4-11 | 27.3 | 2.4 | 0.27 | 0.03 | -0.02 | 2.25 |
| 4-11 | 34.4 | 3.9 | 0.32 | 0.01 | 0.03 | 2.74 |
| 4-11 | 36.3 | 4.1 | 0.32 | 0.01 | -0.05 | 2.87 |
| 4-11 | 44.4 | 5.3 | 0.41 | 0.01 | 0.03 | 3.73 |
| 4-11 | 47.0 | 5.6 | 0.43 | 0.02 | 0.06 | 4.04 |
| 4-11 | 53.2 | 5.0 | 0.55 | 0.11 | 1.41 | 4.66 |
| 4-11 | 59.8 | 5.2 | 0.67 | 0.29 | 3.92 | 5.27 |
| 4-11 | 62.8 | 5.1 | 0.82 | 0.27 | 6.54 | 6.02 |
| 4-11 | 66.9 | 5.1 | 1.01 | 0.41 | 9.36 | 8.93 |
| 4-11 | 71.3 | 5.2 | 0.97 | 0.17 | 8.92 | 7.61 |
| 4-11 | 90.1 | 5.5 | 1.37 | 0.09 | 15.94 | 14.63 |
| 4-11 | 102.2 | 4.8 | 1.40 | 0.08 | 17.33 | 16.20 |
| 4-12 | 8.1 | 3.8 | 0.30 | 0.01 | 0.16 | 0.57 |
| 4-12 | 15.0 | 4.4 | 0.34 | 0.00 | 0.22 | 0.79 |
| 4-12 | 21.5 | 3.6 | 0.36 | 0.00 | 0.29 | 0.83 |
| 4-12 | 27.7 | 3.9 | 0.78 | 0.33 | 5.55 | 5.60 |
| 4-12 | 27.7 | 5.4 | 0.67 | 0.21 | 3.95 | 4.05 |
| 4-12 | 38.3 | 3.0 | 0.75 | 0.29 | 5.19 | 5.18 |
| 4-12 | 44.5 | 3.4 | 1.30 | 0.09 | 15.18 | 14.63 |
| 4-12 | 52.7 | 3.9 | 1.39 | 0.07 | 17.01 | 16.13 |
| 4-12 | 59.7 | 3.7 | 1.62 | 0.05 | 20.19 | 19.60 |
| 4-12 | 68.4 | 4.2 | 1.76 | 0.05 | 22.43 | 22.36 |
| 4-12 | 72.1 | 4.0 | 1.89 | 0.00 | 24.49 | 25.14 |
| 4-12 | 90.9 | 3.5 | 1.96 | 0.03 | 25.86 | 27.70 |

[a] Data (all nutrients) from White et al. 2007 and 2012; Depth bins re-assessed as described in Section 2.2.2.

**Table A.5.** Quantitative ChlA profiles; analysis described in White et al. (2007, 2013). Discrete samples have been binned by density according to mean density profiles (Table A.1) as described in Section 2.2.2. Uncertainty is reported as the standard deviation of replicate samples in bins for which these were available. For each station, the mean percent standard deviation from the replicated depths was applied to the un-replicated samples to generate an estimated uncertainty.

**Table A.5. Chlorophyll A Profiles**

| Station | Depth (m) | σ | ChlA[a] (ng $L^{-1}$) | σ[b] | Station | Depth (m) | σ | ChlA[a] (ng $L^{-1}$) | σ[b] | Station | Depth (m) | σ | ChlA[a] (ng $L^{-1}$) | σ[b] |
|---|---|---|---|---|---|---|---|---|---|---|---|---|---|---|
| *Gulf of California* | | | | | 3-4 | 71.2 | 2.7 | 58 | 20 | 4-9 | 6.5 | 1.3 | 101 | 4 |
| 1-1 | 5.8 | 1.1 | 1467 | 189 | 3-4 | 97.2 | 2.7 | 6 | 2 | 4-9 | 10.3 | 1.3 | 90 | 4 |
| 1-1 | 9.6 | 2.3 | 1823 | 235 | 4-1 | 14.8 | 6.4 | 66 | 4 | 4-9 | 12.6 | 1.6 | 97 | 10 |
| 1-1 | 14.1 | 1.7 | 1199 | 154 | 4-1 | 15.8 | 3.3 | 81 | 7 | 4-9 | 18.8 | 2.9 | 115 | 8 |
| 1-1 | 24.3 | 2.5 | 1777 | 229 | 4-1 | 18.6 | 4.1 | 82 | 15 | 4-9 | 27.0 | 2.5 | 199 | 20 |
| 1-1 | 38.1 | 2.2 | 230 | 30 | 4-1 | 20.7 | 4.6 | 114 | 21 | 4-9 | 30.6 | 2.4 | 162 | 40 |
| 1-1 | 48.5 | 2.5 | 83 | 11 | 4-1 | 21.4 | 4.8 | 95 | 18 | 4-9 | 35.8 | 2.8 | 482 | 65 |
| 1-1 | 68.6 | 3.6 | 42 | 5 | 4-1 | 26.2 | 5.5 | 188 | 36 | 4-9 | 38.5 | 3.3 | 583 | 58 |
| 1-1 | 99.2 | 2.9 | 35 | 4 | 4-1 | 27.5 | 5.9 | 230 | 26 | 4-9 | 41.4 | 3.7 | 612 | 61 |
| 3-1 | 4.0 | 0.0 | 114 | 26 | 4-1 | 30.0 | 4.5 | 319 | 60 | 4-9 | 51.3 | 3.4 | 406 | 24 |
| 3-1 | 7.5 | 1.2 | 119 | 27 | 4-1 | 37.5 | 6.4 | 860 | 163 | 4-9 | 56.1 | 3.7 | 306 | 30 |
| 3-1 | 11.1 | 1.6 | 130 | 25 | 4-1 | 38.8 | 6.4 | 615 | 116 | 4-9 | 67.7 | 3.6 | 137 | 14 |
| 3-1 | 14.3 | 1.7 | 129 | 29 | 4-1 | 42.6 | 6.2 | 539 | 68 | *Eastern Tropical North Pacific* | | | | |
| 3-1 | 16.0 | 2.0 | 223 | 51 | 4-1 | 49.8 | 6.6 | 217 | 123 | 4-10 | 5.8 | 0.5 | 70 | 6 |
| 3-1 | 21.0 | 3.1 | 303 | 40 | 4-2a | 6.1 | 3.9 | 71 | 29 | 4-10 | 9.5 | 3.0 | 83 | 8 |
| 3-1 | 23.3 | 3.1 | 335 | 76 | 4-2a | 10.1 | 5.4 | 104 | 22 | 4-10 | 12.3 | 2.7 | 78 | 7 |
| 3-1 | 26.1 | 3.5 | 450 | 102 | 4-2a | 10.8 | 6.0 | 74 | 11 | 4-10 | 21.3 | 2.3 | 96 | 9 |
| 3-1 | 27.6 | 3.8 | 516 | 117 | 4-2a | 12.8 | 5.0 | 83 | 33 | 4-10 | 21.7 | 2.2 | 89 | 8 |
| 3-1 | 29.0 | 3.7 | 501 | 114 | 4-2a | 14.4 | 6.0 | 108 | 23 | 4-10 | 25.9 | 2.6 | 93 | 8 |
| 3-1 | 30.4 | 3.8 | 857 | 195 | 4-2a | 17.6 | 6.8 | 165 | 102 | 4-10 | 29.7 | 2.6 | 123 | 11 |
| 3-1 | 32.2 | 4.4 | 1268 | 288 | 4-2a | 20.9 | 7.0 | 124 | 21 | 4-10 | 31.3 | 2.7 | 253 | 23 |
| 3-1 | 33.5 | 4.8 | 1429 | 820 | 4-2a | 24.3 | 7.5 | 173 | 87 | 4-10 | 33.2 | 2.7 | 140 | 13 |
| 3-1 | 37.1 | 3.9 | 1005 | 229 | 4-2a | 28.2 | 7.8 | 266 | 157 | 4-10 | 35.2 | 2.8 | 152 | 14 |
| 3-1 | 39.5 | 3.8 | 983 | 224 | 4-2a | 31.8 | 7.4 | 202 | 167 | 4-10 | 39.7 | 2.2 | 224 | 20 |
| 3-1 | 41.9 | 3.6 | 1047 | 238 | 4-2a | 34.7 | 6.8 | 596 | 241 | 4-10 | 42.7 | 2.5 | 463 | 42 |
| 3-1 | 45.9 | 4.1 | 827 | 10 | 4-2a | 36.9 | 6.0 | 362 | 146 | 4-10 | 49.7 | 3.3 | 557 | 51 |
| 3-1 | 59.3 | 6.3 | 330 | 75 | 4-2a | 38.8 | 5.7 | 346 | 188 | 4-10 | 53.5 | 3.2 | 398 | 36 |
| 3-1 | 81.9 | 3.6 | 66 | 15 | 4-2a | 42.4 | 5.3 | 362 | 146 | 4-10 | 61.2 | 3.5 | 389 | 35 |
| 3-1 | 99.9 | 4.0 | 24 | 5 | 4-2a | 44.6 | 5.6 | 278 | 112 | 4-10 | 65.6 | 4.0 | 309 | 28 |
| 3-2 | 14.2 | 2.9 | 263 | 7 | 4-2a | 46.7 | 5.8 | 288 | 116 | 4-10 | 99.4 | 3.4 | 52 | 5 |
| 3-2 | 15.4 | 3.0 | 252 | 11 | 4-2a | 48.9 | 6.4 | 78 | 31 | 4-11 | 3.0 | 2.8 | 61 | 2 |
| 3-2 | 21.0 | 4.9 | 486 | 17 | 4-2a | 51.6 | 7.4 | 98 | 40 | 4-11 | 8.5 | 1.5 | 69 | 4 |
| 3-2 | 25.5 | 1.6 | 509 | 18 | 4-2a | 59.6 | 11.2 | 152 | 61 | 4-11 | 15.1 | 2.0 | 103 | 15 |
| 3-2 | 32.1 | 1.8 | 618 | 22 | 4-2a | 63.1 | 9.9 | 72 | 16 | 4-11 | 23.2 | 2.2 | 105 | 18 |
| 3-2 | 42.0 | 2.1 | 692 | 24 | 4-2a | 97.3 | 7.3 | 35 | 14 | 4-11 | 25.5 | 2.9 | 186 | 27 |
| 3-2 | 48.1 | 1.9 | 504 | 18 | 4-2b | 8.3 | 1.9 | 69 | 8 | 4-11 | 29.4 | 2.8 | 139 | 21 |
| 3-2 | 65.1 | 2.5 | 131 | 5 | 4-2b | 12.8 | 1.6 | 64 | 1 | 4-11 | 33.4 | 3.6 | 278 | 40 |
| 3-2 | 97.6 | 1.6 | 19 | 1 | 4-2b | 16.5 | 1.8 | 87 | 6 | 4-11 | 34.4 | 3.9 | 150 | 21 |
| 3-3 | 3.8 | 1.4 | 161 | 25 | 4-2b | 19.5 | 2.2 | 62 | 4 | 4-11 | 36.3 | 4.1 | 244 | 35 |
| 3-3 | 8.9 | 2.4 | 87 | 13 | 4-2b | 25.4 | 3.0 | 84 | 6 | 4-11 | 38.8 | 4.4 | 313 | 123 |
| 3-3 | 12.7 | 1.5 | 118 | 18 | 4-2b | 28.7 | 3.4 | 161 | 11 | 4-11 | 44.4 | 5.3 | 256 | 36 |
| 3-3 | 13.7 | 2.0 | 90 | 14 | 4-2b | 35.7 | 2.4 | 377 | 26 | 4-11 | 47.0 | 5.6 | 539 | 77 |
| 3-3 | 17.1 | 3.5 | 122 | 19 | 4-2b | 39.9 | 1.6 | 519 | 36 | 4-11 | 49.8 | 5.5 | 549 | 27 |
| 3-3 | 21.7 | 2.7 | 54 | 8 | 4-2b | 43.3 | 1.3 | 1026 | 71 | 4-11 | 56.7 | 4.8 | 390 | 56 |
| 3-3 | 24.3 | 2.9 | 156 | 24 | 4-2b | 46.3 | 1.3 | 1262 | 87 | 4-11 | 59.8 | 5.2 | 432 | 62 |
| 3-3 | 25.8 | 2.7 | 262 | 40 | 4-2b | 53.8 | 2.7 | 679 | 47 | 4-11 | 66.9 | 5.1 | 235 | 33 |
| 3-3 | 28.5 | 3.3 | 170 | 26 | 4-2b | 72.6 | 3.5 | 65 | 4 | 4-11 | 78.7 | 5.1 | 230 | 33 |
| 3-3 | 28.6 | 2.6 | 68 | 11 | 4-2b | 97.3 | 3.7 | 39 | 3 | 4-11 | 94.2 | 5.3 | 76 | 11 |
| 3-3 | 37.1 | 2.8 | 2955 | 456 | *Entrance Zone* | | | | | 4-12 | 8.1 | 3.8 | 217 | 10 |
| 3-3 | 39.5 | 2.9 | 3356 | 518 | 4-8 | 7.5 | 1.2 | 47 | 9 | 4-12 | 15.0 | 4.4 | 284 | 11 |
| 3-3 | 71.5 | 3.4 | 87 | 13 | 4-8 | 8.2 | 2.9 | 88 | 17 | 4-12 | 21.5 | 3.6 | 486 | 15 |
| 3-3 | 104.5 | 1.1 | 31 | 5 | 4-8 | 10.1 | 2.4 | 106 | 20 | 4-12 | 24.4 | 3.8 | 680 | 21 |
| 3-4 | 6.5 | 2.6 | 186 | 115 | 4-8 | 13.1 | 2.9 | 91 | 17 | 4-12 | 26.2 | 4.0 | 612 | 19 |
| 3-4 | 13.9 | 3.1 | 122 | 26 | 4-8 | 17.0 | 3.0 | 75 | 20 | 4-12 | 27.7 | 3.9 | 828 | 25 |
| 3-4 | 19.3 | 2.8 | 110 | 38 | 4-8 | 20.9 | 3.4 | 122 | 37 | 4-12 | 32.7 | 4.1 | 756 | 7 |
| 3-4 | 21.6 | 3.2 | 190 | 65 | 4-8 | 24.4 | 3.8 | 115 | 22 | 4-12 | 40.6 | 3.1 | 838 | 26 |
| 3-4 | 24.6 | 2.6 | 324 | 111 | 4-8 | 32.6 | 4.4 | 163 | 50 | 4-12 | 42.6 | 3.4 | 414 | 13 |
| 3-4 | 30.1 | 2.0 | 640 | 220 | 4-8 | 34.1 | 8.2 | 440 | 83 | 4-12 | 50.5 | 4.2 | 179 | 5 |
| 3-4 | 31.8 | 2.2 | 18 | 6 | 4-8 | 37.4 | 8.0 | 543 | 103 | 4-12 | 52.7 | 3.9 | 136 | 4 |
| 3-4 | 34.5 | 2.2 | 730 | 147 | 4-8 | 40.6 | 7.8 | 157 | 30 | 4-12 | 65.2 | 4.2 | 36 | 1 |
| 3-4 | 37.5 | 1.9 | 965 | 332 | 4-8 | 55.6 | 7.7 | 240 | 41 | 4-12 | 68.4 | 4.2 | 44 | 1 |
| 3-4 | 39.0 | 2.2 | 202 | 69 | 4-8 | 62.6 | 8.8 | 283 | 54 | 4-12 | 97.1 | 3.5 | 20 | 1 |
| 3-4 | 40.2 | 2.4 | 1107 | 381 | 4-8 | 74.7 | 7.5 | 82 | 16 | | | | | |
| 3-4 | 47.5 | 3.2 | 1007 | 346 | 4-8 | 102.8 | 3.1 | 25 | 5 | | | | | |

[a] Data from White et al. 2007 and 2012; Depth bins re-assessed as described in Section 2.2.2.

[b] For depths at which there was not sample replication, σ is determined as the mean percent standard deviation for the station multiplied by the concentration measured at that depth.

**Table A.6.** Profiles of POC concentration, C:N molar ratio, $\delta^{13}$C-POC, and $\delta^{15}$N-POC in suspended particulate material; analysis described in White et al. (2007; 2013). Discrete samples have been binned by density according to mean density profiles (Table A.1) as described in Section 2.2.2. Uncertainty is reported as the standard deviation of replicate samples in depth bins for which these were available. At a given station, the mean percent standard deviation from the replicated depths was applied to the un-replicated samples to generate an estimated uncertainty for POC concentration and C:N ratio. For isotopic properties, mean standard deviation has been used directly at un-replicated depths.

**Table A.6. POC Profiles**

| Station | Depth (m) | σ | POC[a] (μg L$^{-1}$) | σ[b] | C:N (molar) | ± | δ$^{13}$C-POC (‰ vPDB) | σ[c] | δ$^{15}$N-POC (‰ vATM) | σ |
|---|---|---|---|---|---|---|---|---|---|---|
| *Gulf of California* | | | | | | | | | | |
| 1-1 | 5.8 | 1.1 | 232 | 45 | 7.2 | 1.6 | -15.6 | 0.6 | 3.5 | 0.4 |
| 1-1 | 9.6 | 2.3 | 269 | 53 | 6.7 | 1.5 | -15.4 | 0.6 | 3.7 | 0.4 |
| 1-1 | 14.1 | 1.7 | 196 | 38 | 5.7 | 1.3 | -17.4 | 0.6 | 5.5 | 0.4 |
| 1-1 | 19.8 | 2.1 | 119 | 23 | 6.2 | 1.4 | -20.6 | 0.6 | 12.4 | 0.4 |
| 1-1 | 23.0 | 2.2 | 134 | 26 | 6.0 | 1.3 | -19.9 | 0.6 | 9.5 | 0.4 |
| 1-1 | 24.3 | 2.5 | 126 | 25 | 5.7 | 1.3 | -20.1 | 0.6 | 10.2 | 0.4 |
| 1-1 | 32.3 | 2.3 | 73 | 14 | 6.1 | 1.4 | -20.6 | 0.6 | 10.4 | 0.4 |
| 1-1 | 38.1 | 2.2 | 37 | 7 | 6.6 | 1.5 | -22.0 | 0.6 | 10.8 | 0.4 |
| 1-1 | 48.5 | 2.5 | 31 | 6 | 5.9 | 1.3 | -21.6 | 0.6 | 10.6 | 0.4 |
| 1-1 | 68.6 | 3.6 | 20 | 4 | 6.0 | 1.3 | -22.8 | 0.6 | 10.5 | 0.4 |
| 3-1 | 4.0 | 0.0 | 82 | 12 | 8.1 | 1.5 | -21.9 | 0.7 | | |
| 3-1 | 7.5 | 1.2 | 64 | 9 | 6.6 | 1.3 | -21.0 | 0.7 | | |
| 3-1 | 11.1 | 1.6 | 54 | 1 | 6.0 | 0.6 | -20.4 | 0.9 | | |
| 3-1 | 14.3 | 1.7 | 81 | 12 | 5.5 | 1.0 | -19.9 | 0.7 | | |
| 3-1 | 16.0 | 2.0 | 86 | 12 | 6.4 | 1.2 | -20.0 | 0.7 | | |
| 3-1 | 21.0 | 3.1 | 70 | 21 | 6.2 | 1.7 | -20.6 | 0.5 | | |
| 3-1 | 23.3 | 3.1 | 95 | 14 | 7.5 | 1.4 | -20.9 | 0.7 | | |
| 3-1 | 26.1 | 3.5 | 98 | 14 | 6.4 | 1.2 | -22.0 | 0.7 | | |
| 3-1 | 27.6 | 3.8 | 125 | 18 | 7.9 | 1.5 | -22.3 | 0.7 | | |
| 3-1 | 29.0 | 3.7 | 79 | 11 | 6.1 | 1.2 | -21.5 | 0.7 | | |
| 3-1 | 30.4 | 3.8 | 155 | 22 | 7.4 | 1.4 | -22.2 | 0.7 | | |
| 3-1 | 32.2 | 4.4 | 144 | 21 | 6.4 | 1.2 | -21.4 | 0.7 | | |
| 3-1 | 33.5 | 4.8 | 122 | 26 | 6.2 | 2.2 | -21.6 | 1.1 | | |
| 3-1 | 37.1 | 3.9 | 89 | 13 | 6.0 | 1.1 | -21.4 | 0.7 | | |
| 3-1 | 39.5 | 3.8 | 88 | 13 | 5.7 | 1.1 | -21.2 | 0.7 | | |
| 3-1 | 41.9 | 3.6 | 89 | 13 | 5.9 | 1.1 | -21.5 | 0.7 | | |
| 3-1 | 45.9 | 4.1 | 80 | 4 | 5.6 | 0.6 | -21.6 | 0.5 | | |
| 3-1 | 59.3 | 6.3 | 37 | 5 | 5.4 | 1.0 | -21.6 | 0.7 | | |
| 3-1 | 81.9 | 3.6 | 26 | 4 | 5.2 | 1.0 | -21.6 | 0.7 | | |
| 3-1 | 99.9 | 4.0 | 26 | 4 | 5.5 | 1.1 | -21.9 | 0.7 | | |
| 3-2 | 7.0 | 1.4 | 94 | 8 | 7.3 | 0.8 | -23.4 | 0.4 | 5.9 | 0.3 |
| 3-2 | 15.4 | 3.0 | 76 | 11 | 6.7 | 1.1 | -22.1 | 0.2 | 7.8 | 0.3 |
| 3-2 | 22.1 | 6.1 | 70 | 10 | 6.4 | 1.0 | -22.0 | 0.2 | 8.6 | 0.3 |
| 3-2 | 22.2 | 0.6 | 110 | 16 | 6.8 | 1.1 | -22.1 | 0.2 | 8.9 | 0.3 |
| 3-2 | 25.5 | 1.6 | 90 | 7 | 6.4 | 0.6 | -22.1 | 0.2 | 10.0 | 0.1 |
| 3-2 | 25.8 | 4.1 | 63 | 9 | 6.4 | 1.0 | -22.2 | 0.2 | 9.1 | 0.3 |
| 3-2 | 29.3 | 1.1 | 90 | 13 | 6.6 | 1.1 | -23.6 | 0.2 | 9.9 | 0.3 |
| 3-2 | 36.3 | 2.3 | 116 | 32 | 6.0 | 1.7 | -22.7 | 0.1 | 10.1 | 0.6 |
| 3-2 | 40.0 | 1.8 | 72 | 10 | 5.5 | 0.9 | -21.7 | 0.2 | 9.1 | 0.3 |
| 3-2 | 42.0 | 2.1 | 62 | 9 | 5.9 | 1.0 | -22.9 | 0.2 | 10.4 | 0.3 |
| 3-2 | 55.8 | 1.7 | 41 | 6 | 4.9 | 0.8 | -21.6 | 0.2 | 9.0 | 0.3 |
| 3-2 | 72.1 | 3.1 | 20 | 3 | 5.7 | 0.9 | -21.6 | 0.2 | 10.7 | 0.3 |
| 3-2 | 97.6 | 1.6 | 18 | 3 | 6.4 | 1.0 | -21.5 | 0.2 | 11.3 | 0.3 |
| 3-3 | 3.8 | 1.4 | 183 | 58 | 10.6 | 3.7 | -19.9 | 0.1 | 12.5 | 0.5 |
| 3-3 | 8.9 | 2.4 | 68 | 22 | 7.5 | 2.6 | -20.5 | 0.1 | 12.1 | 0.5 |
| 3-3 | 13.7 | 2.0 | 92 | 29 | 8.4 | 3.0 | -20.3 | 0.1 | 10.8 | 0.5 |
| 3-3 | 17.2 | 3.5 | 111 | 35 | 8.3 | 2.9 | -19.6 | 0.1 | 12.5 | 0.5 |
| 3-3 | 19.1 | 3.2 | 136 | 43 | 8.5 | 3.0 | -19.8 | 0.1 | 12.4 | 0.5 |
| 3-3 | 21.7 | 2.7 | 152 | 87 | 9.6 | 6.5 | -20.1 | 0.2 | 11.9 | 0.8 |
| 3-3 | 25.7 | 2.8 | 278 | 89 | 9.9 | 3.5 | -19.8 | 0.1 | 12.8 | 0.5 |
| 3-3 | 25.8 | 2.7 | 247 | 79 | 9.6 | 3.4 | -19.4 | 0.1 | 13.4 | 0.5 |
| 3-3 | 28.5 | 3.3 | 213 | 68 | 11.5 | 4.0 | -20.1 | 0.1 | 13.7 | 0.5 |
| 3-3 | 28.6 | 2.6 | 260 | 83 | 9.6 | 3.4 | -20.1 | 0.1 | 12.4 | 0.5 |
| 3-3 | 32.5 | 2.6 | 745 | 238 | 6.9 | 2.4 | -19.1 | 0.1 | 13.8 | 0.5 |
| 3-3 | 37.1 | 2.8 | 222 | 15 | 6.3 | 0.4 | -19.2 | 0.1 | 10.9 | 0.2 |
| 3-3 | 39.5 | 2.9 | 255 | 81 | 6.0 | 2.1 | -19.4 | 0.1 | 9.5 | 0.5 |
| 3-3 | 41.5 | 3.1 | 148 | 47 | 6.3 | 2.2 | -19.3 | 0.1 | 12.2 | 0.5 |
| 3-3 | 53.0 | 3.8 | 61 | 19 | 6.4 | 2.2 | -20.8 | 0.1 | 14.4 | 0.5 |
| 3-3 | 71.5 | 3.4 | 44 | 14 | 6.2 | 2.2 | -21.1 | 0.1 | 15.4 | 0.5 |
| 3-3 | 104.5 | 1.1 | 34 | 11 | 7.0 | 2.4 | -22.4 | 0.1 | 14.9 | 0.5 |
| 3-4 | 6.5 | 2.6 | 83 | 49 | 7.3 | 4.7 | -21.1 | 1.3 | | |
| 3-4 | 13.9 | 3.1 | 68 | 12 | 6.1 | 1.6 | -20.8 | 0.5 | | |
| 3-4 | 19.3 | 2.8 | 61 | 18 | 6.1 | 2.1 | -20.9 | 0.6 | | |
| 3-4 | 21.6 | 3.2 | 73 | 21 | 5.7 | 1.9 | -20.9 | 0.6 | | |
| 3-4 | 24.6 | 2.6 | 77 | 23 | 6.4 | 2.1 | -21.1 | 0.6 | | |
| 3-4 | 26.3 | 2.2 | 87 | 25 | 6.6 | 2.2 | -20.4 | 0.6 | | |
| 3-4 | 30.1 | 2.0 | 93 | 27 | 6.9 | 2.3 | -21.4 | 0.6 | | |
| 3-4 | 31.8 | 2.2 | 65 | 19 | 6.4 | 2.1 | -23.0 | 0.6 | | |
| 3-4 | 34.5 | 2.2 | 96 | 10 | 6.5 | 0.9 | -21.6 | 0.1 | | |
| 3-4 | 37.5 | 1.9 | 87 | 25 | 6.1 | 2.0 | -21.7 | 0.6 | | |
| 3-4 | 39.0 | 2.2 | 119 | 35 | 5.6 | 1.9 | -21.3 | 0.6 | | |
| 3-4 | 40.2 | 2.4 | 94 | 28 | 6.0 | 2.0 | -22.0 | 0.6 | | |
| 3-4 | 47.5 | 3.2 | 79 | 23 | 5.8 | 2.0 | -22.9 | 0.6 | | |
| 3-4 | 71.2 | 2.7 | 24 | 7 | 6.5 | 2.2 | -22.3 | 0.6 | | |
| 3-4 | 97.2 | 2.7 | 21 | 6 | 6.4 | 2.1 | -22.1 | 0.6 | | |
| 4-1 | 14.8 | 6.4 | 78 | 6 | 8.1 | 0.9 | -21.5 | 0.1 | 10.2 | 0.1 |
| 4-1 | 15.8 | 3.3 | 68 | 13 | 7.8 | 1.4 | -21.7 | 0.3 | 9.8 | 0.7 |
| 4-1 | 25.4 | 5.1 | 85 | 16 | 6.5 | 1.5 | -21.7 | 0.4 | 10.8 | 0.5 |
| 4-1 | 26.2 | 5.5 | 95 | 18 | 6.3 | 1.4 | -21.9 | 0.4 | 10.6 | 0.5 |
| 4-1 | 27.5 | 5.9 | 114 | 39 | 6.9 | 3.3 | -21.7 | 1.0 | 11.0 | 0.1 |
| 4-1 | 30.0 | 4.5 | 126 | 24 | 6.0 | 1.4 | -22.3 | 0.4 | 11.3 | 0.5 |
| 4-1 | 31.8 | 5.7 | 231 | 44 | 8.9 | 2.0 | -22.5 | 0.4 | 10.9 | 0.5 |
| 4-1 | 38.8 | 6.4 | 120 | 23 | 6.3 | 1.4 | -22.7 | 0.4 | 10.3 | 0.5 |
| 4-1 | 40.4 | 6.5 | 124 | 23 | 7.1 | 1.6 | -22.9 | 0.4 | 9.1 | 0.5 |
| 4-1 | 42.6 | 6.2 | 114 | 17 | 6.9 | 1.1 | -23.0 | 0.2 | 10.2 | 1.2 |
| 4-1 | 49.8 | 6.6 | 86 | 16 | 6.2 | 1.4 | -22.0 | 0.4 | 12.2 | 0.5 |
| 4-2a | 6.1 | 3.9 | 75 | 3 | 8.3 | 0.2 | -21.4 | 0.5 | 7.0 | 0.7 |
| 4-2a | 10.1 | 5.4 | 83 | 17 | 7.4 | 1.6 | -21.2 | 0.5 | 8.2 | 0.6 |
| 4-2a | 10.8 | 6.0 | 72 | 7 | 7.7 | 1.1 | -21.2 | 0.0 | 7.9 | 0.1 |
| 4-2a | 12.8 | 5.0 | 74 | 26 | 7.5 | 2.8 | -21.4 | 0.9 | 8.3 | 0.8 |
| 4-2a | 17.6 | 6.8 | 104 | 21 | 8.1 | 1.7 | -22.1 | 0.9 | 8.5 | 0.2 |
| 4-2a | 20.9 | 7.0 | 56 | 21 | 7.3 | 3.5 | -21.4 | 0.3 | 8.2 | 0.9 |
| 4-2a | 24.3 | 7.5 | 98 | 30 | 7.7 | 3.0 | -21.8 | 0.5 | 8.5 | 0.7 |
| 4-2a | 28.2 | 7.8 | 112 | 49 | 7.3 | 3.7 | -21.9 | 0.5 | 8.3 | 0.7 |
| 4-2a | 31.8 | 7.4 | 72 | 12 | 7.1 | 1.5 | -21.6 | 0.4 | 8.5 | 0.7 |
| 4-2a | 34.7 | 6.8 | 76 | 5 | 6.4 | 0.7 | -22.1 | 0.3 | 8.6 | 0.3 |
| 4-2a | 36.9 | 6.0 | 68 | 13 | 6.2 | 1.4 | -22.3 | 0.5 | 7.4 | 0.6 |
| 4-2a | 38.8 | 5.7 | 93 | 26 | 7.9 | 2.9 | -22.6 | 0.4 | 9.0 | 0.2 |
| 4-2a | 40.7 | 5.5 | 58 | 2 | 6.5 | 0.6 | -22.2 | 0.7 | 8.5 | 0.4 |
| 4-2a | 42.4 | 5.3 | 49 | 8 | 6.2 | 1.4 | -22.3 | 0.4 | 7.9 | 0.0 |
| 4-2a | 44.6 | 5.6 | 53 | 6 | 6.5 | 0.7 | -21.5 | 0.6 | 11.8 | 0.9 |
| 4-2a | 46.7 | 5.8 | 48 | 4 | 6.2 | 0.5 | -22.1 | 0.6 | 8.9 | 0.1 |
| 4-2a | 48.9 | 6.4 | 37 | 6 | 6.6 | 1.0 | -21.7 | 1.1 | 11.9 | 0.1 |
| 4-2a | 59.6 | 11.2 | 43 | 8 | 7.0 | 1.8 | -21.2 | 0.4 | 9.8 | 1.1 |
| 4-2a | 63.1 | 9.9 | 37 | 5 | 6.8 | 1.4 | -21.2 | 0.6 | 9.6 | 2.2 |
| 4-2a | 73.0 | 8.9 | 42 | 2 | 6.3 | 0.3 | -21.3 | 0.6 | 9.5 | 0.1 |
| 4-2a | 97.3 | 7.3 | 43 | 14 | 6.3 | 2.8 | -20.5 | 0.4 | 11.7 | 0.5 |
| 4-2b | 8.3 | 1.9 | 59 | 9 | 6.7 | 1.5 | -21.0 | 0.4 | 7.1 | 1.1 |
| 4-2b | 12.8 | 1.6 | 56 | 1 | 7.0 | 1.0 | -21.1 | 0.7 | 7.9 | 1.4 |
| 4-2b | 16.5 | 1.8 | 50 | 0 | 6.5 | 0.7 | -22.0 | 1.3 | 7.0 | 1.6 |
| 4-2b | 22.2 | 2.7 | 59 | 5 | 6.6 | 0.9 | -20.8 | 0.2 | 7.3 | 1.3 |
| 4-2b | 25.4 | 3.0 | 74 | 3 | 7.0 | 0.3 | -21.4 | 0.4 | 7.9 | 0.6 |
| 4-2b | 28.7 | 3.4 | 84 | 18 | 6.7 | 1.8 | -21.6 | 0.2 | 9.0 | 0.1 |
| 4-2b | 31.8 | 3.2 | 66 | 4 | 6.2 | 0.8 | -22.2 | 0.3 | 8.5 | 0.2 |
| 4-2b | 35.7 | 2.4 | 103 | 3 | 6.0 | 0.2 | -21.0 | 0.2 | 9.1 | 0.2 |
| 4-2b | 39.9 | 1.6 | 108 | 41 | 6.1 | 2.9 | -21.6 | 1.5 | 9.2 | 1.2 |
| 4-2b | 46.3 | 1.3 | 110 | 9 | 5.9 | 0.7 | -22.3 | 0.4 | 8.5 | 0.9 |
| 4-2b | 53.8 | 2.7 | 64 | 25 | 6.2 | 3.2 | -21.0 | 1.3 | 9.5 | 1.7 |
| 4-2b | 68.3 | 3.6 | 43 | 9 | 7.2 | 1.3 | -21.3 | 1.9 | 10.7 | 2.1 |
| 4-2b | 94.0 | 3.3 | 33 | 5 | 7.4 | 1.1 | -21.0 | 0.2 | 11.0 | 1.3 |
| *Entrance Zone* | | | | | | | | | | |
| 4-8 | 7.5 | 1.2 | 58 | 4 | 7.4 | 1.0 | -21.4 | 0.7 | 7.4 | 0.5 |
| 4-8 | 8.2 | 2.9 | 65 | 6 | 6.1 | 0.8 | -21.5 | 0.6 | 8.4 | 0.9 |
| 4-8 | 10.1 | 2.4 | 57 | 3 | 6.9 | 0.9 | -21.2 | 0.5 | 7.0 | 0.3 |
| 4-8 | 13.1 | 2.9 | 60 | 3 | 6.9 | 0.4 | -21.3 | 0.5 | 7.8 | 0.2 |
| 4-8 | 17.0 | 3.0 | 64 | 5 | 6.8 | 0.8 | -21.2 | 0.6 | 7.8 | 0.8 |
| 4-8 | 20.9 | 3.4 | 62 | 3 | 7.8 | 1.0 | -20.9 | 0.5 | 8.3 | 0.9 |
| 4-8 | 24.4 | 3.8 | 63 | 4 | 7.1 | 0.6 | -21.5 | 0.4 | 7.4 | 0.6 |
| 4-8 | 27.8 | 4.0 | 68 | 7 | 7.2 | 1.8 | -21.7 | 0.4 | 7.7 | 0.7 |
| 4-8 | 30.2 | 4.5 | 62 | 9 | 6.8 | 1.1 | -22.0 | 0.1 | 7.7 | 1.8 |
| 4-8 | 32.6 | 4.4 | 75 | 10 | 6.8 | 1.0 | -22.1 | 0.6 | 7.8 | 0.3 |
| 4-8 | 34.1 | 8.2 | 69 | 8 | 6.8 | 1.0 | -21.8 | 0.7 | 8.9 | 1.9 |
| 4-8 | 37.4 | 8.0 | 81 | 27 | 7.0 | 2.9 | -22.3 | 0.8 | 7.8 | 0.5 |
| 4-8 | 40.6 | 7.8 | 55 | 5 | 6.3 | 0.9 | -21.5 | 0.6 | 8.6 | 0.9 |
| 4-8 | 44.2 | 7.9 | 66 | 0 | 6.8 | 0.1 | -22.1 | 0.7 | 8.4 | 1.0 |
| 4-8 | 55.6 | 7.7 | 63 | 4 | 6.3 | 0.5 | -22.4 | 0.3 | 8.3 | 0.6 |
| 4-8 | 68.6 | 7.5 | 42 | 3 | 6.0 | 0.6 | -21.3 | 0.4 | 7.9 | 1.0 |
| 4-8 | 70.7 | 7.7 | 43 | 4 | 5.8 | 0.8 | -22.7 | 0.6 | 6.5 | 0.9 |
| 4-8 | 80.0 | 8.5 | 45 | 2 | 5.7 | 0.5 | -22.0 | 0.5 | 8.0 | 0.0 |
| 4-8 | 96.2 | 3.3 | 36 | 0 | 5.5 | 0.5 | -23.5 | 1.3 | 9.1 | 2.0 |
| 4-8 | 102.8 | 3.1 | 24 | 1 | 5.7 | 0.8 | -23.2 | 0.7 | 10.1 | 1.9 |
| 4-9 | 7.6 | 1.2 | 64 | 12 | 6.6 | 1.6 | -21.1 | 0.4 | 9.9 | 0.2 |
| 4-9 | 10.3 | 1.3 | 48 | 4 | 6.3 | 0.9 | -21.0 | 0.3 | 9.3 | 0.2 |
| 4-9 | 15.3 | 2.2 | 62 | 7 | 6.6 | 1.2 | -21.0 | 0.4 | 10.0 | 0.7 |
| 4-9 | 18.8 | 2.9 | 64 | 2 | 5.9 | 0.2 | -20.8 | 0.0 | 9.8 | 0.8 |
| 4-9 | 27.0 | 2.5 | 75 | 0 | 6.2 | 0.2 | -20.9 | 0.4 | 10.6 | 0.7 |
| 4-9 | 30.6 | 2.4 | 64 | 3 | 6.1 | 0.7 | -21.0 | 0.2 | 10.8 | 0.9 |
| 4-9 | 35.8 | 2.8 | 86 | 19 | 5.9 | 1.8 | -22.2 | 0.3 | 10.1 | 0.9 |
| 4-9 | 51.3 | 3.4 | 58 | 7 | 5.7 | 1.3 | -23.3 | 0.5 | 11.6 | 1.2 |
| 4-9 | 56.1 | 3.7 | 52 | 7 | 6.3 | 1.4 | -23.5 | 0.8 | 10.7 | 0.1 |
| 4-9 | 72.2 | 3.8 | 33 | 7 | 6.1 | 1.6 | -22.1 | 0.9 | 11.1 | 1.4 |
| *Eastern Tropical North Pacific* | | | | | | | | | | |
| 4-10 | 9.5 | 3.0 | 51 | 3 | 6.4 | 0.5 | -22.4 | 0.1 | 8.4 | 1.6 |
| 4-10 | 12.3 | 2.7 | 46 | 4 | 6.0 | 0.5 | -22.0 | 0.2 | 7.8 | 2.2 |
| 4-10 | 20.2 | 1.9 | 56 | 6 | 6.1 | 1.0 | -21.5 | 0.3 | 9.1 | 1.4 |
| 4-10 | 21.3 | 2.3 | 68 | 0 | 6.1 | 0.6 | -21.2 | 0.1 | 8.7 | 0.6 |
| 4-10 | 25.9 | 2.6 | 83 | 9 | 6.1 | 1.0 | -21.4 | 0.3 | 9.7 | 1.4 |
| 4-10 | 29.7 | 2.6 | 64 | 7 | 6.8 | 1.1 | -21.4 | 0.3 | 8.6 | 1.4 |
| 4-10 | 31.3 | 2.7 | 68 | 7 | 6.9 | 0.7 | -21.7 | 0.4 | 8.5 | 0.5 |
| 4-10 | 37.4 | 2.5 | 102 | 11 | 5.7 | 0.9 | -22.1 | 0.3 | 9.3 | 1.4 |
| 4-10 | 42.7 | 2.5 | 96 | 11 | 6.6 | 1.4 | -22.4 | 0.0 | 9.4 | 1.0 |
| 4-10 | 46.0 | 3.0 | 86 | 9 | 5.9 | 1.0 | -21.7 | 0.3 | 9.0 | 1.4 |
| 4-10 | 49.7 | 3.3 | 86 | 17 | 6.0 | 1.4 | -23.3 | 0.3 | 8.5 | 0.0 |
| 4-10 | 57.1 | 3.2 | 72 | 12 | 6.5 | 1.4 | -23.4 | 0.4 | 9.7 | 0.3 |
| 4-10 | 65.6 | 4.0 | 52 | 11 | 6.2 | 1.5 | -23.6 | 0.8 | 8.5 | 1.7 |
| 4-10 | 70.1 | 4.2 | 43 | 5 | 6.7 | 1.1 | -23.3 | 0.3 | 8.2 | 1.4 |
| 4-10 | 79.9 | 4.1 | 28 | 3 | 7.1 | 1.2 | -22.9 | 0.3 | 11.6 | 1.4 |
| 4-10 | 105.4 | 3.8 | 16 | 0 | 7.3 | 2.2 | -22.1 | 0.1 | 10.5 | 5.1 |
| 4-11 | 3.0 | 2.8 | 60 | 8 | 7.1 | 1.6 | -22.2 | 0.5 | 7.6 | 0.6 |
| 4-11 | 8.5 | 1.5 | 62 | 8 | 6.8 | 1.0 | -22.3 | 0.7 | 8.3 | 0.6 |
| 4-11 | 21.4 | 2.3 | 80 | 7 | 6.7 | 0.8 | -21.9 | 0.5 | 8.8 | 0.7 |
| 4-11 | 23.2 | 2.2 | 88 | 9 | 7.0 | 0.9 | -21.8 | 0.3 | 8.6 | 0.5 |
| 4-11 | 27.3 | 2.4 | 82 | 4 | 6.8 | 0.3 | -22.1 | 0.3 | 8.8 | 1.0 |
| 4-11 | 29.4 | 2.8 | 82 | 8 | 6.6 | 0.8 | -21.8 | 0.5 | 8.6 | 0.7 |
| 4-11 | 34.4 | 3.9 | 76 | 1 | 6.8 | 0.2 | -22.2 | 0.4 | 8.6 | 0.3 |
| 4-11 | 36.3 | 4.1 | 78 | 7 | 6.6 | 0.7 | -22.5 | 0.6 | 8.0 | 0.0 |
| 4-11 | 38.8 | 4.4 | 68 | 6 | 6.4 | 0.8 | -22.4 | 0.4 | 8.1 | 0.7 |
| 4-11 | 44.4 | 5.3 | 75 | 7 | 6.6 | 0.8 | -22.4 | 0.5 | 9.3 | 0.7 |
| 4-11 | 47.0 | 5.6 | 94 | 10 | 6.1 | 0.8 | -22.7 | 0.6 | 8.6 | 0.9 |
| 4-11 | 49.8 | 5.5 | 96 | 9 | 6.0 | 0.7 | -21.8 | 0.5 | 8.5 | 0.7 |
| 4-11 | 53.2 | 5.0 | 97 | 9 | 5.9 | 0.7 | -22.4 | 0.5 | 8.0 | 0.7 |
| 4-11 | 56.7 | 4.8 | 55 | 5 | 6.2 | 0.8 | -22.0 | 0.5 | 6.6 | 0.7 |
| 4-11 | 59.8 | 5.2 | 62 | 5 | 5.9 | 0.6 | -23.1 | 0.7 | 7.4 | 1.2 |
| 4-11 | 66.9 | 5.1 | 40 | 5 | 6.0 | 1.1 | -22.8 | 0.7 | 10.4 | 1.0 |
| 4-11 | 90.1 | 5.5 | 41 | 4 | 5.6 | 0.7 | -20.0 | 0.5 | 11.1 | 0.7 |
| 4-11 | 102.2 | 4.8 | 22 | 2 | 5.9 | 0.7 | -20.9 | 0.5 | 12.5 | 0.7 |
| 4-12 | 8.1 | 3.8 | 135 | 16 | 6.2 | 0.8 | -21.1 | 0.4 | 10.4 | 0.6 |
| 4-12 | 15.0 | 4.4 | 134 | 13 | 5.9 | 0.6 | -21.1 | 0.4 | 10.3 | 0.5 |
| 4-12 | 21.5 | 3.6 | 129 | 13 | 5.8 | 0.6 | -20.9 | 0.3 | 10.5 | 0.8 |
| 4-12 | 26.2 | 4.0 | 179 | 8 | 6.0 | 0.2 | -20.6 | 0.3 | 10.3 | 0.3 |
| 4-12 | 27.4 | 4.4 | 129 | 0 | 5.7 | 0.2 | -21.5 | 0.0 | 8.3 | 0.1 |
| 4-12 | 27.7 | 3.9 | 127 | 9 | 5.6 | 0.3 | -21.4 | 0.2 | 8.5 | 0.4 |
| 4-12 | 27.7 | 5.4 | 144 | 18 | 5.7 | 0.8 | -21.1 | 0.2 | 8.8 | 0.3 |
| 4-12 | 32.7 | 4.1 | 109 | 4 | 6.1 | 0.2 | -21.5 | 0.1 | 8.9 | 0.4 |
| 4-12 | 38.3 | 3.0 | 88 | 13 | 5.8 | 0.8 | -22.2 | 0.3 | 8.8 | 0.3 |
| 4-12 | 42.6 | 3.4 | 64 | 1 | 6.2 | 0.5 | -22.0 | 0.2 | 10.7 | 0.7 |
| 4-12 | 44.5 | 3.4 | 56 | 8 | 6.5 | 0.9 | -23.3 | 1.1 | 9.4 | 1.1 |
| 4-12 | 52.7 | 3.9 | 42 | 2 | 6.5 | 0.7 | -21.8 | 0.3 | 10.5 | 1.1 |
| 4-12 | 65.2 | 4.2 | 29 | 4 | 6.8 | 0.8 | -20.9 | 0.3 | 11.3 | 1.1 |
| 4-12 | 72.1 | 4.0 | 33 | 8 | 6.5 | 1.4 | -21.0 | 0.3 | 11.9 | 0.8 |
| 4-12 | 90.9 | 3.5 | 27 | 3 | 6.3 | 0.7 | -21.5 | 0.4 | 10.3 | 3.5 |

[a] Data (all properties) from White et al. 2007 and 2012; Depth bins re-assessed as described in Section 2.2.2.

[b] For depths at which there was not sample replication, σ determined as the mean percent standard deviation for the station multiplied by the concentration measured at that depth (abundance and molar properties).

[c] Mean standard deviation for each station used at depths for which there was not sample replication (all isotopic properties).

**Table A.7.** Measured NPP profiles from *in situ* incubation arrays; data from White et al. (2013). For each array depth, the resulting data have been associated with the depth of the density bin (from Table A.1; see Section 2.2.2) whose density corresponds closest to the *in situ* density when water for the incubation was initially collected.

**Table A.7. NPP Profiles**

| Station | Depth (m) | σ | NPP[a] µg C $L^{-1}$ $day^{-1}$ | σ | Station | Depth (m) | σ | NPP[a] µg C $L^{-1}$ $day^{-1}$ | σ |
|---|---|---|---|---|---|---|---|---|---|
| *Gulf of California* | | | | | 4-2b | 31.8 | 3.2 | 7.3 | 1.1 |
| 1-1 | 9.6 | 2.3 | 70.1 | 5.8 | 4-2b | 35.7 | 2.4 | 8.3 | 0.3 |
| 1-1 | 24.3 | 2.5 | 25.2 | 3.6 | 4-2b | 43.3 | 1.3 | 5.0 | 0.8 |
| 1-1 | 35.0 | 2.2 | 3.5 | 1.5 | *Entrance Zone* | | | | |
| 3-1 | 11.1 | 1.6 | 8.3 | 1.1 | 4-8 | 8.2 | 2.9 | 10.6 | 1.6 |
| 3-1 | 16.0 | 2.0 | 11.3 | 3.6 | 4-8 | 20.9 | 3.4 | 7.6 | 0.9 |
| 3-1 | 27.6 | 3.8 | 13.0 | 0.3 | 4-8 | 24.4 | 3.8 | 9.2 | 0.2 |
| 3-1 | 35.0 | 4.3 | 33.3 | 0.5 | 4-8 | 32.6 | 4.4 | 9.1 | 0.9 |
| 3-1 | 39.5 | 3.8 | 7.7 | 0.6 | 4-8 | 34.1 | 8.2 | 10.8 | 1.4 |
| 3-2 | 9.9 | 2.8 | 21.8 | 4.0 | 4-8 | 40.6 | 7.8 | 5.6 | 0.7 |
| 3-2 | 20.2 | 0.5 | 11.9 | 1.7 | 4-9 | 7.6 | 1.2 | 12.1 | 4.1 |
| 3-2 | 32.1 | 1.8 | 15.0 | 1.3 | 4-9 | 10.3 | 1.3 | 7.2 | 1.5 |
| 3-3 | 8.9 | 2.4 | 10.3 | 0.2 | 4-9 | 20.8 | 2.6 | 8.7 | 1.0 |
| 3-3 | 14.2 | 5.0 | 15.1 | 2.8 | 4-9 | 23.8 | 2.5 | 8.1 | 0.5 |
| 3-3 | 24.3 | 2.9 | 16.6 | 15.9 | 4-9 | 28.8 | 2.2 | 4.3 | 0.4 |
| 3-3 | 39.5 | 2.9 | 7.8 | 1.2 | 4-9 | 32.7 | 2.5 | 3.5 | 0.0 |
| 3-4 | 6.5 | 2.6 | 18.0 | 0.1 | 4-9 | 43.0 | 4.0 | 4.2 | 0.3 |
| 3-4 | 13.9 | 3.1 | 18.4 | 5.2 | *Eastern Tropical North Pacific* | | | | |
| 3-4 | 21.6 | 3.2 | 30.7 | 0.1 | 4-10 | 12.3 | 2.7 | 10.6 | 1.5 |
| 3-4 | 34.5 | 2.2 | 12.8 | 2.0 | 4-10 | 27.1 | 2.5 | 11.3 | 1.3 |
| 3-4 | 43.6 | 2.6 | 14.3 | 3.2 | 4-10 | 33.2 | 2.7 | 9.7 | 0.5 |
| 4-1 | 14.8 | 6.4 | 11.9 | 2.5 | 4-10 | 39.7 | 2.2 | 9.3 | 0.5 |
| 4-1 | 15.8 | 3.3 | 23.6 | 0.2 | 4-10 | 49.7 | 3.3 | 6.0 | 0.2 |
| 4-1 | 24.3 | 5.4 | 22.0 | 8.5 | 4-10 | 57.1 | 3.2 | 6.0 | 0.5 |
| 4-1 | 29.3 | 5.9 | 32.6 | 3.8 | 4-11 | 8.5 | 1.5 | 7.3 | 0.5 |
| 4-1 | 37.5 | 6.4 | 25.5 | 0.6 | 4-11 | 23.2 | 2.2 | 5.9 | 1.5 |
| 4-1 | 42.6 | 6.2 | 11.8 | 2.1 | 4-11 | 36.3 | 4.1 | 6.3 | 0.1 |
| 4-1 | 49.8 | 6.6 | 3.5 | 0.0 | 4-11 | 47.0 | 5.6 | 4.9 | 1.2 |
| 4-2a | 12.8 | 5.0 | 16.6 | 0.9 | 4-11 | 56.7 | 4.8 | 5.4 | 0.6 |
| 4-2a | 20.9 | 7.0 | 13.8 | 1.8 | 4-11 | 66.9 | 5.1 | 4.5 | 0.2 |
| 4-2a | 24.3 | 7.5 | 7.5 | 1.5 | 4-12 | 8.1 | 3.8 | 40.4 | 3.0 |
| 4-2a | 28.2 | 7.8 | 5.9 | 1.5 | 4-12 | 15.0 | 4.4 | 41.7 | 1.7 |
| 4-2a | 31.8 | 7.4 | 5.8 | 0.8 | 4-12 | 23.3 | 4.4 | 21.5 | 1.4 |
| 4-2a | 38.8 | 5.7 | 10.0 | 0.2 | 4-12 | 26.2 | 4.0 | 34.3 | 3.4 |
| 4-2b | 6.2 | 0.5 | 12.7 | 2.3 | 4-12 | 35.9 | 3.3 | 13.6 | 0.5 |
| 4-2b | 12.8 | 1.6 | 8.7 | 0.6 | 4-12 | 46.7 | 3.6 | 5.7 | 1.0 |
| 4-2b | 25.4 | 3.0 | 7.4 | 0.3 | 4-12 | 59.7 | 3.7 | 1.9 | 0.2 |

[a] Data (all properties) from White et al. 2007 and 2012; Depth bins re-assessed as described in Section 2.2.2.

**Table A.8.** Profiles of alkenone-producer absolute and relative cell abundance. Data for 1-1 and 3-1 through 3-4 is described in the work of Malinverno et al. 2005, and stations 4-1 through 4-12 are forthcoming from author Rosas-Navarro; depth bins have been re-assessed as described in Section 2.2.2. Uncertainty is reported as the upper 95% confidence interval, using the Poisson cell counting statistics of Bollmann et al. (2002). Gephyrocapsa species include *G. oceanica*, *G. muellerae*, *G. ericsonii*, and *G. ornata*.

**Table A.8. Alkenone Producer Abundance Profiles**

| Station[a] | Depth (m) | σ | *E. huxleyi* (cs $L^{-1}$) | ±[b] | Gephyrocapsa[c] (cs $L^{-1}$) | ± | Fraction *E. hux* + Gephyrocapsa of Total Coccos. |
|---|---|---|---|---|---|---|---|
| *Gulf of California* | | | | | | | |
| 1-1 | 5.0 | 3.5 | 3937 | 3196 | 7046 | 3995 | 0.34 |
| 1-1 | 9.6 | 2.3 | 6700 | 4912 | 11167 | 5961 | 0.62 |
| 1-1 | 15.6 | 2.3 | 29285 | 9825 | 17970 | 8013 | 0.76 |
| 1-1 | 21.2 | 2.0 | 66330 | 26283 | 18090 | 15969 | 0.78 |
| 1-1 | 36.4 | 2.3 | 7787 | 4578 | 2920 | 3221 | 0.46 |
| 1-1 | 51.7 | 3.2 | 2981 | 3110 | 1278 | 2430 | 0.48 |
| 3-1 | 4.0 | 0.0 | 2273 | 2169 | 18471 | 4968 | 0.61 |
| 3-1 | 7.5 | 1.2 | 2635 | 2326 | 22251 | 5485 | 0.69 |
| 3-1 | 11.1 | 1.6 | 2362 | 2160 | 21570 | 5245 | 0.65 |
| 3-1 | 14.3 | 1.7 | 2779 | 2221 | 34335 | 6310 | 0.72 |
| 3-1 | 21.0 | 3.1 | 7330 | 3071 | 13532 | 3956 | 0.69 |
| 3-1 | 24.6 | 3.7 | 5967 | 3093 | 7672 | 3421 | 0.56 |
| 3-1 | 26.1 | 3.5 | 14623 | 4277 | 14884 | 4310 | 0.78 |
| 3-1 | 27.6 | 3.8 | 20340 | 4873 | 17035 | 4505 | 0.92 |
| 3-1 | 29.0 | 3.7 | 9916 | 3566 | 11441 | 3790 | 0.89 |
| 3-1 | 30.4 | 3.8 | 16103 | 4331 | 12634 | 3896 | 0.95 |
| 3-1 | 32.2 | 4.4 | 33167 | 6047 | 24668 | 5282 | 0.94 |
| 3-1 | 33.5 | 4.8 | 25845 | 5275 | 15942 | 4251 | 0.98 |
| 3-1 | 37.1 | 3.9 | 29951 | 5641 | 8937 | 3313 | 0.89 |
| 3-1 | 39.5 | 3.8 | 31781 | 5960 | 10933 | 3717 | 0.87 |
| 3-1 | 41.9 | 3.6 | 18306 | 4650 | 9916 | 3566 | 0.72 |
| 3-1 | 43.9 | 3.6 | 31400 | 5764 | 6280 | 2864 | 0.69 |
| 3-1 | 45.9 | 4.1 | 29493 | 5760 | 9153 | 3448 | 0.71 |
| 3-1 | 59.3 | 6.3 | 14623 | 4277 | 3395 | 2366 | 0.55 |
| 3-1 | 81.9 | 3.6 | 4961 | 2732 | 783 | 1490 | 0.85 |
| 3-1 | 99.9 | 4.0 | 2952 | 2288 | 805 | 1531 | 0.88 |
| 3-2 | 7.0 | 1.4 | 5052 | 1838 | 755 | 902 | 0.40 |
| 3-2 | 15.4 | 3.0 | 7987 | 2206 | 773 | 895 | 0.56 |
| 3-2 | 22.1 | 6.1 | 27911 | 5787 | 1342 | 1764 | 0.80 |
| 3-2 | 22.2 | 0.6 | 12832 | 2973 | 1359 | 1199 | 0.62 |
| 3-2 | 25.5 | 1.6 | 28995 | 5677 | 2178 | 1976 | 0.90 |
| 3-2 | 25.8 | 4.1 | 23645 | 5213 | 1780 | 1857 | 0.83 |
| 3-2 | 28.6 | 2.7 | 34070 | 6152 | 4068 | 2490 | 0.93 |
| 3-2 | 29.3 | 1.1 | 38151 | 6390 | 7432 | 3114 | 0.94 |
| 3-2 | 34.0 | 2.3 | 57384 | 8444 | 10247 | 3924 | 0.76 |
| 3-2 | 36.3 | 2.3 | 51280 | 7328 | 7927 | 3198 | 0.72 |
| 3-2 | 40.0 | 1.8 | 32798 | 6046 | 7628 | 3196 | 0.52 |
| 3-2 | 43.1 | 2.1 | 38646 | 6257 | 5656 | 2705 | 0.60 |
| 3-2 | 55.8 | 1.7 | 10652 | 3621 | 1734 | 1809 | 0.57 |
| 3-2 | 72.1 | 3.1 | 2635 | 1366 | 1255 | 1034 | 0.65 |
| 3-2 | 97.6 | 1.6 | 2230 | 1968 | 248 | 1133 | 1.00 |
| 3-3 | 3.8 | 1.4 | 13204 | 3120 | 161 | 736 | 0.50 |
| 3-3 | 8.9 | 2.4 | 18306 | 4650 | 0 | 957 | 0.61 |
| 3-3 | 12.7 | 1.5 | 24023 | 5328 | 261 | 1194 | 0.64 |
| 3-3 | 13.7 | 2.0 | 21866 | 5033 | 254 | 1162 | 0.59 |
| 3-3 | 17.1 | 3.5 | 38398 | 6409 | 2973 | 2179 | 0.82 |
| 3-3 | 21.3 | 3.6 | 46574 | 7007 | 1982 | 1891 | 0.89 |
| 3-3 | 21.7 | 2.7 | 33692 | 6035 | 1982 | 1891 | 0.91 |
| 3-3 | 24.3 | 2.9 | 47263 | 7257 | 3917 | 2495 | 0.97 |
| 3-3 | 25.8 | 2.7 | 31642 | 5784 | 7488 | 3078 | 0.95 |
| 3-3 | 28.5 | 3.3 | 102844 | 16130 | 14185 | 6785 | 0.98 |
| 3-3 | 30.3 | 2.7 | 39885 | 11574 | 4459 | 2538 | 0.97 |
| 3-3 | 32.5 | 2.6 | 32366 | 8559 | 16908 | 6474 | 0.84 |
| 3-3 | 37.1 | 2.8 | 15000 | 5339 | 15415 | 5347 | 0.82 |
| 3-3 | 41.5 | 3.1 | 3964 | 2426 | 9662 | 3474 | 0.65 |
| 3-3 | 53.0 | 3.8 | 23193 | 1533 | 3764 | 1992 | 0.86 |
| 3-3 | 71.5 | 3.4 | 2273 | 1391 | 995 | 1037 | 0.55 |
| 3-3 | 104.5 | 1.1 | 1675 | 1167 | 773 | 895 | 0.59 |
| 3-4 | 6.5 | 2.6 | 2004 | 1464 | 3558 | 1838 | 0.50 |
| 3-4 | 13.9 | 3.1 | 1977 | 1147 | 1266 | 967 | 0.42 |
| 3-4 | 19.3 | 2.8 | 1699 | 1040 | 849 | 810 | 0.41 |
| 3-4 | 21.6 | 3.2 | 2563 | 1169 | 2169 | 1093 | 0.53 |
| 3-4 | 24.6 | 2.6 | 12787 | 2870 | 2984 | 1546 | 0.79 |
| 3-4 | 31.8 | 2.2 | 27003 | 5456 | 248 | 1133 | 0.72 |
| 3-4 | 34.5 | 2.2 | 19114 | 4076 | 2240 | 1672 | 0.79 |
| 3-4 | 40.2 | 2.4 | 48308 | 7227 | 6865 | 3061 | 0.92 |
| 3-4 | 47.5 | 3.2 | 35178 | 6156 | 6689 | 2983 | 0.51 |
| 3-4 | 59.6 | 1.8 | 1823 | 973 | 1458 | 893 | 0.90 |
| 3-4 | 97.2 | 2.7 | 426 | 811 | 0 | 535 | 0.50 |
| 4-1 | 15.8 | 3.3 | 8030 | 1285 | 780 | 465 | 0.65 |
| 4-1 | 25.4 | 5.1 | 20498 | 3353 | 368 | 715 | 0.70 |
| 4-1 | 33.0 | 6.1 | 58225 | 6641 | 354 | 937 | 0.93 |
| 4-1 | 42.6 | 6.2 | 40094 | 6036 | 4729 | 2368 | 0.79 |
| 4-1 | 46.6 | 6.9 | 25702 | 4424 | 9300 | 2804 | 0.83 |
| 4-1 | 61.1 | 8.1 | 6547 | 1258 | 3960 | 1003 | 0.82 |
| 4-1 | 79.3 | 6.7 | 2695 | 554 | 1706 | 452 | 0.71 |
| 4-2a | 10.1 | 5.4 | 7316 | 2412 | 36426 | 4976 | 0.81 |
| 4-2a | 20.9 | 7.0 | 11867 | 3533 | 31151 | 5447 | 0.88 |
| 4-2a | 31.8 | 7.4 | 24931 | 5471 | 31163 | 6054 | 0.84 |
| 4-2a | 38.8 | 5.7 | 34262 | 6237 | 27259 | 5620 | 0.72 |
| 4-2a | 42.4 | 5.3 | 28499 | 7756 | 19256 | 6543 | 0.52 |
| 4-2a | 46.7 | 5.8 | 15303 | 3507 | 6601 | 2430 | 0.56 |
| 4-2a | 63.1 | 9.9 | 7495 | 1843 | 7317 | 1823 | 0.73 |
| 4-2b | 8.3 | 1.9 | 1270 | 1237 | 14448 | 3289 | 0.55 |
| 4-2b | 19.5 | 2.2 | 2347 | 984 | 9235 | 1791 | 0.40 |
| 4-2b | 35.7 | 2.4 | 17136 | 3974 | 17915 | 4054 | 0.58 |
| 4-2b | 53.8 | 2.7 | 9657 | 2503 | 13680 | 2925 | 0.70 |
| 4-2b | 72.6 | 3.5 | 5952 | 1426 | 7243 | 1557 | 0.61 |
| 4-2b | 97.3 | 3.7 | 6610 | 1287 | 4425 | 1074 | 0.67 |
| *Entrance Zone* | | | | | | | |
| 4-8 | 7.5 | 1.2 | 327 | 688 | 27754 | 3841 | 0.85 |
| 4-8 | 17.0 | 3.0 | 717 | 719 | 25382 | 3206 | 0.77 |
| 4-8 | 24.4 | 3.8 | 2178 | 1688 | 30176 | 5099 | 0.65 |
| 4-8 | 32.6 | 4.4 | 12332 | 4278 | 34701 | 6758 | 0.68 |
| 4-8 | 37.4 | 8.0 | 11690 | 2500 | 24841 | 3536 | 0.84 |
| 4-8 | 55.6 | 7.7 | 30959 | 6940 | 42169 | 7984 | 0.84 |
| 4-8 | 68.6 | 7.5 | 19116 | 2989 | 11865 | 2402 | 0.82 |
| 4-8 | 102.8 | 3.1 | 2353 | 571 | 1801 | 508 | 0.75 |
| 4-9 | 6.5 | 1.3 | 1748 | 778 | 187 | 363 | 0.12 |
| 4-9 | 10.3 | 1.3 | 1890 | 1137 | 1779 | 1111 | 0.14 |
| 4-9 | 18.8 | 2.9 | 3464 | 819 | 1752 | 608 | 0.42 |
| 4-9 | 30.6 | 2.4 | 9617 | 1638 | 5336 | 1253 | 0.91 |
| 4-9 | 35.8 | 2.8 | 53575 | 11911 | 10151 | 5896 | 0.51 |
| 4-9 | 38.5 | 3.3 | 21971 | 3317 | 3737 | 1511 | 0.73 |
| 4-9 | 41.4 | 3.7 | 44850 | 7644 | 9049 | 3778 | 0.78 |
| 4-9 | 51.3 | 3.4 | 41035 | 5710 | 17976 | 3907 | 0.73 |
| 4-9 | 67.7 | 3.6 | 12117 | 1790 | 2759 | 921 | 0.56 |
| *Eastern Tropical North Pacific* | | | | | | | |
| 4-10 | 5.8 | 0.5 | 4804 | 838 | 494 | 318 | 0.94 |
| 4-10 | 9.5 | 3.0 | 4708 | 914 | 2173 | 647 | 0.81 |
| 4-10 | 21.7 | 2.2 | 16069 | 2274 | 1394 | 783 | 0.81 |
| 4-10 | 29.7 | 2.6 | 16833 | 3650 | 8416 | 2688 | 0.68 |
| 4-10 | 33.2 | 2.7 | 28505 | 5273 | 6215 | 2711 | 0.44 |
| 4-10 | 35.2 | 2.8 | 11820 | 2741 | 6313 | 2081 | 0.54 |
| 4-10 | 53.5 | 3.2 | 48535 | 6556 | 7898 | 2903 | 0.46 |
| 4-10 | 65.6 | 4.0 | 141694 | 11696 | 10124 | 3483 | 0.82 |
| 4-10 | 99.4 | 3.4 | 13136 | 2656 | 1395 | 1044 | 0.41 |
| 4-11 | 3.0 | 2.8 | 9936 | 2147 | 5167 | 1608 | 0.64 |
| 4-11 | 8.5 | 1.5 | 8409 | 1576 | 3153 | 1019 | 0.49 |
| 4-11 | 15.1 | 2.0 | 12238 | 1977 | 4580 | 1268 | 0.57 |
| 4-11 | 29.4 | 2.8 | 60854 | 9290 | 24982 | 6193 | 0.63 |
| 4-11 | 38.8 | 4.4 | 33380 | 5053 | 19716 | 3967 | 0.68 |
| 4-11 | 49.8 | 5.5 | 70736 | 11825 | 16210 | 6155 | 0.79 |
| 4-11 | 59.8 | 5.2 | 76933 | 12223 | 14304 | 5805 | 0.54 |
| 4-11 | 90.1 | 5.5 | 4086 | 947 | 882 | 496 | 0.27 |
| 4-12 | 8.1 | 3.8 | 55968 | 7076.5 | 6387 | 2693 | 0.96 |
| 4-12 | 15.0 | 4.4 | 90946 | 12124 | 13735 | 5196 | 0.91 |
| 4-12 | 21.5 | 3.6 | 77136 | 10609 | 5343 | 3337 | 0.98 |
| 4-12 | 24.4 | 3.8 | 52839 | 8000 | 6489 | 3191 | 0.94 |
| 4-12 | 27.8 | 4.6 | 66925 | 8101 | 6561 | 2873 | 0.89 |
| 4-12 | 32.7 | 4.1 | 21441 | 3614 | 4885 | 1878 | 0.85 |
| 4-12 | 40.6 | 3.1 | 49337 | 6612 | 11306 | 3388 | 0.80 |
| 4-12 | 50.5 | 4.2 | 28925 | 5100 | 10606 | 3255 | 0.79 |
| 4-12 | 68.4 | 4.2 | 33801 | 5006 | 7420 | 2536 | 0.96 |
| 4-12 | 97.1 | 3.5 | 18116 | 2261 | 4419 | 1185 | 0.98 |

[a] Data for 1-1 and 3-1 through 3-4 is from the work of Malenverno et al. 2005; 4-1 through 4-12 are from Anaid Rosas-Navarro and Dr. Patrizia Ziveri (personal communication). Depth bins re-assessed as described in Section 2.2.2.

[b] Upper 95% confidence interval, using the Poisson cell counting statistics of Bollmann et al., 2002.

[c] Includes *Gephyrocapsa oceanica*, *G. muellerae*, *G. ericsonii*, and *G. ornata*.

**Table A.9.** Estimated production rate profiles for alkenone producing coccolithophorid cells. Rates are calculated from K37:2 turnover rate (Table A.2) and *E. huxleyi* and Gephyrocapsa cell abundance (Table A.8), interpolated to each density bin, as per Section 2.4.1.

**Table A.9. Estimated Alkenone-Producer Production**

| Station | Depth (m) | σ | Estimated $PR_{cocco}$[a] (cells $L^{-1} d^{-1} \times 10^3$) | ±[b] | Station | Depth (m) | σ | Estimated $PR_{cocco}$[a] (cells $L^{-1} d^{-1} \times 10^3$) | ±[b] | Station | Depth (m) | σ | Estimated $PR_{cocco}$[a] (cells $L^{-1} d^{-1} \times 10^3$) | ±[b] |
|---|---|---|---|---|---|---|---|---|---|---|---|---|---|---|
| *Gulf of California* | | | | | 3-3 | 13.8 | 3.2 | 3.4 | 0.8 | 4-1 | 49.8 | 6.6 | 0.9 | 0.2 |
| 1-1 | 9.6 | 2.3 | 2.3 | 0.9 | 3-3 | 14.2 | 5.0 | 3.6 | 0.8 | 4-2a | 10.1 | 5.4 | 7.8 | 1.0 |
| 1-1 | 11.1 | 2.0 | 3.2 | 1.1 | 3-3 | 15.2 | 3.2 | 4.3 | 0.8 | 4-2a | 10.8 | 6.0 | 8.1 | 1.0 |
| 1-1 | 12.5 | 2.0 | 4.0 | 1.2 | 3-3 | 15.6 | 2.8 | 4.6 | 0.8 | 4-2a | 12.8 | 5.0 | 9.1 | 1.2 |
| 1-1 | 13.1 | 1.4 | 4.3 | 1.2 | 3-3 | 17.1 | 3.5 | 5.7 | 0.9 | 4-2a | 14.4 | 6.0 | 9.0 | 1.2 |
| 1-1 | 14.1 | 1.7 | 4.9 | 1.3 | 3-3 | 17.2 | 3.5 | 5.7 | 0.9 | 4-2a | 17.6 | 6.8 | 8.8 | 1.3 |
| 1-1 | 14.4 | 2.1 | 5.0 | 1.4 | 3-3 | 17.7 | 2.0 | 5.8 | 0.9 | 4-2a | 20.9 | 7.0 | 8.6 | 1.3 |
| 1-1 | 15.6 | 2.3 | 5.7 | 1.5 | 3-3 | 19.1 | 3.2 | 5.9 | 0.9 | 4-2a | 24.3 | 7.5 | 10.6 | 1.5 |
| 1-1 | 15.7 | 1.6 | 5.8 | 1.5 | 3-3 | 21.3 | 3.6 | 6.2 | 0.9 | 4-2a | 28.2 | 7.8 | 13.0 | 1.9 |
| 1-1 | 16.2 | 2.7 | 6.1 | 1.7 | 3-3 | 21.3 | 3.1 | 6.1 | 0.9 | 4-2a | 31.8 | 7.4 | 15.5 | 2.2 |
| 1-1 | 16.9 | 2.4 | 6.7 | 1.9 | 3-3 | 21.7 | 2.7 | 4.5 | 0.8 | 4-2a | 34.7 | 6.8 | 17.2 | 2.4 |
| 1-1 | 17.6 | 2.7 | 7.1 | 2.1 | 3-3 | 22.7 | 2.5 | 5.2 | 0.8 | 4-2a | 36.9 | 6.0 | 18.6 | 2.6 |
| 1-1 | 18.4 | 2.2 | 7.7 | 2.4 | 3-3 | 24.3 | 2.9 | 6.2 | 0.9 | 4-2a | 38.8 | 5.7 | 19.9 | 2.7 |
| 1-1 | 19.8 | 2.1 | 8.7 | 2.9 | 3-3 | 25.7 | 2.8 | 4.4 | 0.7 | 4-2a | 40.7 | 5.5 | 16.6 | 2.8 |
| 1-1 | 21.2 | 2.0 | 9.7 | 3.3 | 3-3 | 25.8 | 2.7 | 4.3 | 0.7 | 4-2a | 42.4 | 5.3 | 13.6 | 2.8 |
| 1-1 | 23.0 | 2.2 | 8.5 | 3.0 | 3-3 | 28.5 | 3.3 | 10.5 | 1.6 | 4-2a | 44.6 | 5.6 | 9.0 | 1.8 |
| 1-1 | 24.3 | 2.5 | 7.7 | 2.7 | 3-3 | 28.6 | 2.6 | 10.1 | 1.5 | 4-2a | 46.7 | 5.8 | 5.3 | 1.0 |
| 1-1 | 26.0 | 2.3 | 6.2 | 2.2 | 3-3 | 29.6 | 3.1 | 6.0 | 0.9 | 4-2a | 48.9 | 6.4 | 4.6 | 0.9 |
| 1-1 | 27.9 | 2.5 | 4.8 | 1.7 | 3-3 | 30.3 | 2.7 | 3.4 | 0.5 | 4-2a | 51.6 | 7.4 | 3.7 | 0.7 |
| 1-1 | 28.9 | 1.7 | 4.1 | 1.5 | 3-3 | 32.5 | 2.6 | 2.9 | 0.6 | 4-2a | 54.3 | 8.7 | 3.0 | 0.6 |
| 1-1 | 30.9 | 2.2 | 2.9 | 1.1 | 3-3 | 34.2 | 2.3 | 1.9 | 0.4 | 4-2a | 55.2 | 9.7 | 2.8 | 0.5 |
| 1-1 | 32.3 | 2.3 | 2.1 | 0.8 | 3-3 | 37.1 | 2.8 | 0.7 | 0.2 | 4-2a | 57.1 | 10.4 | 2.3 | 0.4 |
| 1-1 | 33.6 | 2.1 | 1.5 | 0.6 | 3-3 | 39.5 | 2.9 | 0.1 | 0.0 | 4-2a | 59.6 | 11.2 | 1.7 | 0.3 |
| 1-1 | 35.0 | 2.2 | 1.0 | 0.4 | 3-4 | 6.5 | 2.6 | 1.4 | 0.5 | 4-2a | 61.0 | 10.4 | 1.4 | 0.2 |
| 3-1 | 11.1 | 1.6 | 4.9 | 1.1 | 3-4 | 13.9 | 3.1 | 0.9 | 0.4 | 4-2a | 63.1 | 9.9 | 1.0 | 0.2 |
| 3-1 | 14.3 | 1.7 | 6.8 | 1.2 | 3-4 | 19.3 | 2.8 | 0.6 | 0.3 | *Entrance Zone* | | | | |
| 3-1 | 16.0 | 2.0 | 5.7 | 1.1 | 3-4 | 21.6 | 3.2 | 1.1 | 0.3 | 4-8 | 8.2 | 2.9 | 5.6 | 0.8 |
| 3-1 | 17.6 | 2.3 | 4.9 | 1.0 | 3-4 | 23.0 | 2.9 | 2.4 | 0.6 | 4-8 | 10.1 | 2.4 | 5.3 | 0.7 |
| 3-1 | 19.9 | 2.3 | 3.8 | 0.8 | 3-4 | 24.6 | 2.6 | 4.0 | 0.8 | 4-8 | 13.1 | 2.9 | 4.9 | 0.7 |
| 3-1 | 21.0 | 3.1 | 3.3 | 0.8 | 3-4 | 26.3 | 2.2 | 5.0 | 1.0 | 4-8 | 17.0 | 3.0 | 4.4 | 0.6 |
| 3-1 | 23.3 | 3.1 | 2.5 | 0.7 | 3-4 | 27.6 | 2.0 | 5.8 | 1.2 | 4-8 | 20.9 | 3.4 | 4.6 | 0.7 |
| 3-1 | 24.6 | 3.7 | 2.1 | 0.7 | 3-4 | 29.0 | 2.5 | 6.7 | 1.4 | 4-8 | 24.4 | 3.8 | 5.9 | 1.0 |
| 3-1 | 26.1 | 3.5 | 4.4 | 0.9 | 3-4 | 29.9 | 2.8 | 7.3 | 1.5 | 4-8 | 27.8 | 4.0 | 6.7 | 1.1 |
| 3-1 | 27.6 | 3.8 | 5.4 | 0.9 | 3-4 | 30.1 | 2.0 | 7.5 | 1.5 | 4-8 | 30.2 | 4.5 | 7.3 | 1.2 |
| 3-1 | 29.0 | 3.7 | 4.0 | 0.9 | 3-4 | 31.8 | 2.2 | 8.8 | 1.8 | 4-8 | 32.6 | 4.4 | 7.8 | 1.3 |
| 3-1 | 30.4 | 3.8 | 6.7 | 1.3 | 3-4 | 32.9 | 2.0 | 8.2 | 1.7 | 4-8 | 34.1 | 8.2 | 6.9 | 1.1 |
| 3-1 | 32.2 | 4.4 | 16.7 | 2.3 | 3-4 | 34.5 | 2.2 | 7.4 | 1.5 | 4-8 | 37.4 | 8.0 | 5.1 | 0.6 |
| 3-1 | 33.5 | 4.8 | 13.8 | 2.2 | 3-4 | 34.9 | 2.1 | 8.2 | 1.6 | 4-8 | 40.6 | 7.8 | 5.3 | 0.7 |
| 3-1 | 35.0 | 4.3 | 15.3 | 2.5 | 3-4 | 36.4 | 1.8 | 11.2 | 1.9 | 4-8 | 44.2 | 7.9 | 5.5 | 0.7 |
| 3-1 | 37.1 | 3.9 | 9.6 | 1.6 | 3-4 | 37.5 | 1.9 | 13.5 | 2.1 | 4-8 | 49.6 | 7.8 | 5.3 | 0.8 |
| 3-1 | 39.5 | 3.8 | 4.3 | 0.7 | 3-4 | 39.0 | 2.2 | 16.5 | 2.5 | 4-8 | 55.6 | 7.7 | 4.5 | 0.7 |
| 3-2 | 7.0 | 1.4 | 1.5 | 0.5 | 3-4 | 40.2 | 2.4 | 18.7 | 2.7 | *Eastern Tropical North Pacific* | | | | |
| 3-2 | 9.9 | 2.8 | 1.7 | 0.5 | 3-4 | 42.0 | 2.3 | 17.5 | 2.6 | 4-12 | 8.1 | 3.8 | 23.3 | 3.0 |
| 3-2 | 11.9 | 2.9 | 1.7 | 0.5 | 3-4 | 43.6 | 2.6 | 16.4 | 2.5 | 4-12 | 15.0 | 4.4 | 40.5 | 5.1 |
| 3-2 | 14.2 | 2.9 | 1.6 | 0.4 | 4-1 | 15.8 | 3.3 | 4.4 | 0.7 | 4-12 | 21.5 | 3.6 | 7.9 | 1.3 |
| 3-2 | 15.4 | 3.0 | 1.6 | 0.4 | 4-1 | 16.1 | 6.7 | 4.6 | 0.8 | 4-12 | 23.3 | 4.4 | 0.9 | 0.7 |
| 3-2 | 15.6 | 3.7 | 1.7 | 0.4 | 4-1 | 18.6 | 4.1 | 6.2 | 1.0 | 4-12 | 24.4 | 3.8 | 1.8 | 0.5 |
| 3-2 | 16.5 | 3.1 | 2.0 | 0.5 | 4-1 | 20.7 | 4.6 | 7.6 | 1.2 | 4-12 | 26.2 | 4.0 | 3.8 | 0.5 |
| 3-2 | 18.1 | 4.3 | 2.4 | 0.6 | 4-1 | 21.4 | 4.8 | 8.0 | 1.3 | 4-12 | 26.6 | 3.1 | 3.7 | 0.5 |
| 3-2 | 18.9 | 1.0 | 2.5 | 0.6 | 4-1 | 24.3 | 5.7 | 9.9 | 1.6 | 4-12 | 27.4 | 4.4 | 3.6 | 0.5 |
| 3-2 | 20.2 | 0.5 | 2.7 | 0.6 | 4-1 | 24.3 | 5.4 | 9.9 | 1.6 | 4-12 | 27.7 | 3.9 | 3.6 | 0.5 |
| 3-2 | 21.0 | 4.2 | 3.2 | 0.7 | 4-1 | 25.0 | 5.5 | 10.1 | 1.7 | 4-12 | 27.7 | 5.4 | 3.6 | 0.4 |
| 3-2 | 21.0 | 4.9 | 3.2 | 0.7 | 4-1 | 25.4 | 5.1 | 10.2 | 1.7 | 4-12 | 27.8 | 4.6 | 3.5 | 0.4 |
| 3-2 | 22.1 | 6.1 | 4.1 | 0.9 | 4-1 | 26.2 | 5.5 | 11.8 | 1.8 | 4-12 | 30.1 | 3.9 | 1.9 | 0.3 |
| 3-2 | 22.2 | 0.6 | 2.0 | 0.5 | 4-1 | 26.6 | 5.5 | 12.5 | 1.9 | 4-12 | 30.8 | 4.2 | 1.5 | 0.2 |
| 3-2 | 22.8 | 4.0 | 2.7 | 0.6 | 4-1 | 27.5 | 5.9 | 14.2 | 2.0 | 4-12 | 32.7 | 4.1 | 0.6 | 0.1 |
| 3-2 | 23.5 | 5.0 | 3.4 | 0.7 | 4-1 | 29.2 | 6.2 | 17.0 | 2.2 | 4-12 | 34.4 | 3.9 | 0.5 | 0.1 |
| 3-2 | 25.5 | 1.6 | 6.0 | 1.2 | 4-1 | 29.3 | 5.9 | 17.0 | 2.2 | 4-12 | 35.9 | 3.3 | 0.3 | 0.2 |
| 3-2 | 25.8 | 4.1 | 5.0 | 1.1 | 4-1 | 30.0 | 4.5 | 18.2 | 2.3 | 4-12 | 38.3 | 3.0 | 0.4 | 0.2 |
| 3-2 | 28.6 | 2.7 | 9.1 | 1.6 | 4-1 | 31.8 | 5.7 | 21.0 | 2.5 | 4-12 | 40.6 | 3.1 | 0.6 | 0.3 |
| 3-2 | 29.3 | 3.1 | 11.4 | 1.8 | 4-1 | 33.0 | 6.1 | 22.6 | 2.6 | 4-12 | 42.6 | 3.4 | 0.6 | 0.3 |
| 3-2 | 29.3 | 1.1 | 11.4 | 1.8 | 4-1 | 34.5 | 6.1 | 20.9 | 2.5 | 4-12 | 44.5 | 3.4 | 0.6 | 0.3 |
| 3-2 | 31.3 | 2.0 | 15.4 | 2.2 | 4-1 | 36.5 | 6.3 | 18.8 | 2.3 | 4-12 | 46.7 | 3.6 | 0.6 | 0.3 |
| 3-2 | 32.1 | 1.8 | 17.1 | 2.4 | 4-1 | 37.5 | 6.4 | 17.7 | 2.2 | 4-12 | 48.9 | 4.1 | 0.6 | 0.2 |
| 3-3 | 8.9 | 2.4 | 3.4 | 0.9 | 4-1 | 38.8 | 6.4 | 15.3 | 2.0 | 4-12 | 50.5 | 4.2 | 0.5 | 0.2 |
| 3-3 | 11.1 | 2.6 | 3.7 | 0.9 | 4-1 | 40.4 | 6.5 | 12.8 | 1.7 | 4-12 | 52.7 | 3.9 | 0.5 | 0.2 |
| 3-3 | 11.6 | 2.1 | 3.7 | 0.9 | 4-1 | 42.6 | 6.2 | 9.4 | 1.4 | 4-12 | 55.1 | 3.6 | 0.5 | 0.2 |
| 3-3 | 12.7 | 1.5 | 3.8 | 0.8 | 4-1 | 44.0 | 6.9 | 7.3 | 1.1 | 4-12 | 57.4 | 3.5 | 0.5 | 0.2 |
| 3-3 | 13.7 | 2.0 | 3.3 | 0.8 | 4-1 | 46.6 | 6.9 | 3.8 | 0.6 | 4-12 | 59.7 | 3.7 | 0.5 | 0.2 |

[a] From K37:2 turnover rate (Table A.3) and *E. hux* + Gephyrocapsa abundance (Table A.5) interpolated to each bin. See Section 2.4.1 of text.

[b] Propagated uncertainty from K27:2 turnover rate and cell count profiles.

**Appendix B. Alkenone and $CO_2$ Carbon Isotopic Composition and Ancillary Properties:**

Total dissolved inorganic carbon (DIC) concentration, total alkalinity, and natural abundance $\delta^{13}C_{DIC}$ profiles were collected during the alkenone $^{13}C$ incubation experiments described by Wolhowe et al. (2014). From these properties, Wolhowe et al. calculated $[CO_{2(aq)}]$ and $\delta^{13}C_{CO2}$ via the methods of Laws et al. (1995) and Popp et al. (2006). Profiles of natural abundance $\delta^{13}C_{K37:2}$, measured $\delta^{13}C_{DIC}$, and calculated $\delta^{13}C_{CO2}$ from this work were interpolated to the depths of the $\delta D_{K37}$ measurements and are reported in Table B.1. From these properties, $\varepsilon_p$ was calculated via Equation 3.3.2 (Table 3.2). Uncertainties in $\delta^{13}C_{K37:2}$ and $\delta^{13}C_{CO2}$ were assumed to be 0.1‰ (as per Wolhowe et al. 2014), and an uncertainty of 0.05‰ (Popp et al. 1998b) was assumed for the term $\varepsilon_{cell\text{-}K37:2}$. These values were propagated into Equation 3.3.2 to yield uncertainties in $\varepsilon_p$ of ~0.15‰.

For the calculation of $\mu$ via Equation 3.3.3, surface area to volume ratios were estimated by assuming *E. huxleyi* to be a 5 μm diameter sphere (SA:V = 1.2 $m^{-1}$), and *G. oceanica* to have twice the internal cell volume (SA:V = 0.95 $m^{-1}$). The SA:V value used in Equation 3.3.3 was the weighted average of these two values (Table B.1) based on the *E. huxleyi* vs. *G. oceanica* fractional abundance values in Table 3.2. An uncertainty of the full estimate range (0.25 $m^{-1}$) was assumed. Note that this parameterization only had a minor effect on the resulting profiles of growth rate, which were not appreciably different if a constant value of SA:V was used. In the absence of replicate measurements of $[CO_2]$ with which to assess variability, a generous uncertainty of 10% in dissolved $CO_2$ was assumed, as per Popp et al. (2006). Uncertainties in $\varepsilon_p$ (above), SA:V, and $[CO_2]$ were propagated into Equation 3.3.3 to generate uncertainties in $\mu$ ranging from 0.14 to 0.26 $d^{-1}$.

.

**Table B.1.** Profiles of alkenone and DIC carbon isotopic composition, calculated $CO_{2(aq)}$ isotopic composition and abundance, and estimates surface area:volume at stations/depths for which all data are available as described in Appendix B. All properties are interpolated from the data reported in Wolhowe et al. (2014) to the depth of the alkenone isotopic samples.

**Table B.1.** Values used in Calculation of μ via Eq. 3.3.3.

| Station | Depth (m) | $\delta^{13}C_{K37:2}$ (‰ vs. PDB) | $\delta^{13}C_{DIC}$ (‰ vs. PDB) | $\delta^{13}C_{CO2}$ (‰ vs. PDB) | $[CO_{2(aq)}]$ (μmol $kg^{-1}$) | Estimated SA:V ($m^{-1}$) |
|---|---|---|---|---|---|---|
| 4-1 | 30 | -27.12 | 1.24 | -7.14 | 12.5 | 1.20 |
| 4-2a | 10 | -27.41 | 1.31 | -6.83 | 11.4 | 1.00 |
| 4-2a | 20 | -27.41 | 1.30 | -6.85 | 11.5 | 1.00 |
| 4-2a | 30 | -26.93 | 1.28 | -6.95 | 11.9 | 1.04 |
| 4-2a | 40 | -27.22 | 0.92 | -7.45 | 13.4 | 1.08 |
| 4-2a | 50 | -26.44 | 0.84 | -7.68 | 14.2 | 1.13 |
| 4-8 | 10 | -27.60 | 1.43 | -6.71 | 9.9 | 0.96 |
| 4-8 | 20 | -27.56 | 1.38 | -6.78 | 10.9 | 0.97 |
| 4-8 | 30 | -26.24 | 1.14 | -7.11 | 11.7 | 1.04 |
| 4-12 | 10 | -25.11 | 1.50 | -7.66 | 12.2 | 1.17 |
| 4-12 | 25 | -25.07 | 1.34 | -8.13 | 14.4 | 1.18 |

## Appendix C. Age Models, $\delta^{18}O$ Stratigraphy, and LGM $\delta D_{H2O}$ Estimation:

Below are the dept-age models (Figure C.1; Table C.1) used to identify samples at the 19, 21, and 23 kya horizons as discussed in Sections 4.2.1 and 4.2.2. The benthic foraminiferal $\delta^{18}O$ records used to construct these curves from cores without previously-published age models (EW9504-12PC through -18PC) are illustrated in Figure C.2.

Due to a lack of planktonic foraminiferal data from core LPAZ02MV-21P, surface $\delta D_{H2O}$ had to be estimated as described in Section 4.2.5. The relationship between reconstructed $\delta D_{H2O}$ and reconstructed SST used to do this is shown in Figure C.3.

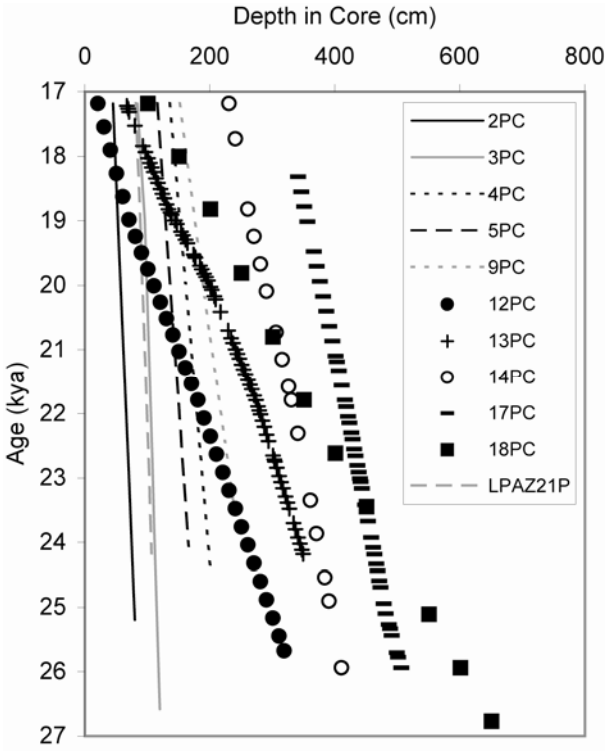


**Figure C.1**. Depth-age models for glacial sampling period (17kya to 25-27kya) for cores used in this study. Cores with existing age models (see Sections 4.2.1 and 4.2.2) are shown as lines, while the age models developed here are shown as points. The data are tabulated in Table C.1.

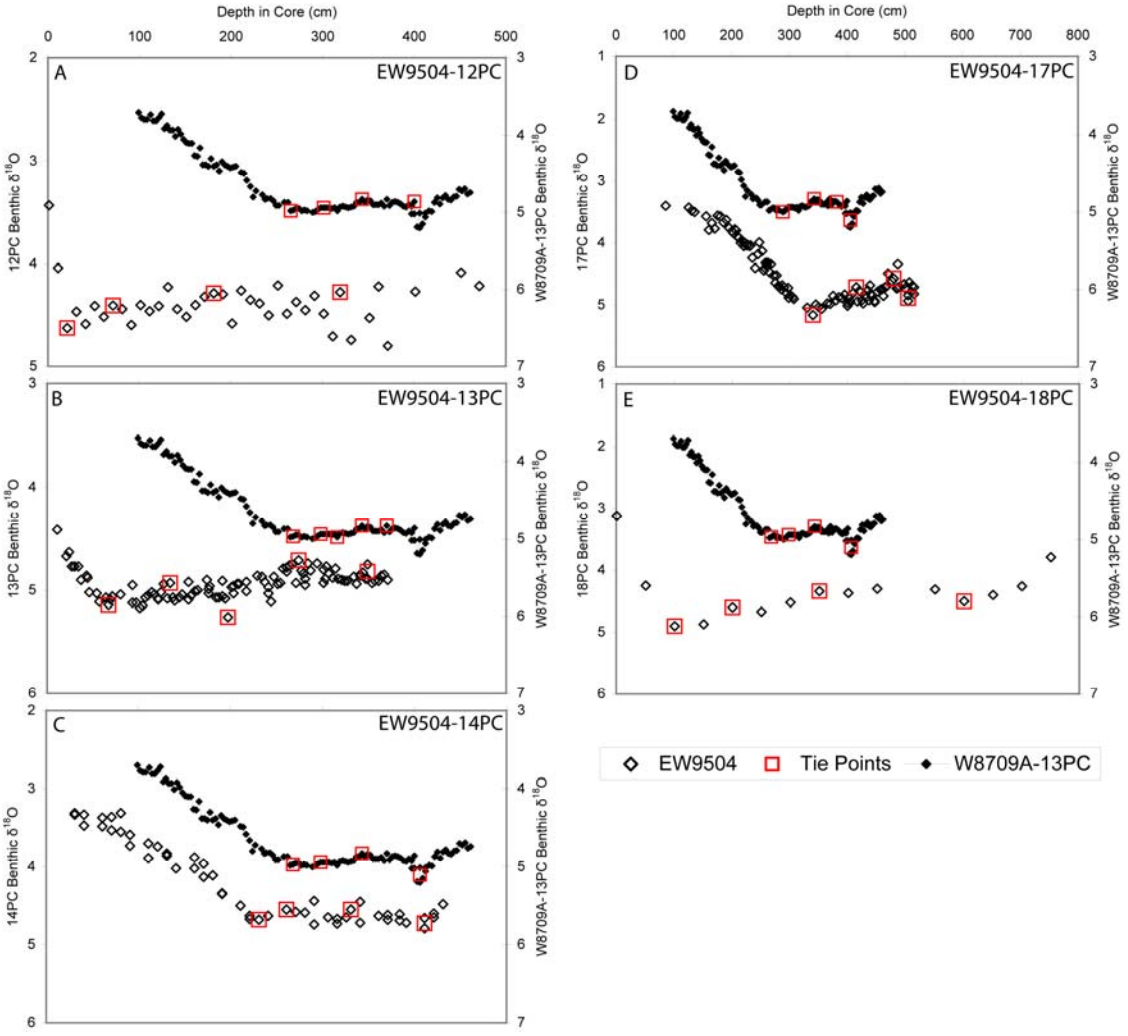


**Figure C.2**. Previously-unpublished EW9504 benthic $\delta^{18}O$ records (Table C.1) compared to W8709A-13PC record of Mix et al. (1999). Tie points from the W8709A-13PC record used to develop the EW9504 age models are highlighted in red. Full Holocene plateaus are missing from the $\delta^{18}O$ records of 12PC, 13PC, and 18PC, suggesting sediment loss during coring (see Section 4.3.1).

**Table C.1.** Depth-age models for the period of ~17-25 kya for all down-core sites as discussed in Section 4.2.2. Included are the depths of each benthic $\delta^{18}O$ sample in this interval, with age estimates either adjusted from those of Stott et al. (2000) and Herbert et al. (2001) or based on the W8709A-13PC chronology via the identified tie points marked in bold, as indicated by footnote.

**Table C.1**. Depth-Age Models for ~17 kya to 25 kya

| Depth (cm) | Age (kya) | Benthic $\delta^{18}O$ (‰ vs. PDB) | Depth (cm) | Age (kya) | Benthic $\delta^{18}O$ (‰ vs. PDB) | Depth (cm) | Age (kya) | Benthic $\delta^{18}O$ (‰ vs. PDB) | Depth (cm) | Age (kya) | Benthic $\delta^{18}O$ (‰ vs. PDB) | Depth (cm) | Age (kya) | Benthic $\delta^{18}O$ (‰ vs. PDB) | Depth (cm) | Age (kya) | Benthic $\delta^{18}O$ (‰ vs. PDB) |
|---|---|---|---|---|---|---|---|---|---|---|---|---|---|---|---|---|---|
| *EW9504-2PC*[a,e] | | | *EW9504-12PC*[c,f] | | | 124 | 18.58 | 5.02 | 303 | 22.72 | 4.89 | 403 | 21.19 | 4.88 | *LPAZ-21P*[d,h] | | |
| 45 | 17.19 | 4.24 | **21** | **17.19** | **4.63** | 127 | 18.65 | 4.94 | 304 | 22.75 | 4.77 | 406 | 21.33 | 4.95 | 81.5 | 17.19 | 3.72 |
| 55 | 19.48 | 4.15 | 31 | 17.55 | 4.47 | 131 | 18.75 | 5.08 | 307 | 22.84 | 4.84 | 411 | 21.56 | 4.80 | 86.5 | 18.50 | 3.65 |
| 60 | 20.63 | 3.95 | 41 | 17.91 | 4.59 | **134** | **18.82** | **4.93** | 311 | 22.97 | 4.88 | **416** | **21.79** | **4.71** | 91.5 | 19.81 | 3.69 |
| 70 | 22.91 | 4.13 | 51 | 18.27 | 4.41 | 137 | 18.87 | 5.07 | 314 | 23.07 | 4.79 | 418 | 21.89 | 4.94 | 96.5 | 21.12 | 3.59 |
| 78 | 24.75 | 4.00 | 61 | 18.63 | 4.52 | 139 | 18.91 | 5.10 | 317 | 23.16 | 4.89 | 421 | 22.05 | 4.77 | 101.5 | 22.53 | 3.72 |
| 80 | 25.20 | 4.17 | **71** | **18.99** | **4.41** | 144 | 18.99 | 5.07 | 321 | 23.29 | 4.90 | 423 | 22.15 | 3.07 | 106.5 | 24.17 | 3.51 |
| | | | 81 | 19.24 | 4.44 | 147 | 19.05 | 5.04 | 324 | 23.39 | 4.91 | 426 | 22.30 | 4.92 | | | |
| *EW9504-3PC*[b,e] | | | 91 | 19.50 | 4.60 | 154 | 19.17 | 5.01 | 327 | 23.48 | 4.91 | 428 | 22.40 | 4.97 | | | |
| 84 | 17.19 | 3.74 | 101 | 19.75 | 4.40 | 157 | 19.22 | 5.05 | 334 | 23.70 | 4.87 | 431 | 22.55 | 4.84 | | | |
| 93 | 18.54 | 3.46 | 111 | 20.01 | 4.46 | 161 | 19.29 | 5.01 | 337 | 23.80 | 4.94 | 433 | 22.66 | 4.88 | | | |
| 96 | 18.99 | 3.77 | 121 | 20.26 | 4.41 | 164 | 19.35 | 5.00 | 341 | 23.93 | 4.86 | 436 | 22.81 | 4.76 | | | |
| 105 | 21.83 | 3.30 | 131 | 20.52 | 4.23 | 174 | 19.52 | 4.90 | 344 | 24.02 | 4.83 | 438 | 22.91 | 4.92 | | | |
| 108 | 22.78 | 3.59 | 141 | 20.77 | 4.44 | 176 | 19.56 | 5.01 | 347 | 24.12 | 4.89 | 440 | 23.01 | 4.68 | | | |
| 111 | 23.73 | 3.23 | 151 | 21.03 | 4.52 | 177 | 19.57 | 4.96 | **349** | **24.18** | **4.82** | 441 | 23.06 | 4.82 | | | |
| 120 | 26.58 | 3.55 | 161 | 21.28 | 4.40 | 184 | 19.70 | 5.07 | | | | 443 | 23.17 | 4.85 | | | |
| | | | 171 | 21.54 | 4.32 | 187 | 19.75 | 5.07 | *EW9504-14PC*[c,f] | | | 448 | 23.42 | 4.94 | | | |
| *EW9504-4PC*[a,e] | | | **181** | **21.79** | **4.29** | 191 | 19.82 | 4.99 | **231** | **17.19** | **4.68** | 453 | 23.67 | 4.78 | | | |
| 136 | 17.19 | 4.05 | 191 | 22.07 | 4.30 | 194 | 19.87 | 5.08 | 241 | 17.73 | 4.63 | 458 | 23.93 | 4.75 | | | |
| 144 | 18.08 | 3.83 | 201 | 22.35 | 4.58 | **197** | **19.92** | **5.26** | **261** | **18.82** | **4.55** | 461 | 24.08 | 4.74 | | | |
| 152 | 18.97 | 3.96 | 211 | 22.64 | 4.26 | 201 | 20.02 | 4.97 | 271 | 19.24 | 4.58 | 463 | 24.18 | 4.85 | | | |
| 161 | 19.97 | 3.84 | 221 | 22.92 | 4.35 | 203 | 20.07 | 5.00 | 281 | 19.67 | 4.59 | 466 | 24.34 | 4.71 | | | |
| 168 | 20.75 | 3.84 | 231 | 23.20 | 4.39 | 207 | 20.17 | 4.94 | 291 | 20.09 | 4.59 | 468 | 24.44 | 4.70 | | | |
| 176 | 21.64 | 3.84 | 241 | 23.48 | 4.50 | 209 | 20.21 | 4.94 | 306 | 20.73 | 4.65 | 471 | 24.59 | 4.49 | | | |
| 184 | 22.53 | 3.76 | 251 | 23.76 | 4.21 | 217 | 20.41 | 4.97 | 316 | 21.15 | 4.7 | 473 | 24.69 | 2.08 | | | |
| 191 | 23.31 | 3.84 | 261 | 24.04 | 4.63 | 229 | 20.70 | 4.86 | 326 | 21.58 | 4.65 | 478 | 24.95 | 4.61 | | | |
| 201 | 24.42 | 3.77 | 271 | 24.32 | 4.37 | 234 | 20.82 | 4.87 | **331** | **21.79** | **4.55** | **481** | **25.10** | **4.57** | | | |
| | | | 281 | 24.61 | 4.45 | 237 | 20.89 | 4.92 | 341 | 22.31 | 4.585 | 486 | 25.27 | 4.73 | | | |
| *EW9504-5PC*[a,e] | | | 291 | 24.89 | 4.31 | 241 | 20.99 | 5.00 | 361 | 23.35 | 4.63 | 488 | 25.34 | 4.53 | | | |
| 116 | 17.19 | 4.61 | 301 | 25.17 | 4.49 | 244 | 21.06 | 5.11 | 371 | 23.87 | 4.65 | 491 | 25.44 | 4.70 | | | |
| 126 | 18.56 | 4.59 | 311 | 25.45 | 4.71 | 247 | 21.14 | 4.87 | 384 | 24.54 | 4.65 | 499 | 25.71 | 4.66 | | | |
| 134 | 19.66 | 4.53 | **319** | **25.68** | **4.28** | 251 | 21.23 | 4.94 | 391 | 24.91 | 4.72 | 501 | 25.77 | 4.73 | | | |
| 142 | 20.76 | 4.55 | | | | 254 | 21.31 | 4.93 | **411** | **25.94** | **4.725** | **506** | **25.94** | **4.89** | | | |
| 150 | 21.86 | 4.52 | *EW9504-13PC*[c,g] | | | 257 | 21.38 | 4.79 | | | | | | | | | |
| 158 | 22.96 | 4.41 | **67** | **17.22** | **5.14** | 261 | 21.48 | 4.80 | *EW9504-17PC*[c,g] | | | *EW9504-18PC*[c,f] | | | | | |
| 166 | 24.06 | 4.31 | 69 | 17.26 | 5.09 | 264 | 21.55 | 4.76 | **341** | **18.32** | **5.16** | **101** | **17.19** | **4.90** | | | |
| | | | 71 | 17.31 | 5.06 | 267 | 21.62 | 4.75 | 346 | 18.55 | 4.99 | 151 | 18.00 | 4.87 | | | |
| *EW9504-9PC*[b,e] | | | 80 | 17.53 | 5.04 | 271 | 21.72 | 4.93 | 351 | 18.78 | 5.03 | **201** | **18.82** | **4.60** | | | |
| 152 | 17.19 | 3.88 | 93 | 17.84 | 5.04 | **274** | **21.79** | **4.71** | 356 | 19.01 | 5.06 | 251 | 19.81 | 4.67 | | | |
| 168 | 18.39 | 3.32 | 97 | 17.93 | 5.12 | 277 | 21.89 | 4.81 | 366 | 19.48 | 4.97 | 301 | 20.80 | 4.52 | | | |
| 184 | 19.59 | 3.81 | 101 | 18.03 | 5.17 | 279 | 21.95 | 4.84 | 371 | 19.71 | 4.98 | **351** | **21.79** | **4.34** | | | |
| 192 | 20.19 | 3.55 | 104 | 18.10 | 5.15 | 281 | 22.01 | 4.92 | 376 | 19.94 | 4.85 | 401 | 22.62 | 4.37 | | | |
| 200 | 20.79 | 3.77 | 107 | 18.17 | 5.07 | 284 | 22.11 | 4.74 | 381 | 20.17 | 4.92 | 451 | 23.45 | 4.30 | | | |
| 208 | 21.33 | 3.77 | 110 | 18.25 | 5.05 | 287 | 22.21 | 4.81 | 386 | 20.40 | 4.87 | 551 | 25.11 | 4.31 | | | |
| 224 | 22.43 | 3.58 | 114 | 18.34 | 5.02 | 291 | 22.33 | 2.79 | 391 | 20.63 | 4.88 | **601** | **25.94** | **4.50** | | | |
| 232 | 22.98 | 3.68 | 117 | 18.41 | 5.04 | 294 | 22.43 | 4.74 | 396 | 20.86 | 4.83 | | | | | | |
| 240 | 23.53 | 3.59 | 121 | 18.51 | 5.09 | 301 | 22.65 | 4.87 | 401 | 21.10 | 4.99 | | | | | | |

[a] Data and age model from Stott et al. (2000), age model shifted based on 17.2 kya 'turning point' as described in Section IV.2.2.

[b] Data from Stott et al. (2000), updated age model from Herbert et al. (2001), age model shifted based on 17.2 kya 'turning point' as described in Section IV.2.2.

[c] New data (see Section IV.2.1). Age model based on tie points (**bold**) to W8709A-13PC chronology of Mix et al. (1999).

[d] Data and age model from Herbert et al. (2001), age model shifted based on 17.2 kya 'turning point' as described in Section IV.2.2.

[e] Data for *C. mckannai*.

[f] Combined record for *C. wuellerstorfi* and *Uvigerina sp.*, with +0.64‰ species offset applied to *C. wuellerstorfi*.

[g] Data for *Uvigerina sp*.

[h] Data for mixed benthic species.

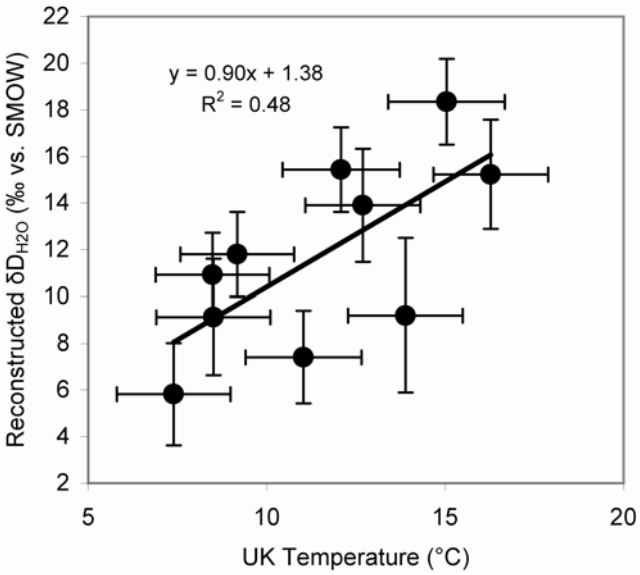


**Figure C.3**. Relationship between mean reconstructed LGM $\delta D_{H2O}$ of surface water (see Section 4.2.5) and mean LGM $U_{37}^{K'}$ temperature. This relationship is used to estimate surface $\delta D_{H2O}$ for LGM samples from LPAZ02MV-21P, from which no planktonic foraminiferal $\delta^{18}O$ data was available.